AD NUMBER
AD889705
LIMITATION CHANGES

TO:

Approved for public release; distribution is unlimited.

FROM:

Distribution authorized to U.S. Gov't. agencies only; Test and Evaluation; 01 NOV 1971. Other requests shall be referred to Air Force Weapons Laboratory, Attn: DEZ, Kirtland AFB, NM 87117.

AUTHORITY
AFWL ltr dtd 19 May 1972

AFWL-TR-70-113, Vol I

AD889705

MULTIPLE-WHEEL HEAVY GEAR LOAD PAVEMENT TESTS

Volume I

Basic Report

R. G. Ahlvin, et al.
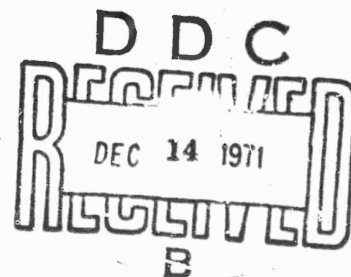
U. S. Army Engineer Waterways Experiment Station

TECHNICAL REPORT NO. AFWL-TR-70-113, Vol I

November 1971

AIR FORCE WEAPONS LABORATORY
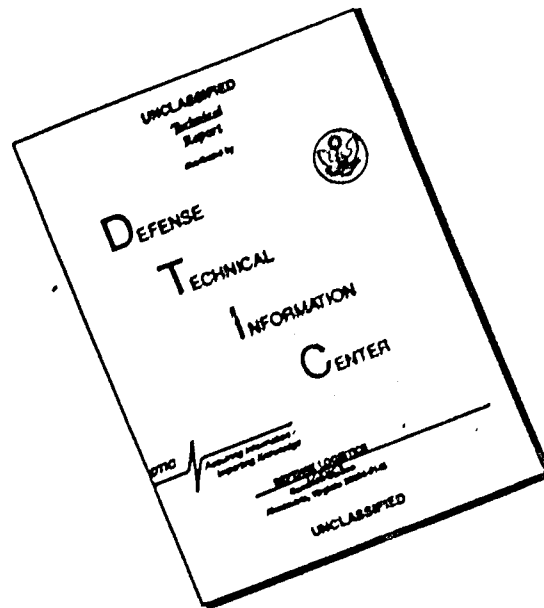Air Force Systems Command
Kirtland Air Force Base
New Mexico

DDC
RECEIVED
DEC 14 1971
B

AD No.
DDC FILE COPY

DISCLAIMER NOTICE

THIS DOCUMENT IS BEST
QUALITY AVAILABLE. THE COPY
FURNISHED TO DTIC CONTAINED
A SIGNIFICANT NUMBER OF
PAGES WHICH DO NOT
REPRODUCE LEGIBLY.

AIR FORCE WEAPONS LABORATORY
Air Force Systems Command
Kirtland Air Force Base
New Mexico 87117

MULTIPLE-WHEEL HEAVY GEAR LOAD PAVEMENT TESTS

VOLUME I

BASIC REPORT

R. G. Ahlvin, et al.

U. S. Army Engineer Waterways Experiment Station

TECHNICAL REPORT NO. AFWL-TR-70-113, Vol I

FOREWORD

This report was prepared by the U. S. Army Engineer Waterways Experiment Station, Vicksburg, Mississippi, under MIPR 68-7. The research was jointly sponsored by the U. S. Air Force under Program Element 64708F, Project 5224, Task 04; the U. S. Army under Task 02, Work Unit 002; and the ⋯⋯ral Aviation Administration under Engineering Requirement FAA-ER-450-034a.

Inclusive dates of research were 1 January 1968 through 1 August 1971. The report was submitted 20 September 1971 by the Air Force Weapons Laboratory Project Officer, Mr. L. M. Womack (DEZ-M).

The following consultants participated in the project and attended the consultants' meeting in January 1970: Professor S. J. Buchanan (Texas A&M University), Professor R. E. Fadum (North Carolina State University), Professor W. H. Goetz (Purdue University), Professor M. E. Harr (Purdue University), Professor W. R. Hudson (University of Texas), Professor C. L. Monismith (University of California), Professor E. G. Nawy (Rutgers University), Professor A. S. Vesic (Duke University), Professor R. K. Watkins (Utah State University), Professor R. W. Woodhead (University of Illinois), and Mr. W. J. Turnbull (Vicksburg, Mississippi).
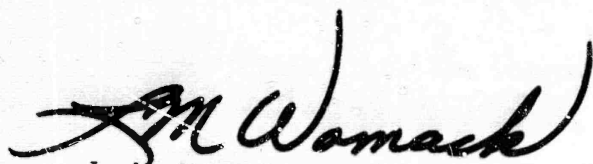
The investigation reported herein was conducted under the overall supervision of Messrs. W. J. Turnbull (retired), J. P. Sale, A. A. Maxwell (deceased), and R. G. Ahlvin, Soils Division, WES. Other Soils Division personnel actively engaged in this study were Messrs. D. N. Brown, C. D. Burns, A. H. Joseph, W. H. Larson, A. L. Mathews, H. H. Ulery, Jr., D. M. Ladd, J. E. Watkins, R. W. Grau, R. H. Ledbetter, D. L. Cooksey, J. W. Hall, Jr., H. R. Austin, M. J. Trawle, and G. M. Hammitt II, and Dr. O. O. Thompson, and Dr. Yu-Tang Chou. Personnel of the WES Instrumentation Services Division engaged in the study were Messrs. L. M. Duke, G. C. Downing, W. S. R. Beane IV, and J. L. Ferguson. Messrs. W. O. Tynes and W. F. McCleese of the WES Concrete Division supervised the concrete laboratory testing.

Personnel of CERL actively engaged in the investigation were Messrs. J. J. Healy, R. L. Hutchinson, J. L. Rice, F. W. Kearney, and J. B. Gambill.
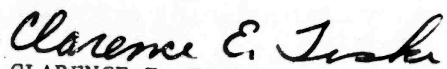
The flexible pavement portions of the report were written by Messrs. Ahlvin and Ulery, and the rigid pavement portions of the report were written by Messrs. Hutchinson and Rice. Coordination between WES and CERL in preparation of the report was by Mr. Ulery.

FOREWORD (cont'd)

This technical report has been reviewed and is approved.

L. M. WOMACK
Project Officer

CLARENCE E. TESKE
Lt Colonel   USAF
Chief, Aerospace Facilities Branch

WILLIAM B. LIDDICOET
Colonel   USAF
Chief, Civil Engineering Research
    Division

ABSTRACT

(Distribution Limitation Statement B)

Flexible and rigid pavements were constructed and tested to obtain data on pavement and soil behavior under large aircraft loadings for use in developing criteria for evaluating and designing airfield pavements subjected to multiple-wheel heavy gear loads (MWHGL).

The test sections incorporated instrumentation systems designed to determine the response of the pavement structures to static, dynamic (slowly moving), and vibratory loads and to traffic by full prototype loadings of a 12-wheel assembly (one main gear of a C-5A aircraft), a twin-tandem assembly (one twin-tandem component of the Boeing 747 assembly), and a single wheel.

Analysis of static load response data from the flexible pavement instrumentation program resulted in the establishment of maximum elastic deflection and vertical elastic stress versus depth curves. Comparisons showed that the same relationships were true for static and dynamic load tests, as well as for speed tests. The findings for the rigid pavement test section indicated that the Westergaard algorithm can be used for reasonable prediction of pavement response to test loadings.

The data from the instrumentation program and the traffic tests were used in the analysis of the flexible and rigid pavement test sections. The analysis resulted in a modification of the basic flexible pavement CBR design method. The recommended method reflects a reduction of existing Corps of Engineers (CE) thickness requirements that is especially significant for multiple-wheel assemblies in the higher operational level. Current CE evaluation and design methods for rigid pavements are based on stress in the concrete pavement as calculated from the Westergaard analysis; extrapolations to the existing criteria were found to be valid for MWHGL assemblies insofar as pavement thicknesses were concerned. Rigid pavement testing indicated that current jointing recommendations allowing keyed construction joints may be unconservative for MWHGL assemblies trafficking a pavement overlying a low-strength subgrade.

CONTENTS

ILLUSTRATIONS

ILLUSTRATIONS (cont'd)

ILLUSTRATIONS (cont'd)

ILLUSTRATIONS (cont'd)

ILLUSTRATIONS (cont'd)

TABLES

TABLES (cont'd)

CONVERSION FACTORS, BRITISH TO METRIC UNITS OF MEASUREMENT

British units of measurement used in this report can be converted to metric units as follows:

Multiply	By	To Obtain
inches	2.54	centimeters
feet	0.3048	meters
miles (U. S. statute)	1.609344	kilometers
square inches	6.4516	square centimeters
square feet	0.092903	square meters
cubic yards	0.764555	cubic meters
gallons (U. S.)	3.785412	cubic decimeters
pounds	0.45359237	kilograms
kips	453.59237	kilograms
pounds per square inch	0.070307	kilograms per square centimeter
pounds per cubic inch	27.67984	grams per cubic centimeter
pounds per cubic foot	16.0185	kilograms per cubic meter
feet per second	0.3048	meters per second
miles per hour	1.609344	kilometers per hour
Fahrenheit degrees	5/9	Celsius of Kelvin degrees*

---

* To obtain Celsius (C) temperature readings from Fahrenheit (F) readings, use the following formula: $C = (5/9)(F - 32)$. To obtain Kelvin (K) readings, use: $K = (5/9)(F - 32) + 273.15$.

SECTION I

INTRODUCTION

1. PURPOSE

This investigation was conducted mainly to validate present criteria, to establish modifications to present criteria, or to develop new criteria for the evaluation and design of both flexible and rigid airfield pavements to be subjected to multiple-wheel heavy gear loads (MWHGL). MWHGL as used in this report denotes aircraft gross loads in excess of 600 kips.[1] A purpose of this study was to collect instrumentation and traffic behavior data for future use in the evaluation of the applicability of theoretical treatments of pavement design.

2. BACKGROUND

Development of a new giant jet transport aircraft by the U. S. Air Force (AF) has led to a significant increase in aircraft size and weight to be accommodated by existing and future airfields. This giant aircraft is the C-5A Galaxy (figure 1) built by Lockheed Aircraft Company. The C-5A has a gross weight of over 750,000 lb with growth potential. In the design competition for the giant transport, Boeing, Lockheed, and Douglas Aircraft Companies were prime participants. Boeing has built the 747 aircraft, and Lockheed and Douglas are building the L-500 and the DC-10, respectively, all of which are in the general gross weight range of the C-5A.

Since these aircraft will be twice as heavy as their predecessors and will impose loads on pavements that are radically different from those previously encountered, there is wide concern over requirements for pavements to support them. Extensions to the existing criteria for pavement evaluation and design are necessary to evaluate the effects of these loads. Data are also required to determine the relative destructive effects of new and proposed aircraft on pavement performance.

Increase in aircraft size and weight has been experienced repeatedly in the past. Following World War II, the need to spread aircraft loads to

---

[1]A table of factors for converting British units of measurement to metric units is presented on page xiv.

more wheels became apparent and led to two- and four-wheel gear configurations. With the advent of the C-5A and equivalent large civil aircraft came the need for substantially more wheels beneath the aircraft. The many supporting wheels are needed to provide ground flotation compatible with existing pavement systems and, in the case of the C-5A, with expedient military airfields. Aircraft ground-flotation criteria, by which the individual wheel loads, tire pressures, and wheel spacings are selected to provide desired flotation, have been developed by the U. S. Army Corps of Engineers (CE) for the AF (references 1, 2, and 3) and were specifically applied in design of the C-5A and apparently also for the above-mentioned 747, L-500, and DC-10 aircraft.

The C-5A was designed with flotation sufficient to permit its unrestricted use on medium-load AF airfields. A medium-load pavement, as defined for AF use, is one that is capable of supporting aircraft with a 100-kip load on a gear with twin wheels spaced 37 in. center-to-center (c-c) and having tire contact areas of 267 sq in. Such a pavement will also support KC-135 aircraft at 300-kip gross weight. The KC-135 aircraft is the military version of the Boeing 707 and has requirem nts about the same as those for an unstretched DC-8 aircraft. The Boeing 747 has apparently been designed for use on civil airfields capable of sustaining regular operations of a 350-kip DC-8. Medium-load pavement design requirements formed the basis for design of the test pavements in the investigation reported herein. Landing gear complexes of 18 to 28 wheels are the result of providing medium-load pavement flotation in the C-5A and flotation comparable to that of previous commercial jet transports in the current very large civil aircraft. For flexible pavements, this puts new emphasis on the effect of wheel interaction and the broader deflection basin commensurate with the multiple-wheel landing gear complexes. For rigid pavements, the distribution of wheel loadings over nearly an entire single pavement slab raises doubts as to the adequacy of assumptions of interior corner or edge loadings on slabs assumed to extend to infinity and the adequacy of present means of measuring subgrade support. Also, it raises questions in regard to conventional assumptions of degree of load transfer across joints. The investigation reported herein was undertaken to provide better information to resolve these problems.

The AF, Army, and Federal Aviation Administration (FAA) jointly sponsored

this investigation. The specific AF objective was to provide means for designing and evaluating flexible and rigid pavements for very heavy multiple-wheeled aircraft. The effects of these loads on an overlay pavement were also studied. The C-5A and other similar aircraft will be operating in support of the Army. Since these aircraft will be required to operate from Army airfields, the Army must have a means of evaluating Army airfields for multiple-wheeled heavy-load aircraft. The objective of this investigation, therefore, was to provide the Army with a means of evaluating airfields for C-5A-type loadings. The Army is also interested in operation of heavy transport-type aircraft on membrane-encased soil layer (MESL) construction. After failure, part of the flexible pavement test section was replaced with MESL construction. The effects of the C-5A load on MESL test items were determined and are discussed in a separate report (reference 4). The FAA is concerned with the operation of the Boeing 747, SST, and even heavier future aircraft on existing airfields and the effects that these aircraft will have on the pavement structures. This investigation will provide methodology for use in developing airfield design and evaluation criteria for such aircraft.

3. SCOPE

The purpose of this investigation was accomplished by the construction and testing of a specially designed test section consisting of both flexible and rigid pavements as described herein. Testing consisted of instrumentation measurements of deflection, strain, and stress resulting from applied static and dynamic (slowly moving) single- and multiple-wheel loads; nondestructive vibratory testing to determine wave velocity and stiffness; and traffic testing with multiple- and single-wheel gear assemblies.

The MWHGL study represented such an extensive effort that the report of the study was divided into the following volumes:

    I - Basic Report (background, summary of entire study, conclusions, and recommendations)

    II - Design, Construction, and Behavior Under Traffic

    III - Presentation and Initial Analysis of Stress-Strain-Deflection and Vibratory Measurements

        A. Instrumentation

        B. Data and Analysis

3

IV - Analysis of Behavior Under Traffic

This volume presents the background, summary of the entire study, examples of pavement thickness criteria, conclusions, and recommendations.

Volume II is limited to the design, construction, instrumentation system, physical properties, and behavior under traffic of the MWHGL test section.

The subject matter of Volume III was too broad to be presented in a single report. Therefore, Volume III-A mainly describes the flexible and rigid pavement instrumentation system and its installation and operation to collect the data required to determine the stresses, strains, and deflections under various static and dynamic loads and wheel configurations, temperature and pore pressure effects, and soil behavior patterns. Volume III-A also includes descriptions of the preliminary test program conducted to evaluate the performance of the system and the tes procedures and application of loads for the major test program. Volume III-B describes the major test program and the interpretation and limited analysis of instrumentation data collected during static and dynamic load tests, i.e., stress, consolidation, deflection, pore pressure, temperature effects, and pavement strain. Volume III-B also describes the results of the tests to determine the effects of the speed of the vehicles during the dynamic load tests, as well as a limited analysis of the soil behavior patterns. Tabulations of selected actual data are presented in the appendixes to Volume III-B. Complete data are on record at WE. The analysis was fairly extensive but was not intended to be completely comprehensive under the current investigation.

Volume IV presents a summary of the investigation of various theoretical concepts of pavement behavior with advantages and limitations of each concept. Following a discussion of these concepts, a review of the development of the current CE methods of design for rigid and flexible pavements is presented, and the analysis of data from the MWHGL test section is given. Data used in the analysis and criteria development were selected from Volumes II and III-B.

4.   HISTORY AND CHRONOLOGY

Work began on the site selection, planning, and design phases of the

investigation in February 1968. The initial funding of the investigation
was by the AF in January 1968. Original Army funding was authorized in March
1969. Funding by the FAA was by FAA interagency agreement in May 1969.

Construction of the test section was initiated in July 1968. The flex-
ible pavement portion of the test section was completed in November 1968,
and the rigid pavement portion was completed in December 1968. All work was
accomplished by WES personnel except for placement of the portland cement
concrete pavement, which was accomplished under contract.

During the period April to July 1969, instrumentation tests were con-
ducted. Trafficking of the test section began in August 1969, and all field
testing was completed in February 1970.

During the conduct of the investigation, five MWHGL consultants' meet-
ings were held at WES for the purpose of reviewing progress of the investi-
gation. These meetings were held on the following dates: 13-14 June 1968
(before start of construction), 6 November 1968 (during construction),
27-28 May 1969 (after construction was completed and shortly after start of
the instrumentation tests), 8-9 October 1969 (after instrumentation tests
were completed and during actual test traffic), and 26-28 January 1970 (after
traffic testing and data collection were essentially completed).

The consultants' meeting held on 26-28 January 1970 was particularly
significant in that the analysis of MWHGL test results had progressed to the
point that preliminary pavement design and evaluation criteria for the C-5A
and Boeing 747 aircraft had been developed and were made available to the
sponsors.

SECTION II

DESIGN AND CONSTRUCTION

1. GENERAL

   The multiple-wheel gear configuration selected for the traffic testing
of the test sections was that used for the C-5A aircraft. The C-5A aircraft
was designed for use on medium-load AF pavements; therefore, when possible,
medium-load pavement requirements were used in the design of the pavement
test items. The greatest influence of combined loadings from a number of
wheels is effective at substantial depths. In order for this influence to
occur within the pavement structure, it was necessary to use a low-strength
subgrade, which would require large structural thickness. Accordingly, all
of the rigid pavement items and flexible pavement items 1, 2, 3, and 5 were
designed for a constant-strength subgrade with a modulus of soil reaction
k of 100 lb/cu in. or a California Bearing Ratio (CBR) of 4 to a depth of
12 ft.

   The AF medium-load criteria for flexible pavements, as shown in TM 5-
824-2/AFM 88-6, Chapter 2 (reference 5), require a minimum pavement and base
thickness of 9 in.: 3 in. of hot-mix surfacing on a 6-in. base course.
These minimum thicknesses were used in all test items, but the total thick-
ness of the flexible pavement test items (thickness above the subgrade) was
varied from 15 to 42 in. so that failures would occur at traffic volume
levels that are expected to occur, under normal operating conditions, from a
few weeks to several years. In order to determine the MWHGL effects on deep
soft layers, item 4 of the flexible pavement section was designed with an
extra weak 36-in. layer of 2-CBR material located 21 in. below the surface
of the 4-CBR subgrade or 54 in. below the surface of the pavement.

   For the rigid pavement, the AF medium-load criteria require thicknesses
in excess of that which would be failed under reasonable volumes of traffic.
Therefore, the thicknesses were selected using current CE design procedures
extrapolated to account for the heavier load and greater number of wheels.
They were varied from 8 to 14 in. so that failures would occur at traffic
volume levels representing that which is expected to occur, under normal op-
erating conditions, from a few weeks to several years. Information available

regarding the concrete strength attainable using locally available gravel aggregates indicated a 28-day flexural strength of 650 psi as reasonable. Therefore, the design thickness of the rigid pavement was based upon a concrete strength of 650 psi and a modulus of soil reaction k value of 100 lb/ cu in. Thicknesses were selected using the Westergaard solution for stress due to edge loading and assuming that 25 percent of the edge loading would be transferred to the adjoining slab through the jointing arrangement. Results of a small-scale static load model study (reference 6) were also utilized in the selection of thicknesses for the test items.

Items 1 and 4 of the rigid pavement test section, which were 10 and 8 in. thick, respectively, were designed to fail under a low volume of traffic. These items were needed to validate current criteria for the evaluation of allowable loadings of pavements for various traffic lives. After each of these items had deteriorated to the point at which an operational pavement would require an extensive strengthening process, a nonrigid overlay was constructed. Traffic was then continued to validate current criteria for strengthening of existing rigid pavements. Nonrigid overlays of 4 and 6 in. were used on the 10- and 8-in. items, respectively, to extend their lives to a volume of traffic that would be anticipated during the life of a pavement under normal operation conditions. Item 2, a 12-in.-thick pavement, was designed to sustain a volume of traffic that would normally be expected to occur during the design life of a pavement. The 14-in.-thick pavement, item 3, was expected to have a traffic life greater than the normal design volume and was not expected to fail. Therefore, the four thicknesses bracketed the thickness believed adequate for the loading to be applied based upon current criteria and should provide information regarding thicknesses needed for low-volume traffic and for strengthening existing pavements.

Weakened-plane transverse contraction joints were used on 25-ft spacings. The 25-ft spacing exceeds that recommended for 8- and 10-in. pavements in reference 7; i.e., AFM 88-6, Chapter 3 (DA Technical Manual TM 5-824-3). Recommended spacings for 8- and 10-in.-thick pavements are 15 and 20 ft, respectively. The 25-ft spacing was used to reduce the number of variables since a 25-ft spacing is recommended for thicker pavements. The greater slab size was also desirable because dimensions of the multiple-wheel gear are such that both six-wheel assemblies will barely fit on a 25-ft slab. Special

7

curing procedures were used to minimize the possibility of cracking in the large slabs during the early curing period. All joints were sealed with a hot-poured joint-sealer material.

2. DESCRIPTION OF TEST SITE AND LAYOUT

The soil in the area in which the test section was located is a lean clay (loess) deposit. The average water table was at a depth of approximately 17 ft. In order to obtain a uniform controlled-strength subgrade to a depth of 12 ft below the surface of the pavement, it was necessary to excavate the existing material from the test site to a depth of 12 ft below finished design grades and backfill with controlled-strength materials. This resulted in an average excavation of about 6 ft of material from under all test items of the flexible and rigid pavements.

The rigid pavement test items were each 50 ft square and composed of four 25-ft-square slabs separated by a longitudinal construction joint and a transverse weakened-plane joint. The rigid pavement test items were separated by 25-ft-long by 50-ft-wide transition slabs, which were heavily reinforced to prevent the migration of cracks from one test item to another. The flexible pavement test items were each 60 ft square. A plan and profile of both the flexible and rigid pavement test sections are shown in figure 2.

3. PAVEMENT ELEMENTS

a. Lean Clay Subgrade

The natural soil at and near the test site was utilized for the bottom portion of the controlled-strength subgrade. The soil had a liquid limit (LL) of 34 and plasticity index (PI) of 12 and was classified as a lean clay (CL) according to the Unified Soil Classification System (reference 8).

b. Heavy Clay Subgrade

The top 3 ft of subgrade under all rigid pavement test items and flexible pavement test items 1, 2, 3, and 5 consisted of a heavy clay (CH) material. This material had an LL of 73 and a PI of 48. The clay, locally known as buckshot, was obtained from a backswamp deposit along the Mississippi River near Vicksburg, Miss. Experience has shown that heavy clay will retain a constant water content and strength over a longer period of time than will lean clay. Therefore, this soil was selected for use in the upper 3 ft of

the controlled-strength subgrade for both the flexible and rigid pavement test items except in item 4 of the flexible pavement. Item 4 was constructed with an extra weak 36-in. layer of 2-CBR heavy clay located 21 in. below the 4-CBR heavy clay subgrade.

c. Subbase Course

The subbase material consisted of a nonplastic gravelly sand (SP). The gravelly sand material met all requirements of Guide Specification CE-807.02 (reference 9) and TM 5-824-2/AFM 88-6, Chapter 2 (reference 5). In the design of the flexible pavement test section, the major variable in the various items was total thickness of construction over the subgrade. This variation was accomplished by varying the thickness of the subbase course as indicated in section A-A of figure 2.

d. Base Course

A 6-in.-thick crushed-stone base course was specified for all test items of the flexible pavement section. The material used (crushed limestone) met all requirements of Guide Specification CE-807.07 (reference 10). No base course or filter course was used in the rigid pavement test items because an increase in foundation strength (subgrade modulus) was not a part of the test and, considering the relatively short time of the test, pumping was not expected to be a problem.

e. Asphaltic Concrete

A mix design for the asphaltic concrete surfacing layer was prepared utilizing 3/4-in. maximum-size crushed limestone, sand filler, and 85-100 penetration-grade asphalt. The gradation met the requirements of Table II, Gradation 11, of Guide Specification CE-807.22 (reference 11). A design asphalt content of 5 percent was selected for the asphaltic concrete mixture. The same mixture was used for the full 3-in.-thick asphaltic concrete surfacing.

f. Portland Cement Concrete

A natural sand and 1-in.-maximum nominal-size gravel aggregate (chert) were selected by the contractor. A concrete mix study was conducted by the WES Concrete Division, and, based upon the study, a mixture having a cement factor of 5.0 bags/cu yd, water content of 5.0 gal/bag of cement,

slump of 2 in., and 5.0 percent entrained air was selected to yield a 28-day design flexural strength of 650 psi. Type I portland cement from the Dundee Cement Company was used. The concrete was dry batched at the plant of the Vicksburg Concrete Co., Inc. It was transit mixed and delivered to the construction site, a distance of about 2-1/2 miles.

g. Nonrigid Overlay

The mix design for the asphaltic concrete used for the nonrigid overlay was the same as that used for the asphaltic concrete surface layer on the flexible pavement test items except that a leaner mix was used to resist excessive plastic flow under traffic. All of the overlay was placed using an asphalt content of 2.6 to 2.8 percent.

4. CONSTRUCTION

The test section was constructed during the period July-December 1968. All work was accomplished by WES personnel except for the portland cement concrete section, which was placed under contract. Details of the construction operations are given in Volume II.

5. TESTING AND SAMPLING DURING CONSTRUCTION

a. Water Content, Density, and CBR

Water content, density, and CBR determinations were made at the bottom of the excavation and at the surface of each lift of material as placed in the test section. These tests were performed for control purposes; when the values were not in the desired range, corrective action was taken prior to proceeding with construction. At completion of construction of the base course in the flexible pavement portion of the test section, test pits were excavated in each test item, and water content, density, and CBR determinations were made at the surface of the base, subbase, subgrade, and at approximately 1-ft intervals to some depth into the subgrade. The density determinations were made in the granular base and subbase materials by the sand-displacement method, i.e., MIL-STD-621A, Method 106 (reference 12), and in the fine-grained subgrade materials by the drive-cylinder method, i.e., MIL-STD-621A, Method 103 (reference 12). In addition, measurements were made of the thickness of various elements of the structure above the subgrade.

10

b. Plate Bearing Tests

Plate bearing tests were made on the finished subgrade of the rigid pavement portion of the test section. These tests were made in each test item immediately prior to the paving operations.

c. Vibratory and Seismic Tests

Vibratory and seismic tests were performed at the bottom of the excavation and on the surface of each element of the pavement structure.

d. Concrete Samples

Samples of concrete were taken from the concrete mixtures as they were discharged from the ready-mix trucks. Beams 6 by 6 by 36 in. and cylinders 6 in. in diameter by 12-in. high were taken that were representative of the concrete placed in each test item of each paving lane. In each case, one beam and one cylinder were field cured, and one beam and one cylinder were standard cured.

e. Sampling

Disturbed samples of the subgrade, subbase, and base course materials were obtained and stored for future testing as needed. Also, undisturbed samples (10 by 10 by 10 in.) of the compacted subgrade material were obtained from both the rigid and flexible pavement portions of the test section for future testing.

6. PROPERTIES OF AS-CONSTRUCTED PAVEMENTS

A summary of the as-constructed thickness, CBR, water content, and density of the various elements of the flexible pavement structure is shown in table 1. The field data measurements were obtained from test pits excavated from the surface of the base course prior to placement of the asphaltic concrete pavement.

A summary of stability, flow, voids, and density data for laboratory- and field-compacted asphaltic concrete specimens is shown in table 2. Data from the field-compacted mixture are shown for cores cut immediately after compaction and after various coverages of traffic with the 12-wheel assembly.

A summary of the as-constructed properties of the foundation and concrete materials is shown in table 3. Density and water content data are averages

11

of results of tests conducted on each lift of the subgrade material after it was placed and compacted during construction. The plate bearing tests were conducted on the surface of the subgrade after it had been brought to proper grade and just before paving operations. Concrete flexural and compressive strength data are shown in tables 4 and 5, respectively.

As-constructed density data for field-compacted asphaltic concrete specimens are shown in table 6. It should be noted in table 6 that the same in-place density was obtained in the nonrigid overlay regardless of the thickness of the layers.

The relatively low CBR values indicated for the crushed-stone base course in the west maneuver area and test item 1 of the flexible pavement test section were due to the thin cover of the subbase and base over the low-strength subgrade, which resulted in high deflection and yielding of the subgrade under the compaction roller and thus in the inability to obtain adequate compaction.

The measured CBR values of the gravelly sand subbase material were low in all items of the flexible pavement test section. This was due to the cohesionless nature of the material and the lack of confinement in the field test pits. The effective strength of the subbase material confined in the pavement structure is probably much greater than indicated by the field in-place CBR test. The as-constructed subgrade strengths were generally slightly less than the design value of 4 CBR. However, this was desired as it was anticipated that the subgrade strength would increase slightly prior to traffic and during the traffic testing period. The test pit in test item 3 was extended through the full thickness of the controlled-strength subgrade, and, as can be noted, the measured CBR values in the lean clay material from elevation 184.8 to 181.8 averaged about 2 CBR. This was considered to be representative of the strength under all test items at comparable depths.

SECTION III

INSTRUMENTATION

Instrumentation data were collected for use in this investigation as described in Section I.1 as well as for future use in evaluation of the applicability of theoretical treatments of pavement design. Detailed discussions of instrumentation are presented in Volumes III-A and III-B. Appendixes A and B to Volume III-B present selected actual data; other data are available at WES and CERL.

1. FLEXIBLE PAVEMENT

Instrumentation for the measurement of vertical stress, vertical deflection, and strain was included in items 3 and 4 of the flexible pavement test section, as shown in figure 3. Other measuring devices installed were two cells for measuring pore pressures and thermistor probes for measuring temperatures at the surface and bottom of asphaltic concrete pavement. A total of 52 data points were established. A brief description of the instrumentation is given in the following paragraphs; a detailed discussion is presented in Volume III-A.

a. Deflection Gages

Vertical deflections were measured with DC linear variable differential transformer (LVDT) displacement transducers mounted within WES deflection gage housings. The LVDT produces DC output voltages directly proportional to the movement of the sensing unit. The transducer consists of a main body, which houses the sensing coil and its associated electronics, and a core, which is movable through the center of the sensing coil. The mechanical movement of the core generates a change in an electrical signal in the coil. The LVDT transducers were mounted on reference rods that extended to reference flanges located 12 ft below the top of the asphalt pavement. A total of 18 deflection gages were installed at five different elevations in the flexible pavement test section. Also, two reference rods for use in the optical determination of deflections were installed to a 12-ft depth.

b. Pressure Cells

Seventeen WES earth pressure cells were installed. The cells are

6 in. in diameter, are fabricated from stainless steel, and use a mercury-filled fluid chamber with diaphragm and a full wheatstone bridge circuit consisting of four SR-4 strain gages hermetically sealed within the cell. Pressure applied to the faceplate of the cell is transmitted through the mercury in the fluid chamber to an internal flexible diaphragm and produces deflection of the diaphragm proportional to the load. The four SR-4 strain gages are mounted on the diaphragm and are actuated by its deflection. The full wheatstone bridge circuit practically eliminates the effects of temperature and of resistance variations in the lead wires. The cells used are rated at either 50- or 100-psi capacity but can withstand greater pressures without damage.

Three commercially available pressure cells were also installed. These cells were developed by Scientific Advances, Inc., Columbus, Ohio, and are described under rigid pavement instrumentation.

c. Strain Gages

Eight direct embedment-type strain gages manufactured by Microdot, Inc., South Pasadena, Calif., were placed at the bottom of the asphaltic concrete pavement. The gages consist of strain-sensitive insulated wire encased in a stainless steel tube. Perforated metal disks are attached to the ends of the strain tube. Electrical termination is through flexible waterproof cables. The electrical conductivity of the resistance wire varies with the strain in tension or compression.

d. Pore Pressure Cells

The CEC type 4-312 transducer is a small, single-diaphragm, hermetically sealed, fluid pressure cell manufactured by Consolidated Electrodynamics Corporation (CEC) of Pasadena, Calif. In this study, the CEC cell was mounted in a WES porous-stone soil-exclusion housing. Two of these cells were installed in item 3 of the flexible pavement test section at depths of 7.5 and 12 ft below the surface of the asphaltic concrete pavement.

e. Thermistors

Four thermistor probes manufactured by United Systems Corporation, Dayton, Ohio, were installed in the flexible pavement test section. Two probes were installed in the top of the asphaltic concrete pavement for

measuring surface temperatures, and two probes were placed at the bottom of the pavement.

2.   RIGID PAVEMENT

The instrumentation for the test section was selected to record pavement behavior at various locations under static and dynamic loading conditions in order to validate the various methods of pavement analysis available and to provide data on failure modes and rates of failure. Pavement deflection, concrete strain, and soil pressure were the parameters selected for measurement. A total of 67 data points were established in the four test items, as shown in figure 4. A brief description of instrumentation is given in the following paragraphs; a detailed discussion is contained in Volume III-A.

a.   Deflection Gages

The deflection gages chosen were DC LVDT displacement transducers, the same as described for the flexible pavement instrumentation. In the rigid pavement test section, the main body of the gage was embedded in the concrete, and the core was mounted to a reference rod that was anchored at some depth in the subgrade. This displacement gave a measurement of the deflection of the pavement relative to the anchorage point of the reference rod. Gages were placed along the longitudinal joint and at the slab midpoint in all four test items and along the transverse joints in items 1, 2, and 3. Reference rods were anchored at depths of 3, 5, and 9 ft in the subgrade in test items 1, 2, and 3 and at 13 ft in test items 1, 2, 3, and 4.

b.   Strain Gages

Two types of strain gages were used to measure the top and bottom surface strains in the concrete. The strain in the bottom surface was measured with an embedment-type (Valore) gage installed during construction of the concrete. The Valore gage consists of a wire sensing element enclosed in a hermetically sealed metal envelope, which provides mechanical protection plus a bonding surface completely surrounding the gage for embedment. Twelve such gages were installed, four in each of items 1, 2, and 3 to measure the strains adjacent and parallel to the longitudinal and transverse joints. Strain in the top surface was measured with an etched foil-type strain gage cemented to the pavement surface. The gage consists of a flat metal-foil sensing element bonded to a thin flexible epoxy base that is used for bonding

15

to the test surface. Six such gages were installed, two in each of items 1, 2, and 3 at the center of the slabs. The two gages in each item were oriented to measure strains both parallel and normal to the direction of traffic. Because of the difficulty of maintaining the foil-type strain gages, those in items 2 and 3 were replaced with the Valore-type gage described above. During the time between construction and the beginning of traffic, several of the bottom surface strain gages became inoperable, and supplemental strain gages were installed to measure the surface strains at points directly over the bottom gages. Additional surface strain gages were installed in the north paving lane prior to traffic in that lane. Valore-type strain gages bonded to the pavement surface were used for these supplemental surface strain measurements. A total of ten such gages were used: two in each of the southwest slabs of items 2 and 3 and three in each of the northwest slabs of items 2 and 3. The gages in the southwest slabs were located adjacent and parallel to the longitudinal and transverse joints. In the northwest slabs, two gages were located at the middle of the slabs in each item to measure strains both parallel and normal to traffic and one gage was located adjacent and parallel to the transverse joint in each item.

c. Pressure Cells

The soil pressure cell selected was a resistance strain-gage-type cell that consists of four strain-gage elements mounted on a thin metal diaphragm. The diaphragm forms one end of a metal cylinder 3 in. in diameter by 5/8 in. long. The cylinder forms the differential pressure chamber and provides mechanical and moisture protection for the strain-gage elements. The strain-gage elements are connected in a four-arm bridge configuration. The electrical output changes in direct proportion to the deformation of the diaphragm. Pressure gages were placed in 12 locations in test item 2. Gages were placed at the pavement-subgrade interface and at depths of 3 and 7 ft in the subgrade below this interface.

SECTION IV

TEST LOADING AND BEHAVIOR UNDER TRAFFIC - FLEXIBLE PAVEMENT

1. TEST CONDITIONS AND PROCEDURES

   a. General

   Traffic tests were performed on five separate lanes of the 80-ft-wide and 300-ft-long test section. The test lanes, test traffic, traffic patterns, pavement conditions, and failure criteria are summarized in the following paragraphs.

   b. Test Lanes

   The layout shown in figure 5 indicates the location, width, and length of items for each test lane. These five lanes were identified as lanes 1, 2, 2A, 3A, and 3B. Each lane consisted of a portion of the test section on which no traffic had previously been applied. Although the outrigger wheels of the test carts traveled on a portion of the adjacent lane, this area was not considered to be trafficked due to the low contact pressure of the outrigger tires.

   Test lane 1 was 16 ft wide through all five test items (300 ft long) and was subjected to traffic by the 12-wheel test cart (figure 6) loaded to 360,000 lb. Test lanes 2 and 2A were 8 ft wide through test items 1 and 2 only (120 ft long) and were subjected to 50,000-lb single-wheel-assembly traffic. Traffic was applied to lanes 2 and 2A to determine whether pavement temperature had any effect on the performance of the asphaltic concrete. The traffic was applied to lane 2 only when the pavement temperature was 90 F or higher, while the traffic was applied to lane 2A only when the pavement temperature was 70 F or lower. Test lane 3A was 8 ft wide through items 1 and 2 (120 ft long) and was subjected to the 30,000-lb single-wheel-assembly traffic. Test lane 3B was 10 ft wide through test items 3, 4, and 5 (180 ft long) and was subjected to traffic of a twin-tandem test cart (figure 7) loaded to 240,000 lb. The wheel spacing duplicated one twin-tandem component of the Boeing 747 assembly. All test-wheel assemblies were equipped with 49x17, 26-ply rating tires.

c. Traffic Patterns

Three types of traffic patterns were used in applying the test traffic. Layouts of these patterns are shown in figure 8. The traffic patterns were varied for each wheel configuration in order to get the desired distribution of traffic over the width of the traffic lane. The coverage levels referred to in this report are the total number of coverages applied in the 100 percent coverage zone. All traffic was applied at a rate of speed of approximately 3 mph.

Traffic was applied with the 12-wheel assembly by following five guidelines, which were painted on the pavement on 16-in. centers (approximately one tire print width). The distribution of traffic coverages[2] over the 16-ft-wide traffic lane after one complete pattern of traffic is shown in figure 8c. This distribution resulted in a total of 22 passes of the test cart for each pattern of test traffic. Each pattern of traffic resulted in 32 coverages of a test wheel over the center 60 in. (100 percent coverage zone) of the test lane.

In the application of single-wheel traffic across the 8-ft lanes, when the test cart had traversed the full distance across the test lane, a total of two coverages had been applied over the test lane. Traffic was applied in an approximately normal distribution pattern, as shown in figure 8a, and the interior 42 in. of the traffic lane received 100 percent of the applied traffic.

Traffic was distributed over a 10-ft-wide lane, as shown in figure 8b, by the twin-tandem assembly following five guidelines. A total of 30 passes of the test cart were required to apply one pattern of test traffic. Each pattern of traffic resulted in 20 coverages of a test wheel over the center 60 in. of the test lane.

d. Collection of Instrumentation Data

Static and dynamic load instrumentation tests using single-wheel, 4-wheel, 6-wheel, and 12-wheel gear configurations were completed prior to the start of actual test section traffic. (Dynamic load measurements were

_____

[2]The term coverages as used for the traffic tests on the flexible pavement indicates a measure of wheel-load repetitions on any given area of the pavement surface.

made using a slowly moving test cart.) During trafficking of lane 1, all
measuring instruments, which were installed in items 3 and 4, were read
daily before the start of traffic. In addition, static load tests were made
at selected locations using the 12-wheel assembly after 438 and 3334 coverages
of item 3 and after 447 and 3343 coverages of item 4. Also, selected dynamic
tests were run after 1718 coverages on item 3. Results of these tests are
presented in Volume III-B.

e. Pavement Temperature

Traffic was applied to the five traffic lanes of the test section
during the period 6 August - 10 November 1969. The average pavement tempera-
ture, as determined from measurements at the surface and the bottom of the
asphaltic concrete layer, ranged between 60 and 133 F during this period.
Also during this time, approximately 6-1/2 in. of rain fell. However, only
a small amount of traffic was applied during a rain because the pavement tem-
perature fell below the minimum temperature required for traffic.

Traffic and pavement temperature distribution curves for each of the
five lanes are shown in figure 9. These curves were derived from the records
of the pavement temperature and number of coverages made hourly during the
traffic of each lane. As can be seen in figure 9, no traffic was applied to
lanes 1, 2, and 3A until the pavement temperature was 90 F or greater (hot-
weather traffic). These three lanes were trafficked when the pavement tem-
perature ranged between 90 and 133 F. To compare the behavior of the test
section under the same loading condition but at a lower temperature, traffic
was applied to lane 2A with the same loading condition as that in lane 2 but
when the pavement temperature was below 70 F (cold-weather traffic). All the
test traffic was applied to lane 2A when the pavement temperature was between
60 and 70 F. No maximum or minimum pavement temperature limits were required
during the trafficking of lane 3B. Approximately 80 percent of the traffic
was applied to this lane when the pavement temperature was between the upper
limit of the cold-weather traffic and the lower limit of hot-weather traffic,
i.e., 70 to 90 F; the remainder of traffic was applied when the pavement
temperature was between 64 and 70 F.

f. Failure Criteria

In judging failure of the flexible pavement test items, distinction

was made between settlement due to traffic compaction and distortion due to shear deformation. Settlement, which is the result of densification of the base and subbase under accelerated traffic, was anticipated because it was not possible to apply a heavy compaction effort on the lower layers of the subbase or base course materials in the thinner test items. The term shear deformation as used herein refers to excessive plastic movement or, in the extreme, to rupture of any element in the pavement structure.

A pavement item was considered failed when either of the following conditions occurred:

(1) Surface upheaval of the pavement adjacent to the traffic lane reached 1 in. or more.

(2) Surface cracking occurred to the point that the pavement was no longer waterproof.

2. SUMMARY OF TEST RESULTS

a. General

Visual observations of the behavior of the test items were recorded throughout the traffic test period of each lane. These observations were supplemented by photographs. Figure 10 shows the flexible pavement test section prior to traffic. Level readings were taken on the pavement prior to and at intervals during traffic to show the development of permanent pavement deformation and deflection of the pavement under the assembly load for the lane being observed. After failure, a thorough investigation was made by excavating test trenches across the traffic lane, by establishing profiles of the surface of various layers in the structure, and by conducting CBR and other pertinent tests to determine where failure had occurred. A summary of the after-traffic test pit investigations is shown in table 7. A summary of the traffic test results for the various loading conditions used on the flexible pavement is shown in table 8. Most of these data are self-explanatory; however, some columns need further explanation as given in the following paragraphs.

b. Rated Subgrade CBR

The rated CBR values of the subgrade are based on the numerical averages of the CBR values measured immediately after construction (table 1)

and after traffic (table 7). In general, the CBR values used were from the tests conducted at the surface of the subgrade and at subgrade depths of 12 and 24 in. The strength of the subgrade below the 24-in. depth was generally slightly less than the rated value. All values obtained in a given test item from the various traffic lanes were used in the average for rating the strength of the test item. Therefore, more data were available for rating the subgrade strength in some items than in others, as all test items were not trafficked by the various load assemblies. In general, the CBR of the subgrade was quite uniform in all test items, and the values measured after traffic were only slightly higher than the as-constructed values. The rated subgrade CBR values were 3.7, 4.4, 3.8, 4.0, and 4.0 for test items 1, 2, 3, 4, and 5, respectively.

c. Pavement Deflection

Surface deflection measurements were made at one location per item on the flexible pavement prior to traffic and at various intervals during traffic. The term deflection as used in this report indicates the total vertical movement that occurred with a single load application. These measurements were obtained with level instruments by reading rods (engineer scales) at prearranged positions on lines parallel and transverse to the direction of traffic. Readings were taken adjacent to and between the load wheels. Rod readings were first taken with the load off the pavement; then the test cart was moved forward until the centroid of the assembly was at a prearranged position, and a second series of readings was taken with the load on. The difference in rod readings indicated the total vertical movement of the pavement. Measurements were made both parallel and transverse to the direction of traffic. The deflection values shown in table 8 represent the maximum values measured prior to traffic and at the coverage level indicated.

d. Maximum Permanent Pavement Deformation

Level readings were taken prior to traffic and at various intervals of traffic across the test lane at predetermined stations. Similar readings were taken along the center line of the traffic lane. These observations were made to determine the magnitude of pavement deformation resulting from traffic. The values listed in table 8 were obtained from cross-section

21

elevation measurements taken prior to traffic and at the coverage level indicated. The maximum deformation normally occurred at or near the center line of the traffic lane.

e. Upheaval

The upheaval values tabulated were obtained from cross-section elevation measurements taken prior to traffic and at the coverage level indicated. Upheaval adjacent to the traffic lane is an indication of shear deformation in some element of the pavement structure. In this study, a test item was considered failed when upheaval of 1 in. or more occurred.

f. Pavement Cracking

Pavement cracking through the full 3-in. thickness of asphaltic concrete was another condition considered in the failure criteria. Where pavement cracking is indicated as severe, this condition did exist and the pavement items were considered failed. Slight cracking indicates narrow, shallow surface cracks that did not extend through the asphaltic concrete layer.

g. Rating of Test Items

It can be noted that pavement failure developed in all test items with the exception of the 12-wheel test item 5 of lane 1 and the single-wheel test item 2 of lane 3A. Traffic was discontinued in these items prior to failure because the performance during traffic indicated that many coverages would be required to produce failure. From failure investigational test trenches, it was determined that subgrade shear deformation was the primary cause of failure in the 12-wheel test item 1 of lane 1, in single-wheel test items 1 and 2 of lanes 2 and 2A, and in twin-tandem items 3, 4, and 5 of lane 3B (see figures 11-18). Cracking of the pavement also developed in these items due to the very high deflections, as indicated in table 8. Test items 2, 3, and 4 of test lane 1 (12-wheel) failed primarily from pavement cracking due to high deflections (see figures 19-21). In these items, evidence of subgrade shear deformation was not distinct. The granular subbase material did move laterally from under the load wheels, which resulted in the upheaval at the surface of the pavement. This movement of the subbase was related to the deflection of the subgrade, which was a function of total thickness of construction over the subgrade. Thus, for a given loading, the

22

service life of the pavement increased as the total thickness increased and deflection decreased.

Comparative pavement performance in single-wheel lanes 2 and 2A indicated that temperature variations within the range experienced during traffic testing had no significant effects upon behavior.

SECTION V

TEST LOADING AND BEHAVIOR UNDER TRAFFIC - RIGID PAVEMENT

The testing phase of the MWHGL study involved three major types of loads: static, dynamic (slowly moving), and simulated trafficking. A limited amount of testing was accomplished using Dynaflect equipment. Each phase of the testing program will be discussed separately.

1. STATIC LOAD TESTS

This series of tests was performed following completion of the instrumentation hookup and electronic checkout. Tests were conducted with one main 12-wheel landing gear of the C-5A Galaxy, a 6-wheel component of the main C-5A gear, a twin-tandem component of the Boeing 747 landing gear, and a single wheel. All assemblies were used with 15,000- and 22,500-lb wheel loads except the 6-wheel assembly, which was tested with the 22,500-lb wheel load only. To avoid the possibility of premature cracking, the 22,500-lb wheel load was not used on test item 4. These tests were intended to provide a checkout of the instrumentation and to provide data points for future correlation with various analytical techniques for predicting pavement slab behavior under load. Complete descriptions of the test procedures and results are contained in Volume III-B.

2. DYNAMIC LOAD TESTS

The dynamic load tests were run in conjunction with the static load tests at the same load levels on the same load carts. These tests consisted of recording pavement response to a slowly moving load which was run forward and backward along six parallel lines. These tests were designed to provide comparative data on static and slowly moving loads and to attempt to detect differences which may occur between loads traveling forward and backward. This was of particular interest for the 12-wheel assembly, as the load wheels were arranged in an axisymmetrical pattern. Loads were run along lines near the longitudinal construction joint and down the center of the test slabs. No difference in strain or deflection histories could be detected when the load was run forward or backward. A complete description of these tests is presented in Volume III-B.

3.   SIMULATED TRAFFIC

a. General

The simulated traffic portion of the tests was run in two parts:
12-wheel assembly and twin-tandem assembly. The layout of the test lanes
is shown in figure 22, and a typical rigid pavement prior to traffic is shown
in figure 23. Traffic was applied at a volume necessary to simulate the
traffic anticipated on an airfield pavement under operational conditions over
its entire life. Data were collected continuously from the transducers onto
tape during the simulated traffic period and were reduced to hard copy peri-
odically throughout the entire test. The data collected during the traffick-
ing period are listed in Volume III-B. Observed pavement behavior under sim-
ulated traffic was also noted during the test, and a brief discussion of the
performance of each test item follows.

Failure criteria have been established for rigid pavement by the
CE. These criteria were applied to the test track pavements and are as
follows:

(1) Initial failure is the condition that exists when a crack re-
sulting from traffic loading is visible at the top slab surface and extends
through the depth of the concrete slab.

(2) Shattered-slab failure condition exists when visible cracks re-
sulting from traffic loading subdivide the pavement slabs into six pieces.

(3) Complete failure is the condition that exists when the visible
cracking subdivides the pavement slabs into about 35 pieces (approximate area
15-20 sq ft each). Complete failure is characterized by relatively large
nonrecoverable deformations and faulting cracks or joints.

Failure of a nonrigid overlay is said to have occurred when the base
pavement is in the complete failure condition with nonrecoverable deforma-
tions of 1.0 to 1.5 in. and recoverable deformations of 0.5 in. Only one
degree of failure has been established for nonrigid overlays. Criteria for
nonrigid overlay failure were developed from previous test track work and
from AF operational policies.

b. 12-Wheel-Assembly Traffic

The first part consisted of trafficking the south paving lane with

25

the 12-wheel assembly loaded to 30,000 lb per wheel. Traffic was applied along five regularly spaced parallel lines in a predetermined sequence to achieve a reasonable distribution of the traffic volume across a 200-in.-wide traffic area. The trafficking sequence produced an approximation of a distribution curve typical of aircraft operational wander. Traffic volume will be described in the following sections of this report as traffic patterns and coverages.[3] A pattern consisted of 22 passes of the load cart and produced 16 coverages within the trafficked area. The five regularly spaced parallel lines were 16 in. apart and were numbered from south to north as lines 1 through 5. Traffic was run along line 1 from east to west and then backed along line 1 from west to east. The load cart was then moved to line 2 and the same procedure was followed. This procedure was followed for lines 1, 2, 3, 4, 5, 5, 4, 3, 3, 2, and 1. A cross section of traffic distribution is shown in figure 8c.

(1) Test item 1. Test item 1 was a nominal 10-in.-thick slab that contained cracks prior to trafficking. The southwest slab was essentially quartered by longitudinal and transverse cracks, and the southeast slab developed diagonal cracks. An inspection pit was dug in the south shoulder where the transverse crack ended, and the crack was found to extend completely through the slab. The other cracks also were assumed to extend completely through the slab. These cracks were assumed to have occurred because of stresses developing from expansion and contraction of the pavement.

The initial crack in test item 1 due to traffic occurred after 12 traffic patterns (192 coverages) in the southeast slab and after 15.7 traffic patterns (251 coverages) in the southwest slab. Traffic was halted on this test item after 37 traffic patterns (592 coverages) because the cracks were spalling and raveling badly (figure 24), and it was feared that more

---

[3]For rigid pavements, coverages is a measure of the number of maximum stress repetitions that occur in the pavement due to the applied traffic. A coverage occurs when each point of the pavement within the test lane has been subjected to a maximum stress, assuming that the stress is equal under the full tire print width. For the 12-wheel assembly, separate and distinct maximum stresses occur under front and rear 6-wheel arrays. Considering only one 6-wheel array, the 2- and 4-wheel-abreast arrangements are sufficiently close that they produce only one maximum stress. For the twin-tandem gear, the front and rear twin wheels are sufficiently far apart that two maximum stress repetitions occur for each pass of the gear.

trafficking would destroy the aggregate interlock across the cracks and thus influence the performance of the nonrigid overlay.

Nonrecoverable deformations averaged about 0.24 in. after 37 traffic patterns, and recoverable deformations averaged about 0.11 in. at the start of traffic and about 0.15 in. at the end of 37 traffic patterns. Differential settlement between the untrafficked north and south lanes averaged about 0.25 in. after 37 traffic patterns. It was concluded that the keyed longitudinal construction joint had failed. Some minor pumping was noted along the cracks in the southeast slab, but the pumping did not appear to materially affect the pavement performance.

(2) Test item 1 - nonrigid overlay. A polypropylene membrane was applied on the southwest slab of item 1 prior to the overlay to evaluate the ability of such a membrane to prevent or retard reflection cracking in the overlay. All four slabs of test item 1 were overlaid with 4 in. of asphaltic concrete after 37 traffic patterns (592 coverages). Traffic was continued in order that the behavior of nonrigid overlay pavements could be studied. The overlay item was subjected to a total of 276 traffic patterns (4416 coverages). Reflection cracking in the overlay coincident with the joints and cracks in the base pavement began to develop immediately after traffic was commenced and continued to progress until the full crack pattern in the base pavement was evident in the overlay. The crack pattern at the conclusion of traffic is shown in figure 25. Examining the crack pattern in the overlay at the conclusion of traffic (figure 25) and comparing it with the crack pattern in the rigid pavement prior to overlay (figure 26) show very little additional cracking in the base pavement after the overlay was applied. In addition, the final crack pattern in the overlay indicated that the test item was not cracked to the degree associated with failure of a nonrigid overlay, and it was concluded that after 276 traffic patterns (4416 coverages) the item was not failed.

Nonrecoverable deformations averaged about 0.74 in., and recoverable deformations averaged about 0.133 in. immediately after the overlay was applied and increased to about 0.250 in. Faulting along the longitudinal joint increased with increasing traffic and at the conclusion of traffic reached a maximum of 1.20 in. at the middle of the southeast slab. For the

remainder of the joint, the faulting was less severe and ranged from 0.36 to 0.72 in.

Pumping, which had been only moderate prior to the application of the overlay, was arrested by the overlay. On a few occasions, some muddy water was pumped out along the south edge of the southeast slab and at the juncture between the rigid and flexible pavement maneuver areas. It is believed that the pumping had very little, if any, effect on the performance of the nonrigid overlay. The polypropylene membrane was considered ineffective in retarding reflection cracking. Only a very slight benefit in the rate of progression of reflection cracking was noted, but this conclusion is questionable as only one test was performed and no statistical data could be devel.

(3) Test item 2. Test item 2 contained a longitudinal crack in the southeast slab which was observed after the load cart had made the first pass. It is probable that the crack had occurred prior to traffic and was not detected. The first structural crack which occurred in test item 2 was a transverse crack in the southeast slab after 247.7 traffic patterns (3963 coverages). A diagonal crack occurred in the southwest slab after 281 traffic patterns (4496 coverages). The final condition of item 2 after 313 traffic patterns (5008 coverages) is shown in figure 27.

Spalling along the longitudinal joint was noted after 136 traffic patterns (2176 coverages) and continued throughout the trafficking. The spalls were approximately 2-3 in. deep at the longitudinal joint and feathered out to the surface about 10-12 in. from the joint. The spalls were due to compression in the top portion of the slabs due to joint faulting. The spalls were repaired and periodically filled with cold-mix asphaltic concrete to avoid debris formation.

Nonrecoverable deformation averaged about 0.78 in., and recoverable deformation along the longitudinal joint in the southwest slab averaged about 0.074 in. at the beginning of traffic and 0.139 in. at the conclusion of traffic. In the middle of the southwest slab, the average maximum recoverable deformation was 0.026 in. and was nearly constant until the 282nd traffic pattern (4512 coverages). At this coverage level, the deformation dropped to 0.014 in. This reduction was attributed to a diagonal crack that

developed during the 281st traffic pattern (4496 coverages). Faulting along the longitudinal joint was first noted after 62 traffic patterns (992 coverages), and the faulting continued to increase until it measured as much as 0.60 in. at the conclusion of traffic.

Pumping at the transverse and longitudinal joints and along the south edge of the slab in this item was moderately heavy. Slight pumping was first noted after only 26 traffic patterns (416 coverages); however, the pumping continued to increase until it was moderately heavy after 48 traffic patterns (768 coverages). Pumping continued intermittently (generally following rainfall) during the remainder of the traffic testing but was never considered severe.

(4) Test item 3. There were no structural cracks in item 3 before traffic was started. Two minor defects consisting of a small spall along the transverse joint between the southeast slab and transition section and an uncontrolled transverse contraction crack at the northwest corner of the southwest slab were noted.

The first crack due to traffic was a longitudinal and transverse crack in the southeast slab that occurred during the 37th traffic pattern (592 coverages). The first crack that occurred in the southwest slab of the item was a transverse crack that developed during the 138th traffic pattern (2208 coverages). Nonrecoverable deformations averaged about 1.08 in., and recoverable deformations in the center of the southwest slab averaged about 0.029 in. at the beginning of traffic and 0.078 in. at the conclusion of traffic. Along the transverse joint of the southwest slab, the recoverable deformation ranged from 0.087 to 0.156 in. from the start of traffic until the end of traffic.

A spall similar to those occurring on test item 2 developed along the longitudinal joint after 195 traffic patterns (3120 coverages). This was the only spall along the longitudinal joint which developed during the entire trafficking period.

The final condition of item 3 is shown in Figure 28 after 313 traffic patterns (5008 coverages).

Faulting of the longitudinal joint ranged from 0.36 to 0.66 in. but was as high as 1.08 in. in the northeast corner of the southeast slab.

Pumping was quite severe on this test item and did materially affect the performance of the pavement. The pumping was most severe at the northeast corner of the southeast slab and along the transverse joint between the southeast slab and transition slab.

(5) Test item 4. There were no defects in item 4 prior to traffic. The first structural crack was a transverse crack in the southwest slab after 11.2 traffic patterns (179 coverages), and on the next pass, a diagonal crack occurred in the southeast slab. After this, cracking occurred rather rapidly. After 15 traffic patterns (240 coverages), traffic was stopped because the pavement was extensively cracked. The final condition of the item prior to placement of the nonrigid overlay is shown in figure 29.

Nonrecoverable deformation in the test lane averaged about 0.42 in., but due to gage failure, no data were available on recoverable deformations. Faulting along the longitudinal joint was not noted except at a corner break in the southwest slab. Pumping started quite early on this test item; however, it was not considered to be severe enough to materially affect the performance of the pavement.

(6) Test item 4 - Nonrigid Overlay. All four slabs of item 4 were overlaid with 6 in. of asphaltic concrete after 15 traffic patterns (240 coverages), and traffic was continued in order that the behavior of nonrigid overlay pavement could be studied.

The overlay was subjected to a total of 276 traffic patterns (4416 coverages). Reflection cracking in the overlay, coincident with the joints and cracks in the base pavement, began to develop immediately after traffic was started and continued to progress until the full crack pattern in the base pavement was evident in the overlay. The crack pattern at the conclusion of traffic is shown in figure 30. (It is noted here that the 313 traffic patterns shown on the board in figure 30 is in error and should read 291 traffic patterns - 276 traffic patterns on the overlay and 15 traffic patterns before the overlay was constructed.) Examining the crack pattern prior to the overlay (figure 29) and at the conclusion of traffic on the overlay (figure 30) indicates only a small amount of additional cracking of the base pavement due to the traffic on the overlay. After traffic, the

asphaltic concrete overlay was removed, and a study of the crack pattern indicated that the overlay had not failed.

Nonrecoverable deformations within the test lane averaged about 1.10 in. Crude optical measurements indicated recoverable deformations on the order of 0.1 and 0.2 in.

Faulting along the longitudinal joint averaged about 0.56 in., with a maximum of 1.56 in. at the northwest corner of the southwest slab.

Pumping, which had been moderately severe prior to the overlay, was arrested by the overlay until the 173rd traffic pattern (2868 coverages) when pumping of fairly heavy mud (figure 31) began at the south end of the transverse joint between the southwest slab and transition slab. Pumping at this point continued intermittently for the remainder of the traffic; however, no pumping developed at other locations in the item.

c. Twin-Tandem-Assembly Traffic

The second part of the traffic test program consisted of trafficking the north paving lane with a 44- by 58-in. twin-tandem assembly loaded to 41,500 lb per wheel and having a contact area of 207 sq in. Traffic was applied along five regularly spaced lines in a predetermined sequence to achieve a crude approximation of a typical operational distribution curve across the 120-in.-wide traffic area. As with the simulated 12-wheel-assembly traffic, traffic was applied along five parallel lines spaced 16 in. apart. The trafficking sequence in this case was forward and backward along lines 1, 2, 3, 4, 5, 4, 3, 2, 2, 3, 4, 4, 3, 2, and 3, in that order. This traffic is referred to herein as a traffic pattern and consists of 30 passes (15 forward and 15 reverse) of the load cart and produces 10 coverages within the trafficked area. A sketch of the traffic pattern is shown in figure 8b. The traffic area was centered in the north paving lane. The north paving lane was instrumented with a total of eight surface gages, four each located in test items 2 and 3. Readings from these gages were continuously recorded on magnetic tape and periodically reduced from hard copy oscillograph traces. A total of 68 traffic patterns (680 coverages) were applied with the twin-tandem assembly.

(1) Test item 1 - nonrigid overlay. A defect consisting of a transverse crack was evident in test item 1 before the start of twin-tandem simulated traffic. This crack was due to migration of a crack from the south paving lane that had developed under 12-wheel-assembly traffic. The crack was in the northwest slab of item 1 and had reflected through the nonrigid overlay. After four traffic patterns (40 coverages), the beginning of a transverse crack in the northeast slab could be detected, and the crack continued to progress and extended across the slab after 19 traffic patterns (190 coverages). After 15 traffic patterns (150 coverages), a longitudinal crack in the northwest slab commencing at the transverse joint was detected. It progressed to the transverse crack in this slab after 29 traffic patterns (290 coverages) and across the entire slab after about 41 traffic patterns (410 coverages). After 41 traffic patterns, longitudinal and diagonal cracking commenced in the northeast slab, and additional cracking was detected in the northwest slab. The cracking had progressed to the degree shown in figure 32 when traffic was stopped after 68 traffic patterns (680 coverages).

Nonrecoverable deformations averaged about 0.74 in.; however, since there were no electronic deflection gages installed in the test lane, no measure of recoverable deformation was obtained. Based on examination of the crack patterns in the overlay and base pavement and on measurements of permanent deformation, it was concluded that the item had not failed after 68 traffic patterns, but failure was probably imminent.

(2) Test item 2. There were no visible defects in test item 2 prior to traffic. The first crack observed under traffic was a longitudinal crack commencing at the transverse joint and progressing into the northwest slab after four traffic patterns (40 coverages). After 15 traffic patterns (150 coverages), a longitudinal crack commenced at the transverse joint and progressed into the northeast slab. After 41 traffic patterns (410 coverages), a transverse crack occurred in the northeast slab, and cracking progressed rather rapidly until traffic was stopped after 68 traffic patterns (680 coverages). The final condition of item 2 is shown in figure 33.

The average nonrecoverable deformation was 0.40 in.; no recoverable deformation measurement could be obtained since electronic deflection gages were not installed in the test lane.

(3) <u>Test item 3</u>. There were no visible defects in test item 3 prior to traffic. The initial crack, which occurred after 15 traffic patterns (150 coverages), was longitudinal, commencing at the transverse joint and progressing in an easterly direction in the northeast slab. The first crack in the northwest slab, also longitudinal, occurred after 26 traffic patterns (260 coverages). A diagonal crack began to form in the northwest slab after 53 traffic patterns (530 coverages) but had not progressed far when the traffic was concluded at 68 traffic patterns (680 coverages). The final condition of the item is shown in figure 34.

The average nonrecoverable deformation was about 0.36 in. Recoverable deformations were not measured. Slight pumping occurred at the transverse joints, especially at the transverse joint between the northeast slab and transition slab. It is believed that the pumping was not severe enough to have a material effect on the pavement performance.

(4) <u>Test item 4 - nonrigid overlay</u>. The only visible defects in test item 4 were the beginnings of transverse cracks along the longitudinal joint, which were the result of the 12-wheel-assembly traffic. Additional cracking was visible in the nonrigid overlay surface almost as soon as traffic was begun, and after only four traffic patterns (40 coverages), the progression of one of the short transverse cracks across the slab was observed. The progression of cracking in the item was minimal through 20 traffic patterns (200 coverages), but the rate of cracking increased rapidly. After 68 traffic patterns (680 coverages), the final condition was as shown in figure 35.

Nonrecoverable deformations averaged about 1.36 in. Recoverable deformations were not measured; however, it was the consensus of those at the site that deflections could be detected visually as the test cart passed over the test item.

Based on examination of the crack patterns in the overlay and base pavement and on measurements of nonrecoverable deformations, it was concluded that test item 4 failed under 68 traffic patterns (680 coverages) of simulated twin-tandem traffic.

4. DYNAFLECT MEASUREMENTS

Data were collected periodically with a Dynaflect testing device during

the 12-wheel-assembly trafficking period. A partial listing of these data is presented in Volume III-B. The results of the Dynaflect testing program were inconclusive as anomalies were found even in data collected on untrafficked portions of the test section. The data do indicate that the Dynaflect testing device may be useful for comparing the structural integrity of one pavement with that of another since the deflection basins were larger for the thinner items than for the thicker ones. Also, there was some evidence that the device would reflect differences in subgrade support such as when the slab was warped upward or when the subgrade support was lost due to pumping. However, all attempts to analyze the data to evaluate the applicability of the device for making quantitative evaluation of the load-carrying ability of pavements were unsuccessful. The difficulties encountered in making an analysis of the voluminous data collected may well have been due to the lack of knowledge regarding the state of the pavement system at the exact time that the Dynaflect measurements were made. There was some evidence that readings made at any one time of day, for example, showed agreement; however, readings made at different times or under various climatic conditions showed poor correlation.

SECTION VI

FLEXIBLE PAVEMENT INSTRUMENTATION TESTS AND RESULTS

1. INTRODUCTION

Static and dynamic load tests were conducted on the flexible pavement
test section, and the response of the pavement-soil system was monitored by
an instrumentation installation. The instrumentation system and the related
equipment necessary to operate and accurately monitor the system are de-
scribed in detail in Volume III-A.

2. TESTING EQUIPMENT

Full-scale loads and wheel assemblies were used for conducting the
static load, dynamic load, and traffic tests. Tests were conducted with one
main 12-wheel landing gear of the C-5A Galaxy, a 6-wheel component of the
main C-5A gear, a twin-tandem component of the Boeing 747 landing gear, and
a single wheel. The tires used in all of the test carts were 49x17, 26-ply
rating, which is the design tire for both the C-5A Galaxy and the Boeing 747.

3. PRELIMINARY TESTING PROGRAM

Prior to commencement of the major instrumentation testing program, a
number of preliminary tests were performed to establish procedures to be
followed in the test program. All of the preliminary tests except those for
the tracking device were performed using the single-wheel 30,000-lb test
cart, which was a C-5A tire mounted in a load vehicle. The 180,000-lb
12-wheel assembly was used in developing and checking the tracking device.
The preliminary tests are summarized below; details of the tests are given
in Volume III-A.

a. Performance of Instrumentation System

Data collected for study of soil response time lag with depth and
load-position effect were used in determining the performance of the instru-
mentation system. The system was shown to be functioning correctly, and the
response of the system was considered to be consistent to an acceptable
degree.

b. Time-Lag Study

To determine the time response of the soil, representative gages and cells at each depth were statically loaded and the response timed. The indicated time lags were used for conducting the regular static load tests by allowing 2 min to elapse after loading before deflection gage responses were recorded and allowing a 30-sec lapse between loading and recording pressure cell responses.

c. Position Effects Study

Representative gages and cells were statically loaded to determine the effects of the load cart being offset either longitudinally or perpendicularly with the direction of travel (east-west) of a test vehicle. The conclusion was drawn that in order to achieve the best accuracy and consistency possible for all static load tests, the loading points for each wheel configuration would have to be centered as accurately as possible over the gage and cell positions.

d. Response of Reference Plane

Movement of the reference rods during static loading was monitored optically to determine if the 12-ft-deep reference plane was experiencing load-induced movements. The responses indicated that (1) the reference plane was within the zone of the test loads; (2) load-induced movements were occurring at the selected reference depth; and (3) the optical monitoring system was adequate and accurate enough to measure these deflections.

e. System Response to Dynamic Loading

The single-wheel test cart was run down the test section over the instrumentation in items 3 and 4. Runs were made slowly and at 1, 3, and 6 mph. All gages and cells were monitored during the dynamic loadings and all functioned properly during the tests.

f. Effect of Temperature on Instrumentation Response

For studying the temperature effects on the asphalt and pavement structure behavior, static load tests with the single-wheel 30,000-lb load were conducted when the asphaltic concrete was cool and again when the asphaltic concrete was hot. Also, the surface strain gages were monitored for several days to determine the temperature-pavement strain effects. The

temperature range during the temperature-effects static load tests is shown
in table 9. Greater temperature extremes were not possible at the time of

Table 9

Temperature Ranges

Location	Temperature, deg					
	Minimum		Maximum		Range	
	F	C	F	C	F	C
Ambient	78	26	72	22	10	6
Top of pavement	79	26	97	36	18	10
Bottom of pavement	78	26	83	28	5	2

the tests (April) in the temperature zone where the test area was located.
The static load tests did not show a temperature effect on the pavement sys-
tem in the ranges of temperatures investigated, and the conclusion was drawn
that there was an insufficient amount of data and insufficient range of tem-
peratures to formulate any definite conclusions.

g. Tracking System

Comparison of the results of dynamic load runs made with the 180,000-
lb 12-wheel assembly traveling down the center of the instrumentation pattern
demonstrated the necessity for developing a tracking system. Tests indicated
discrepancies of about 25 and 70 percent when the wheel position was 4 and
7 in. off center, respectively. A bank of photoelectric cells mounted on
each wheel assembly was used to accurately monitor the positions of the wheel
assembly during dynamic runs. Details of the tracking system are given in
Volume III-A.

4. MAJOR TESTING PROGRAM

The major instrumentation testing program was conducted after the pre-
liminary tests had been completed and before traffic tests were initiated.
Additional static and dynamic load tests were conducted during the traffic
testing and after completion of the 12-wheel traffic on items 3 and 4. Table
10 shows the chronology of the test loadings. The static test loadings were
always conducted first and the dynamic runs second, both with the same

assembly at a given load and tire inflation pressure. Summaries of the major instrumentation test program are shown in tables 11 and 12.

The static load tests were conducted by moving a loaded test cart or an empty prime mover into position over a test section loading point and then recording the responses of the appropriate cells and gages. In conjunction with each of the static load tests, the same test cart traveled slowly over the same instrumentation, and the reactions of soil and pavement were recorded (dynamic load tests). In addition, speed tests were performed to study the effects of varied rates of loading and unloading of the pavement system; instrumentation responses were monitored with the single-wheel assembly 30,000-lb load moving at speeds of 1 to 10 mph. Test procedures, summarized below, are described in detail in Volume III-A.

a. Test Vehicle Load Points

The wheel configurations used were 12 wheel, 6 wheel, twin tandem, and single wheel. Each configuration had its own distinct points of maximum loading, as shown in figure 36. These loading points were chosen as the points at which the maximum stress, strain, and pore pressure would be induced in the pavement system being loaded. The load points were used in positioning the test cart for static tests and for positioning and traffic guidance during dynamic runs.

The maximum stress under the 12-wheel configuration migrated with depth from the surface under either of the back inside tires of the front six wheels, in to the geometric center of the back axle of the front six wheels at depths of 2.5 to 12 ft, and then to the geometric center of the 12-wheel configuration at greater depths. For the 12-ft-deep pavement structure of the test section, point 1 under the center of the back axle of the front six wheels and point 2 under either of the back inside wheels represented the maximum load points (figure 36). The 6-wheel configuration was the front 6 wheels of the 12-wheel configuration, and points 1 and 2 were the same as for the 12-wheel configuration.

For the twin-tandem wheel arrangement, the maximum stress was considered to migrate with depth from the surface under the left rear wheel to the geometric centroid of the configuration at depth. These two maximum load points were used as load points 1 and 2.

The point that gave the maximum stress path with depth for the single-wheel assembly was always directly beneath the geometric centroid of the tire.

b. Instrumentation Load Patterns

Static and dynamic instrumentation loading patterns that were the same for both items 3 and 4 were designed and utilized in all of the instrumentation testing. A complete static load pattern consisted of stopping the test cart on each location (X) in an item, shown in figures 37 and 38, and recording all of the instrumentation responses. A partial loading pattern consisted of stopping only on each location on the four instrumented rows in each item. A selected-location pattern was a modified partial loading pattern consisting of static loading only at selected or representative cells and gages in one or both items.

The dynamic loading pattern included collection of data from all instrumentation as the load cart traveled on each of the 23 rows shown in figure 39.

c. Application of Loads

Prior to each series of static load tests, all gages, cells, and reference rods were monitored to establish initial no-load responses. Pertinent ambient and pavement temperatures and barometric pressure readings were recorded. Similar no-load readings were made at the completion of a run on each static or dynamic load row, after interruption of loading in excess of 30 min, and upon completion of each static load test.

The static load tests were conducted by starting on static row 1 in item 4 and successively loading each pavement loading point. The test cart then traveled in reverse back to the east maneuver area, and no-load readings were made for both items. The test cart returned down the same row to item 3 and stopped on the first position to be loaded. The loading procedure used in item 4 was followed in item 3, and the test cart returned to the east maneuver area traveling in reverse. Series of no-load readings were made for both items before the test cart was maneuvered into alignment with the next row to be loaded.

In order to determine the magnitude of the effect of the dead load

39

of the prime movers on the soil response, static and dynamic load tests were performed using the empty 12-wheel and twin-tandem prime movers. Measurements indicated that the vehicle used in the single-wheel assembly had only a negligible effect on soil response; therefore, no corrections were necessary.

After each static load grid pattern, dynamic load tests were made with the same test cart. The test cart followed each of the dynamic rows from t' e east maneuver area across items 4 and 3 and then covered the same row in both items traveling in reverse.

d. Monitoring Soil Instrumentation

Technicians read and recorded all instrumentation responses, temperature, and barometric pressure for each static load test. At the same time, the movement of the reference plane was monitored optically and recorded.

For all of the dynamic load tests, including the speed studies, monitoring of all of the instrumentation and tracking systems was accomplished by oscillograph recorders. No-load and temperature readings were made and recorded directly on appropriate oscillograph records to serve as reference readings.

5. ANALYSIS OF DATA FOR FLEXIBLE PAVEMENT TESTS

Because of the great volume of both static and dynamic load test data obtained during the testing periods, only a very limited analysis of the data was completed. Details of the analysis are presented in Volume III-B. Analysis of the maximum responses on the soil instrumentation in items 3 and 4 under both static and dynamic loadings was considered to be of primary importance and was undertaken first. These maximum responses, which are the combined results from load points 1 and 2 (discussed previously), are presented as depth versus maximum elastic deflection and maximum elastic stress curves. Comparisons are made between soil response to static and dynamic loads and also between responses from the two instrumented items.

A thorough analysis of the soil deflections under load, as depicted by the deflection gages, resulted in identification of a load-position history-dependent moving zero reference level for each deflection gage with no residual strains being induced. Under this hypothesis, the true initial no-load reference point is not known, and the only truly known point of

reference is the rebound value, which defines the moving reference level. Using this hypothesis, equivalent elastic deflections resulted on a gage and on duplicate gages at symmetrical loading points of a wheel assembly.

An analysis of the induced soil stresses resulted in an almost constant horizontal changing zero reference and also in active residual stresses. Equivalent elastic stresses resulted from responses of a cell and from duplicate cells at symmetrical loading points of a wheel assembly.

A portion of the actual instrumentation data was reduced and is presented in Volume III-B, Appendix A, along with evaluation of the consistency and reproducibility of the measuring instruments and the loss of instrumentation. The data are presented for both static and dynamic load tests of the 30,000-lb-per-wheel loads, the static 50,000-lb single-wheel load, and the static 240,000-lb twin-tandem load.

The results of the maximum responses of the instrumentation are presented in figures 40-47. Figures 40-43 show deflections under both static and dynamic loads; figures 44-47 give stresses from both static and dynamic load testing. The actual data points used for developing each of the curves are shown on the curves. These data points represent averages of the responses of the gages or cells at each location.

a. Deflection Test Results

(1) Static versus dynamic loading. Figures 40 and 41 show comparisons of static and dynamic load maximum elastic vertical deflection curves for each item. These curves are plotted on a variable deflection axis for the purpose of getting all comparisons on one plot with a minimum of overlap. If these curves are to be used for obtaining specific values, the reference value for each loaded assembly on the deflection axis must be used to calculate deflection values for the particular loaded assembly.

As can be seen in figure 40, the dynamic load deflections in item 3 are in very close agreement with the static load deflections below a depth of about 3 ft. Also, it can be noticed that all dynamic load deflection curves lie to the left of the static load curves. Elastic deflections should not be dependent upon slow-speed load application; in other words, the speed of a slowly moving vehicle should not appreciably affect elastic deflections. Elastic deflection is not time-dependent, whereas plastic

deflection or deformation is time-dependent. The difference in the curves
can be accounted for by the static load elastic deflection including delayed
rebound and the dynamic load elastic deflection not including this delayed
action. All speeds for the dynamic load test carts were approximately 2 to
3 mph.

Comparisons of static and dynamic load tests for item 4 are
shown in figure 41, plotted the same way as for item 3. The previous dis-
cussion for item 3 also applies to these curves; however, the static and
dynamic load data do not agree as well as those for item 3. This difference
between the static and dynamic load curves in item 4 could be caused by the
influence of the soft 2-CBR layer increasing the time-dependent action more
than that in item 3.

(2) <u>Item 3 versus item 4</u>. Figure 42 gives a comparison of maximum
elastic deflection curves for static loading of item 3 versus item 4. These
comparisons are also plotted on a variable deflection axis. In this figure,
the soft 2-CBR layer in item 4 is delineated, and, as can be seen, this soft
layer greatly affects the strain distributions under all loaded assemblies
in item 4. This effect also increases with load, and the action of this soft
layer can be seen to be mainly effective from the bottom of the layer (7.5 ft)
upward, with the main difference between item curves occurring within the
soft layer. Deflections at the 7.5-ft level are approximately equal in both
items for the lighter loads, with the difference increasing with increase in
load.

Figure 43 gives the comparison of maximum elastic deflection
curves for dynamic load tests of item 3 versus item 4. As is evident from
the previous comparisons of dynamic to static loading in each item and then
comparisons of static load test results in item 3 to item 4, these curves
show the exact same relationships as previously discussed for item 3 versus
item 4 static load comparisons.

The conclusion from comparisons of static and dynamic load de-
flection curves of item 3 versus item 4 must be that each item has different
soil strain distributions as a result of the soft 2-CBR layer in item 4.
This soft layer appeared to have large elastic deflections; however, it was
deep enough that its action was not detrimental to the overlying pavement

structure. It appears to be acting almost as a layer of springs beneath a semirigid structure.

(3) Theoretical versus measured deflections. Figures 48 and 49 show plots of the theoretical elastic deflections (see references 13 and 14) as compared to the actual measured elastic deflections for the 12-wheel 360,000-lb static load tests for items 3 and 4, respectively. The theoretical elastic deflection curves were computed for a homogeneous, isotropic, linearly elastic half-space with a Poisson's ratio of 0.5; the curves were forced to match the actual data curve at the surface. Matching was accomplished by using the known elastic deflection and solving for the modulus of elasticity; therefore, this modulus was used to calculate the theoretical deflections to a depth of 12 ft. As can be seen, the comparison is better for item 3 than for item 4.

Figure 50 shows for item 3 a comparison of the measured elastic deflection basin (offset versus deflection) at a depth of 7.5 ft with the theoretical basin (reference 13). At a point on a horizontal plane in a mass, the assumptions of a linearly elastic, homogeneous, isotropic half-space should be approximately valid, and the theoretical elastic deflection basin should also be approximately valid. However, as can be seen, the comparison between the theoretical and measured maximum elastic deflection is not good. A similar plot for item 4 is not shown, but it would show the same results.

In figure 51, the theoretical equivalent single-wheel load (ESWL) curve has been plotted for each item versus the ESWL curve calculated from the actual instrumentation deflection data. These curves are for the 12-wheel 360,000-lb load. Discussion of ESWL is presented in Section VIII.

b. Comparison of Stress Curves

(1) Static versus dynamic loads. Figures 44 and 45 give the comparisons of maximum elastic stress curves of static and dynamic load tests in items 3 and 4, respectively. These curves are plotted for comparative purposes only and are plotted on a variable stress axis.

Figure 44 is the comparison of static and dynamic load stresses for item 3. As can be seen, the stresses are in very close agreement, as were the deflections in this item. The discussion for the deflection comparisons also applies to these stress comparisons. Figure 45 gives stresses for

static and dynamic loads in item 4. As for item 3, these stresses are also in good agreement.

(2) Item 3 versus item 4. Figure 46 gives the comparison of static load maximum elastic stress curves for item 3 versus item 4. The comparisons are plotted on a variable stress axis similar to all other comparisons. In this figure the soft 2-CBR layer in item 4 is delineated, and, as can be seen, it influenced the stress distributions. This soft layer appears to have influenced the stress distributions more with increase of load and was effective for the full 12-ft depth of the test section.

Figure 47 gives the comparison of the dynamic load maximum elastic stress curves for item 3 versus item 4. These curves are on a variable stress axis. The soft layer of item 4 is again delineated in this plot. These curves show exactly the same relationships as previously discussed for item 3 versus item 4 static load comparisons, as is evident from the static versus dynamic load comparisons.

These comparisons of item 3 versus item 4 for both static and dynamic load vertical elastic stresses show that the stress distributions of each of the items are different. This difference must be concluded to be due to the soft 2-CBR layer in item 4.

6. PORE PRESSURES AND TEMPERATURE EFFECTS

Pore pressures in the soil were not induced except for the negligible pore pressures that developed under two maximum load tests: 50,000-lb single-wheel loads and 240,000-lb twin-tandem loads. Therefore, no analysis of pore pressures is made in this report. The fact that no pore pressures were induced under load was completely consistent with laboratory tests on the soil showing that the soil was not at 100 percent saturation. With no pore pressures developing, the soil pressure cell responses under load were the effective stresses induced in the soil.

A few load tests were conducted specifically at different temperatures of the air and pavement, but the temperature differential was not sufficient to cause measurable effects in the pavement structure. Therefore, no correlation between temperatures and pavement or soil behavior could be made.

7. PAVEMENT STRAIN RESULTS

The results presented here were the best obtained and are included only to give an indication of the induced strains at the bottom of the asphaltic concrete pavement of the test section. These results are from one strain gage in item 4 that measured strains transverse (north-south) to the direction of travel. Also these strains are for static load tests; no strains are available for dynamic load tests.

The results are presented in figures 52 and 53. Figure 52 shows offset strains at distances parallel to the direction of forward movement for assembly load point 2 of the 360,000-lb 12-wheel assembly. As can be see, the gage did respond to the different wheels in alignment with load point 2 (see figure 36). In figure 53, strains at offset distances from load point 1 of the same 12-wheel assembly are plotted. At the top of the figure are offsets perpendicular to forward movement versus strain for which the row numbers correspond to the row on which point 1 was located when the strain was measured (figure 38 should be used with this figure). The plot at the bottom of figure 53 is for strains at offset distances parallel to the forward movement for assembly load point 1. This plot, as does figure 52, shows the effects of the different sets of wheels. In figures 52 and 53, the letters on the offset axis correspond to the grid in figure 38.

8. SPEED TEST RESULTS

The speed tests were conducted at four speeds: slow, about 1-2 mph; normal, about 2-3 mph; twice normal, about 5-6 mph; and fast, about 9-10 mph. From the results of these tests, it was concluded that the speeds had a negligible effect on results of tests; therefore, the curves for all speeds are the same as the dynamic single-wheel curves for the 30,000-lb loads presented previously. Also, these curves add evidence to the discussion presented earlier for the dynamic load elastic deflections at slow speeds being approximately equal to the static load elastic deflections.

SECTION VII

NONDESTRUCTIVE VIBRATORY TESTS

A program was conducted to obtain nondestructive vibratory tests of both
the flexible and rigid MWHGL test pavements. The nondestructive tests were
performed during construction of the test section, during application of traf-
fic, and at the completion of traffic in order to develop nondestructive test-
ing techniques that might provide a method of evaluating the load-carrying
capability of airfield pavements. Testing was continuing at the time this
series of reports was written. Most of the data obtained on the MWHGL pave-
ments are included in Volume III-B, and a more detailed report containing
analysis of the data and a preliminary evaluation procedure will be published
at the completion of the nondestructive testing program (reference 15).

There are two basic techniques, both of which involve steady-state vibra-
tion testing of pavements: (a) determination of the rate of wave propagation
through the layers of the pavement system, and (b) measurement of the rela-
tionship of applied dynamic force to corresponding dynamic deflection. Equip-
ment used in these tests consists of an electromagnetic vibrator with a fre-
quency range of 40 to 10,000 Hz and a force output of 50 lb (figure 54a) and
a large eccentric-mass (counterrotating) vibrator with a frequency range of
5 to 60 Hz and a force output of 8000 lb (figure 54b).

1. WAVE-VELOCITY MEASUREMENTS

    a. Test Procedure

    Wave-velocity measurements employ both the low-frequency mechanical
vibrator and the high-frequency electromagnetic vibrator. A vibrator is
placed on the pavement surface, and a transducer is placed on the surface at
various distances from the vibrator. By means of an appropriate phase-marking
circuit and an oscilloscope, the length of the wave being propagated can be
determined. This is done by locating a point on the surface where the phase
marker coincides with the peak (or trough) of a wave on the oscilloscope and
then moving the transducer to another point where the marker coincides with
the next corresponding peak (or trough). The distance measured on the surface
between the two points is one wavelength. By knowing the frequency, the ve-
locity V_s can be determined from the simple relation:

$$V_s = f\lambda \tag{1}$$

where

f = frequency, Hz

λ = wavelength, ft

The process is repeated with other frequencies, and data are thus obtained to establish the relationship between wavelength and velocity.

Wave-velocity data were obtained on both the flexible and rigid pavement sections. One-half of the wavelength has been found to be approximately the effective depth of the measurement; therefore, the wave velocities were plotted at a depth equal to one-half the wavelength.

Ordinary seismic refraction measurements were made on the flexible pavement items to determine compression wave velocities. Equipment used for the refraction seismic measurements is shown in figure 55. These compression wave velocities V_c and the shear wave velocities V_s from above were used to determine Poisson's ratio ν for each pavement layer from the relation:

$$\nu = \frac{1 - 2\left(\dfrac{V_s}{V_c}\right)^2}{2 - 2\left(\dfrac{V_s}{V_c}\right)^2} \tag{2}$$

Dynamic moduli of elasticity (E moduli) were determined using the shear wave velocities in the following relation:

$$E = 2(1 + \nu)\rho V_s^2 \tag{3}$$

where

ρ = mass density = $\dfrac{\gamma}{g}$

γ = wet density of soil, pcf

g = acceleration due to gravity = 32.2 ft/sec^2

V_s = shear wave velocity, fps

b. Test Results

Wave-velocity tests were made on the flexible pavement items on top of the various pavement layers during construction. A typical data plot is shown in figure 56. There is an apparent increase in the velocities of the underlying layers due to the overburden effect. Typical wave velocities prior to application of traffic are presented in figure 57 for the south lane of the rigid sections. Actual pavement thicknesses are also shown in figures 56 and 57; these indicate that the half-wavelength theory is not exact, especially in determining thickness of the upper layers.

2. PAVEMENT RESPONSE TO VIBRATORY LOADING

a. Test Procedure

In order to determine the degree and the depth to which steady-state vibratory loading affects pavements, the large WES vibrator was operated over the instrumentation (pressure and deflection gages) in item 4 of the flexible sections and items 2 and 4 of the rigid sections. Both frequency of loading and force (by changing eccentric settings of counterrotating weights) were varied. The vibrator was placed directly over the selected gages, and responses of all adjacent gages were read. Contact area of the vibrator was 284 sq in. Data were obtained in the same manner used for recording deflection and stress in load cart tests. Reduction of the data was difficult due to the small order of magnitude of the deflection and stress values; information from the rigid pavement sections is not presented because it could not be accurately read.

b. Test Results

Figures 58 and 59 present plots of elastic deflection and elastic stress, respectively, with depth for various conditions of vibratory loadings and static loadings on item 4 of the flexible test section. Deflection and stress produced by the vibrator, although only a fraction of corresponding values beneath the static loads, are proportional with depth. Deflection at a depth of 12 ft was read from a reference rod with the load cart located adjacent to the rod; the 12-ft deflection was not obtained beneath the vibrator.

3. SURFACE DEFLECTION TESTS

   a. Determination of Dynamic Force

   Relationships of dynamic force to elastic surface deflection were ob-
tained for each pavement test item using the large eccentric-mass vibrator.
The dynamic force applied to the pavement varied with changes in the frequency
of loading and eccentric setting of the rotating masses. The phase shift be-
tween the rotating masses and the displacement was measured with a sin-cos po-
tentiometer. The dynamic force was determined through use of the following
equation:

$$F = M\omega^2_x + me\omega^2 \cos \theta \qquad (4)$$

   F = dynamic force coincident with the maximum deflection

   M = mass of vibrator

   m = mass of eccentric weights

   e = eccentricity

   ω = angular frequency

   x = dynamic deflection

   θ = phase shift

   Force was applied to the pavement on a circular steel plate with a
contact area of 284 sq in., which was equivalent to the contact area of the
load wheel during tests with the load cart. Deflection of the pavement was
measured with a velocity-type pickup placed at the center of the contact
plate.

   b. Load-Deflection Relationships

   Vibratory load-deflection data were obtained prior to the applica-
tion of traffic on the pavements for comparison with deflections measured be-
neath static single-wheel loads. Data were obtained after traffic to deter-
mine the change in the vibratory load-deflection relationship with application
of traffic at different pavement temperatures.

   Vibratory load-deflection data obtained prior to application of traf-
fic to the pavement test items are shown in figures 60 and 61. The data
points for each test item represent frequencies of 5 to 15 Hz. Also shown

in these figures are deflections measured beneath static single-wheel loads with contact areas of 285 sq in. In figure 60, except for the 40-kip load, items 3 and 4 measurements were obtained from instrumentation responses. All other measurements were obtained optically.

c. Vibratory Pavement Stiffness

The ratio of the applied force to the measured vertical deflection is termed the dynamic stiffness of the pavement structure. The load-deflection ratio is determined at various frequencies and an elastic stiffness for zero frequency is found by linear extrapolation in a plot of load-deflection versus the square of the frequency.

Stiffness values measured on the flexible test items prior to application of traffic were found to correlate with total pavement thickness above the subgrade, as can be seen in figure 62. Thickness of the portland cement concrete also showed a relationship to stiffness as shown in figure 63. The data used in figure 63 were taken on 16 October 1969 after trafficking had begun because pretraffic data were not believed to be as reliable due to equipment problems.

d. Deflection Basins

By placing velocity-type pickups on the pavement surface at increments away from the base of the large vibrator, the magnitudes and shapes of the deflection basins were determined at each frequency of a particular test. These data did not show a good correlation between deflection basin and pavement performance.

SECTION VIII

ANALYSIS OF BEHAVIOR UNDER TRAFFIC - FLEXIBLE PAVEMENT

1.   GENERAL

An effort was made to establish a theoretical basis for flexible pavement design and the recent concepts, theories, and computer programs shown in table 13 were examined to determine their applicability to analysis of the results of the MWHGL test sections.

Table 13

Sources for Theoretical Study

Type	Reference No.
Layered system	16-18
Energy method	19-22
Stiffness method	23-25
Finite difference method	26
Finite element method	27-31
Mechanistic models	32, 33
Viscoelastic models	34, 35
WES viscoelastic, multilayered, half-space system	36
Discontinuous orthotropic plates and pavement slabs	37
Elastic plate on dense-liquid bottom layer	38
Elastic plate on elastic solid subgrade	39-41
Barenberg shear layer	42
Single-layer elastic theory program	43, 44

Although some of the methods showed promise, the inability to totally apply any one theoretical concept to the total problem of the design and evaluation of airfield pavements within the time frame available led to an anal is of the MWHGL flexible pavement test data based on present CE

methods (CBR). Further work using these and other methods to analyze the data obtained from the behavioral tests should be continued.

2. COMPARISON WITH EXISTING CRITERIA

The analysis of the MWHGL test section data was based on the as-constructed values shown in table 1, the traffic test data shown in table 7, and the vertical deflection measurements obtained from instrumentation in items 3 and 4.

The test section was designed based on AF medium-load pavement requirements, consisting of a design loading of 100 kips, twin wheels spaced 37 in. center-to-center, and a tire contact area of 267 sq in. Items 1, 2, 3, 4, and 5 were designed for 8, 40, 200, 200, and 1000 coverages, respectively, based on a 4-CBR subgrade. The existing flexible design equation

$$t \rightarrow (0.23 \log C + 0.15) \sqrt{\frac{ESWL}{8.1\ CBR} - \frac{A}{\pi}} \tag{5}$$

was used to determine thickness requirements (t) for the above-mentioned coverage levels where:

t = design thickness (total thickness required above supporting layer), in.

$0.23 \log C + 0.15$ = percent of design thickness (repetitions effect)

C = coverages (sufficient wheel passes to cover every point of a traffic lane once)

$ESWL$ = equivalent single-wheel load (load on a single tire of an assembly that produces the same vertical deflection on the supporting medium as that particular multiple-wheel assembly), lb

CBR = measure of supporting layer's strength

A = measured contact area of tire, sq in.

The ESWL (reference 45) is based on the ratio of maximum deflections beneath a multiple-wheel group and one wheel of that group computed assuming a homogeneous, isotropic half-space loaded by uniformly distributed circular loads. The ESWL varies with depth and is determined at pertinent depths or at sufficient depths to form a curve of ESWL versus depth. At the time the test section was designed, the ESWL for the 12-wheel gear was determined by using a modification of the single-layer elastic theory. This modification

adjusts the deflection based on a subtraction of the deflection factor at the 20-radii offset (cutoff) and proportionate values at lesser offset positions to zero beneath the center of the load (see figure 64). The ESWL's for all other gear configurations were computed using the single-layer elastic theory without any modification.

As can be seen in table 1, the as-constructed subgrade CBR varied slightly; however, except for item 5, the as-constructed thicknesses were the same as design thicknesses. Using the design equation, as-constructed thickness values, and rated CBR values, the design coverages for the 12-wheel assembly become 9, 79, 206, 248, and 810 for items 1, 2, 3, 4, and 5, respectively. A comparison of existing criteria with the performance of the MWHGL test section is shown in table 14.

After testing, the failure coverages were used in the design equation to determine the thicknesses. These values are shown in column 5 of table 14 (Indicated Thickness). A comparison of indicated and actual thicknesses reflects the close agreement between predictions based on the present criteria and the actual behavior of the thinner items at low coverage levels. The agreement is not as good for lane 1, item 5, in which present criteria indicate that 810 coverages (t = 41.0 in.) should have failed the item, but the item actually withstood 3850 coverages without developing a failure. Also in lane 3B, item 5, present criteria indicated a required thickness of 47.0 in. for 280 coverages, but actually 41.0 in. sufficed. A plot of thickness versus failure coverages for the 12-wheel loading (figure 65) shows this divergence at higher coverage levels. Curve A represents actual performance data, and curve B represents design thickness requirements by the existing criteria.

3. EQUIVALENT SINGLE-WHEEL LOAD

The ESWL can be computed by rearranging equation 5 to the following form:

$$ESWL \rightarrow 8.1 \ CBR \left[\frac{A}{\pi} + \frac{t^2}{(0.23 \log C + 0.15)^2} \right] \qquad (6)$$

The ESWL's were calculated using actual test data as shown in figure 65 (curve A) and the flexible pavement design equation (equation 6). These

computations showed a decrease in the 12-wheel ESWL beginning at shallow depths, and also showed a discontinuity at shallow depths. The decrease in ESWL with depth is impossible by definition. The ratio of the deflection under a multiple-wheel assembly to the deflection under any single-wheel assembly must approach unity with depth as the deflections under each assembly approach the same value.

Deflections determined through use of the elastic theory yield values in an elastic, isotropic, homogeneous half-space under a uniformly distributed circular load, and the computations will always indicate some deflection at any distance from the loaded area. In reality, the deflection basin attenuates to insignificantly small values. In an effort to duplicate the theoretical ESWL that most closely represents the behavioral pattern based on the results of actual performance, different cutoff distances in radii were selected and ESWL's computed. These ESWL's were computed using modified deflection curves in which the theoretical deflections for the 12-wheel assembly were made to attenuate to zero at the respective radii cutoff distances. A computer grid and coordinate system was selected by an iterative process to select the location of maximum deflections with depth. Migration with depth is shown in figure 66. The theoretical maximum deflection occurs under the tire at the surface (point A). The maximum deflection actually never reaches the centroid of the six wheels (point B) but at greater depths, approaches the centroid of the 12 wheels (point C).

The instrumentation results for vertical deflections Δ with depth for item 3 are shown in figure 67, and the ESWL's were computed from this plot. The ESWL's were determined from figure 67 in the following manner:

$$\text{ESWL, percent assembly load} = \left(\frac{30,000\Delta_{12\text{ WH}}}{\Delta_{SW}}\right)\left(100 \, \frac{1}{360,000}\right) \qquad (7)$$

For example, using data from the 9-in. depth, the ESWL would be computed as follows:

$$\frac{0.215}{0.098} \times \frac{30}{360} \times 100 = 18.28\%$$

The ESWL's are shown in figure 64 for comparison of the measured and computed values.

Of the relationships of ESWL with depth shown in figure 64, the 10-radii cutoff values agree best in the thickness design relationship, equation 5, as shown in table 15.

Table 15

Thickness Calculated by 10-Radii Cutoff Versus Actual Value

Item	CBR	Failure Coverages	ESWL lb	A sq in.	Thickness t, in. Calculated (approximate)	Actual	Comments
1	3.7	8	44,000	285	13.3	15	
2	4.4	104	51,500	285	22.6	24	
3	3.8	1500	59,400	285	37.7	33	
4	4.0	1500	59,400	285	36.7	33	
5	4.0	>3850	67,250	285	43.4	41	Nonfailure

The calculated t is approximate, since the ESWL is dependent on the calculated t, and the value is shown only for first-order accuracy.

A similar type of approach was then directed toward the data from traffic by the twin-tandem gear spaced 44 by 58 in. on test items of lane 3B. A plot of ESWL, percent of assembly load, versus depth from computations using elastic theory, modified elastic theory, and instrumentation deflection values is shown in figure 68. It is noteworthy that the instrumentation ESWL curve for the twin-tandem gear loading more closely approximates the values derived from the elastic theory than for the radii cutoff modification of the elastic theory. This is also true for the 12-wheel gear loading at shallow depths, but the ESWL curve for the 12-wheel gear is best approximated by the modified elastic theory, 20-radii cutoff, at greater depths (figure 64).

Analysis of traffic test data with the two gear configurations did not yield values of ESWL consistent with the elastic theory or any one modification thereof. The elastic theory without modification was selected as best representing the relationship of ESWL for all multiple-wheel assemblies. This decision was also supported by related work (reference 43). The difference in the behavior of the nonmoving single-wheel, twin-tandem, and 12-wheel assemblies can be related to their different configurations, spacing, and,

consequently, different load-distributing characteristics. However, the effects of the total number of wheels, method of application of traffic, and load repetitions must also be considered.

4. TRAFFIC STUDY

a. Repetitions Effect

The factor f , which equals (0.23 log C + 0.15), employed in the current design of flexible pavements accounts for the effect of traffic repetitions. This factor was developed from previous studies (reference 46). Using the MWHGL test section data and the elastic theory for ESWL determination, the following analysis was made. The flexible pavement equation (equation 5) was rewritten as

$$t_a \rightarrow \alpha \sqrt{\frac{ESWL}{8.1 \, (CBR)} - \frac{A}{\pi}} \qquad (8)$$

then

$$a \rightarrow \frac{t_a}{\sqrt{\frac{ESWL}{8.1 \, (CBR)} - \frac{A}{\pi}}} \qquad (9)$$

where

t_a = actual test section thickness, in.

α = load repetitions factor

ESWL = equivalent single-wheel load, lb, at the depth t_a

CBR = measure of supporting layer's strength

A = measured tire contact area, sq in.

The α factors or the effect of repetitions on the total thickness requirements were computed and are shown in table 16.

Figure 69 shows a semilog plot of the α values versus coverages. For comparison, the existing relationship of f versus coverages is also shown. The existing criteria for low-intensity traffic seem adequate for all wheel gears shown (reference 47). However, as noted, with an increase in coverages, the present load repetition factor is too large and hence yields too great a thickness. Curves 1, 2, and 3 in figure 69 represent failure envelopes for the single-wheel, twin-tandem, and 12-wheel gear, respectively. An additional point was obtained for curve 3 for the 12-wheel assembly. This

56

was obtained by extrapolating the nonfailure of item 5 to failure at about 15,000 coverages as shown in curve A, figure 65.

A statistically weighted curvilinear regression (references 48 and 49) was performed on the MWHGL failures, given in table 16, to determine the best-fit curve for coverages and α. The results are shown in figure 70. Curve B represents the best-fit curve, and curve A is the existing design curve. Curve B is a good estimate for the twin-tandem assembly but requires too much thickness for the 12-wheel gear. If curve B were shifted downward a constant amount to include the 12-wheel data, it would not require enough thickness for the twin-tandem assembly. This would indicate a need for a separate α versus traffic volume factor for each of the assemblies used.

Using the relationships for α_i shown in figure 69 and earlier conclusions, the following design pattern was developed for thickness requirements to protect supporting layers.

$$t \rightarrow \alpha_{SW} \sqrt{\frac{ESWL}{8.1\ CBR} - \frac{A}{\pi}} \qquad \alpha_{SW} = \text{equation of curve 1} \qquad (5a)$$
$$\text{figure 69}$$

$$t \rightarrow \alpha_{TT} \sqrt{\frac{ESWL}{8.1\ CBR} - \frac{A}{\pi}} \qquad \alpha_{TT} = \text{equation of curve 2} \qquad (5b)$$
$$\text{figure 69}$$

$$t \rightarrow \alpha_{12WH} \sqrt{\frac{ESWL}{8.1\ CBR} - \frac{A}{\pi}} \qquad \alpha_{12WH} = \text{equation of curve 3} \qquad (5c)$$
$$\text{figure 69}$$

Using the above relationships, computations were made to check predictions of the pattern with performance of the test section. As shown in table 17, this method of predicting required thickness is in agreement with the performance of the test pavements.

b. Traffic Distribution Studies

During the early stages of development of criteria for the design and evaluation of pavements, it became apparent that a method was needed to account for repetitions of traffic. To simply count the number of aircraft using an airfield is not adequate. The incremental detriment to a pavement resulting from a particular aircraft wheel at a specified location on pavements is influenced by many factors. Some of the more important factors are: (1) number of wheels, (2) wheel configuration, (3) tire contact area,

(4) tire inflation pressure, and (5) location of wheel on pavement.

In an attempt to normalize these factors so that one number could be obtained to reflect their collective influence on the total system of design and evaluation, the concept of coverage was introduced where coverage is defined as sufficient contiguous wheel passes so that every point in a traffic lane has been touched one time by a moving wheel.

In the past, traffic on test sections was programmed so that successive wheel paths were not overlapping, and an accurate value of coverages resulted. It was assumed that coverages on a test section related directly to coverages on airfield facilities (runways, taxiways). However, the random traffic on runways and/or taxiways can only be conveniently counted as aircraft passes. The general equation currently used for determining pass per coverage ratios (sometimes called operation per coverage ratio), given as equation 7 in reference 50, is:

$$p/c = \frac{W_t + S + W_w}{0.75 \; N \; W_t} \tag{10}$$

where

p/c = pass per coverage ratio

W_t = tire width, in.

S = wheel spacing, in.

W_w = wander width (40 in. assumed for channelized traffic of military aircraft on a taxiway)

N = number of wheels in traffic lane

In accordance with the traffic pattern used on the C-5A test sections (Volume II) where the traffic was programmed in such a manner that 22 passes of the load cart generated 32 coverages, p/c equaled 22/32 or 0.68. In comparison, when the dimensions for the C-5A gear are substituted in equation 10 ($W_t = 14.3$ in., $S = 121$ in., and $N = 12$), then p/c equals 1.36. Thus, the pass per coverage ratio determined from the current method for aircraft operating on runways and/or taxiways does not agree with the actual pass per coverage ratio for the test section. In addition, there has been considerable confusion and some misunderstanding relative to the use of coverage as a means of accounting for traffic repetitions and some indication that the current method of converting coverages into passes (or vice versa)

may contribute to some of the difficulty encountered in analysis of test
section data. For these reasons, a revised method, based on statistical
analysis, for determining pass per coverage ratios has been developed. The
revised method and its application are described in the following paragraphs.
The background and details of the development and application of the method
are given in reference 50.

c. Development of Revised Traffic Distribution Concepts

Statistical analysis combined with actual traffic distribution data
has been used to develop a new method for determining pass per coverage ra-
tios. A fundamental assumption is made that airfield traffic is normally
distributed instead of uniformly distributed as was assumed in the develop-
ment of equation 10. For a large number of aircraft passes, the lateral
placement of the center line (of the aircraft) will be, statistically, as
shown in figure 71. The general shape is assumed to be normal, while the
specific shape depends on the standard deviation σ. The specific shape may
also be described by prescribing the wander width W_w, which is defined as
that width over which the center line of the aircraft traffic is distributed
75 percent of the time. It has been determined, on the basis of an analysis
of a small amount of actual military aircraft traffic distribution, that
wander widths of 40 and 80 in. should be used in determining pass per coverage
ratios for taxiways and runways, respectively. These values represent the
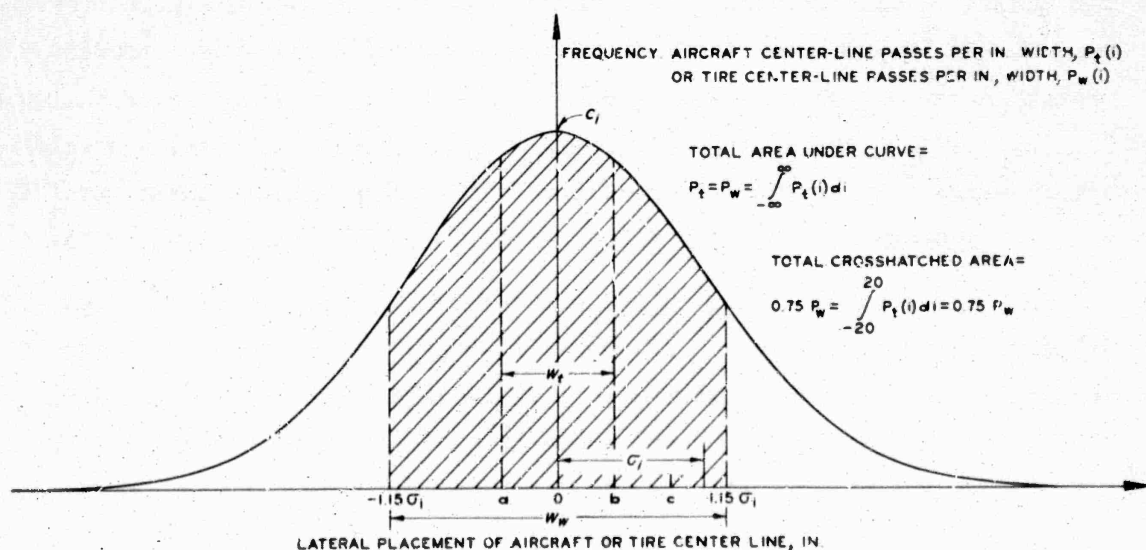
Figure 71. Theoretical Normal Distribution of Aircraft Traffic

59

best values obtainable from existing data and are subject to change if and when additional actual traffic distribution data are obtained.

The definition for coverage was revised for the traffic distribution study. It was considered that coverage represents the maximum number of tire prints or partial tire prints applied to the pavement surface at that point where maximum accumulation occurs. In figure 71, the distribution curve also represents the distribution of the center line of one wheel on the aircraft. When the wheel center line is at $a = -\frac{W_t}{2}$, wheel passes accumulate at 0. Similarly, when the wheel center line is between $a = -\frac{W_t}{2}$ and $b = \frac{W_t}{2}$, there will be accumulations at 0 equal to:

$$\int_{-\frac{W_t}{2}}^{\frac{W_t}{2}} P_t(i) \, di \tag{11}$$

As can be seen, this is approximately equal to $(C_i)(W_t)$. It is assumed in equation 11 that the effect of the edge of a tire at 0 is as detrimental as the effect of the tire center line at 0. This is not necessarily true and a further refinement could be made through use of a location weighting factor as discussed in detail in reference 50. However, for the present this refinement will not be used. Instead, the simplified definition for coverage, $C = (C_i)(W_t)$, will be used. This method can be extended to aircraft having many wheels by graphical addition of any number of single-wheel traffic distribution curves, such as that shown in figure 71. The area under the cumulative traffic distribution curve will then represent the total number of wheel passes. Pass per coverage ratios based on an assumed normal traffic distribution can be developed as described in the following paragraphs.

The standard normal distribution (SND) curve is shown in figure 72. Properties of the SND curve are tabulated in numerous standard references for statistics and tables of probability functions. and these tabulated values can be used to determine the properties of a general normal distribution (GND) curve, figure 73. In the SND, standard deviation $\sigma = 1$, area under the curve $A = 1$, maximum ordinate $C = 0.399$, and 75 percent A lies

60
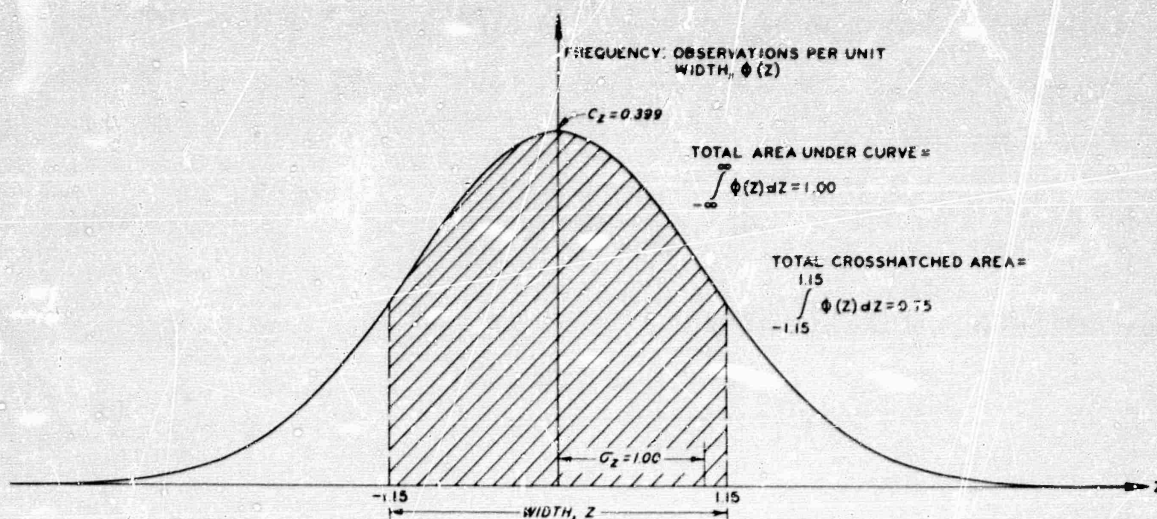
Figure 72. Standard Normal Distribution (SND) Curve
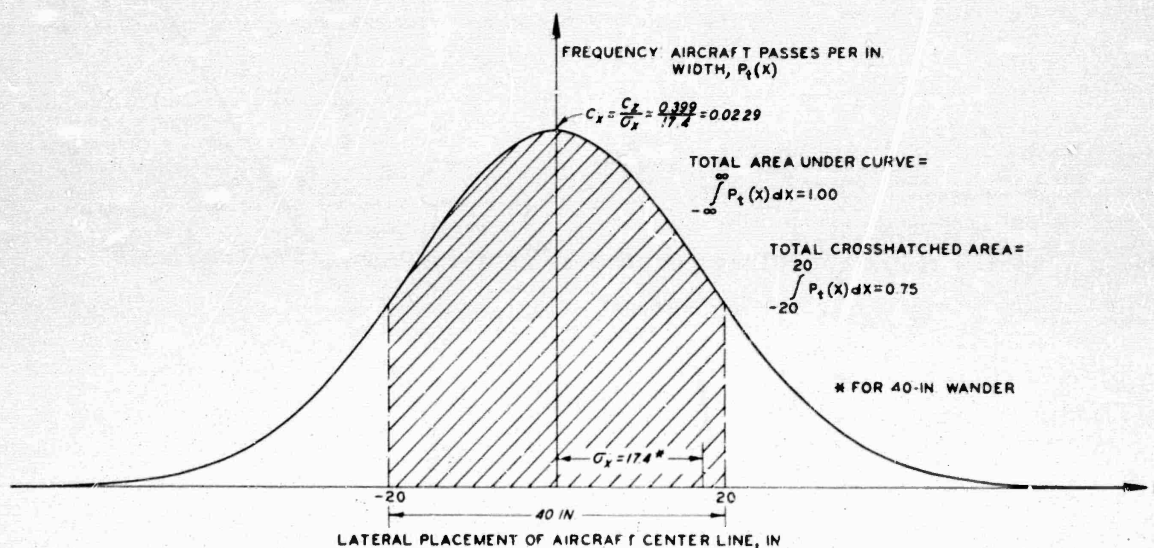
Figure 73. General Normal Distribution (GND) Curve for Aircraft Traffic

between $-1.15 < z < + 1.15$. The GND curve may be related to the SND curve using the following substitution:

$$z = \frac{x - u}{\sigma_x} \qquad (12)$$

where

z = a variable in SND

x = a variable in GND

u = mean value in GND

σ_x = standard deviation in GND

61

Then, where the wander width W_w equals 40 in. (or $2x$), $x = 20$ in., and $u = 0$, by substitution, $1.15 = \dfrac{20 - 0}{\sigma_x}$, or σ_x for the GND = 17.4 . Now the SND curve has the equation

$$\phi z = \frac{1}{\sqrt{2\pi}} e^{-\frac{z^2}{2}} \tag{13}$$

and the GND curve has the equation

$$P_t(x) = \frac{1}{\sigma_x \sqrt{2\pi}} e^{-\frac{1}{2}\left(\frac{x-u}{\sigma_x}\right)} \tag{14}$$

wherein substitution of $z = \dfrac{x - u}{\sigma_x}$ yields

$$P_t(x) = \frac{1}{\sigma_x}(\phi z) \tag{15}$$

and

$$C_x = \frac{1}{\sigma_x} C_z \tag{16}$$

where C_x is the maximum ordinate on the GND curve. Also, the area under the GND curve A is equal to:

$$A = \int_{-\infty}^{\infty} P_t(x)\, dx$$

$$= \int_{-\infty}^{\infty} \frac{1}{\sigma_x}\left[\phi(z)\right]\sigma_x d_z$$

$$= \int_{-\infty}^{\infty} \phi(z)\, dz = 1.00$$

Note, however, that as wander width W_w is changed, σ_x must be recalculated as indicated above.

The GND curve can now be applied to the study of real aircraft traffic distribution. For example, using an aircraft with a single-wheel tricycle landing gear (figure 74) and neglecting the nose gear, plot the GND of each
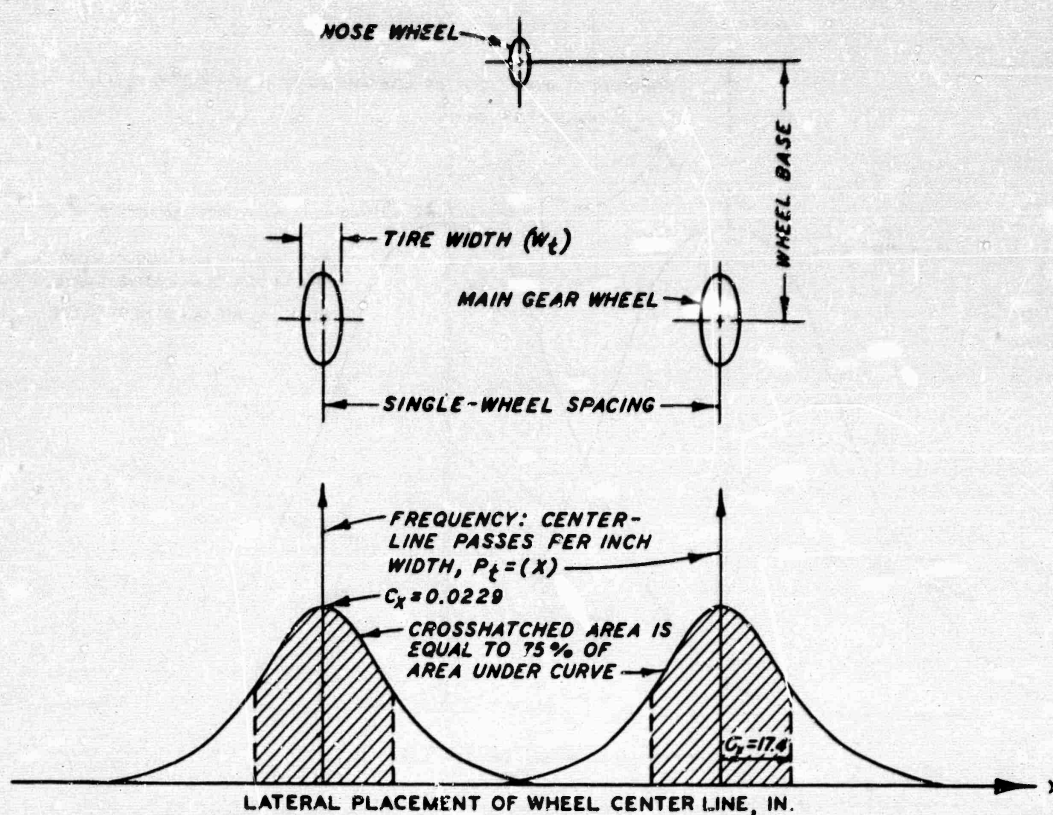
Figure 74. General Normal Distribution for Nonoverlapping Wheels for the Typical Single-Wheel Tricycle Landing Gear

wheel, both on the same plot, as shown in figure 74. Graphically adding these curves results in a cumulative curve identical (for all practical considerations) with the GND curve. The total area under the cumulative curve is equal to two wheel passes (wp) or one aircraft pass (ap), and the maximum number of coverages C is: $C = (C_x)(W_t)$ and

$$p/c = \frac{1}{(C_x)(W_t)} \left(\frac{ap}{wp}\right) \qquad (18)$$

As the wheel spacing S becomes smaller, the GND curve for each single-wheel overlap and the distribution pattern shown in figure 75 are obtained. In this case, graphical addition of the individual single-wheel curves results in a cumulative distribution curve with a maximum ordinate larger than that of either single-wheel curve. The area under the cumulative curve is still 2.00. Now, however, the maximum number of coverages is the maximum area under the cumulative curve with a width of W_t. This value may
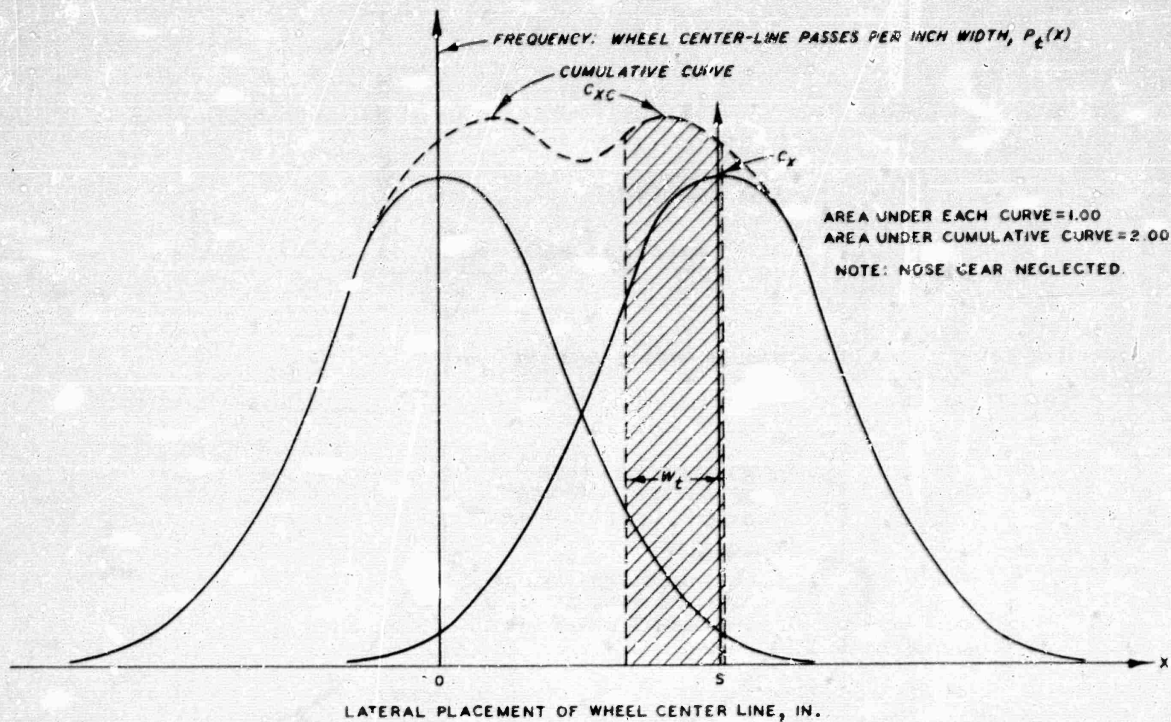
Figure 75. GND Curve for Overlapping Single Wheels

not necessarily occur under one wheel and its location must be determined by trial and error. For example, the maximum area may be as shown by the cross-hatched area in figure 75. Such a refinement is not considered warranted, and for simplicity, the value $(C_{xc})(W_t)$ will be used as the maximum value for coverages. Values for C_{xc} developed in this study have been obtained graphically. The determination of C_{xc} could easily be a programmed determination using a computer, but this has not been done because the determination need be made only once for each aircraft.

Thus

$$p/c = \frac{1}{(C_{xc})(W_t)} \left(\frac{ap}{vp} \right) \qquad (19)$$

As an aid in determining the magnitude of C_{xc}, figure 76 has been prepared. This figure shows C_{xc} versus wheel spacing for 40- and 80-in. wander widths. For a wander width of 40 in., $C_{xc} = C_x = 0.0229$ when the wheel spacing is greater than 60 in. (nonoverlapping wheel paths). When the wheel spacing is 0, $C_{xc} = 2C_x = 0.0458$ (tandem assembly). When the wheel spacing is greater than 0 and less than 60 in., C_{xc} can be read from
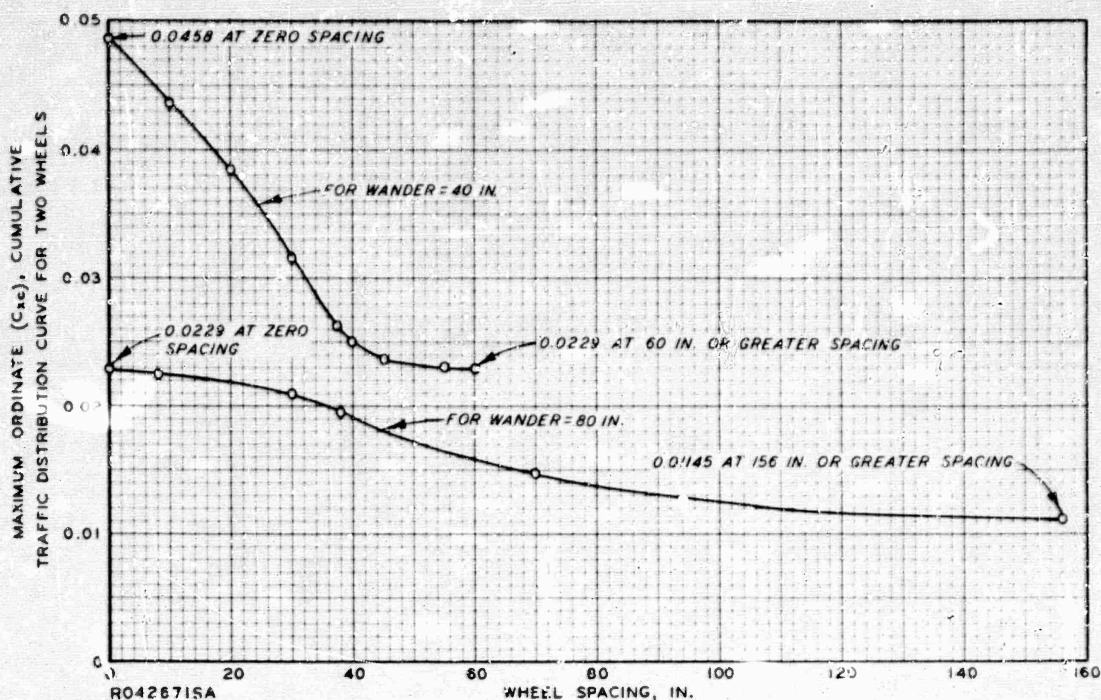
Figure 76. Maximum Ordinate on Cumulative Traffic Distribution Curve
for Two Wheels Versus Wheel Spacing

figure 76. For a wander of 80 in., $C_{xc} = C_x = 0.01145$ when the wheel spacing is greater than 156 in. (nonoverlapping wheel paths). When the wheel spacing is zero, $C_{xc} = 2C_x = 0.0229$ (tandem assembly). When the wheel spacing is greater than 0 and less than 156 in., C_{xc} can be read from figure 76. The values read from figure 76 are applicable to the following landing gear configurations without exception: single conventional, single tricycle, single-tandem tricycle,[4] and twin bicycle[4] and to the following landing gear configurations when the tread is greater than 60 in. (for $W_w = 60$ in.) or 156 in. (for $W_w = 80$ in.): twin conventional, twin tricycle, twin-tandem tricycle,[4] and twin-twin bicycle.[4] For other landing gear configurations, C_{xc} can be determined by plotting the individual wheel distribution and determining the cumulative distribution curve by graphical addition as demonstrated in figure 77.

The versatility of this method is demonstrated with the determination

---

[4]Note that for these configurations, C_{xc} will be twice the value read from figure 76 because there are two wheels in line in the direction of travel.
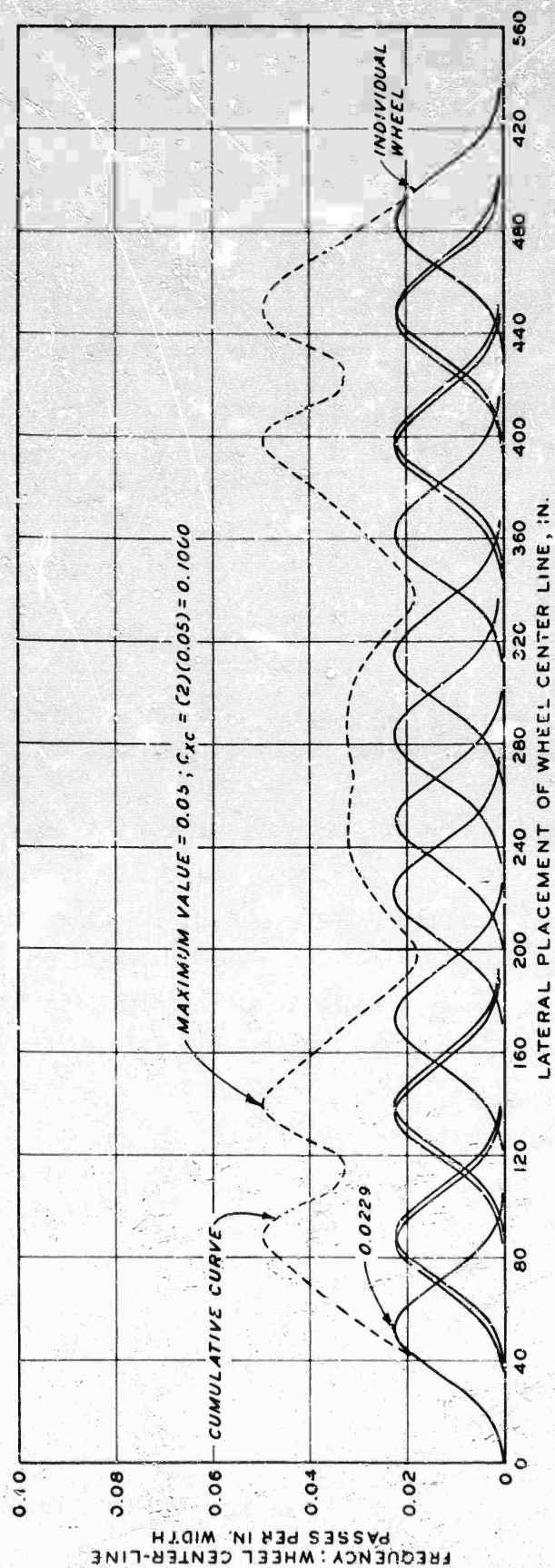
Figure 77. Theoretical Normal Distribution for C-5A Gear (Partial). Note: The Distribution Curve Shown Is for Wheel Groups A, E, and B As Shown in Figure 78.

of p/c ratios for the C-5A and Boeing 747 landing gear wheel configurations
and a wander of 40 in. as shown in the following paragraphs.

(1) p/c ratio for the C-5A. The C-5A wheel configuration is shown
in figure 78. The normal distribution curves for wheel groups A, B, and E
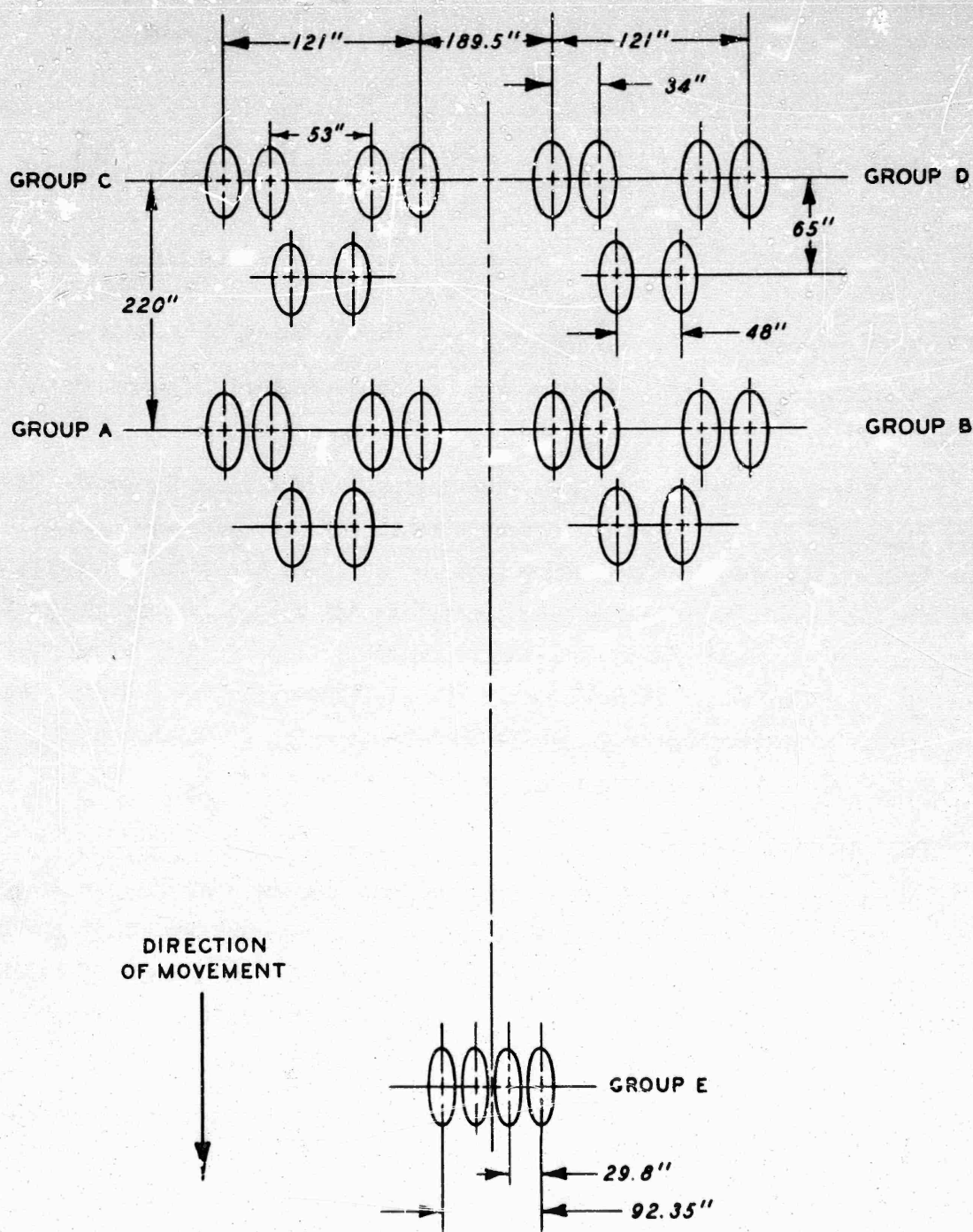
Figure 78. C-5A Landing Gear Configuration

are shown in figure 77 where the cumulative distribution curve was obtained by graphical addition of individual wheel distribution curves. By inspection, it can be seen that the maximum ordinate for Group A plus Group C (or Group B plus Group D) on the cumulative curve is the maximum ordinate for the assembly. Thus $C_{xc} = 2(0.0500) = 0.1000$. For the entire assembly, total number of wheel passes = 28. However, 28 wheel passes = 1 aircraft pass. Thus,

$$p/c = \frac{1}{28}\left(\frac{ap}{wp}\right)\frac{28}{1}(wp)\frac{1}{(0.1000)(W_t)}\left(\frac{in.}{wp}\right)\left(\frac{1}{in.}\right) = \frac{1}{(0.1000)(W_t)}\left(\frac{ap}{wp}\right)$$

Or as before (equation 19), $p/c = \frac{1}{(C_{xc})(W_t)}\left(\frac{ap}{wp}\right)$. Therefore, for the C-5A, where $W_t = 15.1$ in., $p/c = \frac{1}{(0.1000)(15.1)} = 0.662$, which is in general agreement with the operations per coverage ratio determined from actual test traffic.

(2) **p/c ratio for the 747.** The Boeing 747 wheel configuration is shown in figure 79. The pass per coverage ratio for the Boeing 747 can be determined by the graphical procedure used for the C-5A aircraft. However, since the individual twin-tandem gear assemblies are spaced far enough apart to prevent any overlap between twin-tandem assemblies for a 40-in. wander, the value of C_{xc} can be determined through use of figure 76. For a 44-in. twin-wheel spacing, the maximum ordinate for a 44-in. spacing is 0.024 and $C_{xc} = (2)(0.024) = 0.048$. Therefore, for the Boeing 747, where $W_t = 12.9$ in., $p/c = \frac{1}{(0.048)(12.9)} = 1.62$.

Pass per coverage ratios for the various landing gear wheel configurations used in the MWHGL investigations reported herein and for other similar data obtained from related studies have been determined through use of equation 18 or 19. Values for C_x and C_{xc} were read from figure 76 or were determined by the graphical procedure just demonstrated.

Using these p/c factors, the test section failure coverages were converted to actual field facility failure passes. This conversion is shown in table 18. The α factors versus passes were plotted, as shown in figure 80, and limiting failure envelopes were drawn for the 12-wheel,
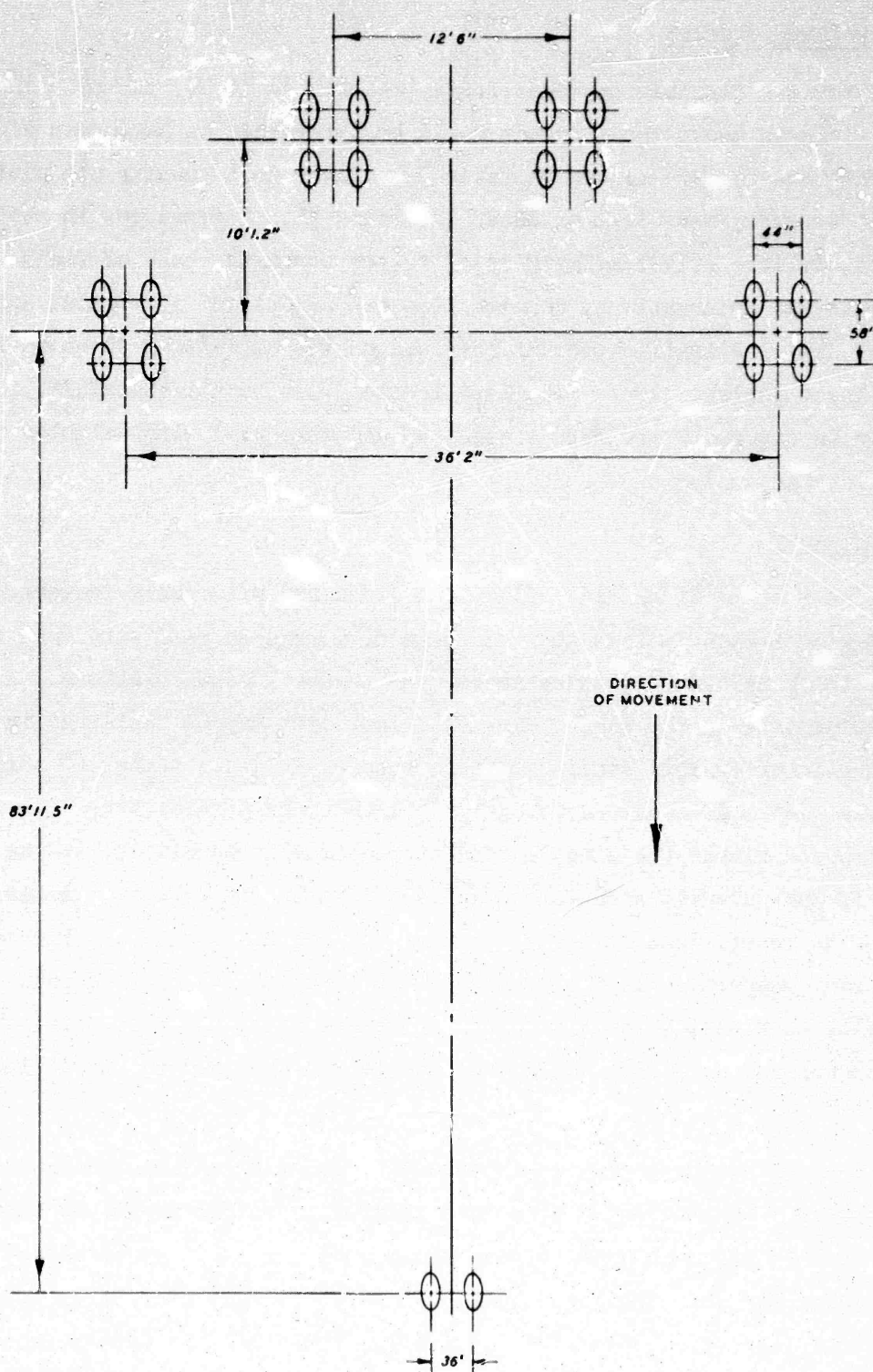
Figure 79. Boeing 747 Landing Gear Configuration

twin-tandem, and single-wheel gear configurations.

d. Related Studies

Previous flexible pavement tests (references 51-58) in which insufficient thickness above the subgrade could be determined as having an effect on pavement behavior are listed in table 19. These test results are plotted in the α versus passes form as shown in figure 81. Differences in test objectives, failure criteria, methods of rating strength, rate of field measurements and observations, construction techniques and materials, and methods of applying traffic account for some of the variations shown in figure 81. These variables were minimized in the MWHGL tests; therefore, the data shown in figure 80 are more consistent and were used with weighted emphasis in this analysis.

e. Summary

The results of the investigations discussed previously indicate that load repetitions factors α_i decrease at a reduced rate with repetitions for the single-wheel, twin-tandem, and 12-wheel configurations. A better performance as the number of wheels increases may be explained in part by the interior soil confinement afforded by a larger number of perimeter wheels. An additional advantage may be that the partial stress reversals imposed within the elastic domain are actually beneficial to the performance of the pavement structure. The decrease in the rate of thickness increase with repetitions reflects the past and recent testing experience in protecting supporting layers from shear deformation. Figure 82 shows a plot similar to figure 80 with a logarithm extension of the test pattern shown to encompass different numbers of wheels and extended to one million passes.

The α_i curves have been developed using the load on one landing gear assembly of an aircraft. In actual practice, designs are to be based upon the load on all main gear tires. Therefore, the α_i versus passes curves (figure 82) show the total number of aircraft main gear tires represented by the gear type. Use of the criteria, therefore, is accomplished by determining the ESWL and the α_i for all main gear tires, which generally results in maximum thickness requirements for a specific aircraft. However, where it is shown that some combination or grouping of tires other than all

main gear tires will produce a greater thickness requirement, then the other combination or group will be used. Use of the criteria for aircraft having a number of wheels other than shown requires interpolation between the curves. The unique limiting curve shown from 1 to 100 passes represents a composite of the single, twin-tandem, and 12-wheel curves shown in figure 80. Actually, the composite curve for the very low operational level is used for convenience because there is such a small difference in repetitions effect and because it is difficult to differentiate failure at a low operational level.

5. STATIONARY REQUIREMENTS

The static requirements, i.e., requirements other than those due to repetitions, may be well defined by the two basic parameters, $\frac{t}{\sqrt{A}}$ and $\frac{CBR}{p_e}$. These parameters may be reduced to a single plotted curve that separates service-behavior data with regard to failures and nonfailures (reference 59). Results from the MWHGL tests and those from earlier related tests are generally separated by this curve with the failures located above this curve and the nonfailures below. In the region of higher $\frac{CBR}{p_e}$ and lower $\frac{t}{\sqrt{A}}$ values, certain minimum requirements (i.e., stability and longevity requirements) are considered in the total thickness requirements. To incorporate these parameters of design and extreme cases of high tire pressure, light loads and low tire pressure, or heavy loads, the service behavior curve was developed. This curve represents an average of these extremes in the upper region of $\frac{CBR}{p_e}$ and approximately the same as the curve shown in reference 59 in the lower regions of $\frac{CBR}{p_e}$. The statistical equation of the best-fit cubic curve is

$$
t \to \left\{ \sqrt{A} \left[-0.0481 - 1.1562 \left(\log \frac{CBR}{p_e} \right) - 0.6414 \left(\log \frac{CBR}{p_e} \right)^2 \right. \right.
$$
$$
\left. \left. - 0.4730 \left(\log \frac{CBR}{p_e} \right) \right] \right\} \qquad (20)
$$

where

p_e = ESWL or SWL tire pressure, psi. For multiple-wheel gear, p_e = ESWL/A where ESWL is determined by the method shown in reference 45 and for single-wheel gear, p_e = SWL/A . This is an artificial tire pressure for multiple-wheel loads consistent with use of contact area of one tire and has no relation to actual tire inflation pressure. However, for single-wheel loads, this pressure is the actual average contact pressure and is nominally the same as the tire inflation pressure.

6. DESIGN METHOD

The cubic equation yielded the best statistical curve fit for the separation of failures and nonfailures. The equation can be used for the computation of thicknesses of overlying layers required to prevent shear deformation in supporting layers. With the cubic equation representing the static condition and the α_i factors developed previously representing the effect of repetitions, the thickness requirement equation is thus finalized in the following form:

$$t \rightarrow \alpha_i \left\{ \sqrt{A} \left[-0.0481 - 1.1562 \left(\log \frac{CBR}{P_e} \right) - 0.6414 \left(\log \frac{CBR}{P_e} \right)^2 - 0.4730 \left(\log \frac{CBR}{P_e} \right)^3 \right] \right\} \qquad (20a)$$

where

α_i = load-repetition factor which varies with number of wheels on main gear of aircraft considered and the volume of aircraft traffic, in passes, anticipated as shown in figure 82.

Thicknesses can also be computed by calculating the ESWL as explained in reference 60, using the procedures outlined therein in conjunction with figures 82 and 83 of this report.

7. FLEXIBLE PAVEMENT THICKNESS REQUIREMENTS[5]

Using the results of the preceding analysis, typical examples of evaluation curves for the C-5A aircraft can be developed (figures 84-88). A capacity design category of 12,000 passes for type A traffic areas can be assumed based on expected usage by this aircraft. An estimation of facility usage of 100 passes per month, and 10-year life yielded the 12,000 passes. For this particular aircraft, a pass is defined as one takeoff and one landing. Evaluation curves can also be developed assuming the following: full category, 2400 passes (2 years); minimum category, 480 passes (6 months); and emergency category, 56 passes (2 weeks). These example evaluation curves were also

---

[5] The criteria presented herein for the C-5A and Boeing 747 (figures 84-90) are not to be used as design criteria but serve only as examples of how such criteria can be developed. The methodology used to develop these curves can be used to develop design criteria for any type of aircraft.

based on the gear configuration shown in figure 78 and on the following
assumed conditions:

Design gross loading, lb	769,000
Main gear load per wheel, lb	30,000
Main gear contact area per tire, sq in.	285
Total nose gear wheel load, lb	12,250
Maximum main gear load, percent of gross load	93.6

A typical design curve in FAA format for the Boeing 747 aircraft is shown
in figure 89. The example is for the 100,000-pass level, which was determined
on the basis of 350 days per year use, 20 passes per day, and 15-year life. A
pass is defined by FAA as one movement of the aircraft past one specific point.
The design curve was based on the gear configuration shown in figure 79, and
on the following assumed conditions:

Maximum gross loading, lb	713,000
Main gear load per wheel, lb	42,334
Main gear contact area per tire, sq in.	208
Total nose gear wheel load, lb	17,825
Maximum main gear load, percent of gross load	95

Also for this design, the FAA soil classification system was related to CBR as
shown in table 20.

Table 20

FAA Soil Classification-CBR Relationship

Subgrade Classification	CBR	Subgrade Classification	CBR
F10	3.5	F4	10.0
F9	4.5	F3	12.0
F8	5.5	F2	14.5
F7	6.5	F1	18.0
F6	7.5	Fa	20.0
F5	8.5		

These values represent the median of values shown in reference 61, page 80. A

73

typical design curve for the C-5A aircraft for 50,000 passes is shown in figure 90. The pass level was assumed to represent expected facility usage of 250 days per year, 20 passes per day, and 10-year life.

SECTION IX

ANALYSIS OF MWHGL RIGID PAVEMENT DATA

1. PHYSICAL PROPERTIES

A considerable amount of testing was required after the traffic had been completed to determine the as-built properties of the test section. Actual slab thickness, flexural strength, and subgrade moduli were parameters that had to be measured. Construction control data were available; however, these data were nearly a year old when traffic had been completed. Test pits were opened in each of the four test items in both the north and south paving lanes. In the south lane, a 5- by 6-ft slab was removed from the northeast corner of the southwest slab in each test item. In the north lane, a 5- by 6-ft slab was removed from the southeast corner of the northeast slab in each test item. The test pits were planned so as to yield enough concrete material for flexural test specimens, sufficient space for plate bearing tests, and adequate soil samples for water content and density tests and to permit examination of the keyed longitudinal joint and transverse dummy groove contraction joint. A summary of the physical properties of the test section is shown in table 21.

2. COMPARISON WITH EXISTING CRITERIA

a. 12-Wheel Assembly

A comparison of the service life of the rigid pavement test items under 12-wheel traffic with projected performance based on existing criteria can best be made by showing the predicted and observed service lives for each test item. The observed performance of the test items provides two failure points, since each of the test items was composed of four 25- by 25-ft slabs, two of which carried the bulk of the traffic. Table 22 presents a summary of rigid pavement performance.

Table 22

Summary of Rigid Pavement Performance Under 12-Wheel Traffic

	Coverages to Initial-Crack Failure				Coverages to Shattered-Slab Failure			
	Predicted		Observed		Predicted		Observed	
Item	East	West	East	West	East	West	East	West
1	75	370	192	251	2000	4600	592	592*
2	3600	2250	3963	4496	9000	7300	5008*	5008*
3	3050	5000	592**	2208**	6200	7900	5008*	5008*
4	<10	<10	181	180	490	490	240	240

* Test was terminated before indicated failure condition was reached.
** Premature failure attributed to excessive pumping.

Corps of Engineers rigid pavement failure criteria were used to predict the two failure conditions tabulated above. These criteria are defined in Section V of this report.

During the conduct of the traffic tests, 4- and 6-in. nonrigid overlays were placed on test items 1 and 4, respectively. These overlays were intended to provide a measure of the adequacy of the nonrigid overlay criteria under multiple-wheel loadings. Performance predictions for nonrigid overlays are based on an equivalent single thickness of rigid pavement. The equivalent single thickness of rigid pavement is calculated from the equation:

$$h_e = \frac{1}{F}\left(Ch_b + \frac{t}{2.5}\right) \tag{21}$$

where

h_e = equivalent single thickness of rigid pavement, in.

F = factor relating controlled degree of cracking in base pavement and is dependent on modulus of subgrade reaction and amount of traffic

C = condition factor describing structural condition of base pavement ranging from 1.0 (when slabs contain only nominal cracking) to 0.75 (for slabs with multiple cracking)

h_b = thickness of base pavement, in.

t = thickness of nonrigid overlay, in.

The equivalent single thickness of rigid pavement determined from equation 21

is then used to formulate performance predictions for the nonrigid overlay. The base pavements in nonrigid overlays are allowed to crack extensively as was mentioned in Section V of this report. Performance predictions for nonrigid overlays are thus based on the complete failure condition for the equivalent single thickness of rigid pavement as determined from equation 21.

The design of the nonrigid overlay sections was based on data available from preconstruction tests and results from construction-control test specimens, as no means were available to accurately determine these parameters without destructive testing. In retrospect, the nonrigid overlays were somewhat overdesigned, as the selected values of slab thicknesses, flexural strengths, and subgrade moduli were lower than the actual values determined from the posttraffic testing program. Table 23 gives predicted performance from both the estimated values and the measured values along with the observed performance.

Table 23

Summary of Performance of Rigid Pavement

with Nonrigid Overlay (12-Wheel Traffic)

	Coverages for Nonrigid Overlay Failure					
	Predicted				Observed	
	Construction Control Data		After-Traffic Data			
Item	East	West	East	West	East	West
1	3520	3520	100,000	100,000	4416*	4416*
4	3040	3040	6,000	5,500	4416*	4416*

* Traffic testing was terminated before failure occurred.

The comparison of the observed and predicted performance for initial-crack failure of the various plain rigid pavements subjected to 12-wheel traffic shows reasonable agreement for items 1 and 2. Test items 3 and 4 performed differently than current CE criteria predicted. Test item 3 failed prematurely, and, in the opinion of the personnel involved in testing the rigid pavement, the failure was accelerated because of excessive pumping. Test item 4 performed better than predicted, but the reasons for this have not been completely explained. Some hypothetical explanations have been

offered such as nonrepresentative after-traffic data and absence of environmentally imposed loadings. However, the most probable cause was normal data scatter encountered in low-volume traffic tests.

The observed and predicted performance comparisons for the shattered-slab failure condition are meaningful for only three slabs. Five of the eight test slabs were not trafficked to the shattered-slab failure condition. All three slabs reached the shattered-slab failure condition at a slightly lower coverage level than would be predicted by the current CE criteria. The coverage level at which the shattered-slab condition was reached was relatively low, and the disparity between observed and predicted traffic volumes is considered due to normal data scatter.

The performance of the nonrigid overlay sections was as predicted by current CE criteria, i.e., none of the slabs failed. The overlay pavements were overdesigned and would have required an unreasonable amount of traffic to cause failure. A polypropylene membrane was inserted in the nonrigid overlay on test item 1 at the interface of the asphaltic concrete and portland cement concrete to assess the effects on retardation of reflection cracking. The membrane did seem to retard the rate of reflection crack progression to some small extent. It must be pointed out that the section containing the polypropylene membrane was small (approximately 28 by 28 ft), and the base pavement was spalled more severely than the comparable section without the membrane. Reflection cracks from both structural cracks and the jointing system occurred with little difference between the sections where the polypropylene was and was not used.

b. Twin-Tandem Assembly

The performance of the test items under twin-tandem traffic was compared with that predicted by current Corps of Engineers criteria (table 24). Items 1 and 4 can be analyzed only as nonrigid overlay items since the overlays were placed before the start of twin-tandem trafficking. The same failure definitions and criteria are applicable to the twin-tandem tests and the 12-wheel tests.

Table 24

Summary of Rigid Pavement Behavior Under Twin-Tandem Traffic

	Coverages Required for Failure											
	Initial Crack				Shattered Slab				Overlay			
	Predicted		Observed		Predicted		Observed		Predicted		Observed	
Item	East	West	East	West	East	West	East	West	East	West	East	West
1	N/A	N/A	--	--	N/A	N/A	--	--	100,000	100,000	680*	680*
2	64	88	150	40	1050	2000	680	680	N/A	N/A	--	--
3	3050	1400	150	260	8000	7000	680**	680**	N/A	N/A	--	--
4	N/A	N/A	--	--	N/A	N/A	--	--	12,000	12,000	680	680

* Test terminated before indicated failure condition was reached, but failure was
   imminent.
** Indicates number of coverages at termination of test.

The comparison of predicted and observed pavement performance in regard
to the initial-crack failure as predicted by current CE criteria was applicable
to only four slabs under the twin-tandem-assembly traffic program. Test item
2 failed at approximately the traffic level predicted; the east slab failed
somewhat later and the west slab somewhat earlier. Test item 3 failed earlier
than anticipated under the twin-tandem-assembly loading. Pumping in the north
lane of item 3 was not considered severe enough to adversely affect the pave-
ment performance. One explanation may be that the pass per coverage ratio for
the twin-tandem assembly should have been 1.62 rather than the 3.30 that was
used. The critical stress used for the analysis of these test items was par-
allel to the transverse joint with the gear positioned perpendicular to and
tangent to the transverse joint. The crack development and progression veri-
fied the location of the maximum stress, as the crack originated at the trans-
verse joint and progressed perpendicular to the joint.

The shattered-slab failure condition for twin-tandem-assembly traffic
shows that test item 2 failed slightly earlier than predicted and test item 3
did not fail, which was as predicted. The consensus of the personnel involved
was that test item 3 probably would have failed slightly earlier than pre-
dicted had traffic been continued to 7000 or 8000 coverages.

The nonrigid overlay performance predictions for twin-tandem-assembly
traffic were applicable to the four remaining test slabs in the north lane.

79

Test item 1 was overdesigned for the traffic that was applied for the same reasons given before. Test item 4 reached failure prematurely under the twin-tandem assembly. This premature failure has not been totally explained and may be further indication that the pass per coverage ratio for the twin-tandem assembly should have been 1.62 rather than the 3.30 used.

3. PERFORMANCE OF JOINTS

The keyed longitudinal construction joints failed in all test items relatively early under the MWHGL traffic. The failure was either a shearing of the key or a spalling of the keyway. Both types of failure occurred in each test item, indicating a balanced dimensional design of the key and key-way. Past experience had indicated that the keyed joint was marginal but would perform satisfactorily provided the slabs were adequate for the flexural stresses generated by the load with an appropriate design factor (not overloaded). Thus, the early failure of the joint under the MWHGL traffic points to a difference between these multiple-wheel gears and those comprising fewer wheels, even though the individual wheel loadings are not different. It is believed that the increased flotation realized by the addition of more wheels results in lower bending stresses in the slab; thus thinner slabs can be utilized. This results in smaller keys or keyways and smaller areas of concrete for load transference from one slab to another. Since total load is higher and deflections are increased, the joint attempts to transfer more load across the joint than the available concrete area can achieve and thus failure occurs.

Because both the keys and keyways failed without a significant pattern, the optimal key and keyway dimensions adopted by the Corps of Engineers are considered valid. No purpose would be served by constructing a larger key since this would reduce the keyway section and cause it to fail. The same is true should the keyway be redesigned to give more strength, which would reduce the key size and result in failure. It may be possible to achieve a satisfactory keyed-joint design by thickening the slab edge, which would permit increasing both key and keyway dimensions.

The transverse contraction (weakened-plane) joints, which depend upon aggregate interlock for load transfer, performed satisfactorily under the MWHGL traffic. There was no faulting of the joints, which would indicate loss

80

of the interlock, nor was there evidence of premature longitudinal cracking, which would indicate inadequate load transfer. It is pointed out that the orientation and geometry of the 12-wheel gear were such that these joints were not required to transfer as much shear as the keyed longitudinal joint.

4. SUBGRADE BEHAVIOR

The lean clay (CL) and heavy clay (CH) subgrade materials were placed at a density and water content that would yield the desired CBR of 4 (k value of 100 lb/cu in.) and remain essentially constant during the test program. Laboratory tests indicated compaction water contents of 21 and 30 percent for the lean and heavy clays, respectively, for the desired strength after soaking. The clay subgrade materials were compacted to at least 95 percent of the CE 55 maximum density at these water contents. This resulted in densities of between 80 and 90 percent of the maximum CE 55 density at optimum water content. At the compacted water content and density, both clay materials were essentially saturated.

In rigid pavement design and analysis, the subgrade strength is described by the subgrade modulus or k value. The subgrade modulus is essentially a spring constant that represents the pressure required to produce a unit deflection and is determined by a plate bearing test using an essentially rigid plate. The plate bearing test consists of loading a 30-in.-diam plate and observing the load-deflection curve at incremental loadings up to 30 psi. The k value is defined as the ratio of the 10-psi load to the plate deflection occurring under the 10-psi load. For low-strength subgrades, the requirement to produce a load-deflection curve is waived, and the k value is determined by loading the plate to 10 psi directly and observing the plate deflection. This abbreviated procedure was used to determine the subgrade modulus following construction and before traffic. The k values for the various test items ranged from 62 to 74 lb/cu in., which was slightly lower than the design value of 100 lb/cu in., but indicated very uniform subgrade conditions.

Changes can occur in the subgrade material under rigid pavements as the result of environmental conditions (mainly water content), inherent soil properties such as thixotropy, or manipulation of the soil by traffic loading. Such changes are reflected as changes in the subgrade modulus. Following the completion of traffic, plate bearing tests were performed on the surface of

81

the subgrade directly beneath the pavement in each test item of both paving lanes. The incremental loading procedure was used for these tests, and load-deflection curves were produced at each test location. While this is more accurate than the abbreviated procedure used before traffic, it sometimes requires some judgment in interpretation of results. When the load-deflection curve is nonlinear, a correction is necessary and is accomplished by drawing a straight line through the portion of the load-deflection curve having the least curvature. This straight line is projected through the origin, and the deflection is determined from the straight line at a 10-psi unit load. The load-deflection curves for the plate bearing tests conducted at the conclusion of traffic were nonlinear, requiring the corrections described above (see Volume II). The resulting k values varied from 59 to 169 lb/cu in. a much greater variation than that obtained before traffic and, in general, indicated a significant increase in the k value. The changes in k value appeared to follow the drainage pattern and to be somewhat associated with the pumping that occurred. The low value of 59 lb/cu in. was measured in item 3 in the south lane, which had the lowest elevation and was where the greatest pumping occurred. The highest value of 169 lb/cu in. was measured in item 1 in the north lane, which had the highest elevation and little or no pumping occurred.

In the after-traffic test program, no major variations in water content between as-constructed and after-traffic test values were noted that would explain the relatively large increase in the k values. Densification of the subgrade material due to traffic was ruled out as a possibility, as marked increases in subgrade densities were not found and the water content indicated near saturation of the soil, making undrained compaction almost impossible. It is probable that the increase in the k values was due primarily to the thixotropic properties of the clay soil rather than to envionmental effects or manipulation under traffic.

The permanent deformations experienced under the MWHGL traffic were greater than those encountered previously under more conventional wheel arrangements on other test tracks and operational pavements. Under the 12-wheel traffic, maximum permanent deformations as determined from level readings were 1.08, 0.96, 1.44, and 1.56 in. in test items 1, 2, 3, and 4, respectively. Similarly under the twin-tandem traffic, permanent deformations of 0.84, 0.48, 0.48, and 1.68 in. were recorded in test items 1, 2, 3, and 4, respectively.

Of these, only the permanent deformation in item 3 under the 12-wheel traffic appears out of line with the other items and is undoubtedly due to the excessive pumping that occurred in that item. As with the increases in k values, the large permanent deformations could not be attributed to densification of the subgrade materials. No marked change in water content or density was noted, which is consistent with the fact that the subgrade material was near saturation and undrained consolidation or densification under traffic was almost impossible. Some of the permanent deformation as well as some of the transient deflection, which was also large, probably resulted from the pumping that occurred; however, it is believed that the major portion of the permanent deformations recorded was the result of a lateral plastic flow of the saturated subgrade materials directly beneath the rigid slab. Large permanent and transient deflections should be anticipated on rigid pavements subjected to operations of MWHGL aircraft, and some loss of crown may result. If various soil types are present, some differential settlement may occur. Apparently, multiple-wheel assemblies are quite efficient in distributing flexural stresses in the pavement slab but require more work from the supporting materials than, for example, conventional twin or twin-tandem assemblies. These results point to the need for stronger foundations and increased density requirements in the foundation materials.

5. PAVEMENT REQUIREMENTS

    a. Pavements for the C-5A Aircraft

    Rigid pavements subjected to C-5A operational traffic fall into two categories, each of which requires slightly different criteria: (1) existing pavements, requiring evaluation criteria, and (2) new pavements, requiring design criteria. Existing criteria are available for both evaluation and design of airfield pavements.

    The existing evaluation criteria appear to be applicable for pavements serving the C-5A aircraft with the following exceptions. A major problem in evaluation lies with the jointing and load-transfer systems of existing pavements. Most existing pavements having the thickness required for operation of the C-5A aircraft will have been constructed using keyed construction joints. Based upon the results of the MWHGL traffic tests, such pavements constructed on low-strength subgrades will experience rapid joint deterioration

with a subsequent increase in edge stress and shortened pavement life. Although not demonstrated in the test track, pavements with keyed construction joints on medium- to high-strength subgrades may also experience rapid joint deterioration under C-5A aircraft traffic. Existing pavements resting on pumpable foundations can be expected to experience pumping, depending on soil type, moisture conditions, drainage, and traffic volume, which will result in loss of subgrade support to the pavement slabs and shortened pavement life.

For design criteria, use of the Westergaard analysis for the determination of edge stresses appears to yield reasonable results for multiple-wheel gear loadings under static and quasistatic loading conditions. Typical design curves for new pavements to serve the C-5A aircraft are shown in figure 91. These curves are based on the Westergaard analysis with associated design factors for 12,000 passes of the C-5A aircraft. For the C-5A aircraft a pass is defined as one takeoff and one landing.

For new construction, the use of doweled or thickened-edge construction joints regardless of subgrade strength is preferred over the use of keyed construction joints. The use of adequately designed filter courses of stabilized layers between the rigid pavement and pumpable subgrade materials should be used, and increased compaction requirements for the foundation materials should be considered.

b. Pavements for Boeing 747 Aircraft

The existing Corps of Engineers method of evaluating pavements for the Boeing 747 aircraft is recommended for use insofar as pavement thickness is concerned. Although traffic was applied with only a twin-tandem bogie of the aircraft, inferences can be drawn from such traffic and from the 12-wheel-assembly traffic that would be applicable to the Boeing 747. The keyed construction joints in existing pavements are suspect, and a rapid joint deterioration with subsequently increased pavement stresses and shortened pavement life should be anticipated under Boeing 747 aircraft traffic. This is particularly true for existing civil airports that contain keyed joints with a root dimension of 0.3 times the pavement thickness. This root dimension results in an overly strong key and resulting weak keyway. The design has since been changed but quite a large number of keyed joints were constructed utilizing this design. The above is especially true of pavements constructed on low-strength subgrades, and, while not demonstrated by the MWHGL tests,

is probably true for pavements on medium- to high-strength subgrades. Pavements on pumpable foundations will probably experience some degree of pumping (depending on soil type, moisture conditions, and traffic volumes) with a loss of subgrade support and shortened pavement life.

For new construction to serve the Boeing 747 aircraft, the use of Westergaard equations for computation of pavement stresses and the existing Corps of Engineer design method yield reasonable results for development of rigid pavement thickness requirements. The use of doweled or thickened-edge construction joints in lieu of the keyed construction joint, adequately designed filter or base courses or stabilized layers to prevent pumping, and increased compaction requirements for the foundation materials similar to that discussed for the C-5A aircraft is also recommended for the Boeing 747 aircraft. Typical design curves for the Boeing 747 are shown in figure 92. These curves are based on Westergaard analyses with associated design factors for 100,000 passes of the Boeing 747 aircraft. A pass is defined as one movement of the 747 past one specific point.

6. DESIGN METHOD

Rigid pavement thickness requirements[6] for the C-5A and Boeing 747 aircraft can be determined using figures 91 and 92. Before these figures can be used, the pertinent properties of the foundation and concrete materials must be determined. These properties are the modulus of subgrade (foundation) reaction k, which is determined by plate loading tests, and the modulus of rupture (flexural strength) R of the concrete determined by third-point loading beam tests. The curves (figures 91 and 92) have been prepared assuming a constant modulus of elasticity of concrete of 4×10^6 psi and a Poisson's ratio of 0.20. These values are found to be representative of high-quality paving concrete mixtures. The design curves are entered with R (see figures 91 and 92), and a horizontal projection is made to the line representing the k value. A vertical projection is then made to the intersection of the line representing the design aircraft main assembly load, and a horizontal projection is next made to the scale representing required pavement thickness.

---

[6] The design curves presented herein for the C-5A and Boeing 747 (figures 91 and 92) are not to be used as design criteria but serve only to illustrate the design methods that can be developed.

The thickness thus determined is that required for the volume of traffic used to develop the design curve (12,000 passes for C-5A and 100,000 passes for Boeing 747) and is based upon edge loading and the assumption that 25 percent of the load on the edge of one slab is transferred to the adjoining slab through appropriate load transfer devices constructed in the joint. Design curves can be developed for other concrete properties, loading conditions (interior or corner), joint load transfer, or aircraft traffic volume.

SECTION X

CONCLUSIONS

Based on the results of the tests of the flexible and the rigid pavement sections, the following conclusions are believed justified.

1. FLEXIBLE PAVEMENT

    a. Analysis of Behavior Under Traffic

    (1) Based on the results of the MWHGL tests, the basic CBR design method has been modified to obtain a method of design and evaluation for flexible pavements subjected to MWHGL aircraft traffic. This procedure reflects a reduction of thickness requirements of existing multiple-wheel criteria, especially significant in the higher operational level. Using these concepts and procedures, the following behavioral pattern for thicknesses of pavement layers to properly design underlying layers to resist shear deformation was derived:

$$t \to \alpha_i \left\{ \sqrt{A} \left[-0.0481 - 1.1562 \left(\log \frac{CBR}{p_e} \right) - 0.6414 \left(\log \frac{CBR}{p_e} \right)^2 \right. \right.$$
$$\left. \left. - 0.4730 \left(\log \frac{CBR}{p_e} \right)^3 \right] \right\} \qquad (20a)$$

    (2) The pass concept in lieu of aircraft coverages is presented as being representative of aircraft traffic volume and has been related to actual lateral load applications at airfield facilities. Also, gross aircraft loadings are used to better reflect the total effect of the aircraft and to eliminate the necessity of assembly determination on aircraft similar to the Boeing 747 aircraft.

    b. Instrumentation

    WES-designed soil pressure cells, soil deflection gages, and pore pressure cells functioned satisfactorily with respect to accuracy, consistency, and survival. Only one soil pressure cell of seventeen installed and two of eighteen deflection gages were lost during the instrumentation tests.

    Performances of the commercial soil pressure cells and strain gages

were not acceptable for application in this type of investigation. The temperature probe used was satisfactory.

The optical technique of determining surface and reference-plane deflections was not sufficiently sensitive to reflect the magnitude of movement experienced by the flexible pavement structure.

c. Interpretation of Data

A thorough analysis of the soil deflections under load, as depicted by the deflection gages, was conducted and resulted in identification of a load- and position-dependent moving zero reference level for each deflection gage with no residual strains being induced. The soil at all levels appeared to be behaving as a plastic and elastic mass (for lack of better terms) similar to putty, but not as a viscoelastic material.

(1) Equivalent elastic deflections were found for equivalent loading situations, i.e., either repeated loadings of a gage or loadings at symmetrical loading points.

(2) An analysis of the soil stresses induced under load indicated an almost constant horizontal zero reference per soil pressure cell and the data indicated active residual stresses.

(3) Equivalent elastic stresses were found for equivalent loading situations, i.e., either repeated loadings of a gage or loadings at symmetrical loading points.

d. Results of Instrumentation Measurements

Due to the large amount of data available from both static and dynamic load tests and due to time limitations, only the maximum responses were evaluated.

(1) Maximum elastic deflection and maximum vertical elastic stress versus depth curves were established for static load test results. Data developed in the analysis showed that the same relationships are true for the static and dynamic load tests.

(2) The dynamic load and speed test results showed that elastic deflections and stresses are not affected by the range of speeds used in the

MWHGL tests (1-10 mph) and that the dynamic load test results are approximately equivalent to the static load results.

(3) The pavement temperature effects study was inconclusive due to the limited range of temperatures, and the pavement strains study yielded no appreciable results due to the unreliability of the strain gages used.

e. Analysis of Soil Behavior Patterns

Limited study of soil behavior patterns indicated the following:

(1) Elastic deflection comparisons and elastic vertical stress comparisons for item 3 versus item 4 showed that the stress and deflection distributions of the two items were different. The difference was caused by the soft layer in item 4. Even though the instrumented items have different strain distributions characteristics, if log-log plots of wheel load versus deflection are made, the two items show the same behavior patterns; only the magnitude of the deflection values is different.

(2) Assuming elastic behavior, theoretical predictions of deflection versus depth or of offset versus deflection are not good except for a single-wheel load.

(3) Analysis of behavior patterns shows that behavior under a single-wheel load is different from that under a multiple-wheel assembly.

(4) Based on the analysis, the principle of superposition is not valid, and the stress-strain characteristics of the soil are nonlinear and dependent on stress level.

2. RIGID PAVEMENT

a. Analysis of Behavior Under Traffic

(1) The Westergaard algorithm can be used to calculate strains and deflections in rigid pavements under MWHGL; however, the validity becomes questionable as the number of wheels and wheel spacings increase.

(2) Traffic volume factors developed from previous traffic tests with other gear configurations and loadings were applicable for the MWHGL.

(3) The existing Corps of Engineers evaluation and design methodology will yield reasonable results for pavement thickness requirements for the MWHGL.

(4) Strain measurements indicate higher strains at the edges of the slab under edge loadings than in the interior of the slab under interior loadings.

(5) The keyed longitudinal construction joint failed under traffic, raising a question regarding its applicability in pavements constructed on low-strength subgrades for MWHGL. Although not evaluated in these tests, the adequacy of the keyed joint in pavements constructed on medium- and high-strength subgrades that are subjected to MWHGL is suspect.

(6) Considering the large number of wheels and their arrangement on the multiple-wheel gears and after examining the pavement strain pattern from a pass of the gears, the coverage concept for describing traffic on the pavement is quite difficult to apply and a better method is needed.

(7) When rigid pavements are constructed on fine-grained soil foundations and subjected to MWHGL, severe pumping can be anticipated, and positive protection against pumping must be provided.

(8) MWHGL assemblies will stress the subgrade materials to a much greater depth than current landing-gear assemblies and loads.

(9) Both transient and permanent deflections experienced under the MWHGL assemblies were large and pointed to the need to consider increased compaction requirements in the foundation materials.

b. Instrumentation and Equipment

(1) The techniques employed to install the instrumentation were satisfactory except for those used to install the embedded strain gages. The high loss of the strain gages, which occurred early in the test program, indicates that either different installation techniques are necessary for the Valore-type gage or a different type strain gage should be used. The Valore-type gages that were bonded to the pavement surface rather than embedded in the concrete performed satisfactorily and gave reasonably good results.

(2) The DC LVDT displacement transducers used to measure deflection gave good results; however, a relatively high loss of gages was experienced. The loss was attributed to failures in the gage electronics, probably due to a shorted circuitry.

(3) Very little information of value was obtained from the soil

pressure cells, which were installed at the slab-soil interface and within the soil mass. The signals from the cells were erratic; however, the cause was not definitely established. The performances of these cells were not unlike the performance of the same type cell used in the flexible pavement tests.

(4) A Dynaflect testing device yielded results that indicate that it can be used as a qualitative evaluation device and that seemed to indicate differences in deflection basins for different pavement thicknesses, for when the slab was warped, and for when there was a reduction in subgrade support due to pumping. However, analyses to date of the data obtained indicate that the Dynaflect is of little value in providing quantitative data on airfield pavement strength or condition. This is perhaps due to the lack of correlation between pavement performance and changes in the elastic modulus of the subgrade, which may be resolved by further tests and data analysis.

c. Results of Instrumentation Data

(1) Measured recoverable deformations at the 3-, 5-, and 9-ft depths in the subgrade were less than those predicted by a composite analysis involving the finite element analysis and the semi-infinite elastic half-space analysis. Actually, closer agreement was achieved between theory and the measured nonrecoverable deformations. This is probably a coincidence since both analyses assumed that elastic behavior occurred in the pavement system, which includes the subgrade.

(2) All measured strains were less than those predicted by the finite element representation of the Westergaard analysis.

(3) The strain gage readings indicated that for the 12-wheel gear, maximum strains occurred when the 4 wheels abreast were directly over the gage; however, the strain occurring under the 2 wheels abreast was approximately 80 to 90 percent of the maximum. Between the two 6-wheel arrays, the strain relaxed to about 25 percent of the maximum strain, and between the 2- and 4-wheel-abreast arrays, the strain relaxed to about 60 percent of the maximum strain. This strain pattern indicated that the pavement is subjected to several significant strain excursions as the 12-wheel array passes.

(4) Under the 4-wheel gear, the maximum strain occurs under the 2-wheel array with some strain relaxation between the two 2-wheel arrays.

91

The magnitude of strain relaxation between the two 2-wheel arrays is dependent upon the pavement thickness.

    (5) Generally, there were only slight increases in both strain and recoverable deformation with traffic.

3.   NONDESTRUCTIVE VIBRATORY TESTING

    a. Wave velocity values of the lower layers are slightly greater when measured from the pavement surface than when measured directly on top of the lower layer.

    b. Steady-state vibratory loadings appear to stress the pavement structure in a manner similar to static prototype loads.

    c. Indications are that vibratory load-deflection data can be extrapolated with some degree of accuracy to predict elastic surface deflections beneath prototype loads.

SECTION XI

RECOMMENDATIONS

Based upon the performance of the flexible pavement test items under the various loading conditions as reported herein, it is recommended that:

a. The methodology presented in this report be used for the development of flexible pavement design and evaluation criteria, and all existing criteria be modified to reflect the results of this study. A detailed instruction report should be prepared presenting the procedures to be used in the development of a set of CBR design and evaluation curves.

b. Further theoretical studies be accomplished using the MWHGL traffic and instrumentation data.

c. Further investigations be made of flexible pavement subbase movements under MWHGL traffic.

d. The effect of stabilizing subbases be determined with particular regard to the prevention of subbase movement.

e. Studies be initiated to develop asphalt mix design criteria for pavements subjected to fatigue cracking, as occurred under the MWHGL traffic.

f. A method or instrument for accurately measuring strains in pavements be developed.

Based upon the performance of the rigid pavement test items under the traffic testing, it is recommended that:

a. Doweled, thickened-edge keyed or thickened-edge butt joints be used for new pavements constructed on low-strength foundations to serve MWHGL aircraft; keyed longitudinal construction joints should not be allowed. Additional studies of keyed joint behavior in pavements constructed on medium and strong foundations utilizing filter courses and subjected to MWHGL traffic are also recommended.

b. Consideration be given to increasing the compaction requirements in the foundation materials as a means of reducing excessive permanent deformations under MWHGL traffic. Additional studies to evaluate compaction requirements under MWHGL traffic are recommended. It is also recommended that consideration be given to use of stabilized materials to reduce excessive permanent deformation.

c. Consideration be given to the establishment of maximum allowable

deflections that can be tolerated in a rigid pavement structure.

d. Consideration be given to expanding the work already done in the area of repeated loadings of soils in triaxial compression and the behavior of soils in flexible pavements to establish allowable soil stresses under rigid pavements.

e. Embedment-type strain gages be placed by a method other than that used on this test pavement. Perhaps casting the embedment gages in a beam under laboratory conditions and then embedding the beam in the pavement would yield satisfactory results.

f. Further studies of the data collected be undertaken. For example, no attempt was made to account for environmental effects, which would normalize the data and might indicate trends that are not otherwise apparent.

Recommendations pertinent to both flexible and rigid pavements are as follows:

a. Analysis of data and results should be continued. Further and complete analysis of the large quantity of data and the soil behavior patterns of the MWHGL test section would provide a basis for a completely nonlinear-inelastic constitutive equation in terms of fundamental material constants that would provide a fundamentally correct thesis from which a rational pavement design and evaluation procedure could be developed.

b. The stochastic nature of airfield pavement loading should be approched from a statistical standpoint. Other disciplines have successfully employed statistical analysis of fatigue data. As aircraft increase in size, more emphasis is placed on the maximum utilization of existing and newly constructed pavements for use by the larger aircraft. This, coupled with increasing requirements regarding pavement performance and its effect upon the aircraft performance, points to the fact that much more sophistication is needed in pavement design. Simply designing for some number of loadings by the heaviest load may no longer be realistic. Therefore, designs that incorporate strain and/or deflection histories should be investigated as a means of analyzing the random loading characteristics.

Based on the results of the nondestructive tests, it is recommended that:

a. The equipment used to obtain the vibratory stiffness and deflection

94

basin data be improved and automated so that test results are readily available for inspection in the field.

_b_. The effects of such variables as the temperature of the asphaltic concrete layer and the size of the vibrator plate be further investigated.

_c_. Further analysis of the data collected be made.

Figure 1. C-5A Galaxy (Courtesy of Lockheed-Georgia Company)

96

AFWL-TR-70-113

PLAN VIEW
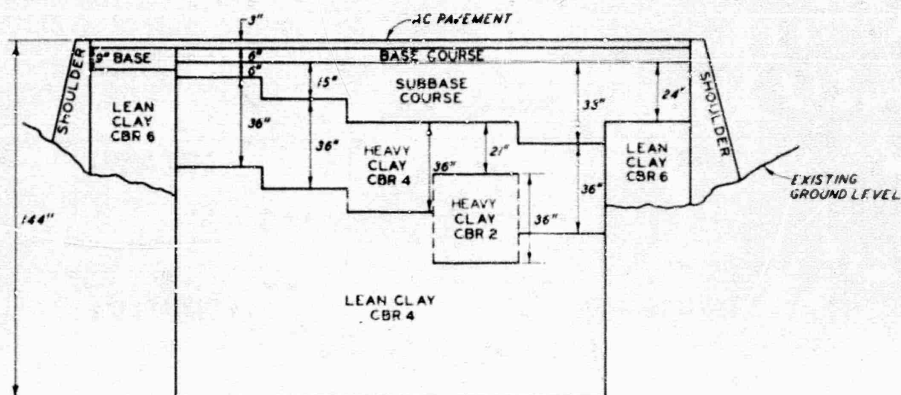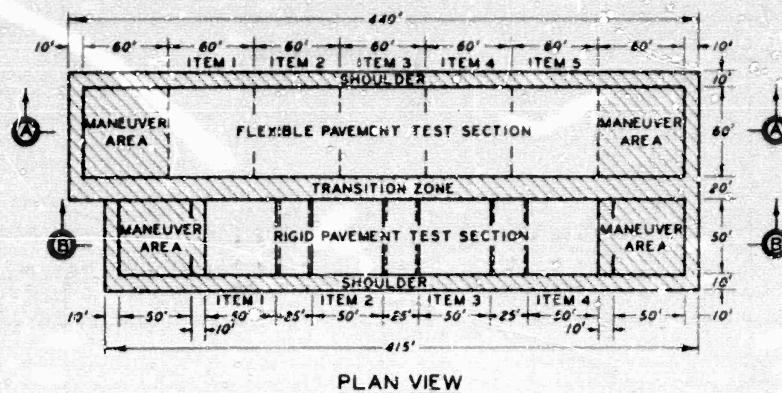
SECTION A-A
FLEXIBLE PAVEMENT TEST SECTION
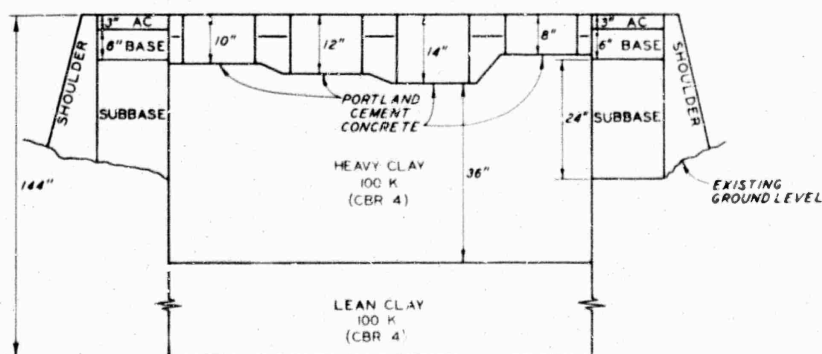
SECTION B-B
RIGID PAVEMENT TEST SECTION

Figure 2. Plan and Profile Views of the Flexible and Rigid
Pavement Test Sections

PLAN
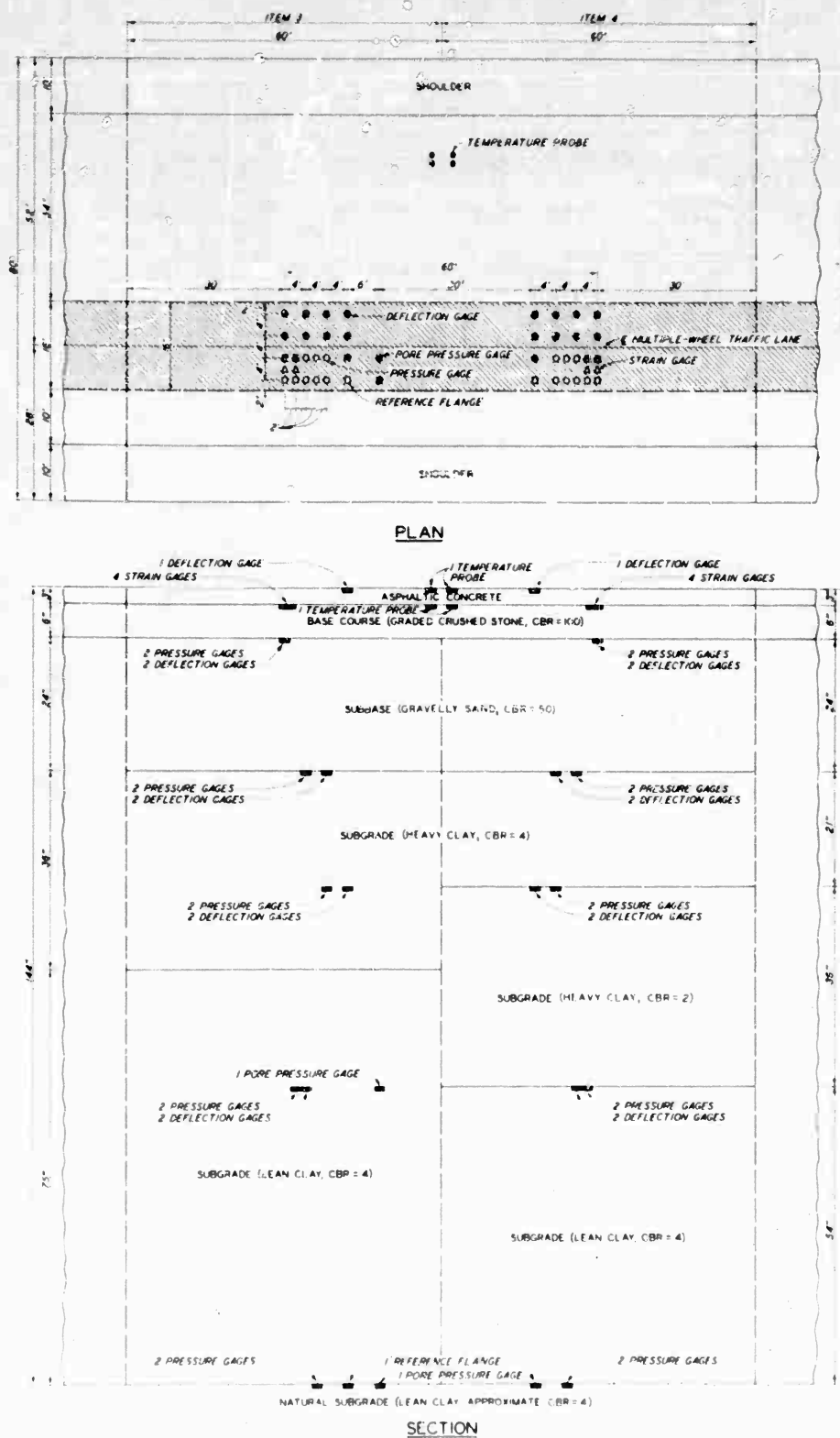
SECTION

Figure 3. Instrumentation Layout for Flexible Pavement Test
Section
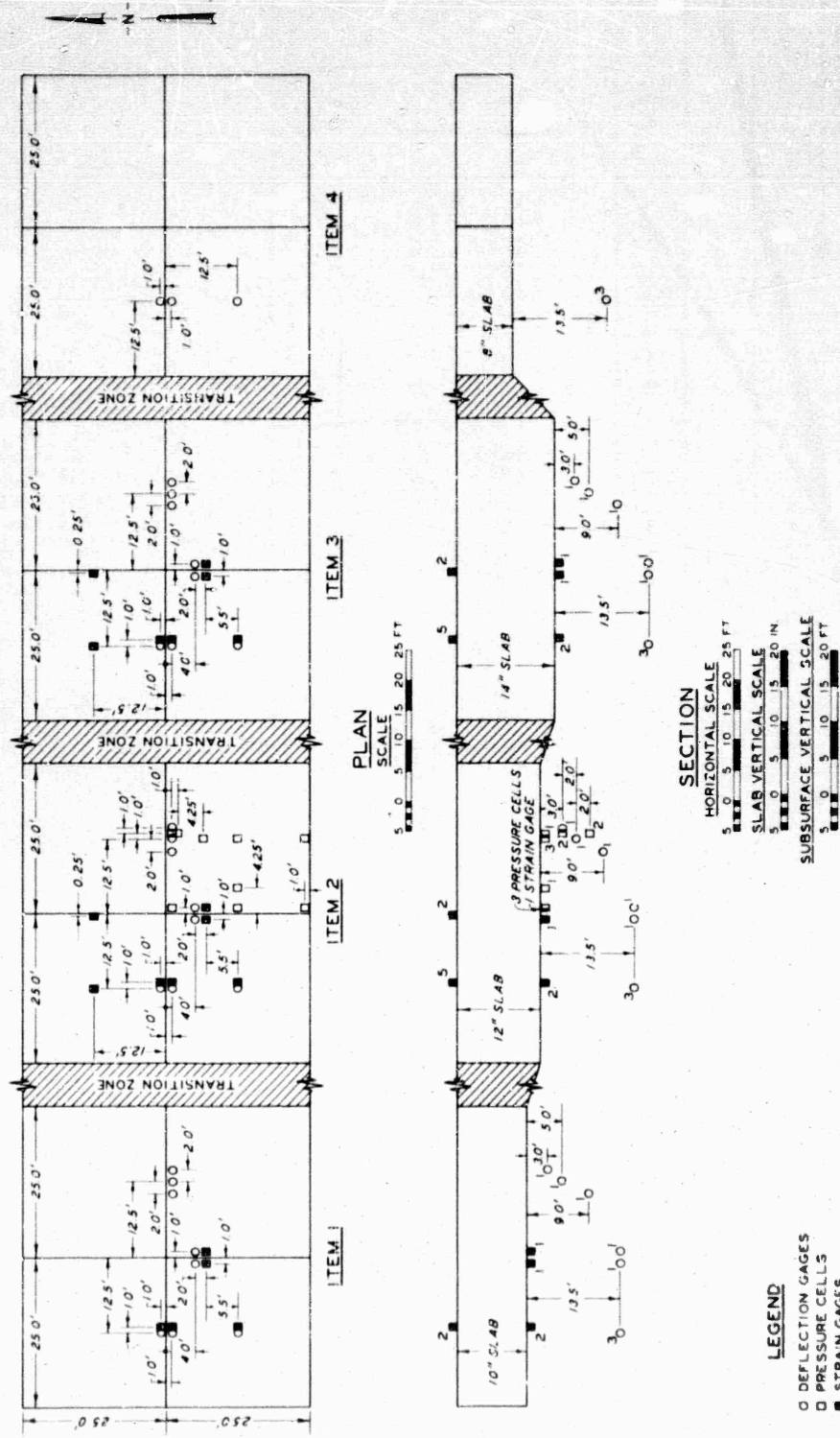
Figure 4. Instrumentation Layout for Rigid Pavement Test Section
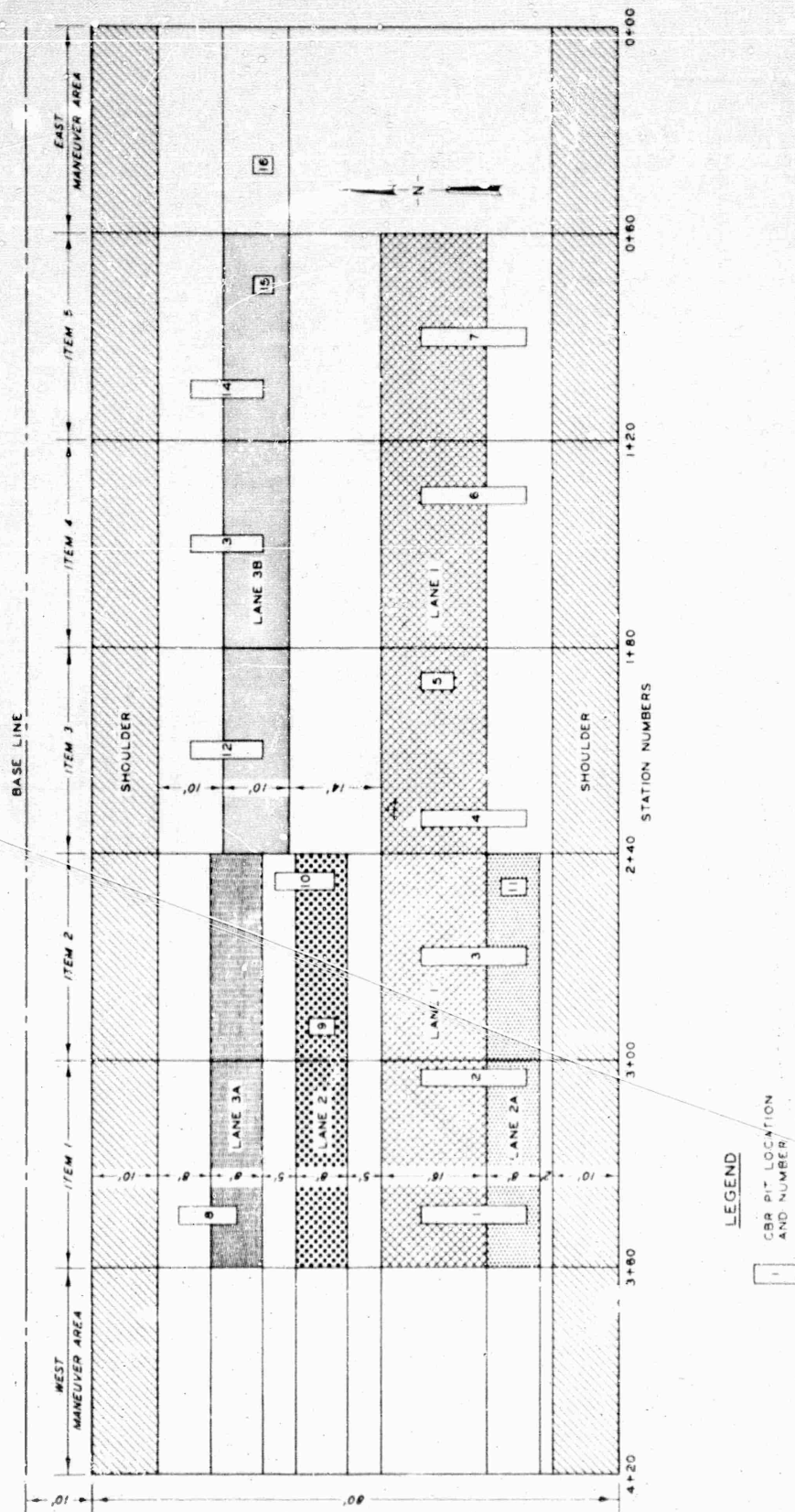
Figure 5. Layout of Flexible Pavement Test Lanes
(See Table 7 for Identification of Lanes)
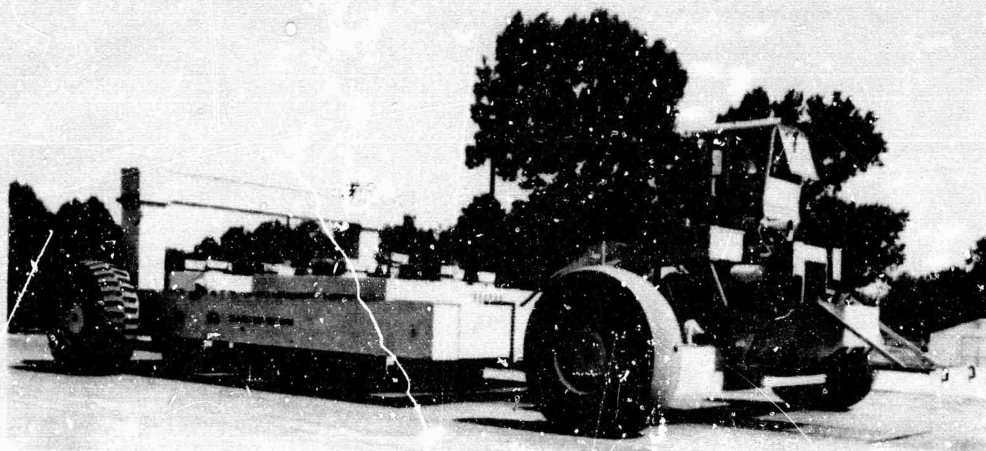
Figure 6. 12-Wheel-Assembly Test Cart
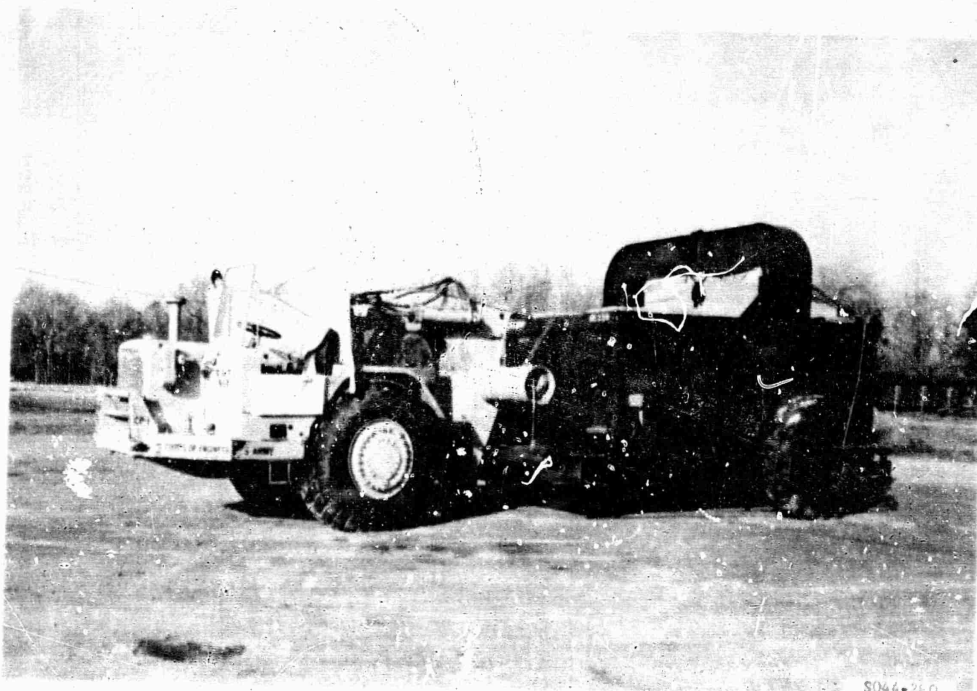
Figure 7. 240-kip Twin-Tandem-Assembly Test Cart

101

Figure 8. Traffic Patterns
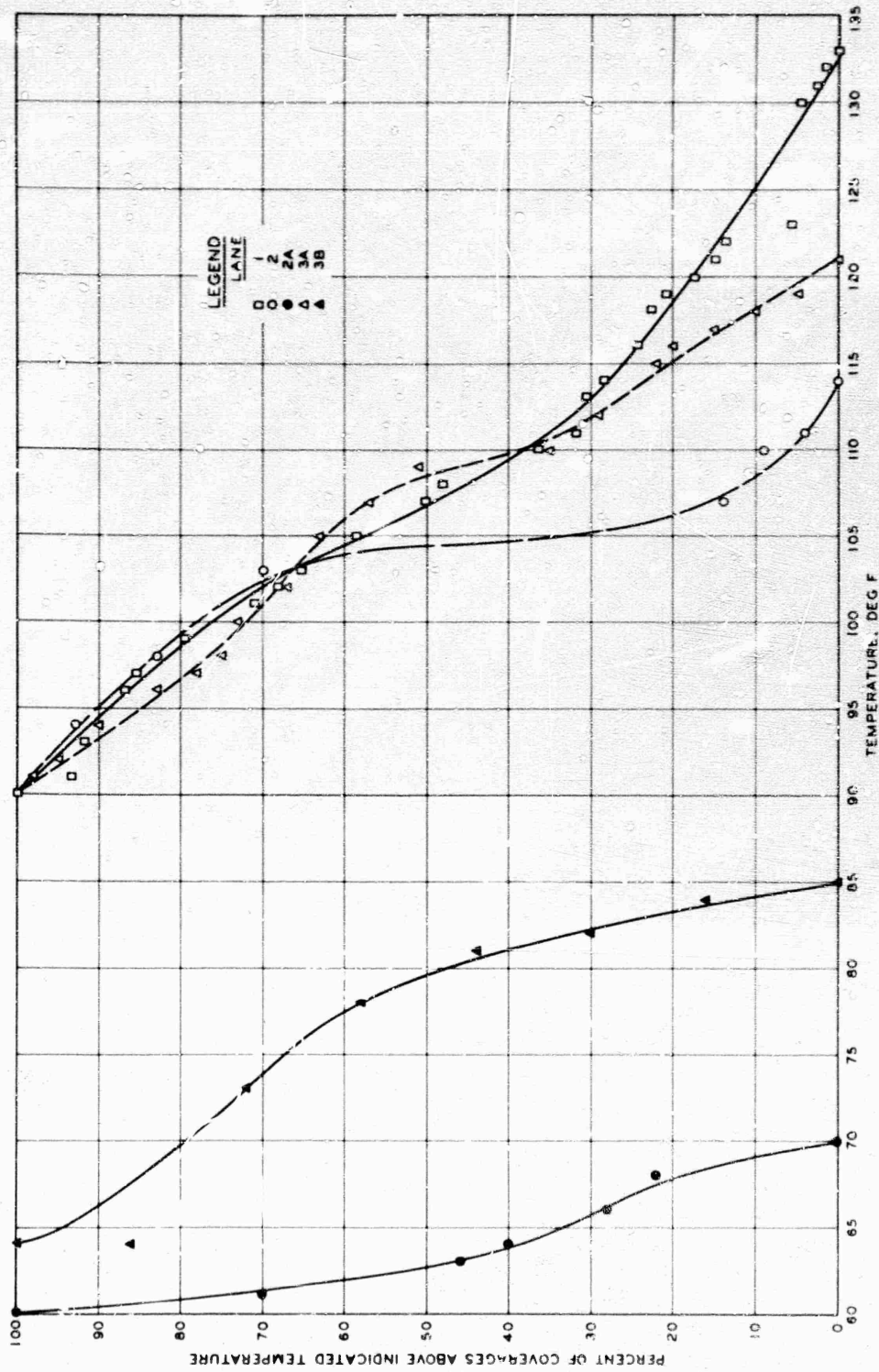
NOTE TEMPERATURES ARE THE AVERAGE OF THAT MEASURED
AT THE TOP AND BOTTOM OF THE PAVEMENT

Figure 9. Traffic and Pavement Temperature Distribution, Flexible Pavement Test Sections
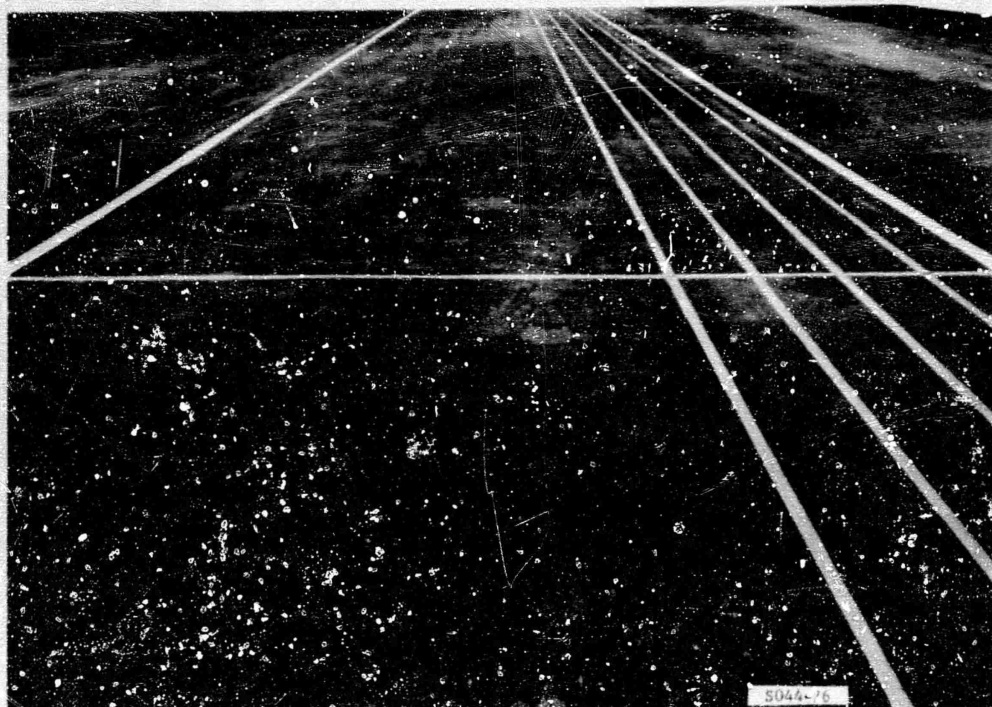
Figure 10. Typical View of Flexible Pavement Test Section Prior to Traffic

Figure 11.   Failure of Flexible Pavement in Item 1, Lane 1, Caused by
             Subgrade Shear Deformation
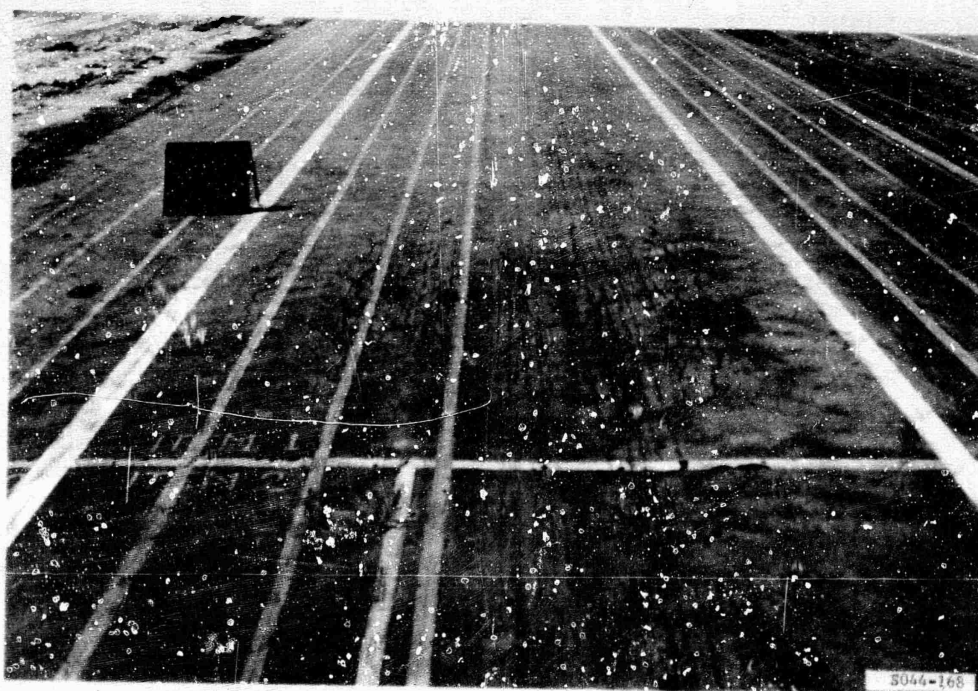
Figure 12.   Failure of Flexible Pavement in Item 1, Lane 2, Caused by
             Subgrade Shear Deformation
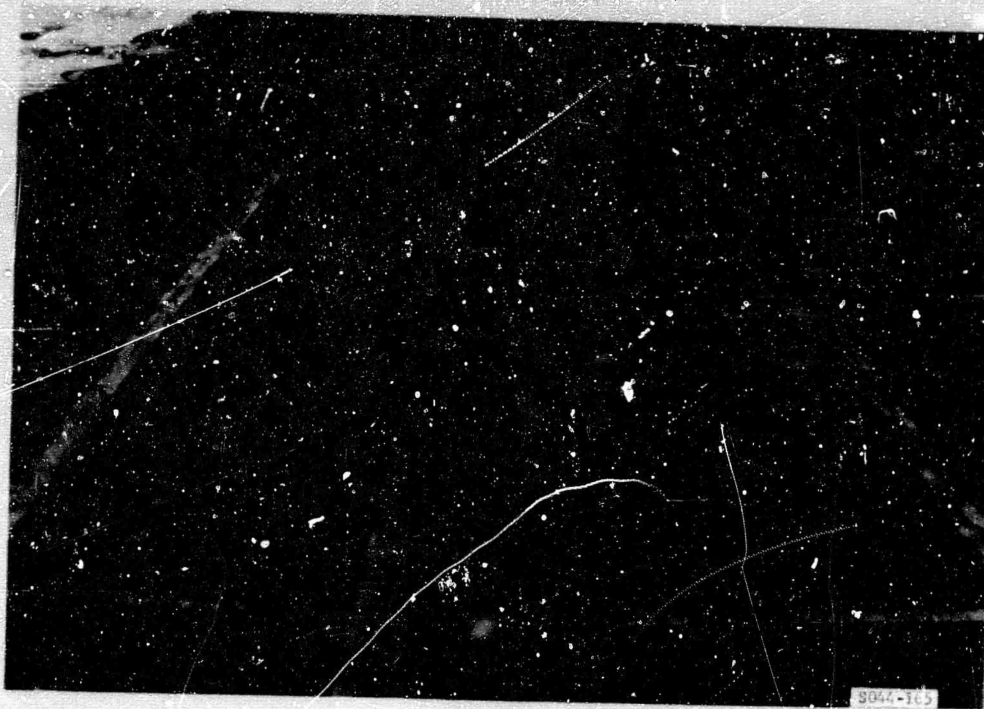
Figure 13. Failure of Flexible Pavement in Item 2, Lane 2, Caused by Subgrade Shear Deformation

Figure 14. Failure of Flexible Pavement in Item 1, Lane 2A, Caused by Subgrade Shear Deformation
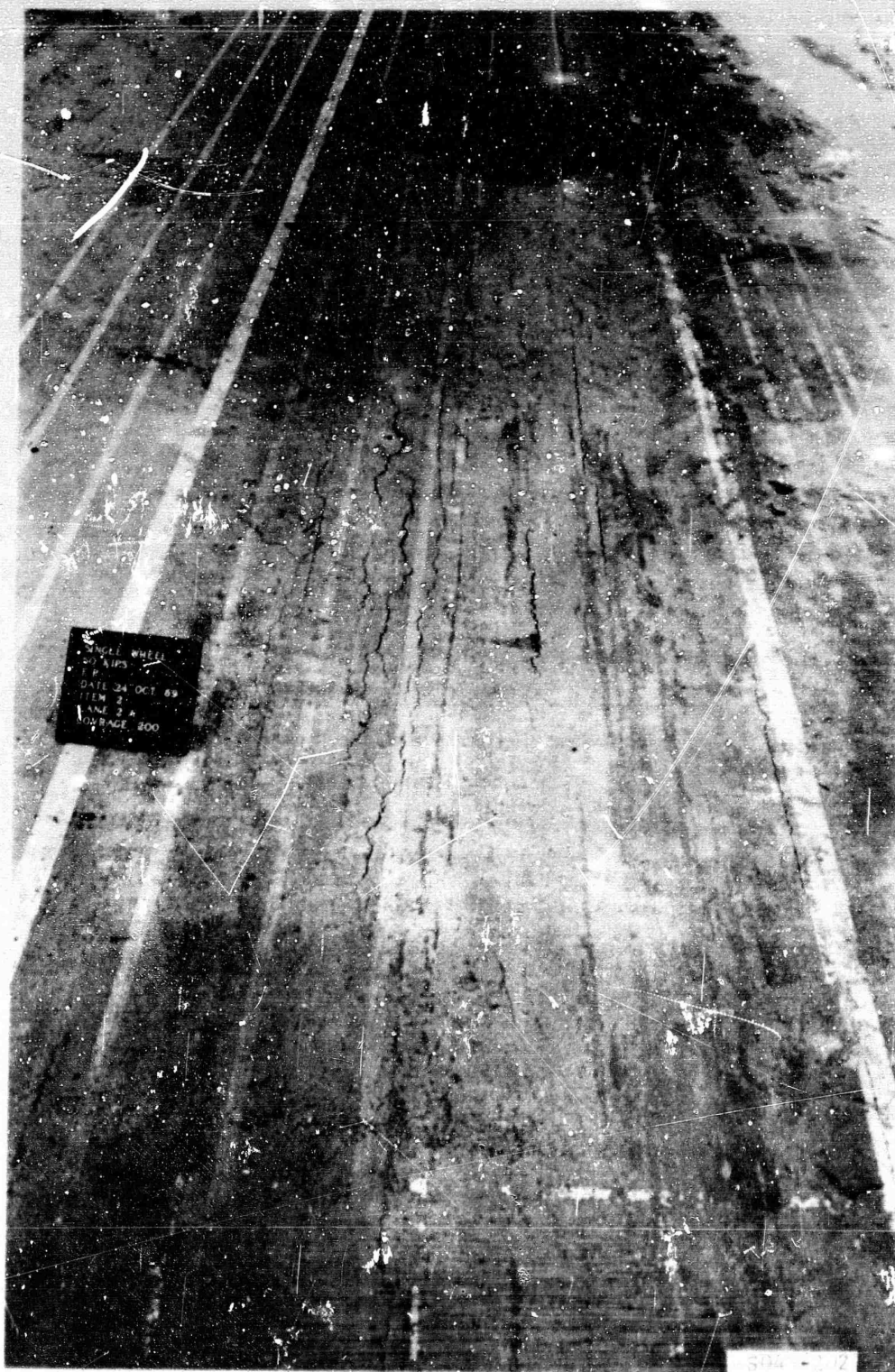
Figure 15.   Failure of Flexible Pavement in Item 2, Lane 2A, Caused by
             Subgrade Shear Deformation
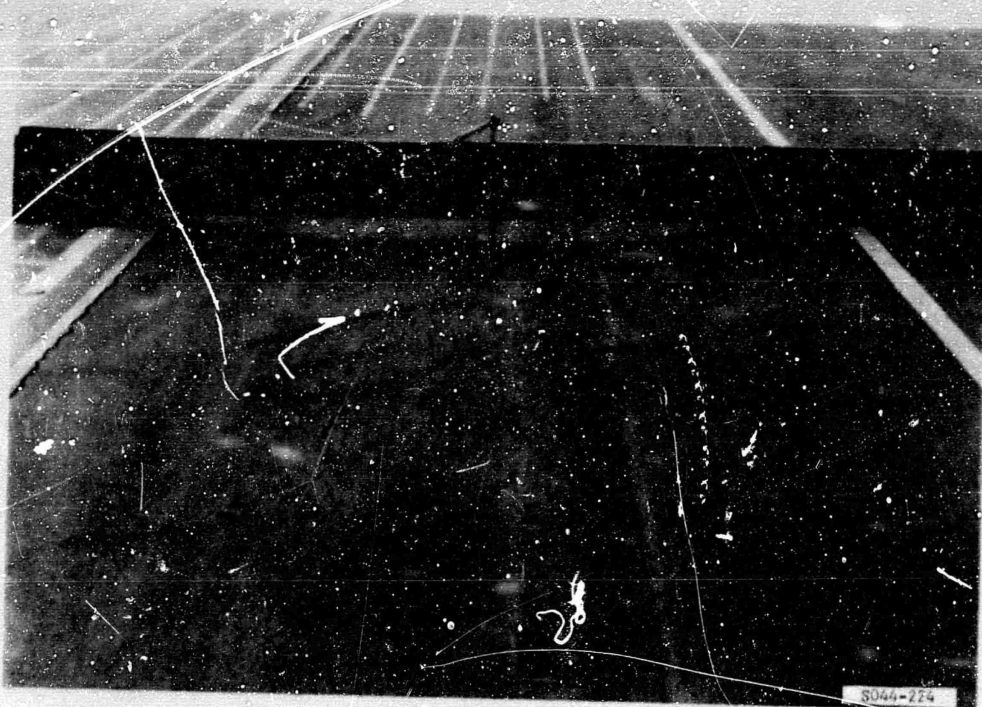
Figure 16. Failure of Flexible Pavement in Item 3, Lane 3B, Caused by Subgrade Shear Deformation
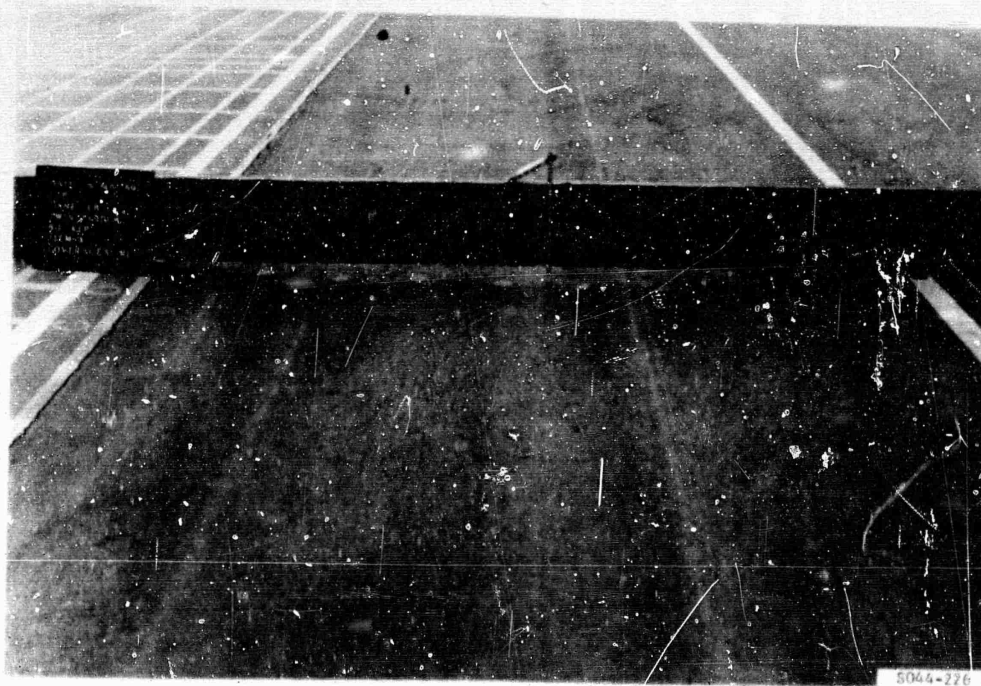
Figure 17. Failure of Flexible Pavement in Item 4, Lane 3B, Caused by Subgrade Shear Deformation
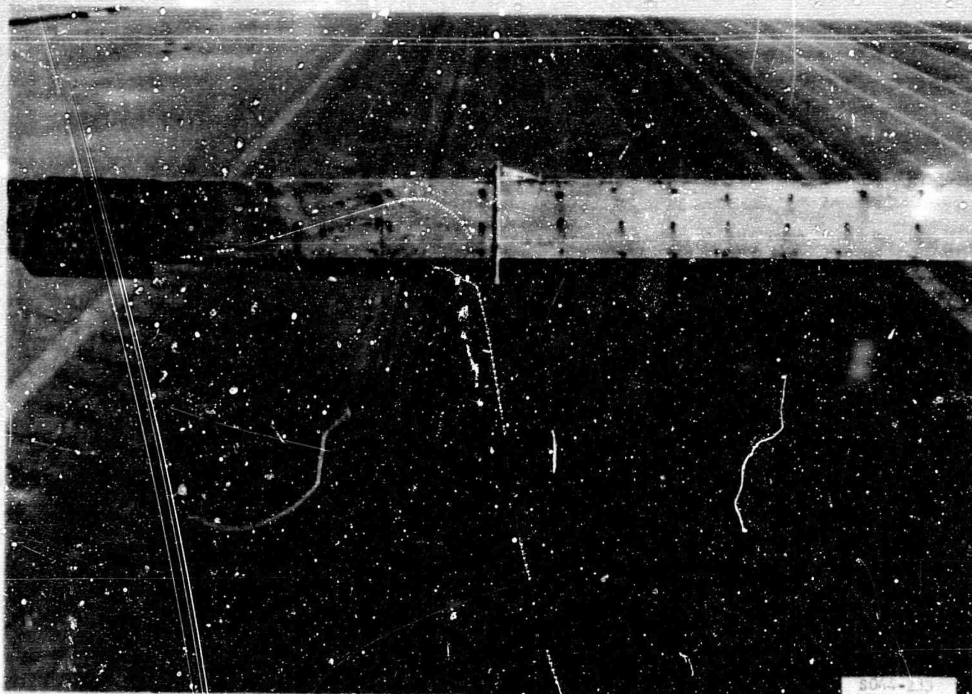
Figure 18. Failure of Flexible Pavement in Item 5, Lane 3B, Caused by Subgrade Shear Deformation
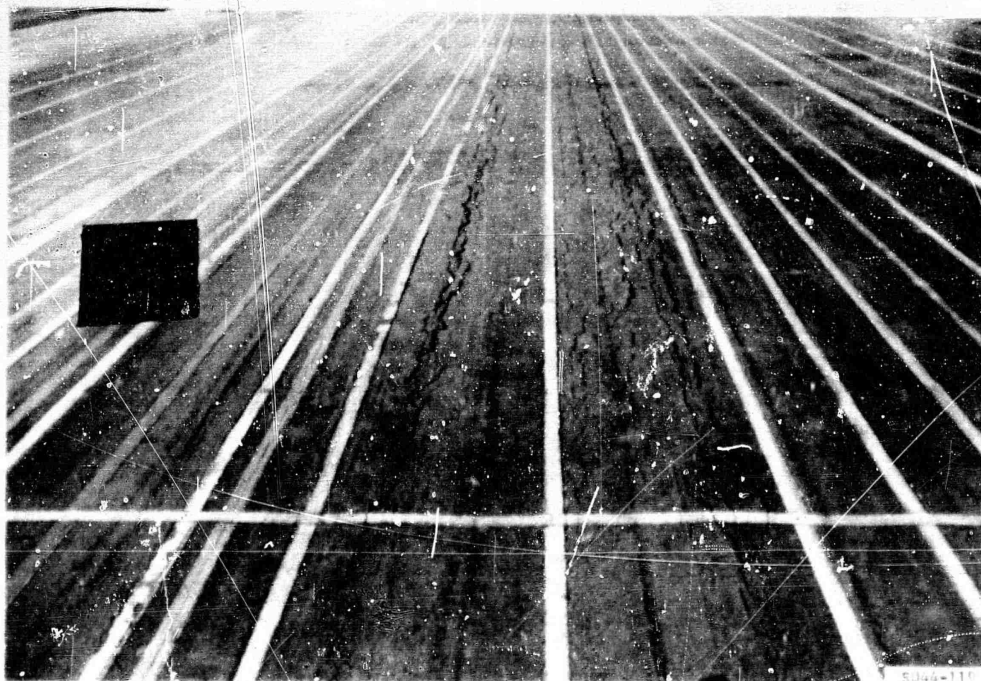
Figure 19. Failure of Flexible Pavement in Item 2, Lane 1, Primarily Caused by Fatigue Cracking Due to High Elastic Deformations

109

Figure 20.   Slab Removed from Flexible Pavement, Item 3, Lane 1,
After Failure, Showing Extent of Fatigue Cracking
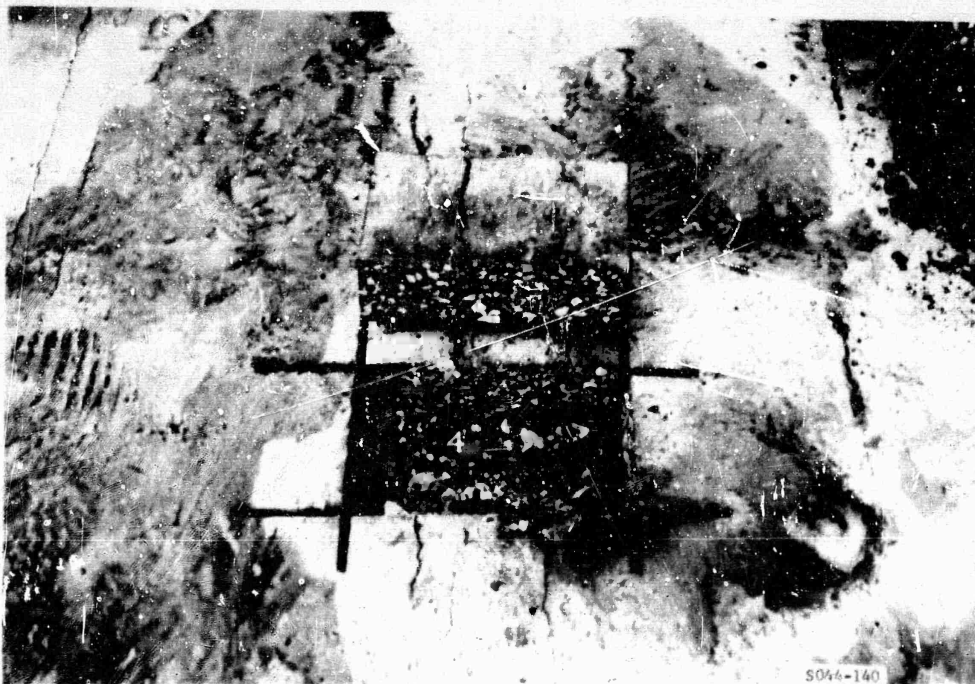
Figure 21.   Slab Removed from Flexible Pavement, Item 4, Lane 1,
After Failure, Showing Extent of Fatigue Cracking

NOT REPRODUCIBLE
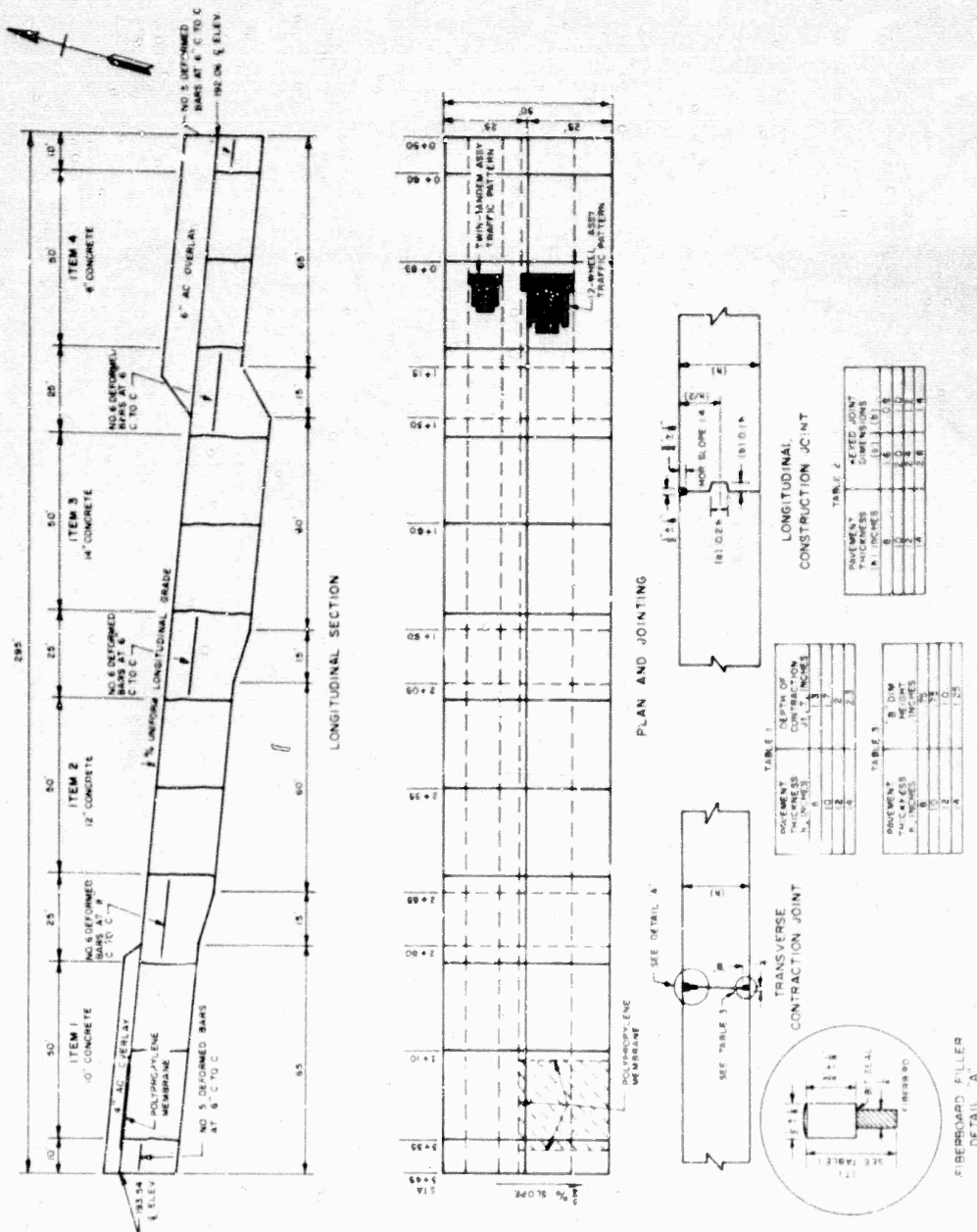
Figure 22. Plan, Profile, and Joint Details of the Rigid Pavement Test Section

111
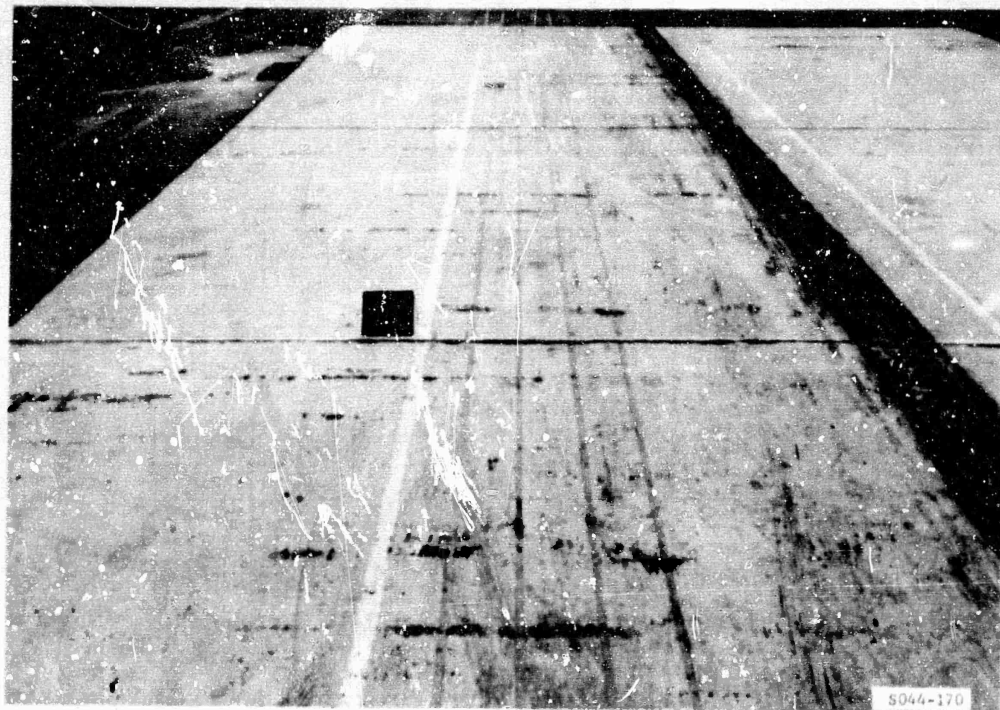
Figure 23. Condition of Rigid Pavement, South Lane, Prior to Traffic

Figure 24. Spalling Along Transverse Crack in SW Slab of Rigid Pavement
Item 1

113

Figure 25. Crack Pattern in Nonrigid Overlay of Item 1, South Lane, at Conclusion of 12-Wheel-Assembly Traffic
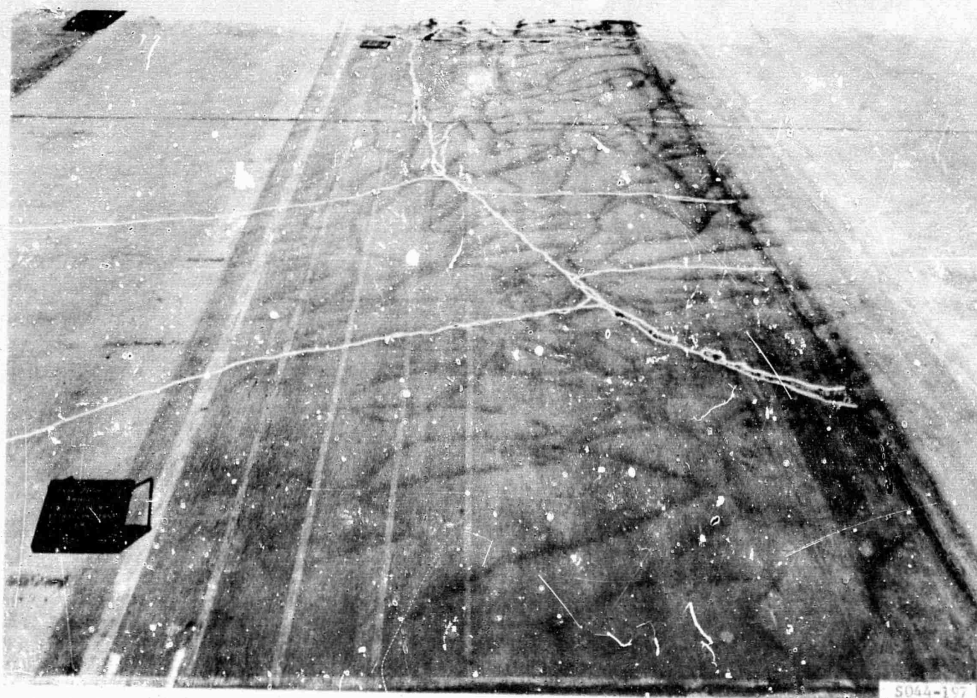
Figure 26. Crack Pattern in Rigid Pavement, Item 1, South Lane, Prior to Placement of Nonrigid Overlay

114 NOT REPRODUCIBLE

Figure 27. Condition of Item 2, South Lane, at Conclusion of 12-Wheel-Assembly Traffic
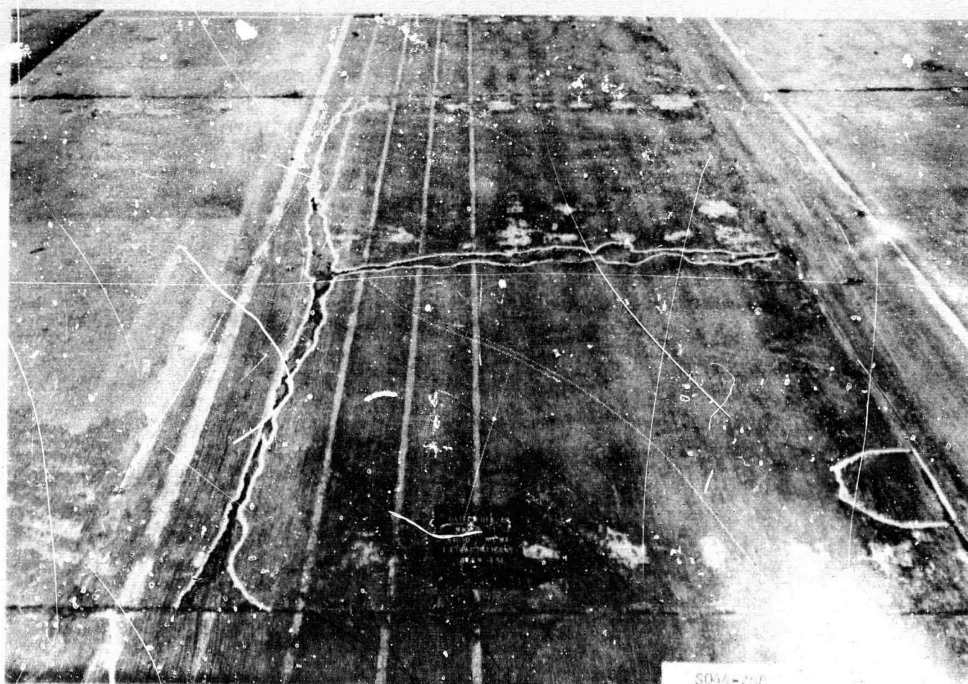
Figure 28. Condition of Item 3, South Lane, at Conclusion of 12-Wheel-Assembly Traffic

NOT REPRODUCIBLE

Figure 29.   Condition of Item 4, South Lane, Prior to Placement of
             Nonrigid Overlay
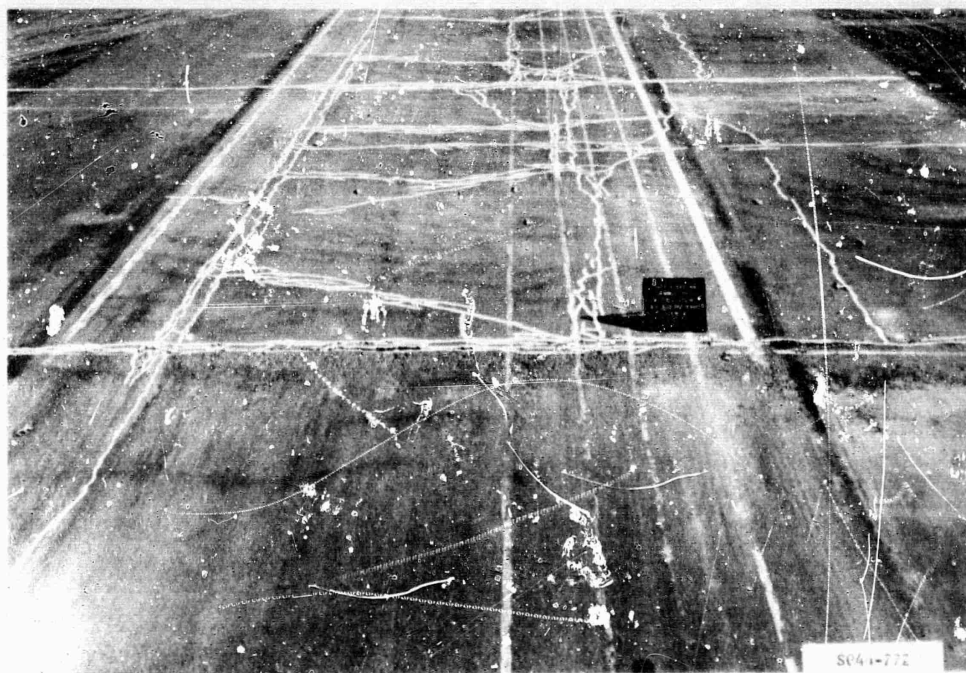
Figure 30.   Crack Pattern in Nonrigid Overlay of Item 4, South Lane, at
             Conclusion of 12-Wheel-Assembly Traffic

116

Figure 31.   Heavy Mud Pumped at South Edge of Item 4 Overlay, South Lane, SE Slab, During 12-Wheel-Assembly Traffic

Figure 32. Condition of Nonrigid Overlay, Item 1, North Lane, at the
Conclusion of Twin-Tandem-Assembly Traffic
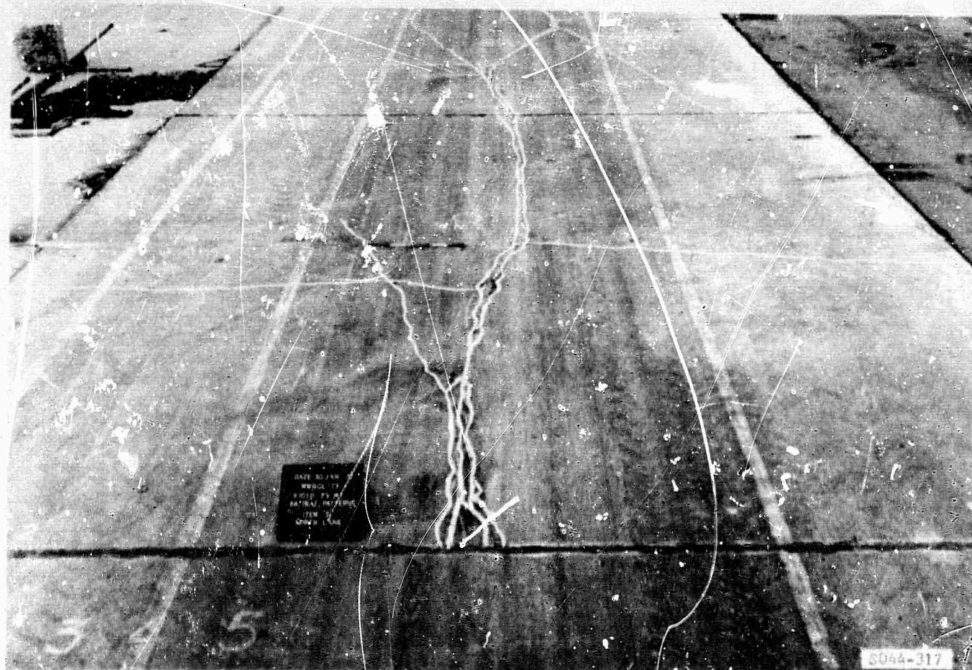
Figure 33. Condition of Item 2, North Lane, at the Conclusion of Twin-
Tandem-Assembly Traffic
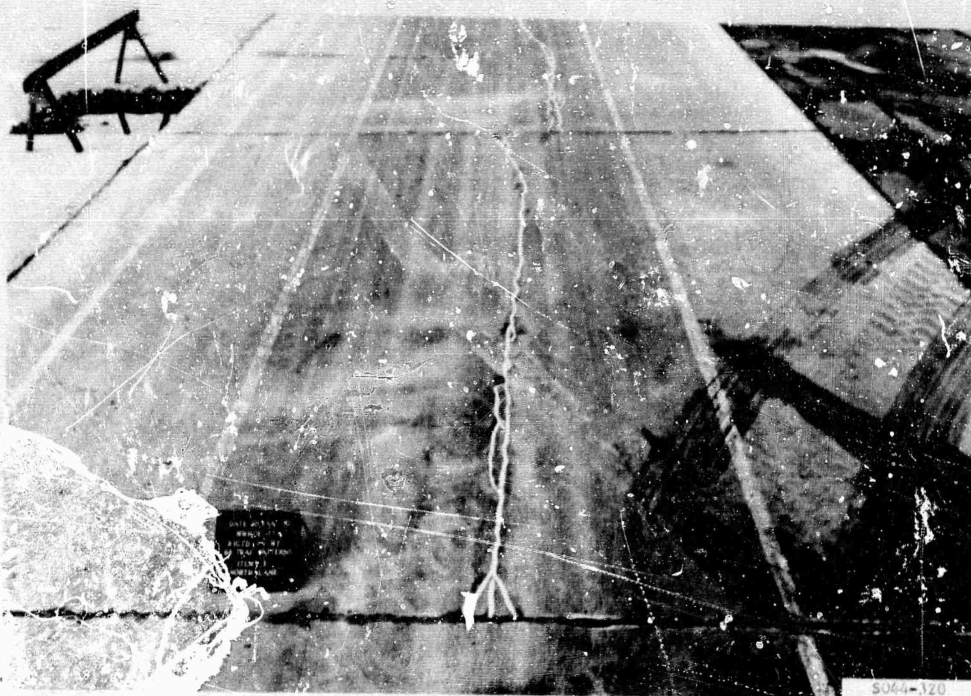
Figure 34. Condition of Item 3, North Lane, at the Conclusion of Twin-Tandem-Assembly Traffic
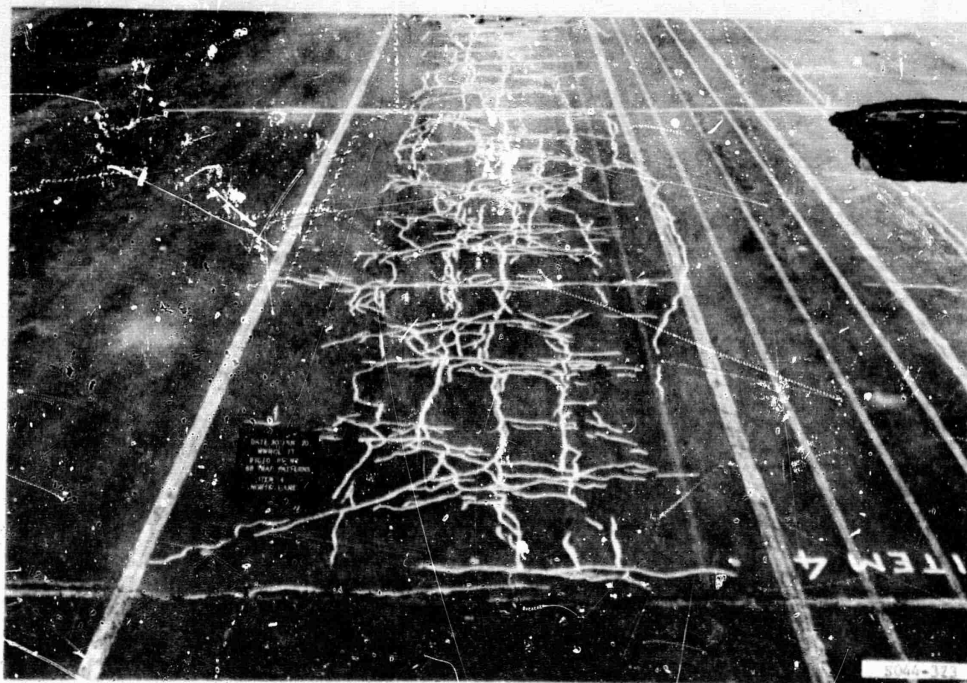
Figure 35. Condition of Item 4 Overlay, North Lane, at the Conclusion of Twin-Tandem-Assembly Traffic
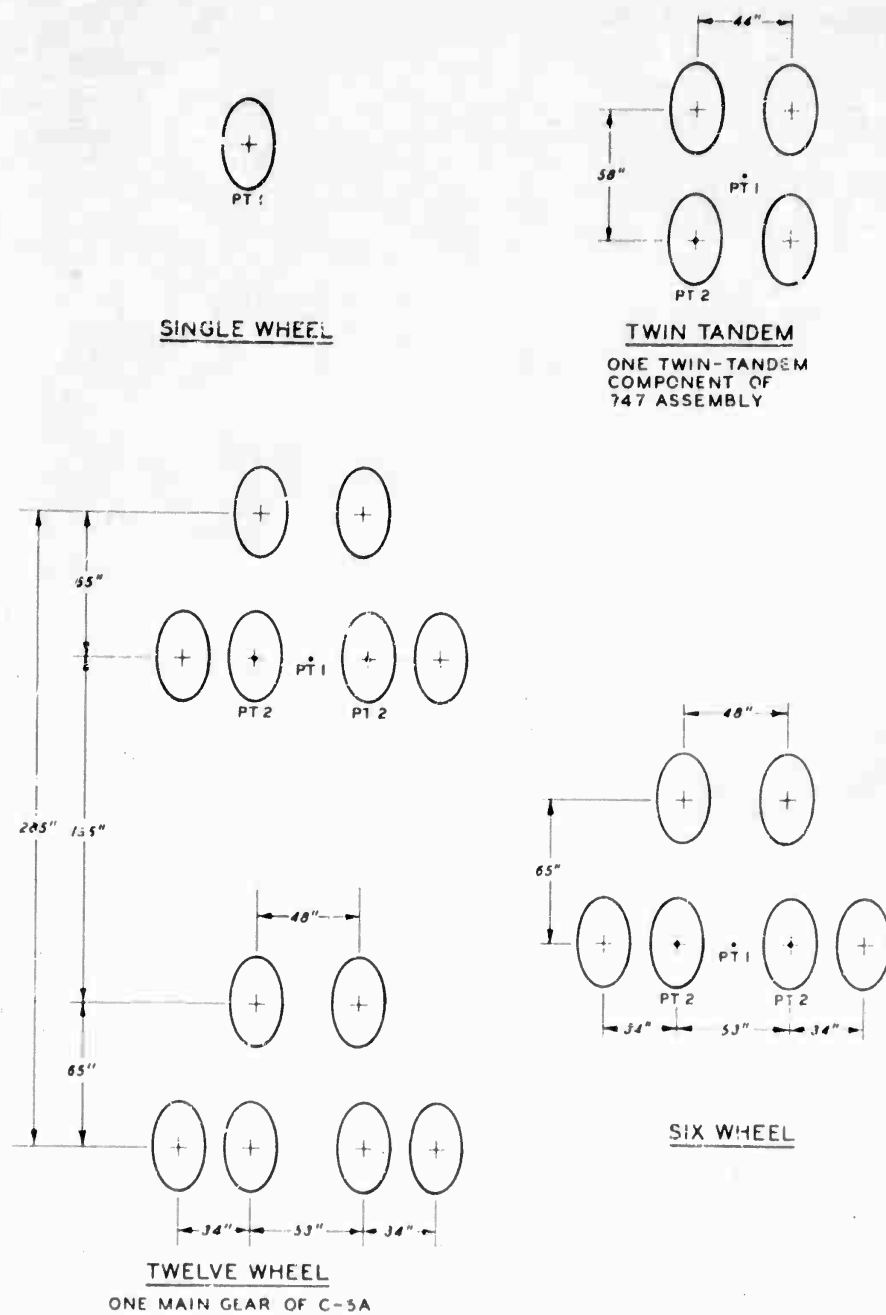
Figure 36. Locations of Loading Points of Wheel Assemblies
Used in the Flexible Pavement Tests
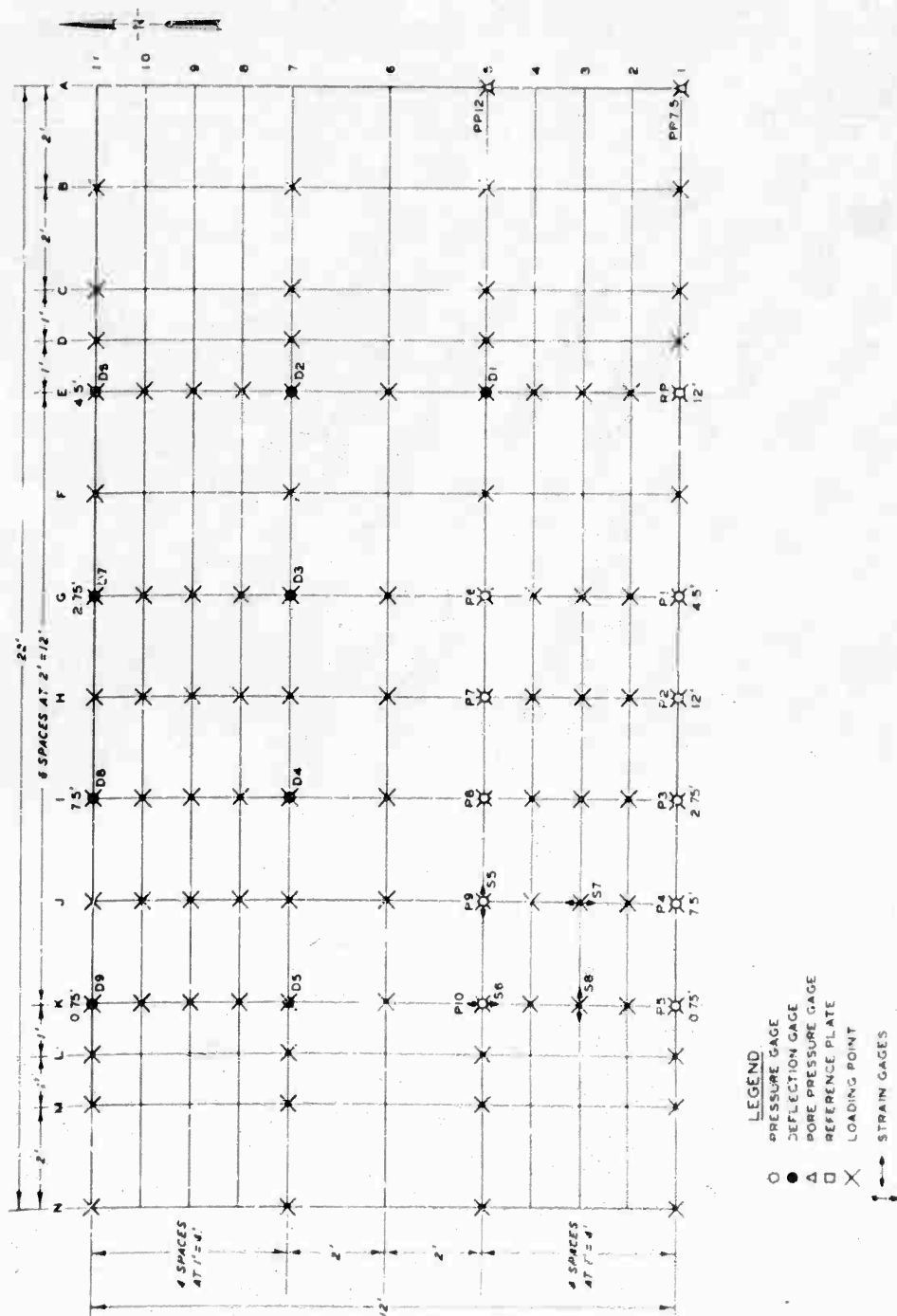
Figure 37. Static Load Grid System, Item 3, Flexible Pavement Tests. Instrumentation Identification (Type, Number) Beside Each Symbol
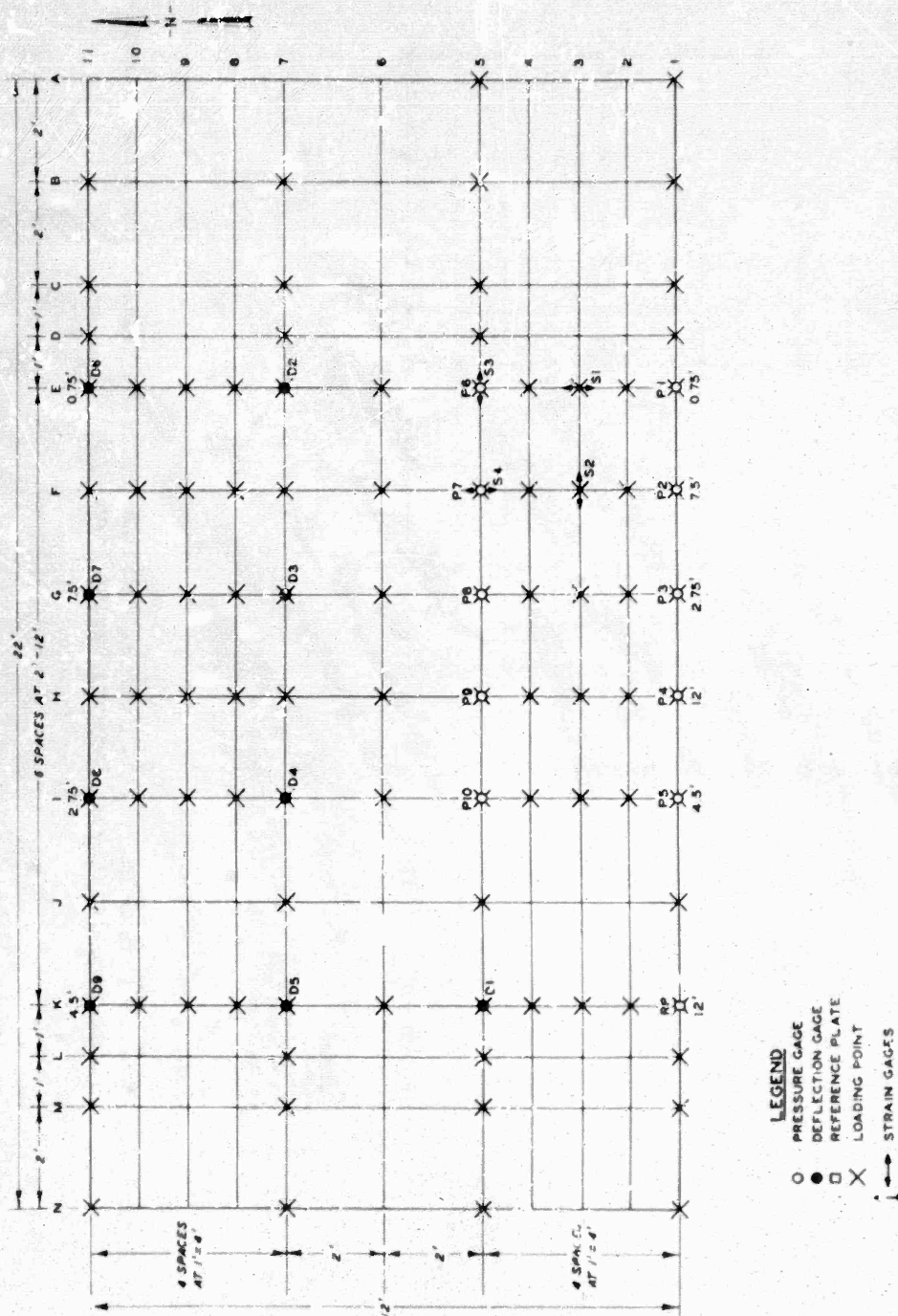
Figure 38. Static Load Grid System, Item 4, Flexible Pavement Tests. Instrumentation Identification (Type, Number) Beside Each Symbol
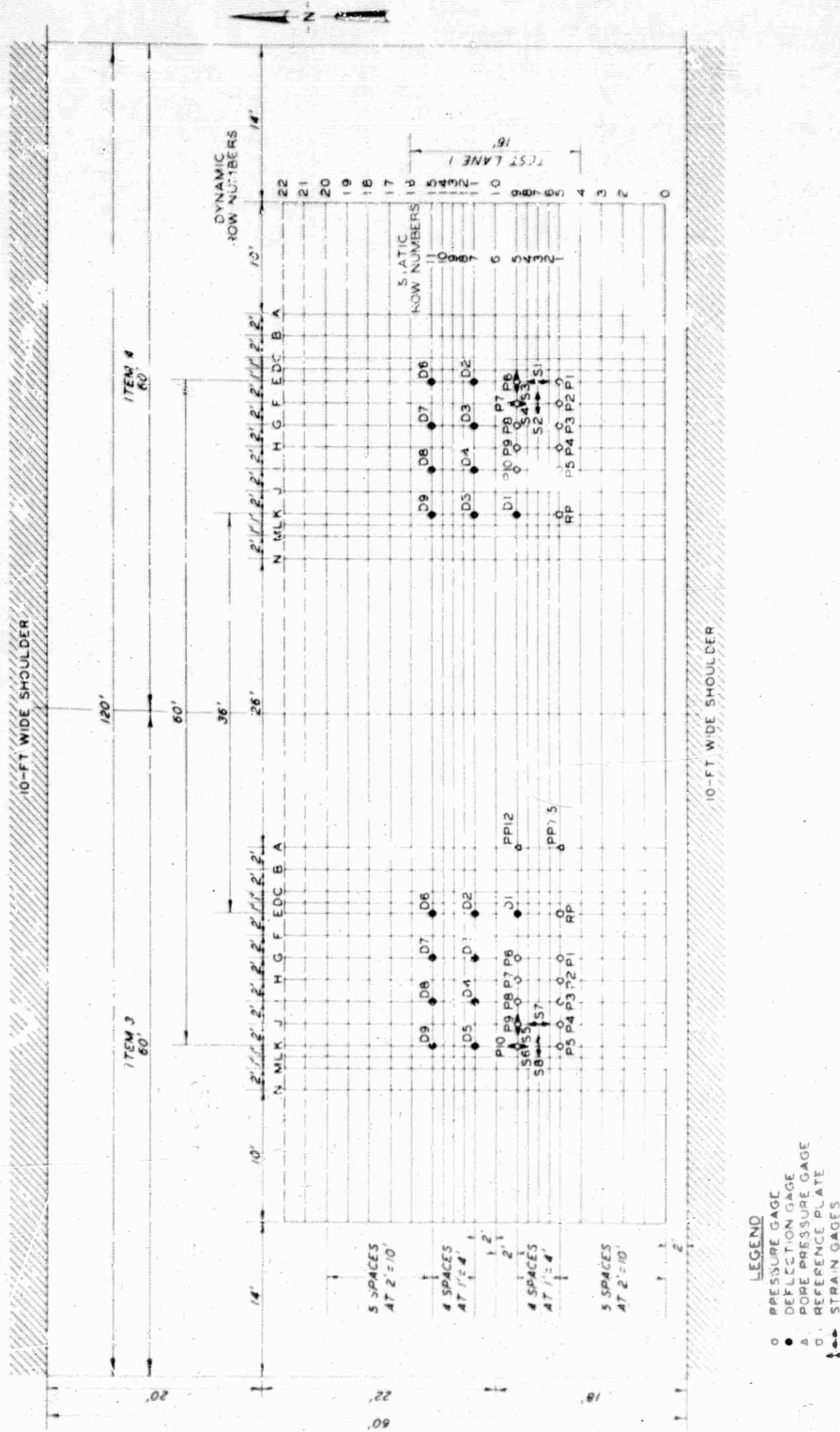
Figure 39. Static and Dynamic Load Grid System Used for Flexible Pavement Tests. Instrumentation Identification (Type, Number) Beside Each Symbol
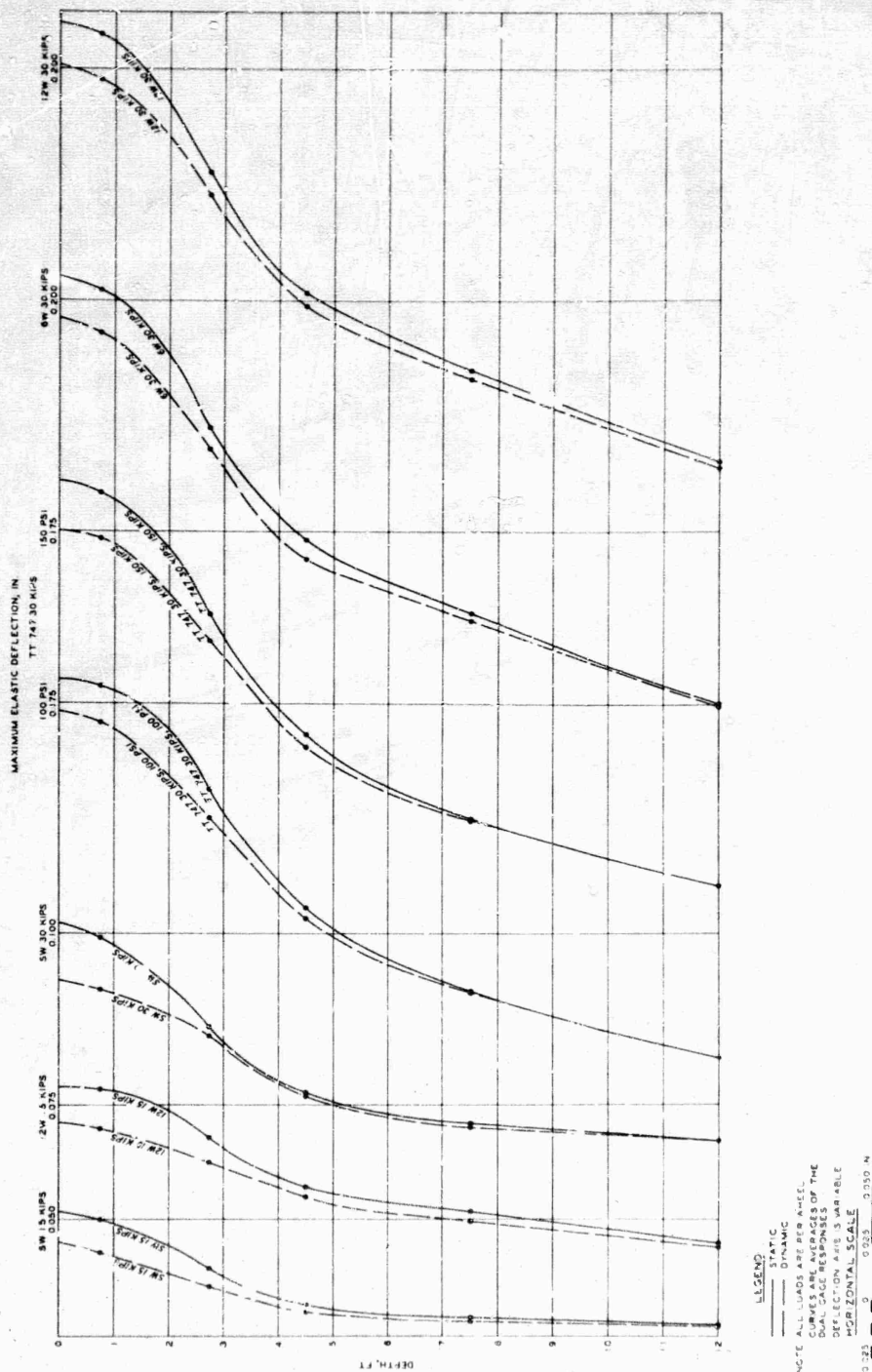
Figure 40. Static Versus Dynamic Load Maximum Deflection Curves, Item 3, Flexible Pavement

124

Figure 41. Static and Dynamic Load Maximum Deflection Curves,
Item 4, Flexible Pavement

125
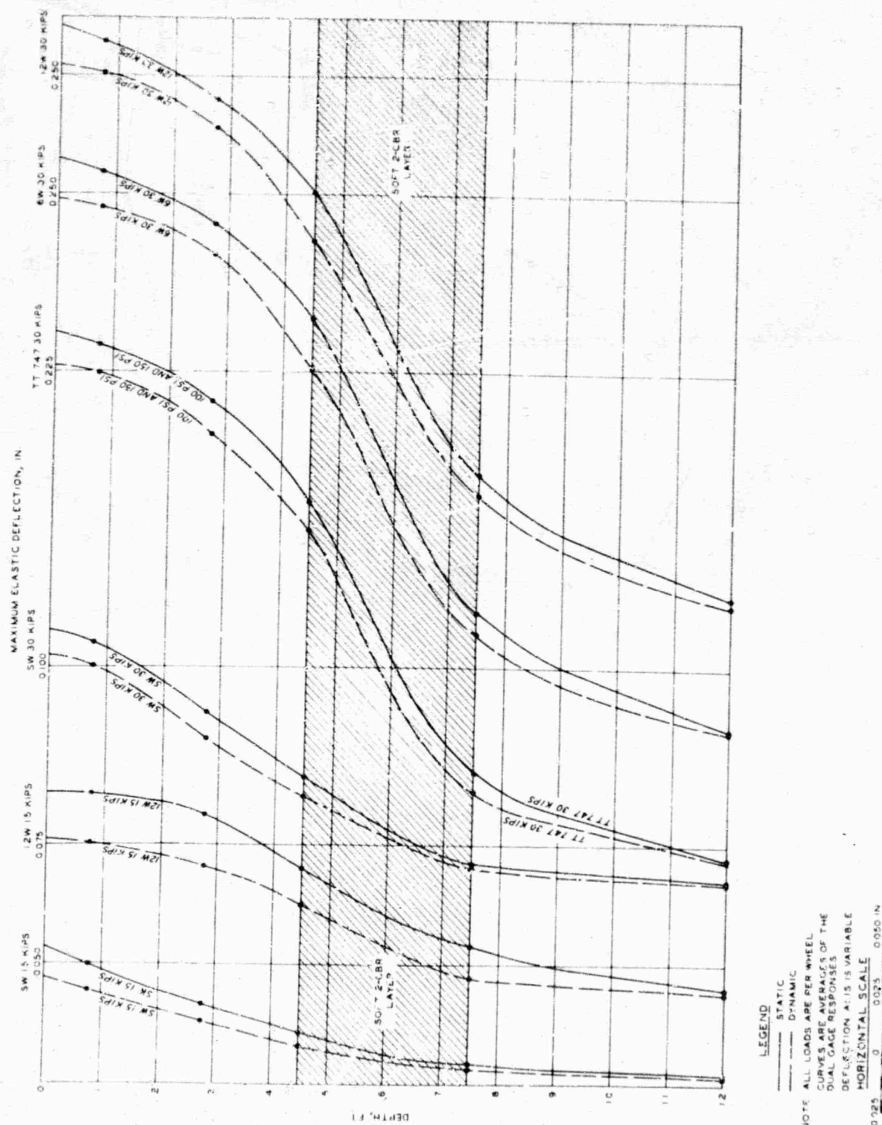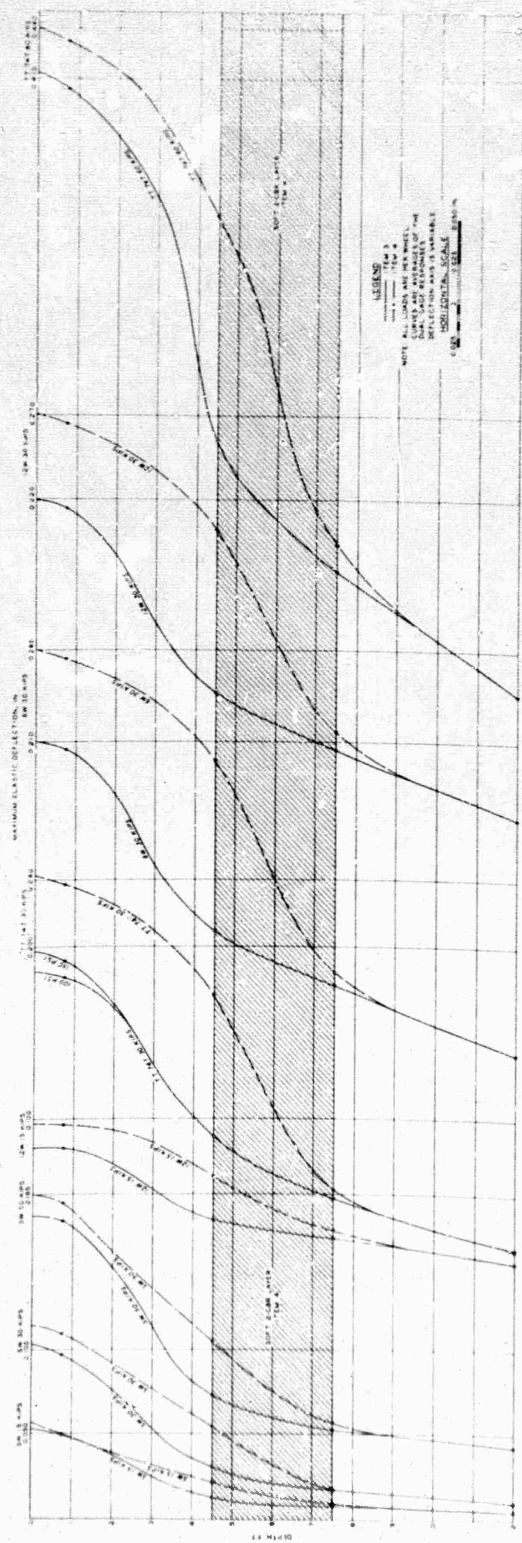
Figure 42. Item 3 Versus Item 4 Maximum Deflection Curves, Static Load Flexible Pavement Tests

Figure 43. Item 3 Versus Item 4 Maximum Deflection Curves, Dynamic Load Flexible Pavement Tests

127
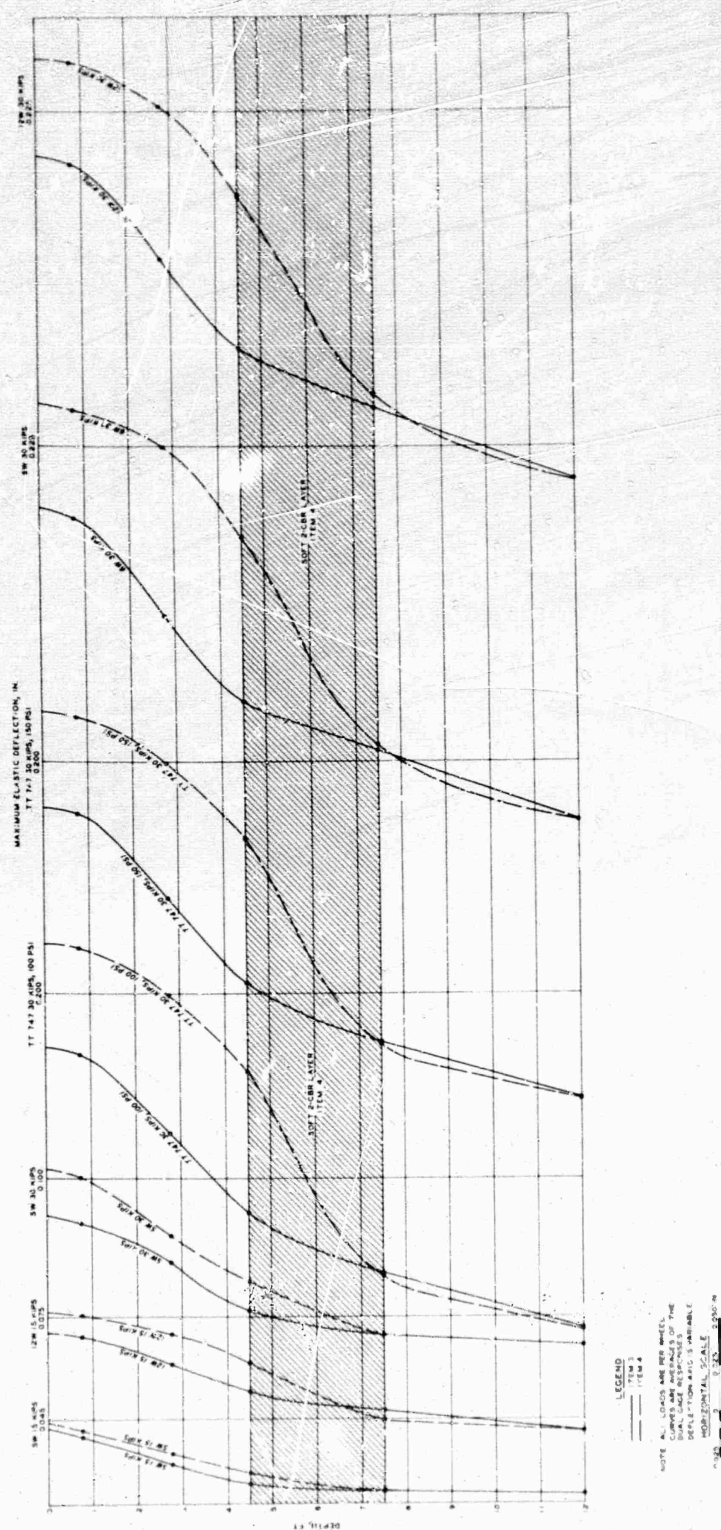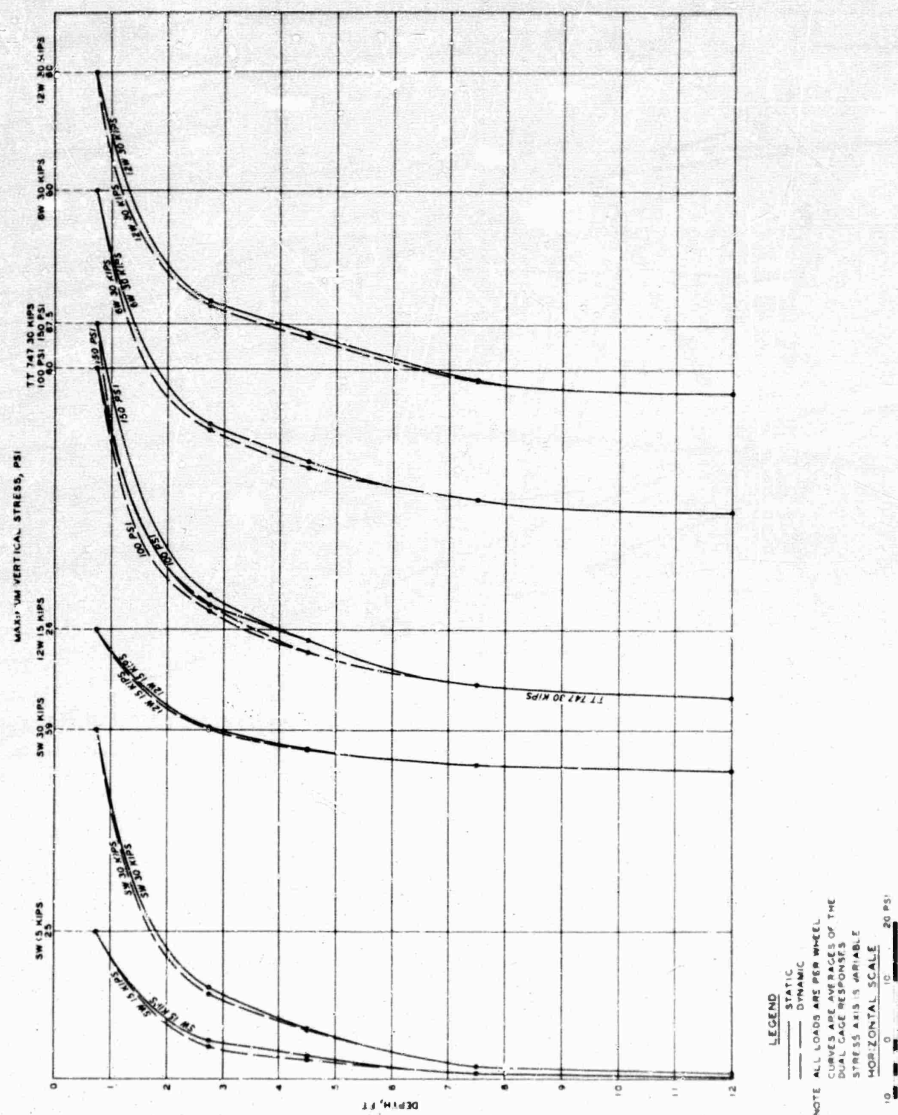
Figure 44. Static Versus Dynamic Load Maximum Vertical Stress
Curves, Item 3, Flexible Pavement
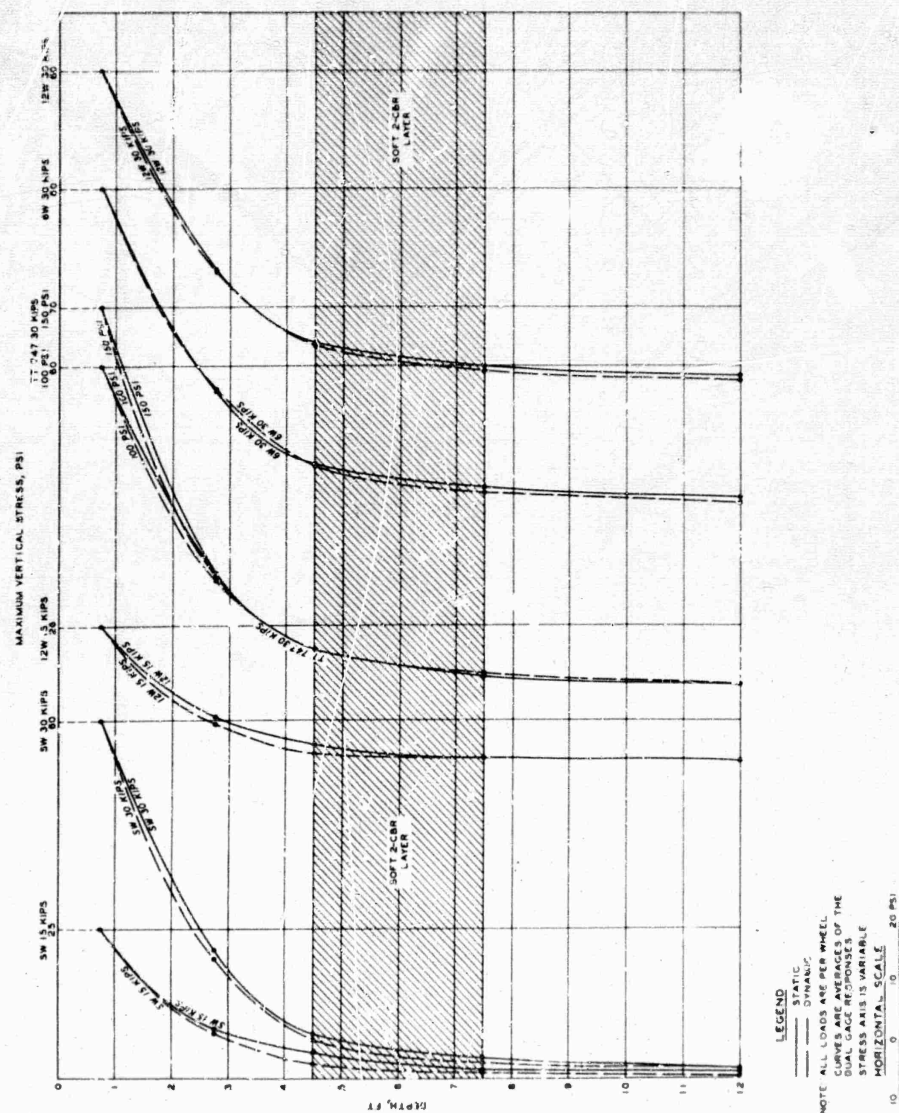
Figure 45. Static Versus Dynamic Load Maximum Vertical Stress
Curves, Item 4, Flexible Pavement
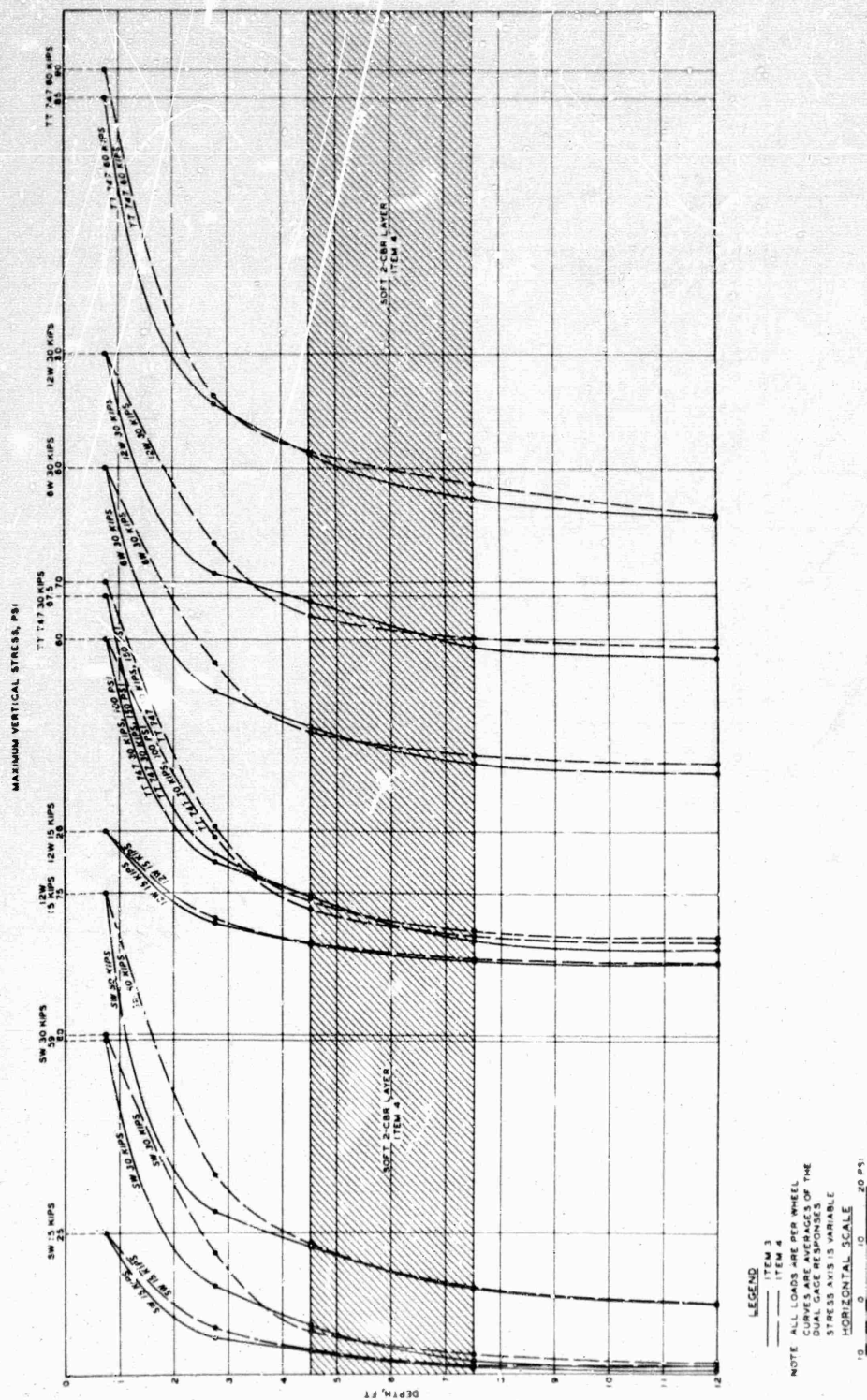
Figure 46. Item 3 Versus Item 4 Maximum Vertical Stress Curves, Static Load Flexible Pavement Tests

130
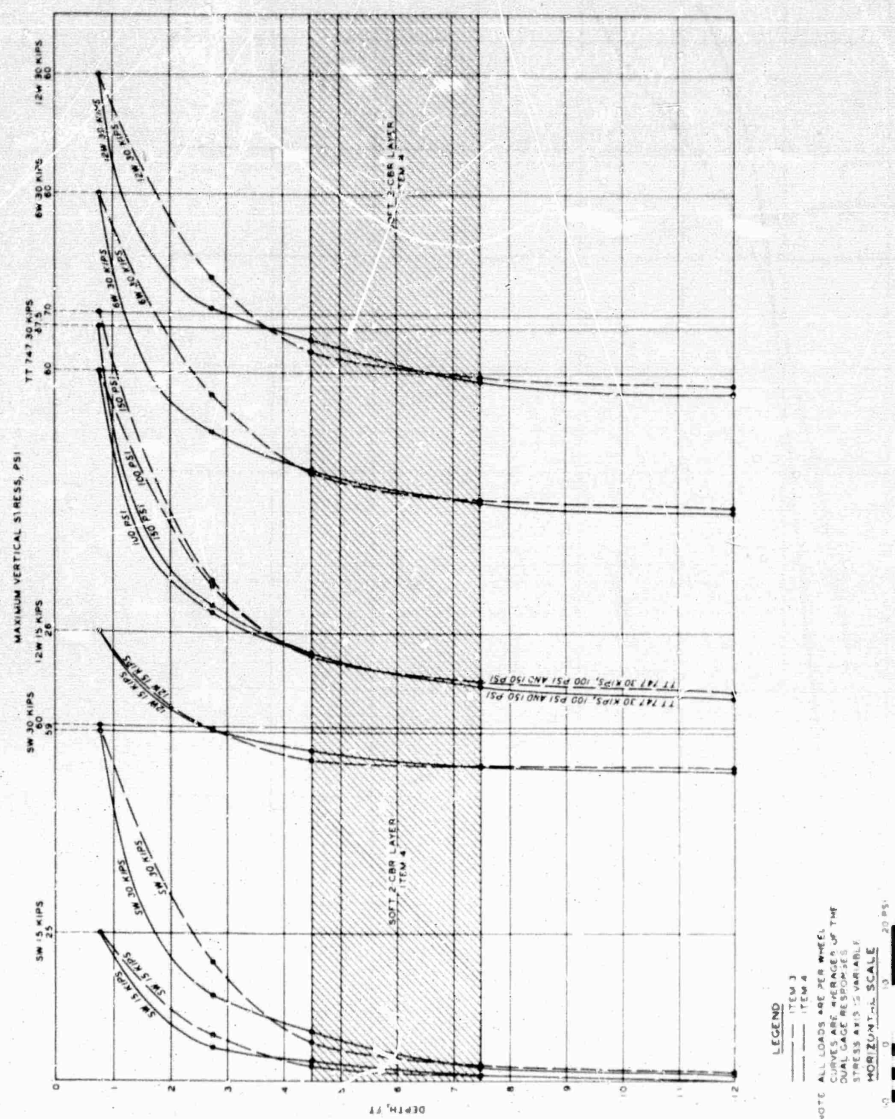
Figure 47. Item 3 Versus Item 4 Maximum Vertical Stress Curves, Dynamic Load Flexible Pavement Tests

Figure 48. Comparison of Computed and Actual Data for
Maximum Elastic Deflection Versus Depth for
12-Wheel, 30-kip Load (100-psi Tire Infla-
tion Pressure), Item 3, Flexible Pavement

MAXIMUM ELASTIC DEFLECTION, IN.

THEORETICAL

ACTUAL DATA

SOFT 2-CBR LAYER
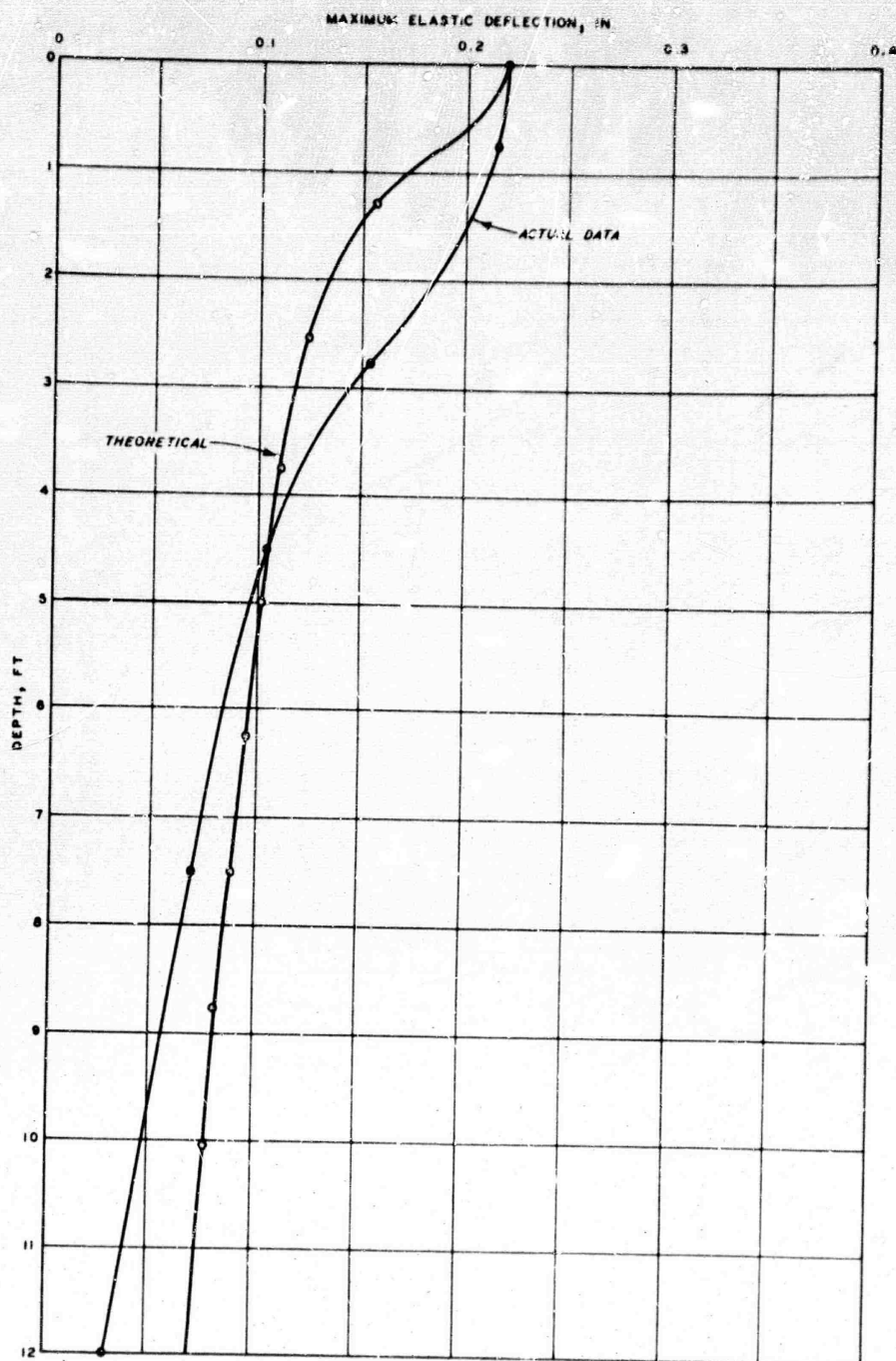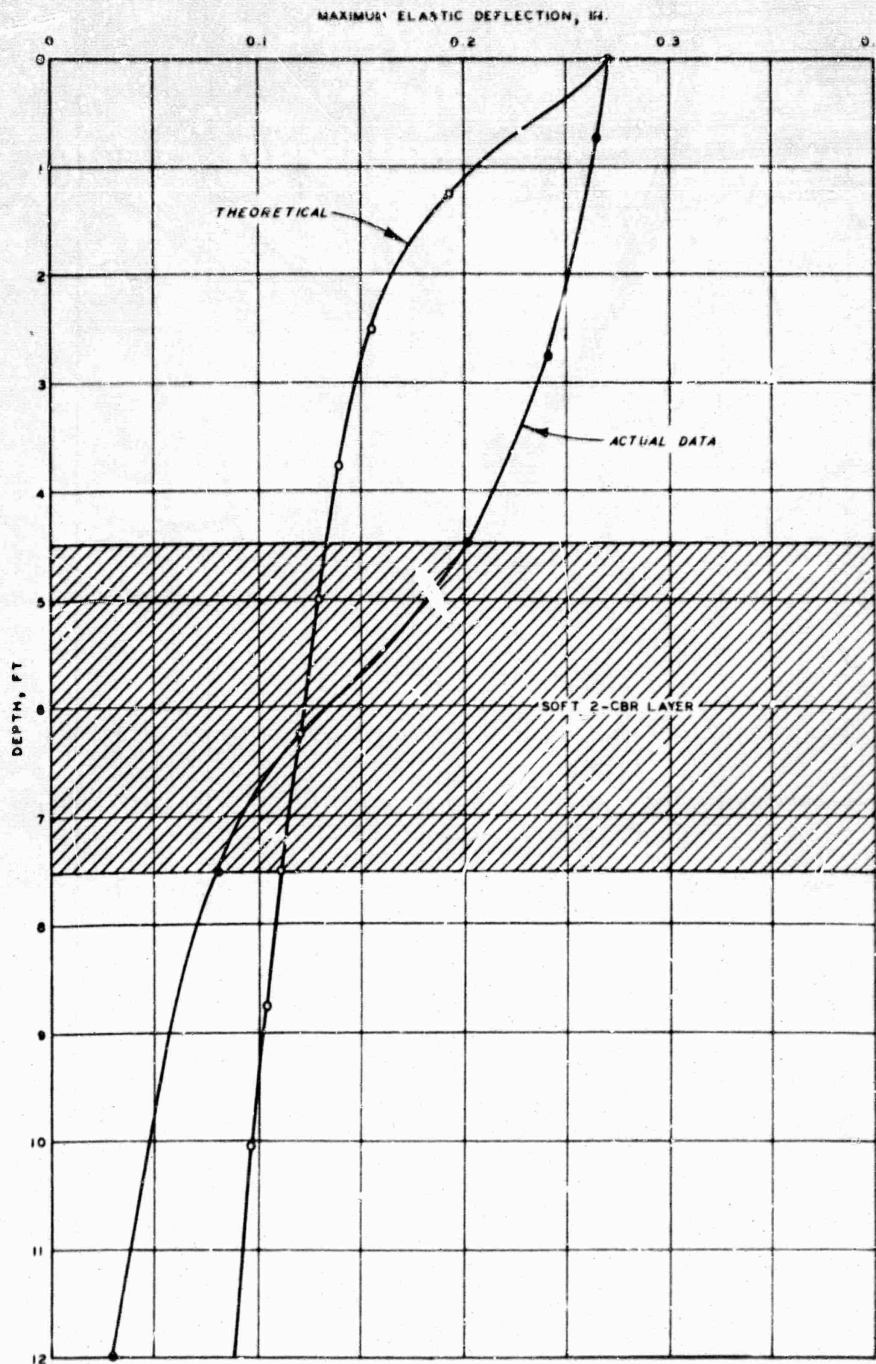
DEPTH, FT

NOTE: CURVE IS AVERAGE OF GAGE RESPONSE.
LOAD IS PER WHEEL

Figure 49.   Comparison of Computed and Actual Data for
Maximum Elastic Deflection Versus Depth for
12-Wheel, 30-kip Load (100-psi Tire Pressure),
Item 4, Flexible Pavement

133
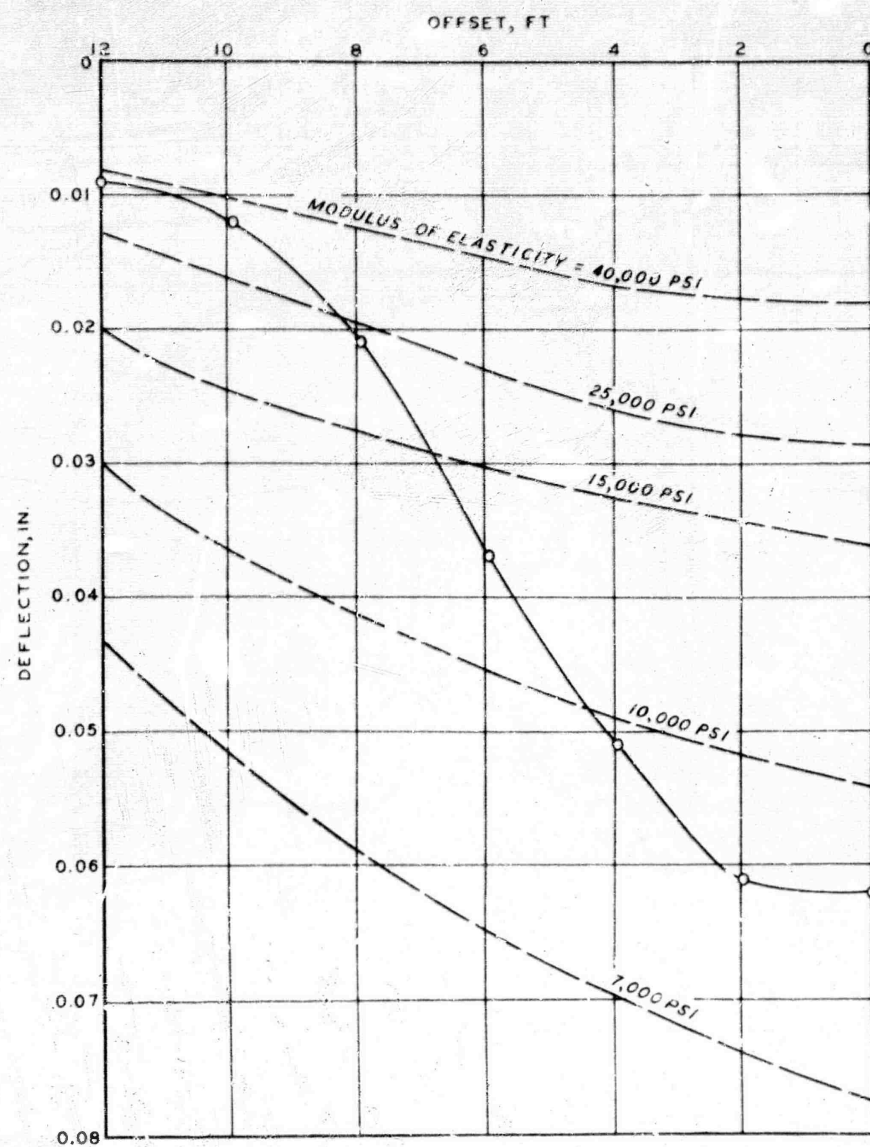
Figure 50. Transverse Offset Versus Theoretical and Measured
Deflection at 7.5-ft Depth, 6-Wheel, 180-kip Load,
Item 3, Flexible Pavement

134
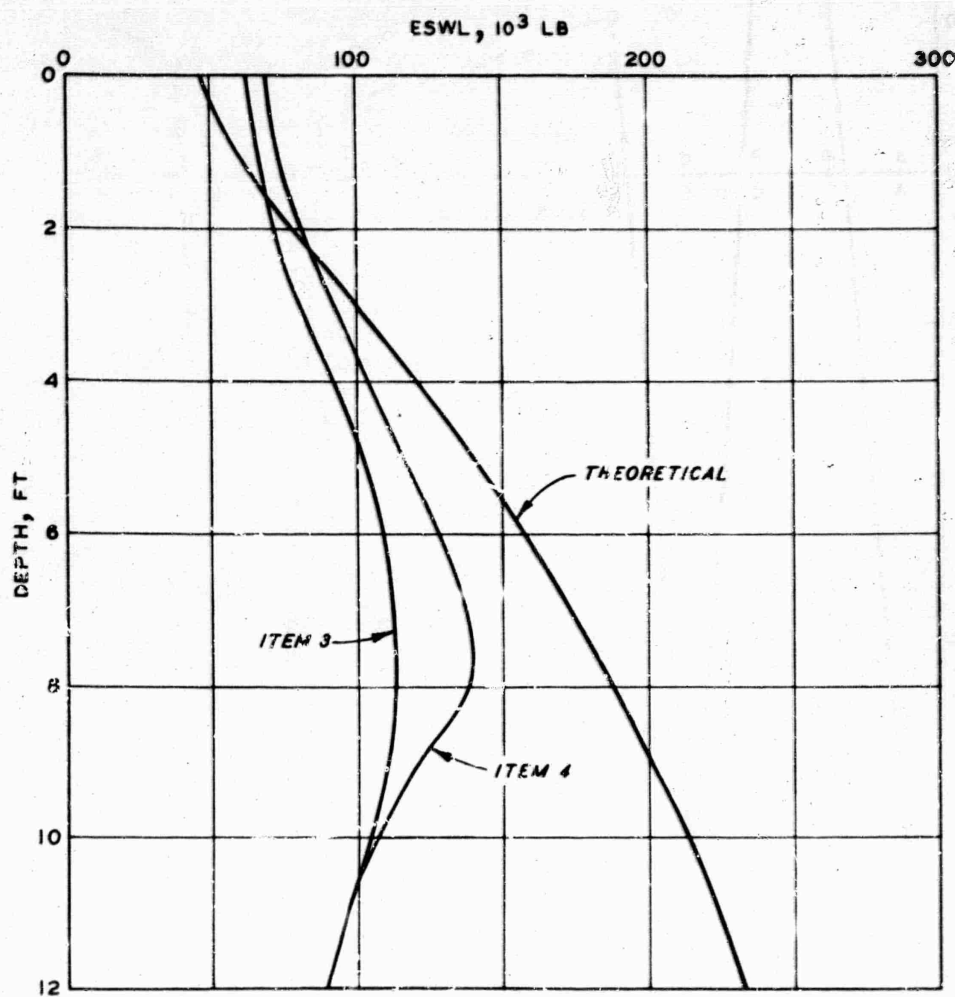
Figure 51. Comparison of Computed Curve with Actual
Data for ESWL Versus Depth, 12-Wheel,
360-kip Load, Flexible Pavement Tests

135
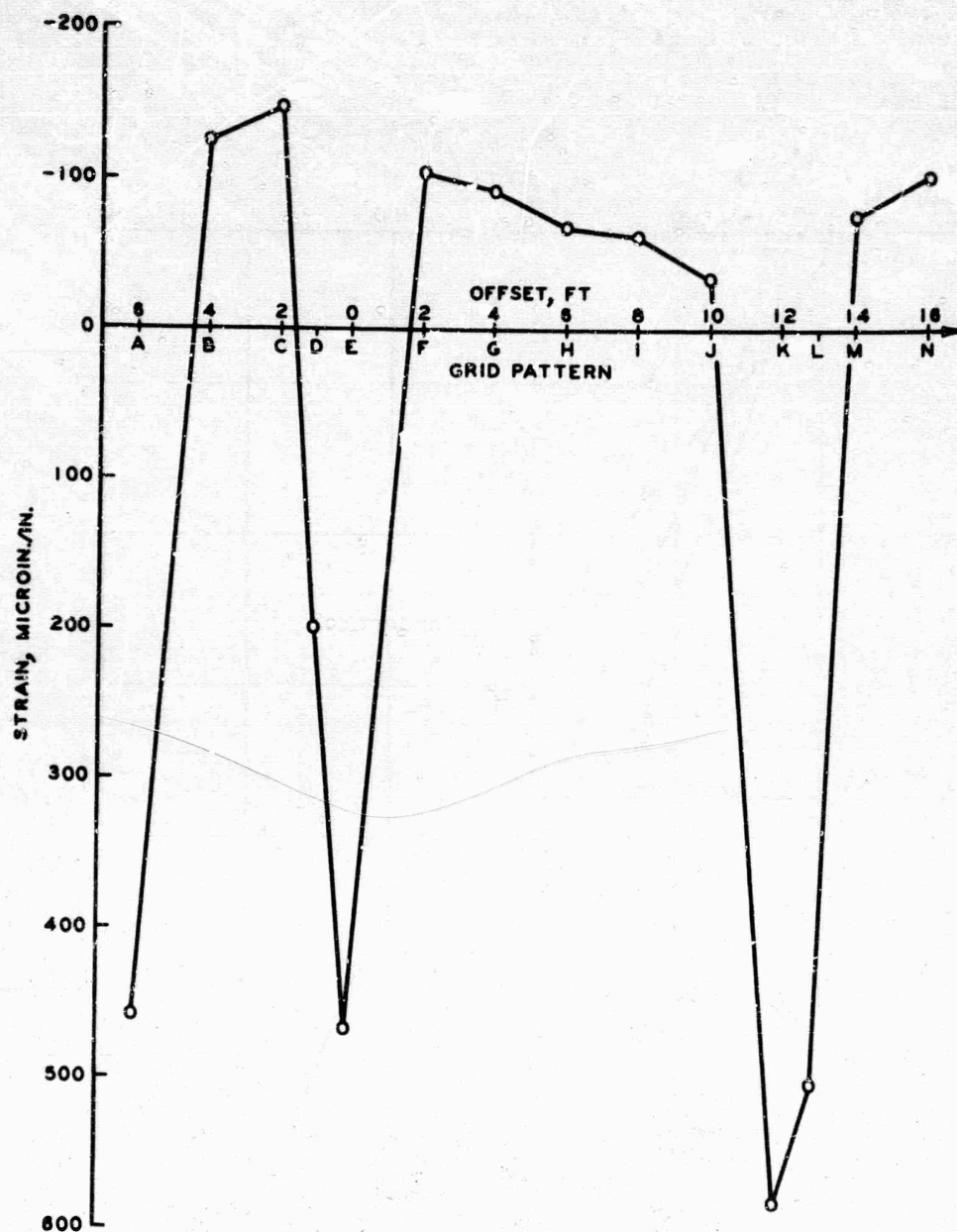
Figure 52. East-West Offsets Versus Pavement Strain for Assembly
Load Point 2, Static Load Tests, 12-Wheel, 360-kip
Load. Gage S1 (‡ N), Item 4, Flexible Pavement. Off-
set Distances Are Parallel to the Direction of Forward
Movement of the Assembly; Offset Distances and Grid
Pattern Are Shown in Figure 38.
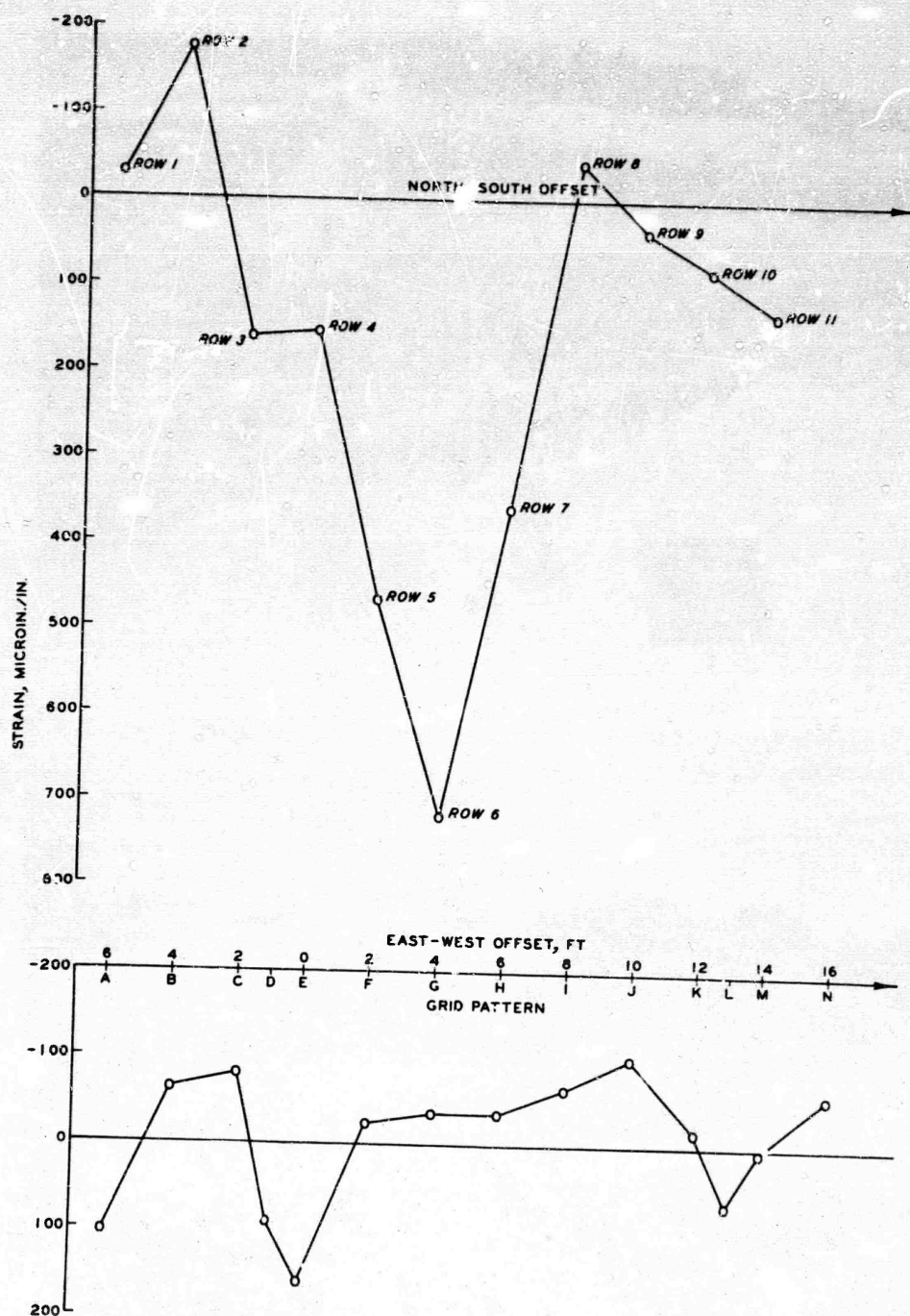
Figure 53. East-West and North-South Offsets Versus Pavement Strain for Assembly Load Point 1, Static Load Tests, 12-Wheel, 360-kip Load. Gage S1 (¢ N), Item 4, Flexible Pavement. N-S and E-W Offset Distances Are Parallel and Perpendicular, Respectively, to the Direction of the Forward Movement of the Assembly. Offset Distances, Row Numbers, and Grid Patterns Are Shown in Figure 38.

137

a. Electromagnetic Vibrator and Transducer Used in High-Frequency Vibratory Tests
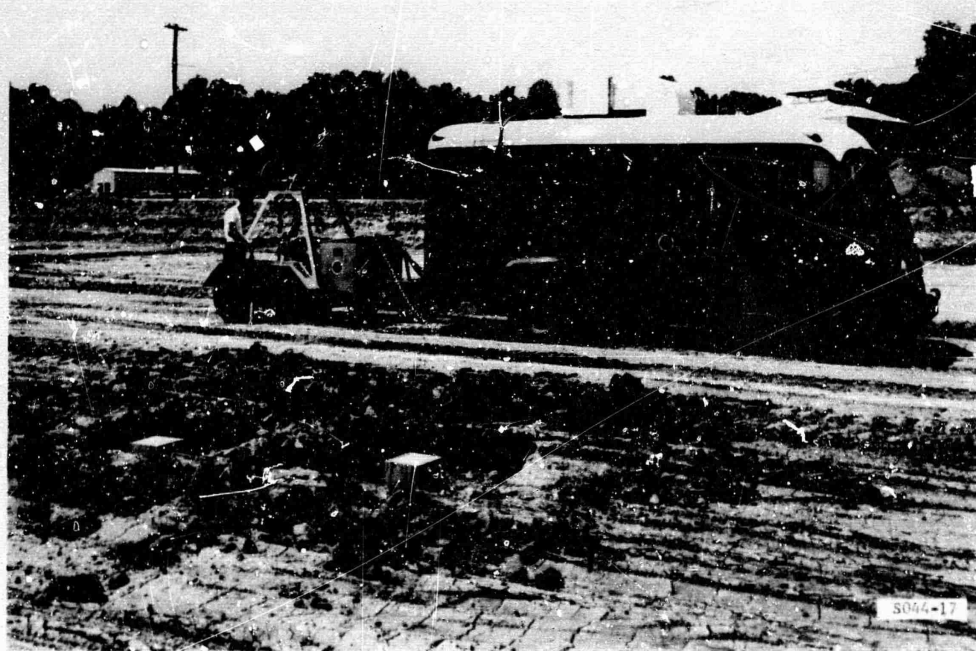
b. Mechanical Vibrator and Instrumentation Van Used in Low-Frequency Vibratory Tests

Figure 54. Equipment Used for Nondestructive Testing

138

Figure 55. Refraction Seismic Test at the Bottom of the Excavation

NOT REPRODUCIBLE
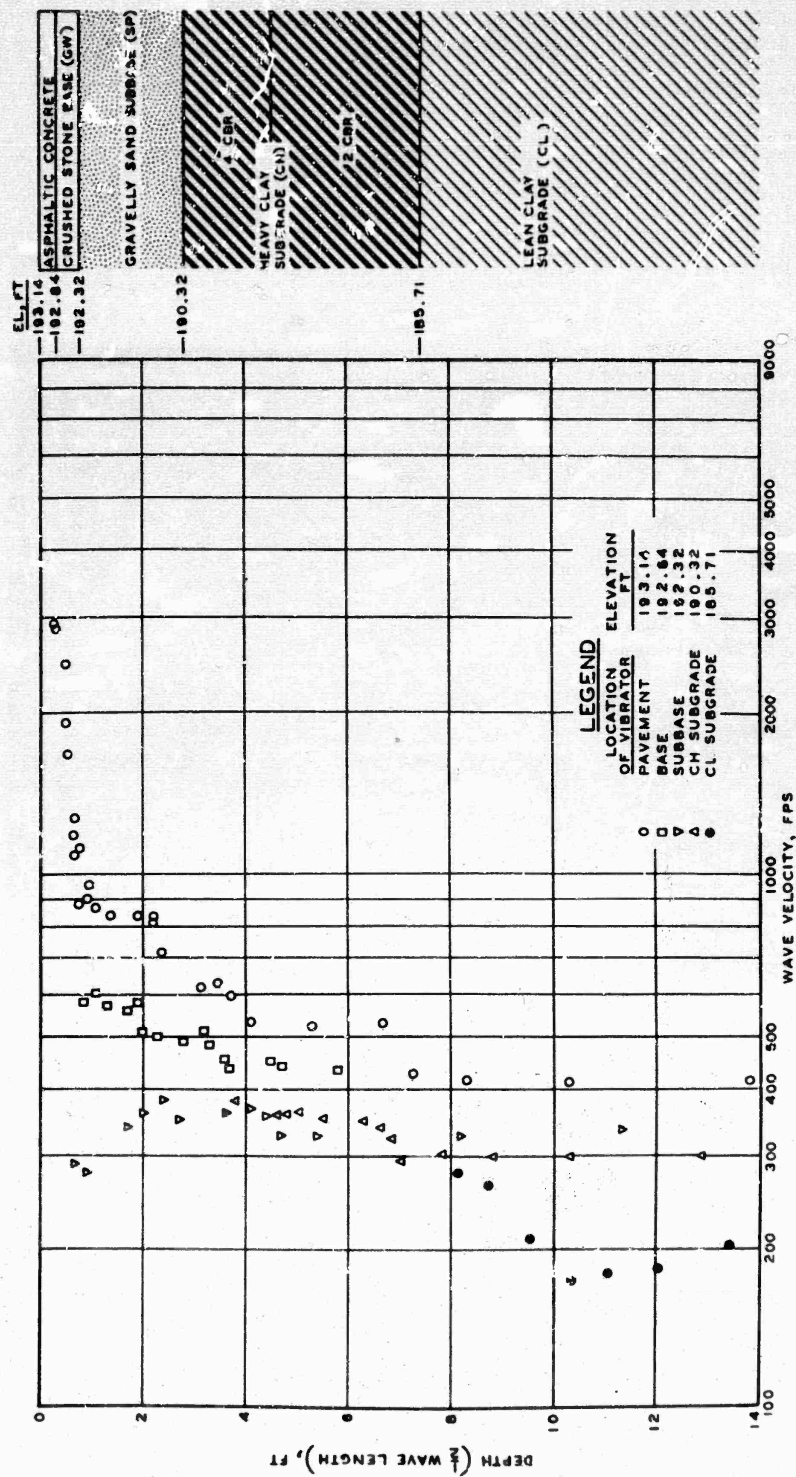
Figure 56. Wave Velocity Versus Depth for Flexible Pavement Lane 1, Item 4, As Constructed
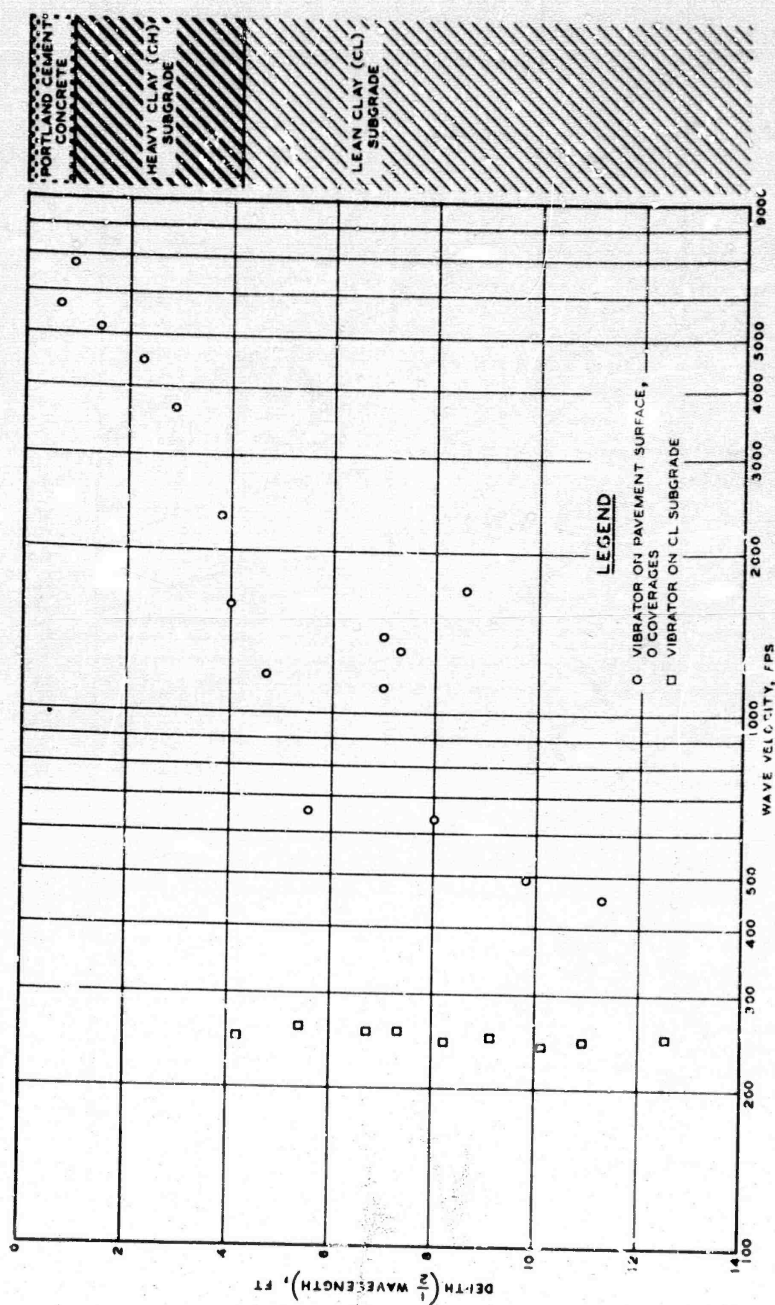
Figure 57. Wave Velocity Versus Depth for Rigid Pavement Item 1, South Lane, As Constructed
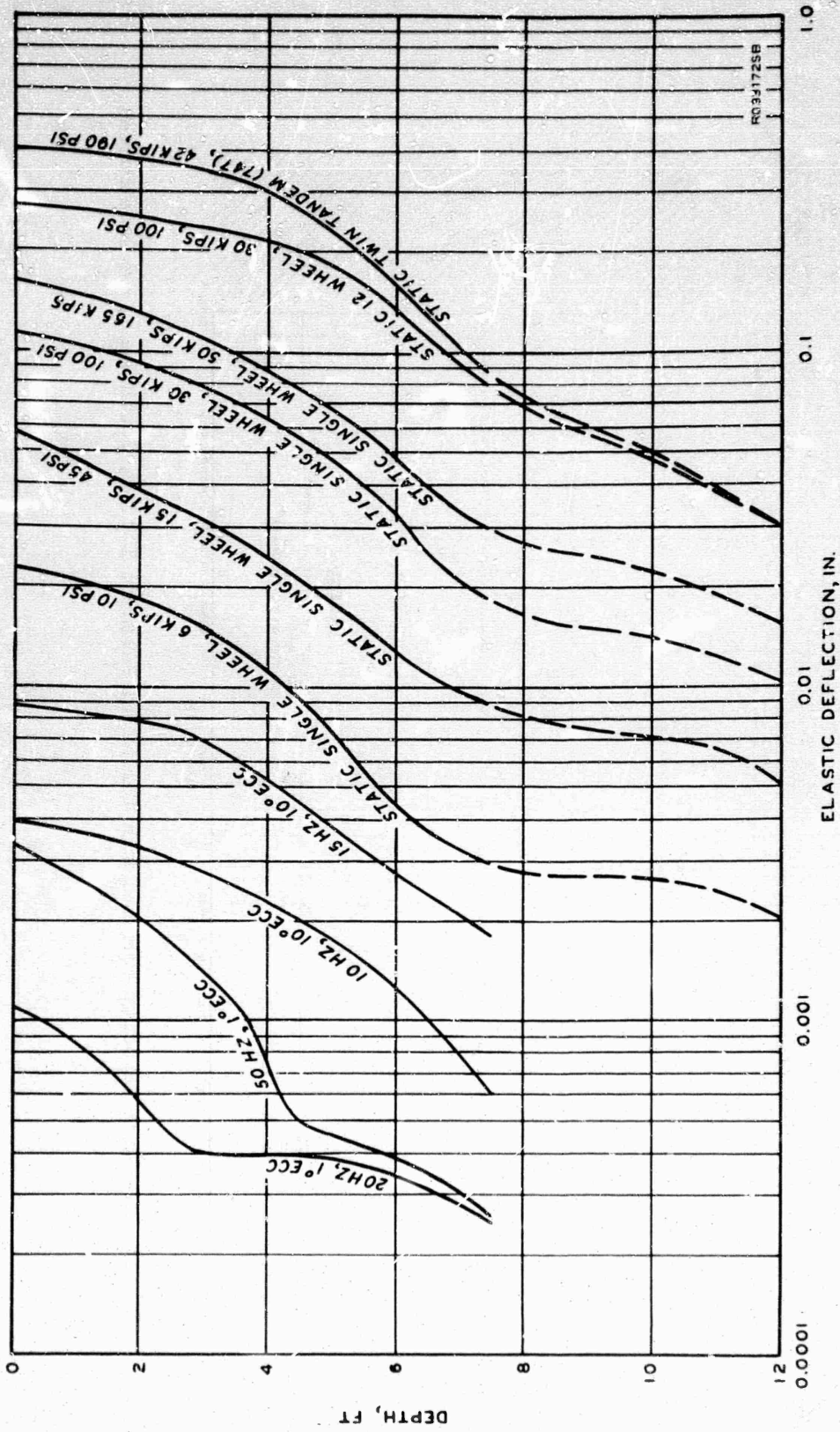
Figure 58. Deflection Versus Depth for Static and Vibratory Loading
of Flexible Pavement, Lane 1, Item 4
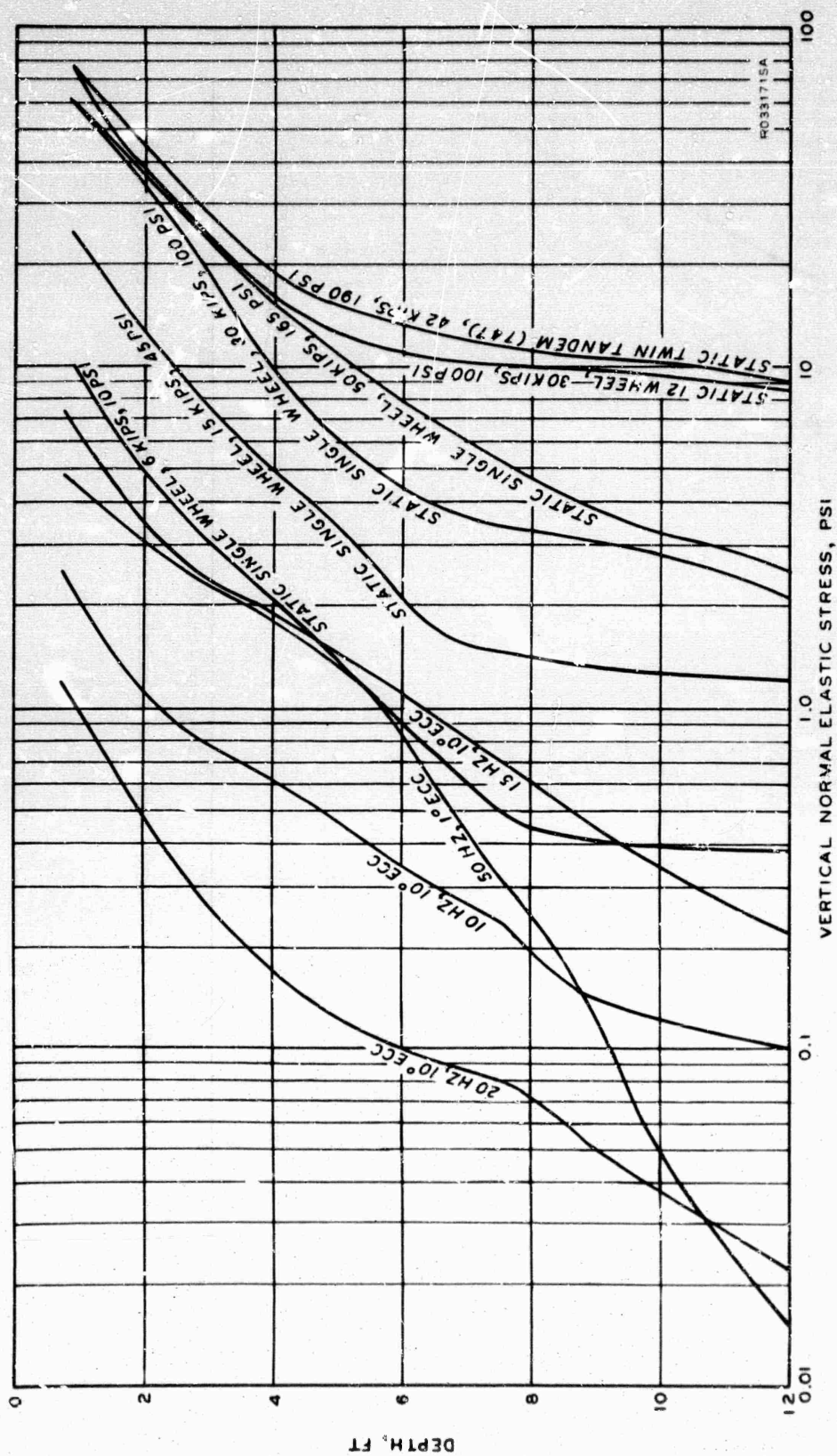
Figure 59. Stress Versus Depth for Static and Vibratory Loading of Flexible Pavement, Lane 1, Item 4

143
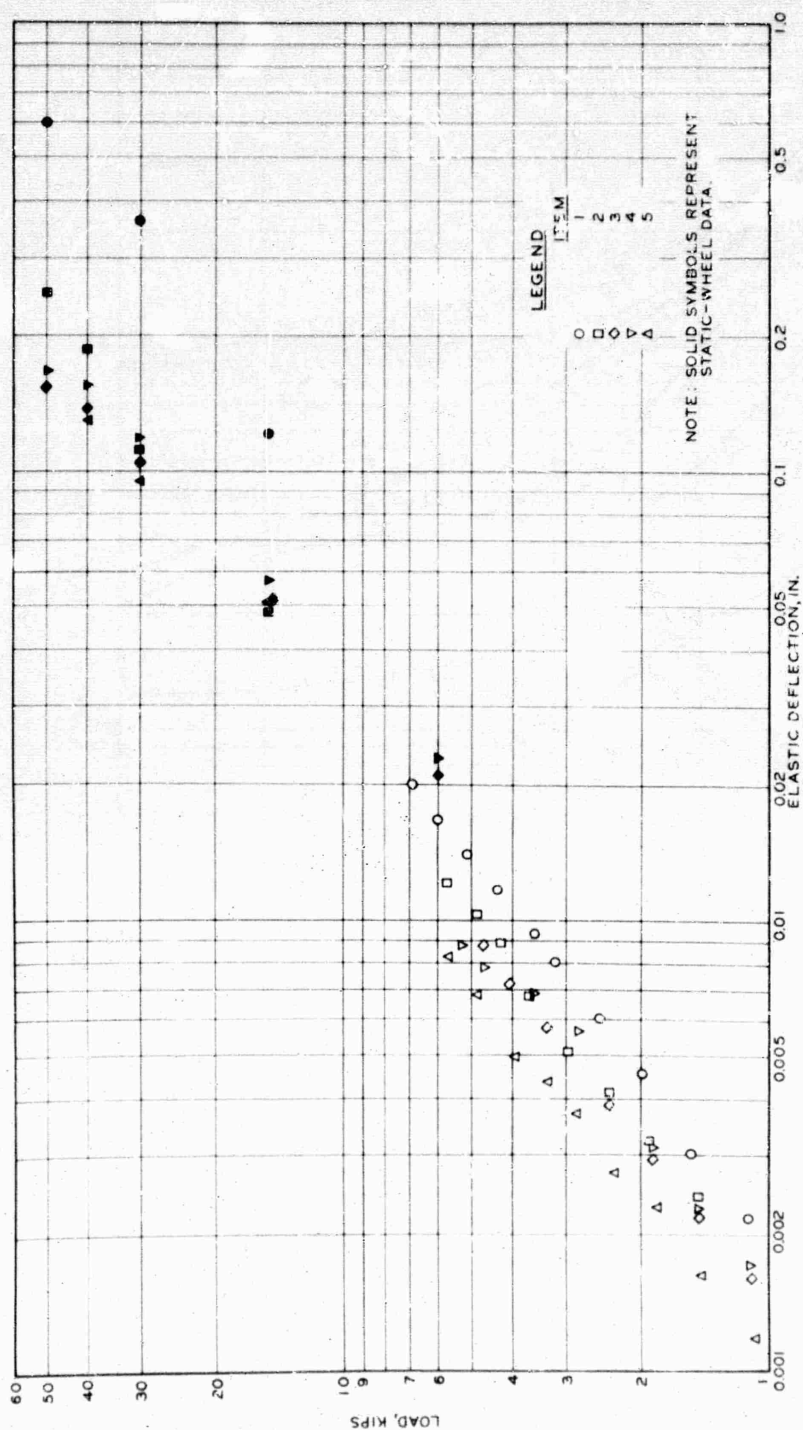
Figure 60. Deflection Versus Load for Flexible Pavement Lane 1, As Constructed
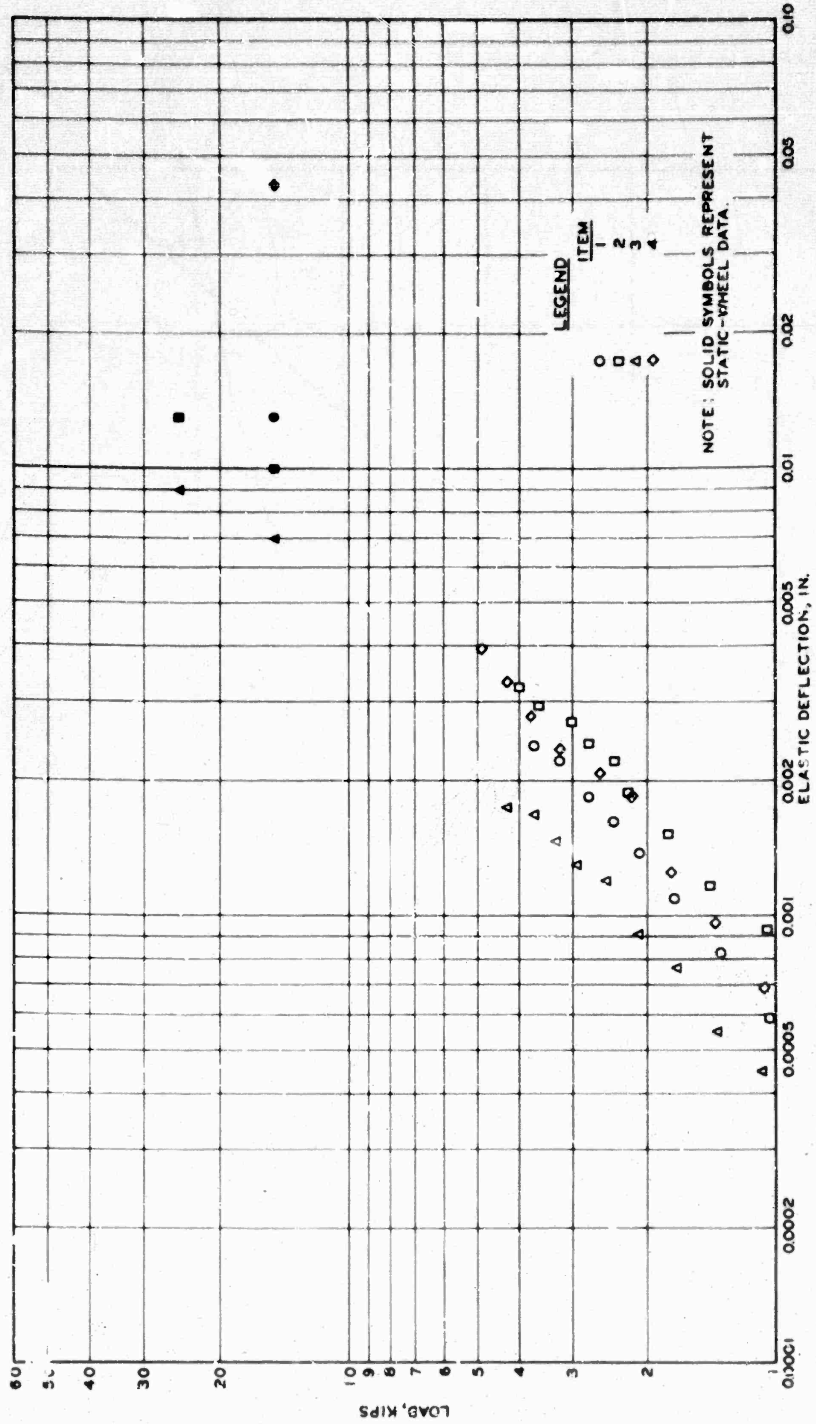
Figure 61. Deflection Versus Load for Rigid Pavement, South Lane, As Constructed
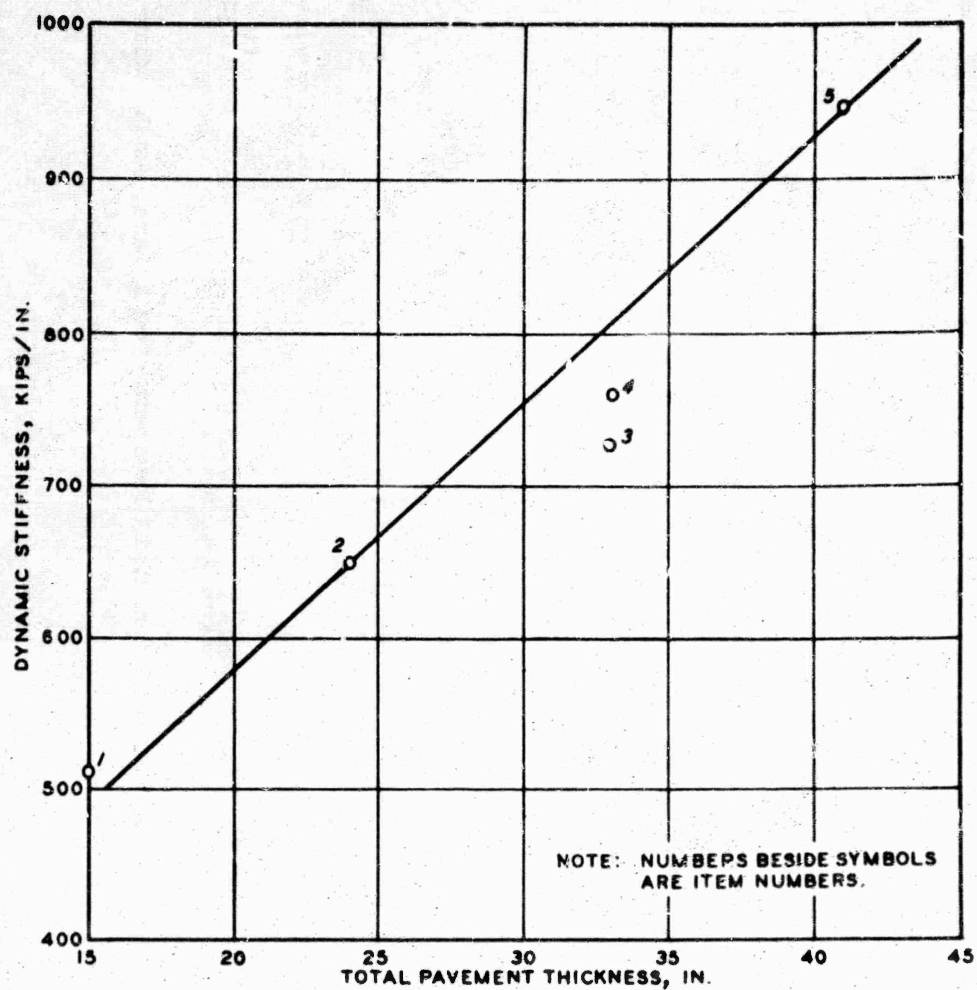
Figure 62. Dynamic Stiffness Versus Total Pavement
Thickness for Flexible Pavement, Lane 1
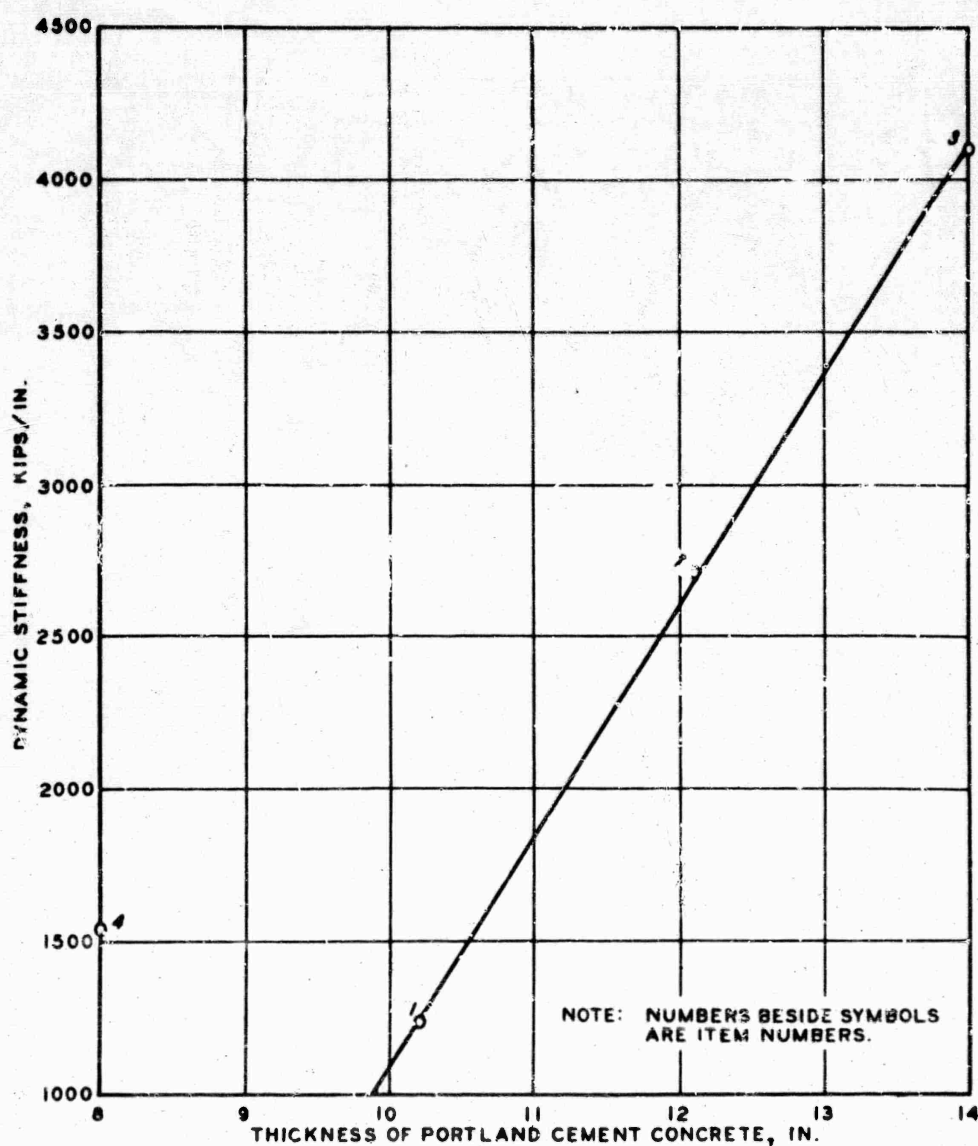
Figure 63. Dynamic Stiffness Versus Pavement Thickness
for Rigid Pavement, South Lane

147
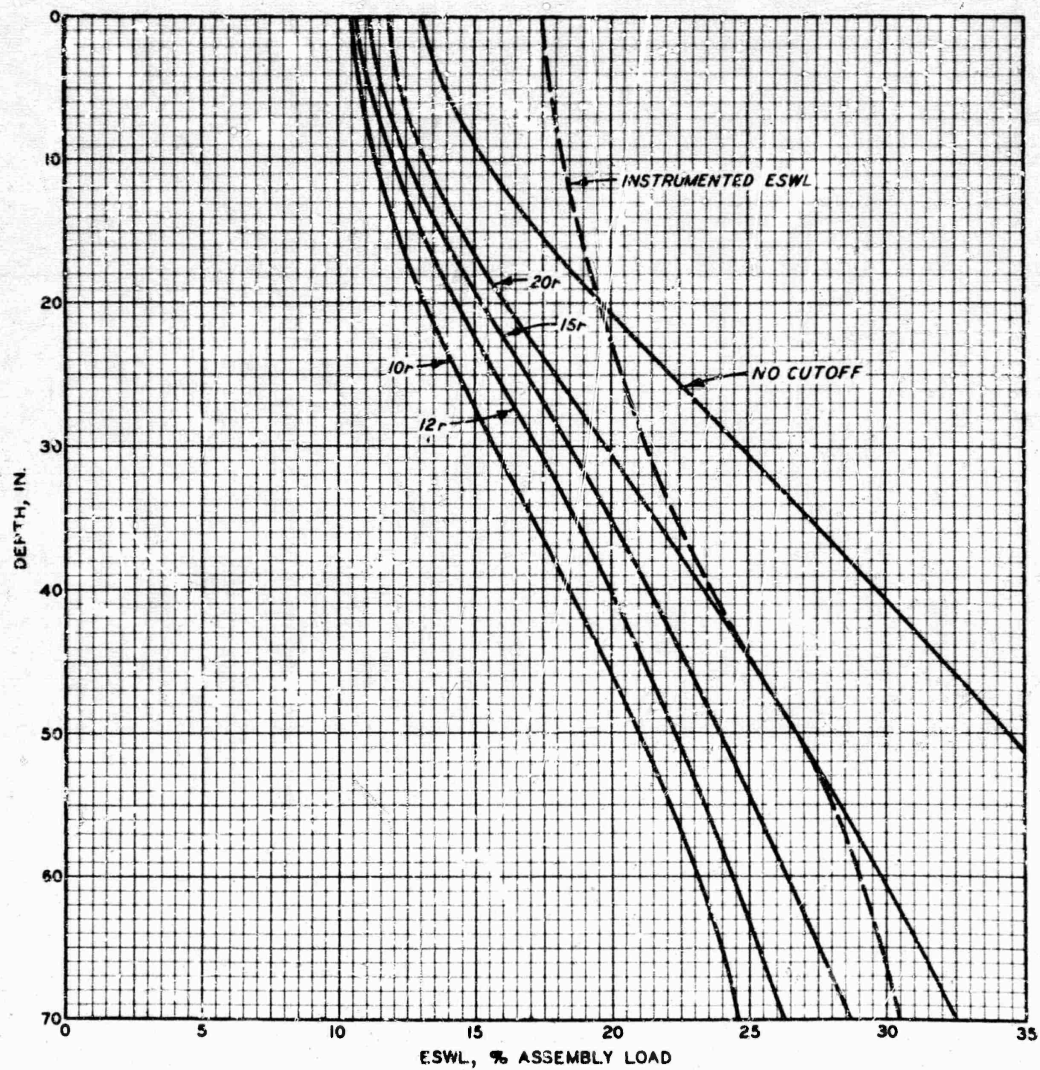
Figure 64. Comparison of Measured and Computed Equivalent Single-Wheel Loads Versus Depth for 12-Wheel Assembly
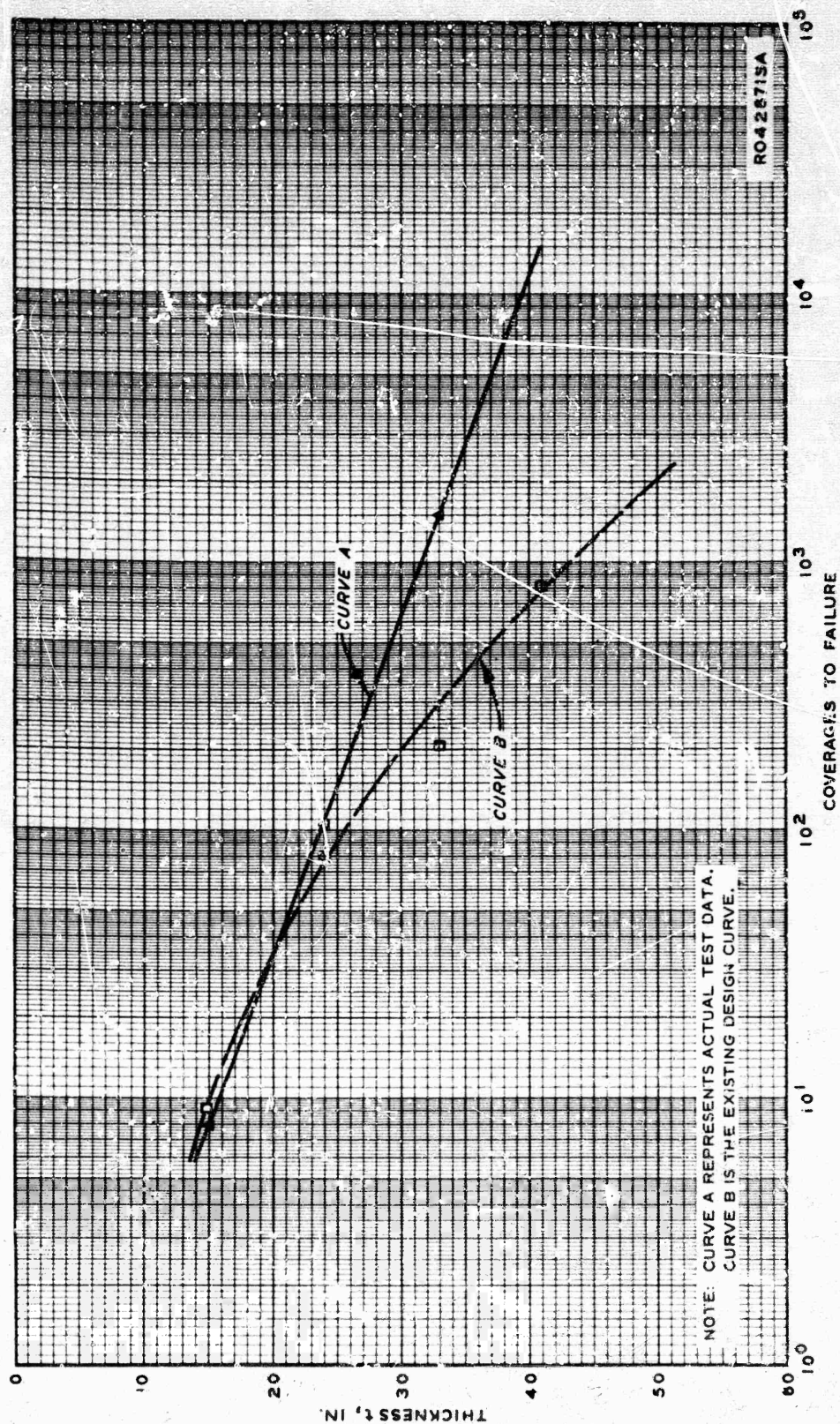
Figure 55. Comparison of Actual Data (Curve A) with Existing Design Curve (Curve B) for Thickness-Failure Coverage Relationship
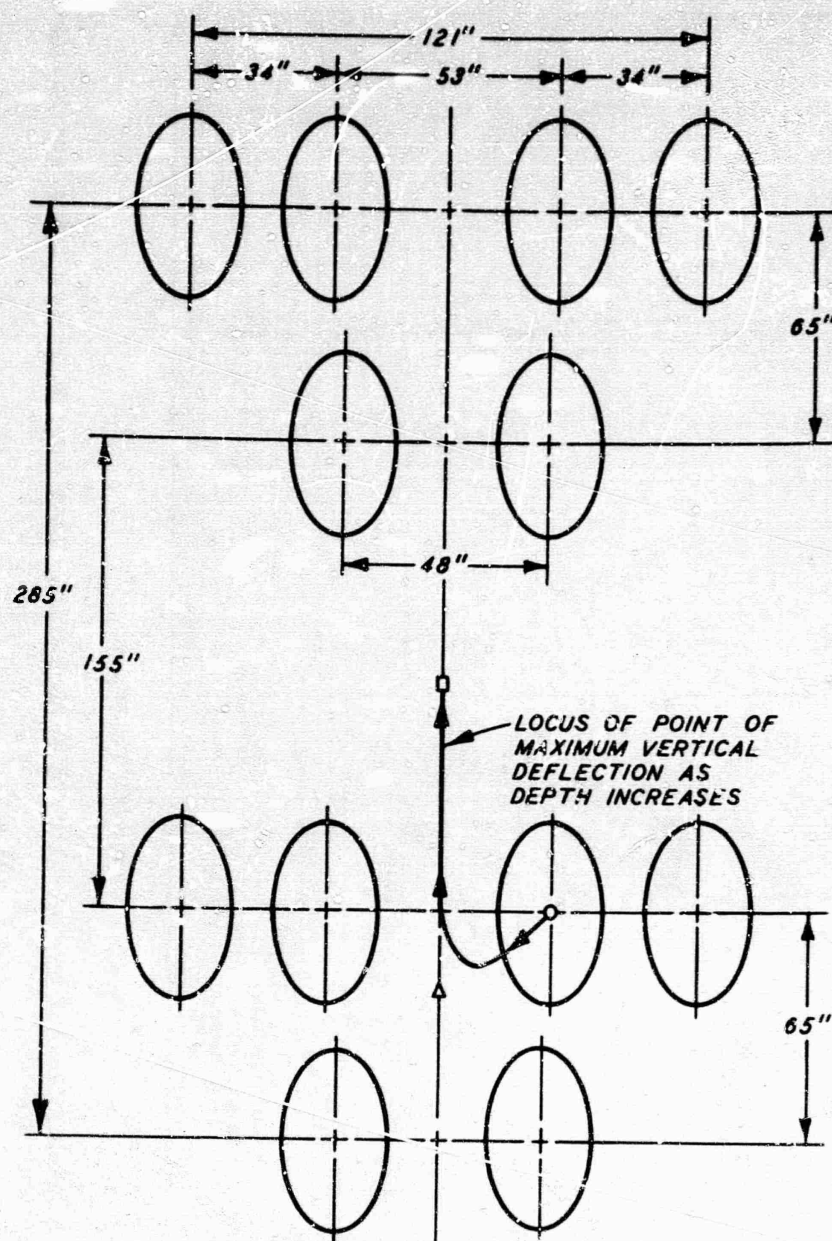
LEGEND

O PT A, CENTROID OF TIRE

Δ PT B, CENTROID OF THE FRONT SIX WHEELS

⊡ PT C, CENTROID OF TWELVE WHEELS

Figure 66. General Flow of Maximum Vertical Deflection with Depth

150
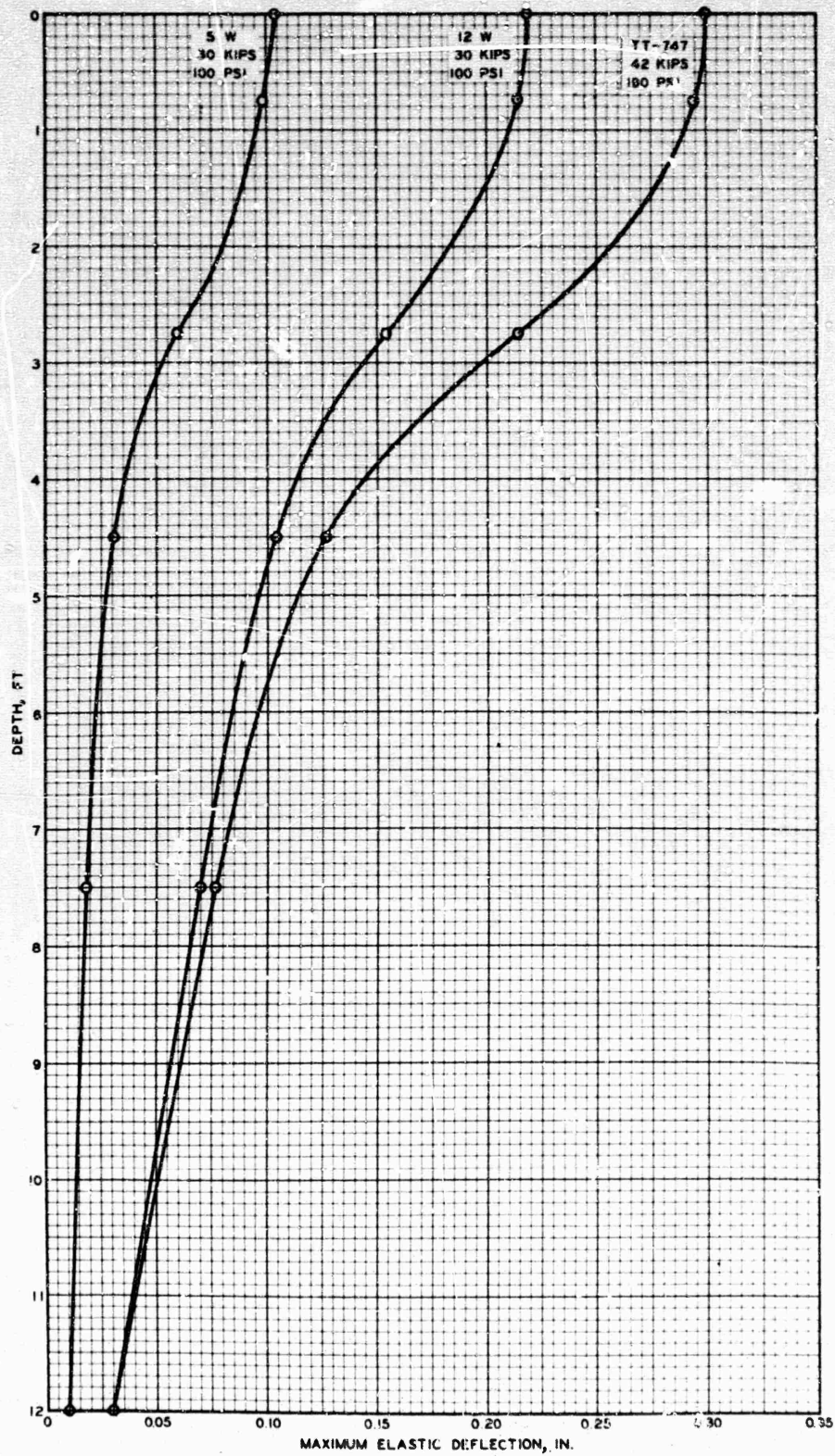
Figure 67.   Vertical Deflection Versus Depth (Data from Volume III-B, Item 3, Static Load)
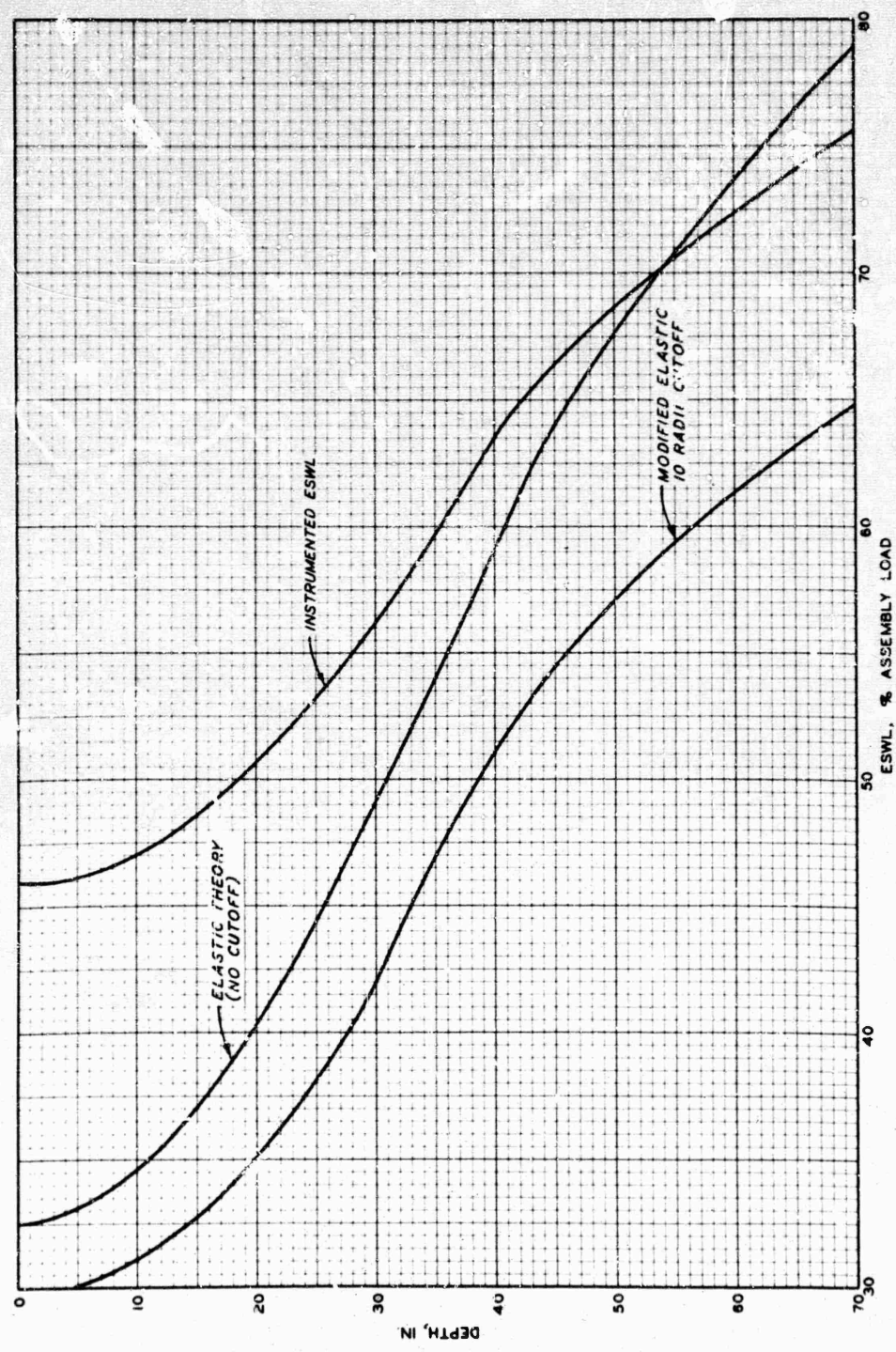
Figure 68. Comparison of Measured and Computed Equivalent Single-Wheel Load for Twin-Tandem Assembly
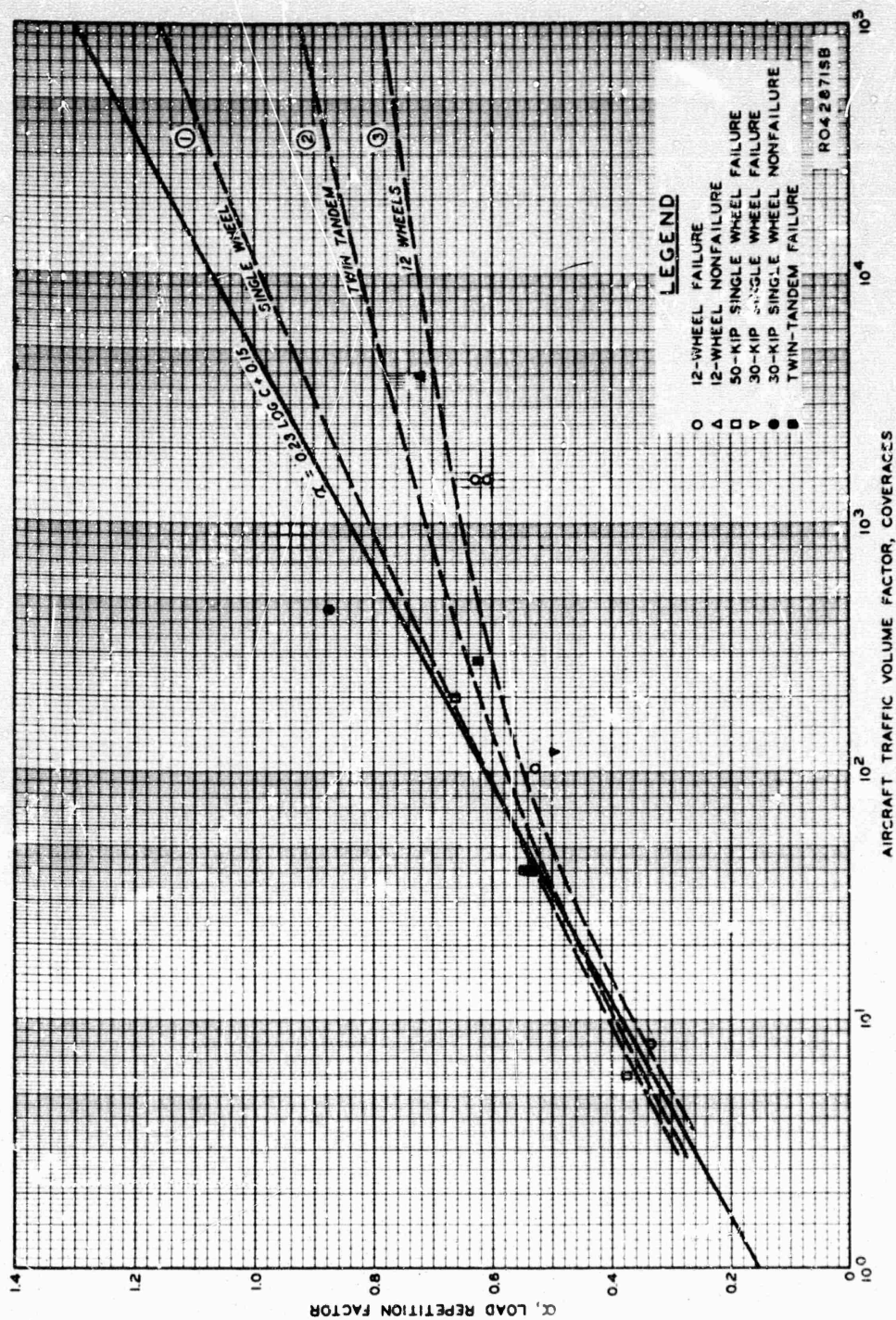
Figure 69. Load Repetition Factors Versus Coverages
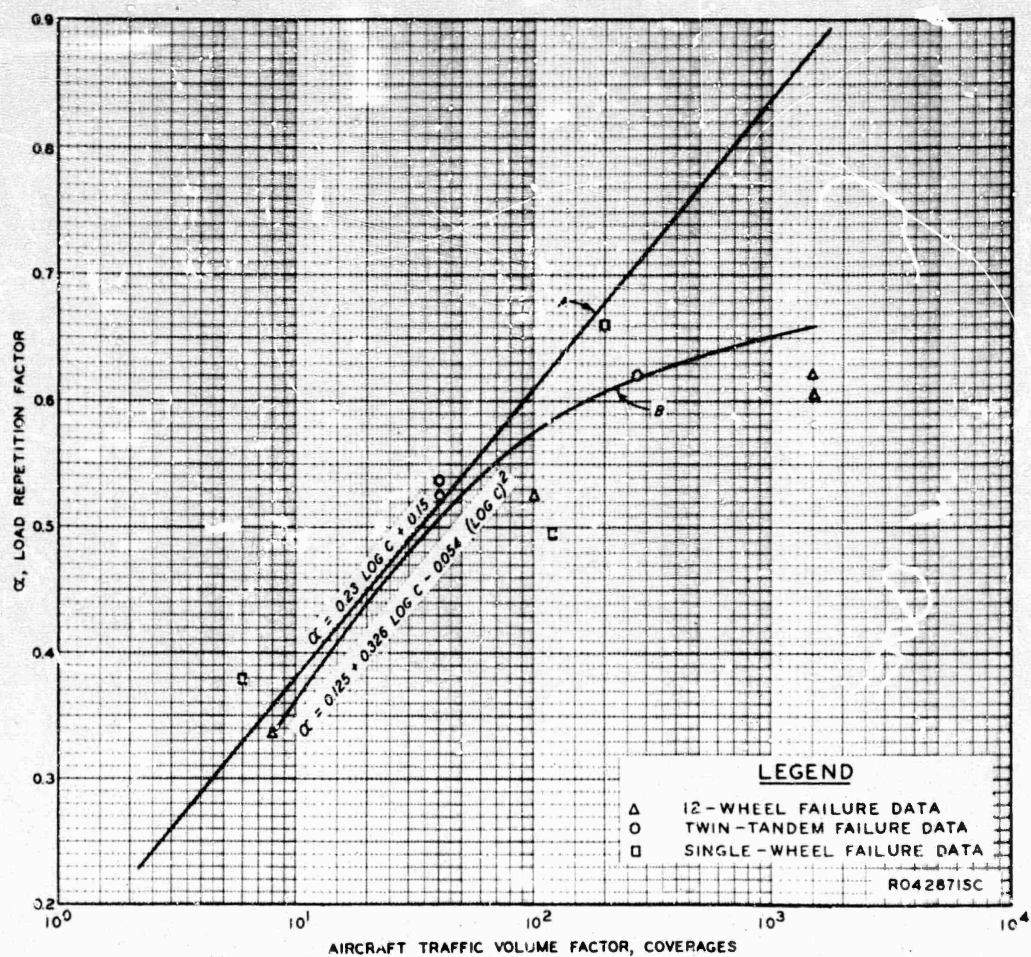
Figure 70. Comparison of Existing Design Curve (A) and Best-Fit Curve (B)

Note: Figures 71 through 79 have been
placed in the text proper for
the reader's convience.

Figure 80. Load Repetition Factor Versus Passes for MWHGL Study
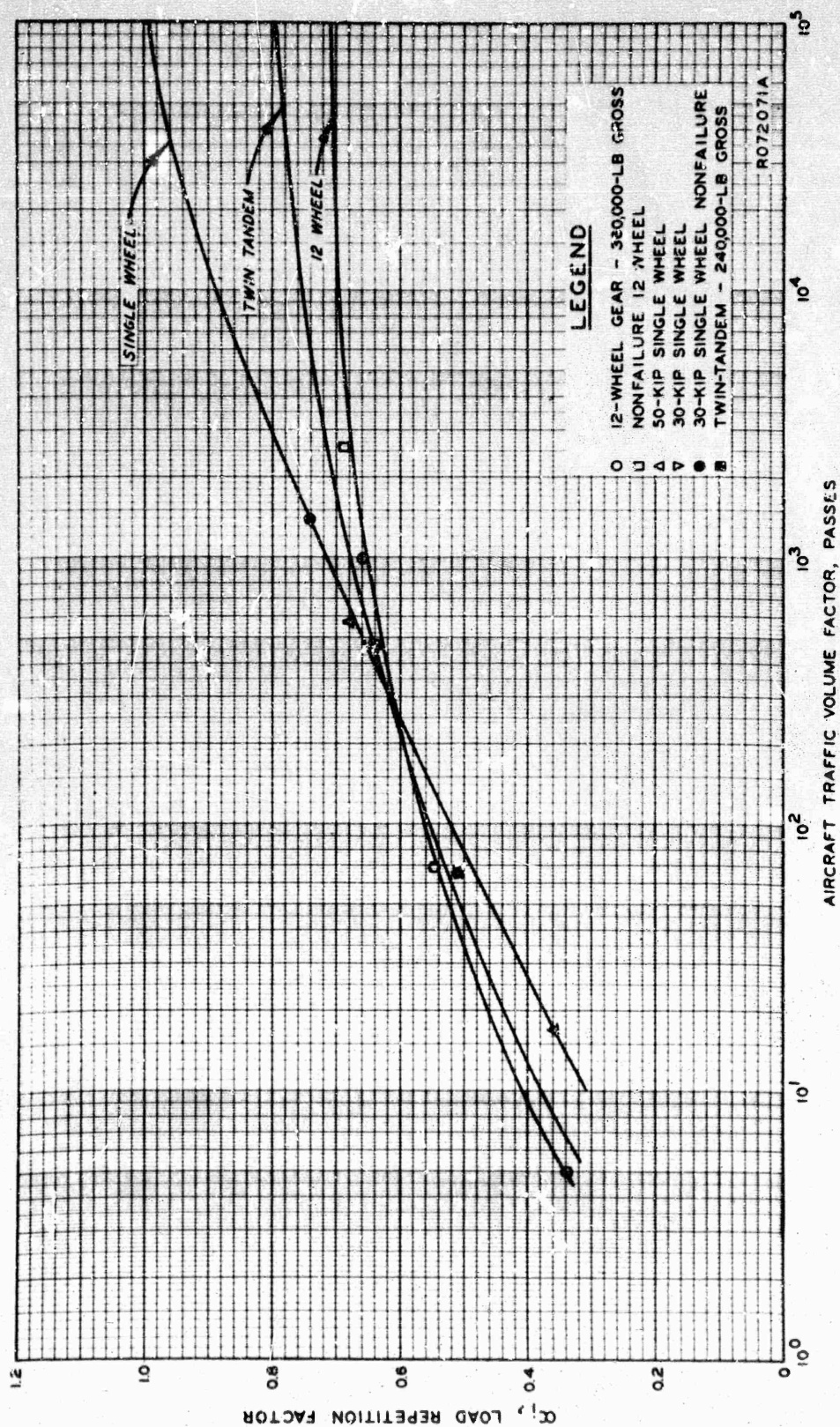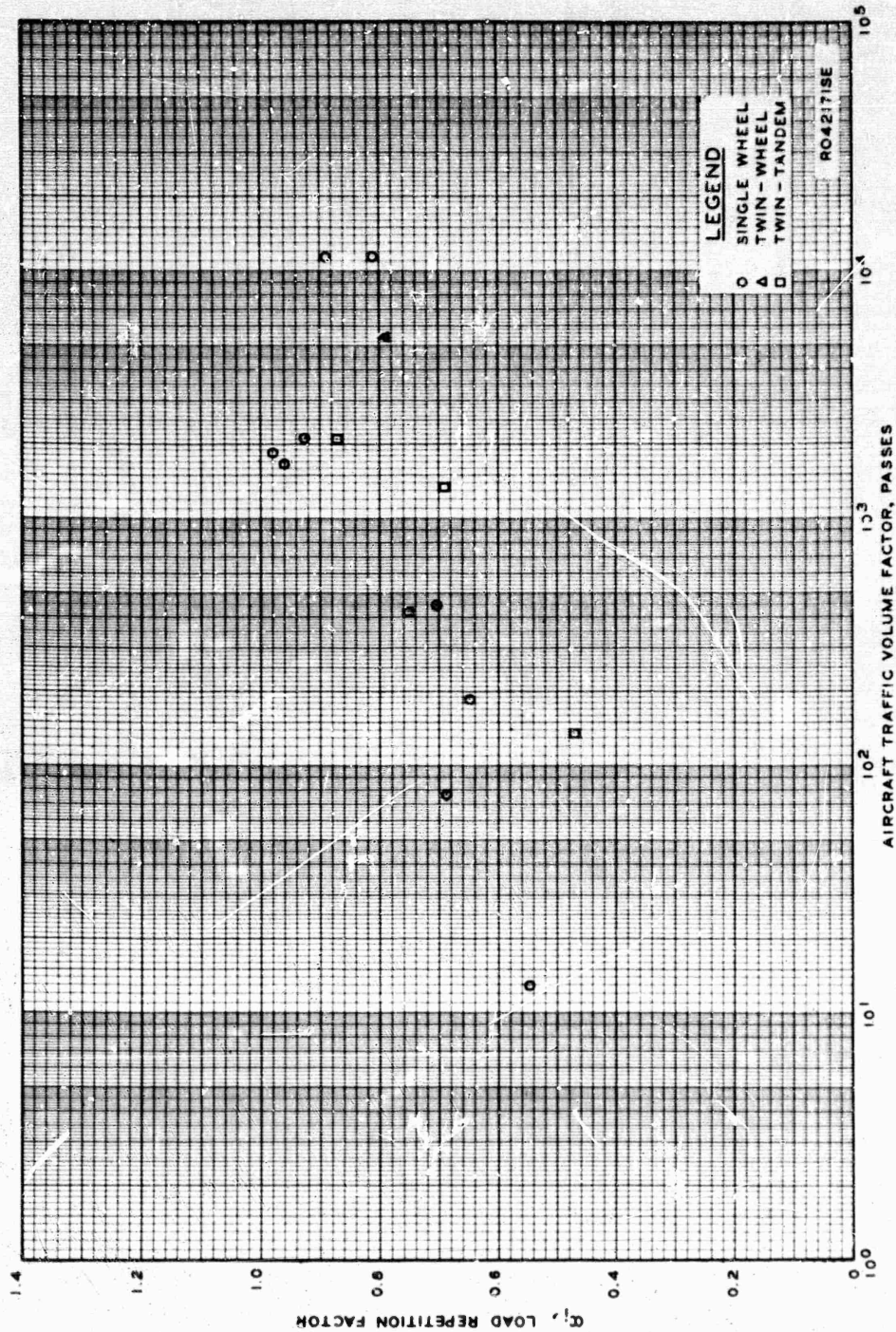
Figure 81. Load Repetition Factor Versus Passes for Related Studies

157
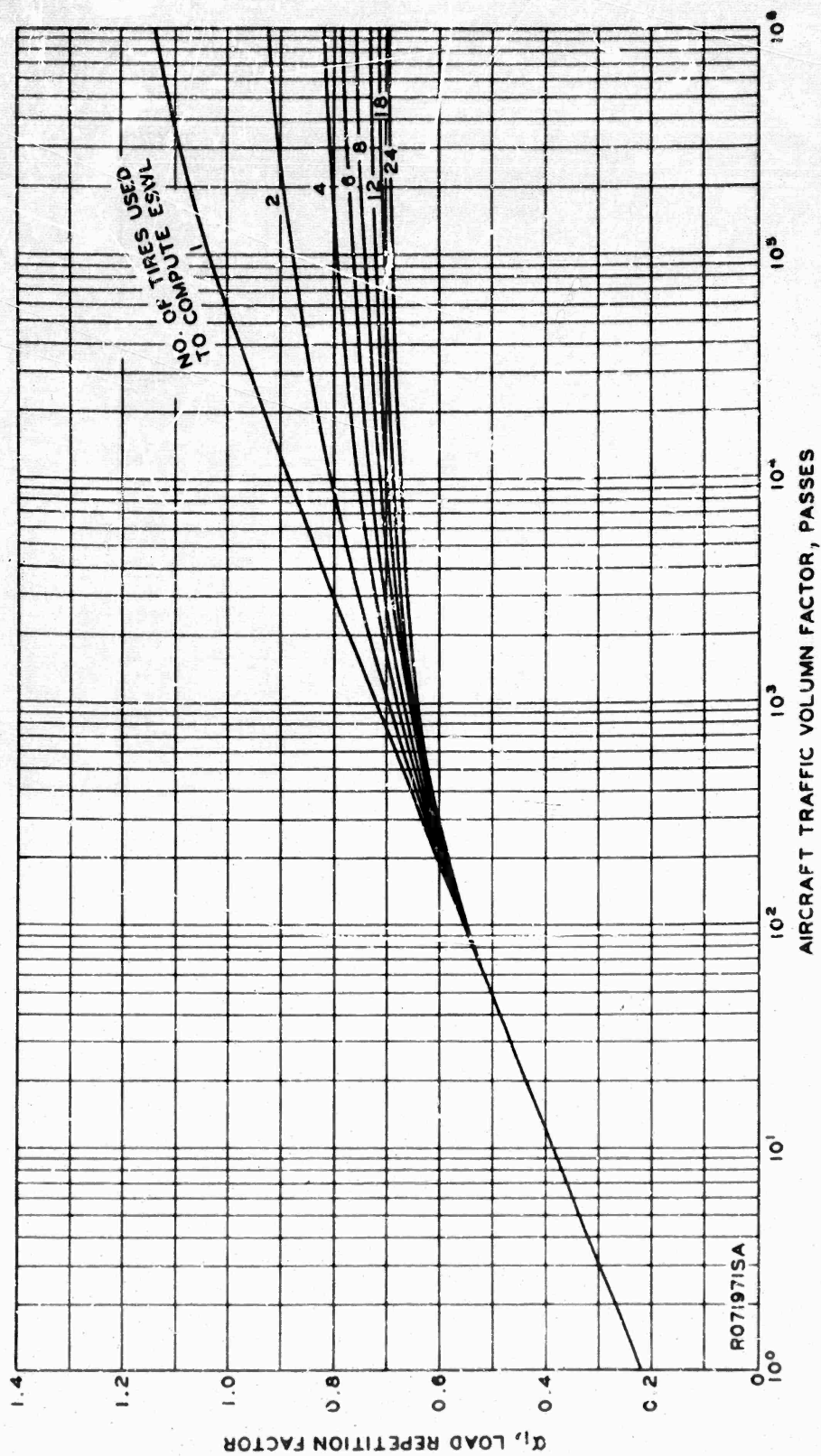
Figure 82. Composite Plot of Load Repetition Factors Versus Passes
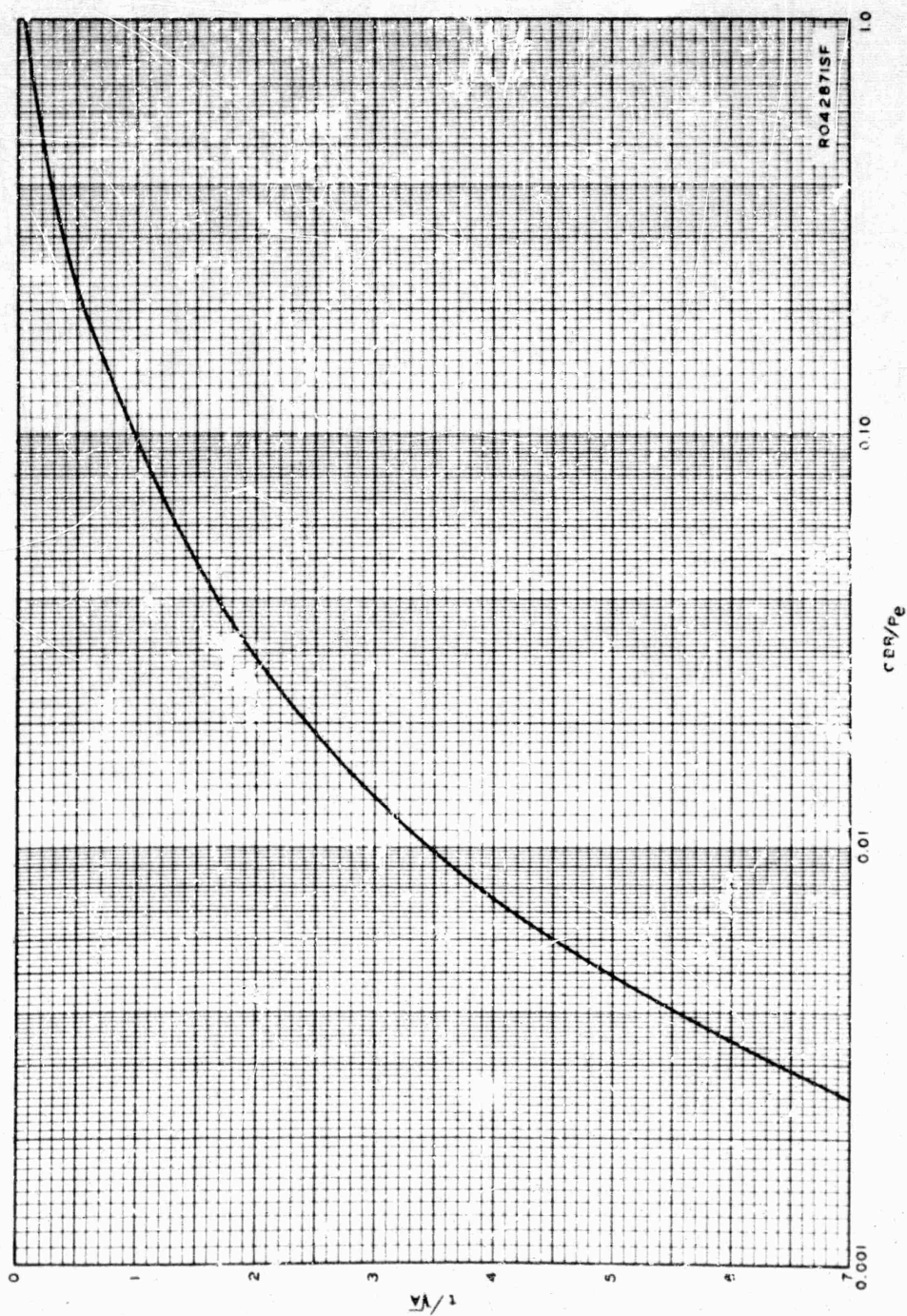
Figure 83. $\frac{t}{\sqrt{A}}$ Versus $\frac{CBR}{p_e}$
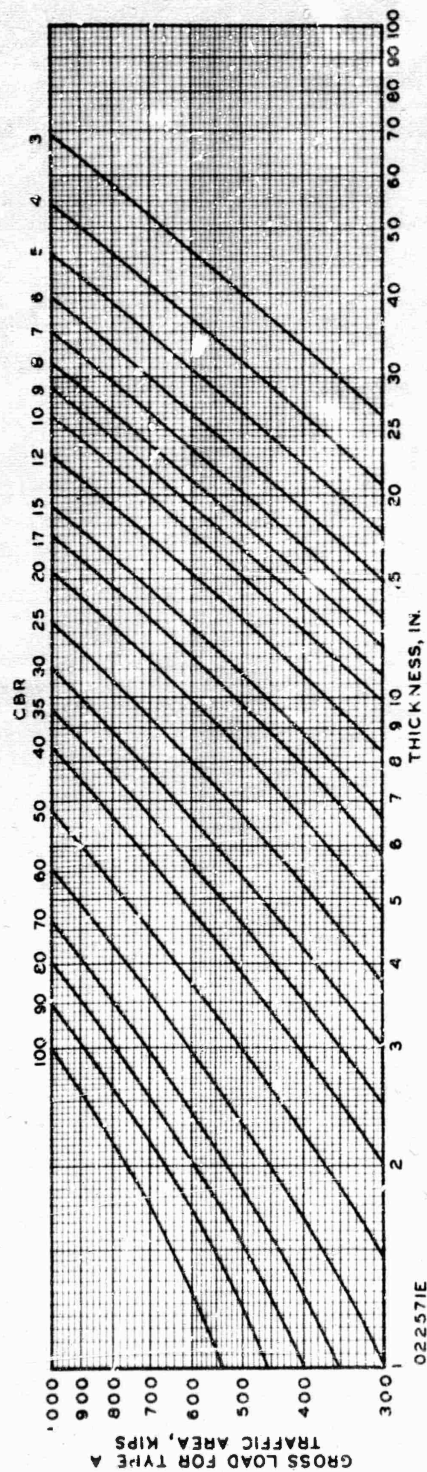
TYPE A TRAFFIC AREA — USE IN-PLACE THICKNESSES WITH THESE CURVES FOR CAPACITY OPERATION.

TYPE B AND C TRAFFIC AREAS — CURVES ARE NOT APPLICABLE.

Figure 84. Flexible Pavement Evaluation Curves for C-5A Capacity Operational Category (Contact Area 285 sq in.)
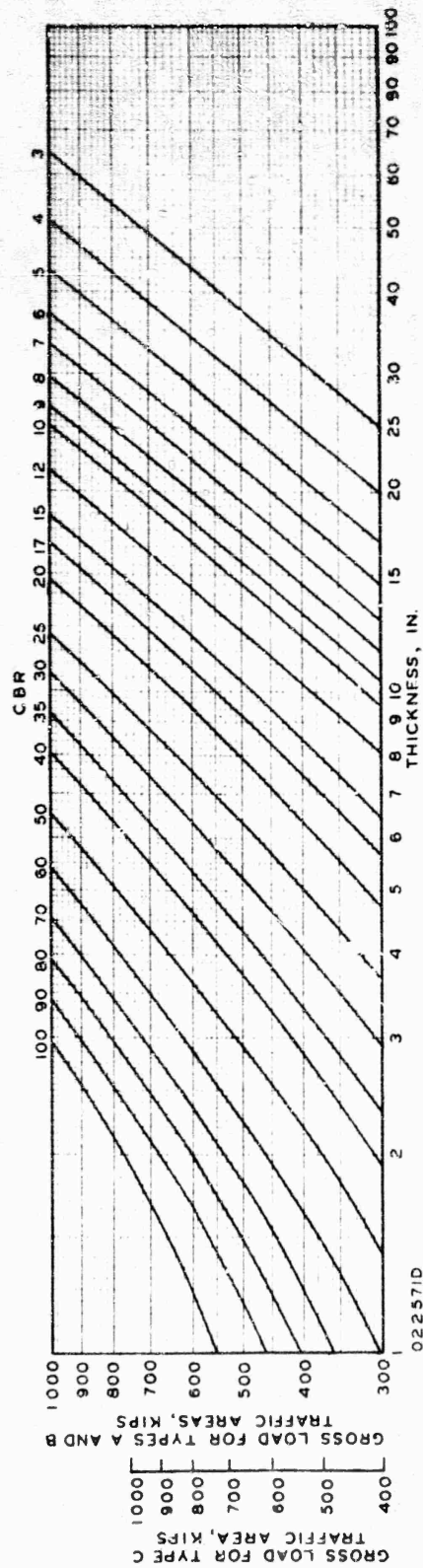
Figure 85. Flexible Pavement Evaluation Curves for C-5A Full and Capacity Operational
Categories (Contact Area 285 sq in.)

161
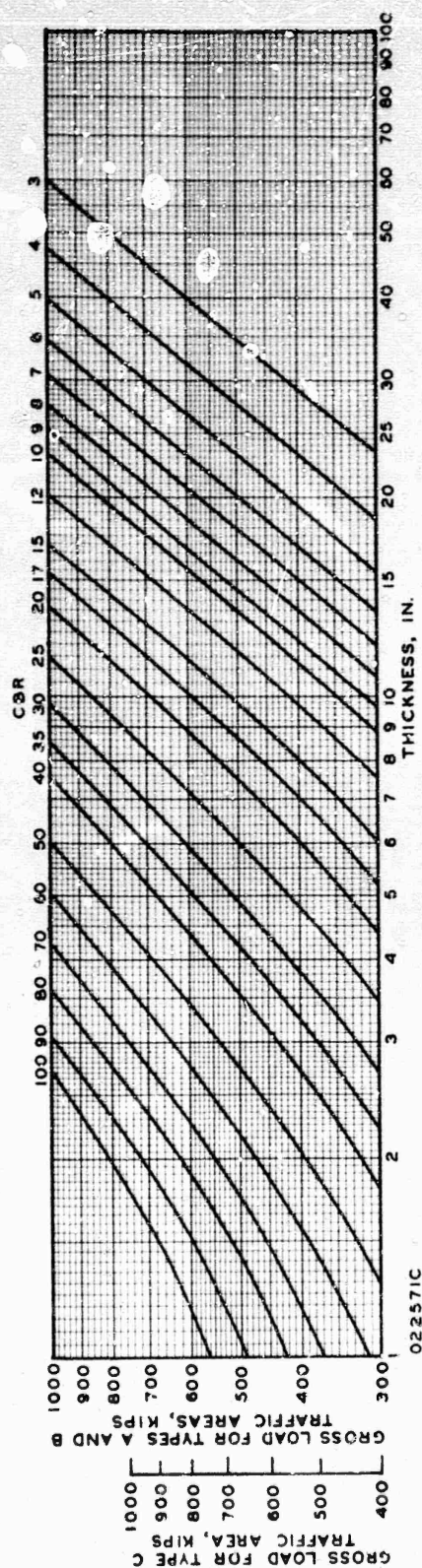
TYPE A TRAFFIC AREA   - USE IN-PLACE THICKNESSES WITH THESE
                         CURVES FOR MINIMUM OPERATION.

TYPE B AND C TRAFFIC AREAS - USE IN-PLACE THICKNESSES WITH THESE
                             CURVES FOR FULL OPERATION.

Figure 86. Flexible Pavement Evaluation Curves for C-5A Aircraft Minimum and Full Operational
            Categories (Contact Area 285 sq in.)

162

Figure 88. Flexible Pavement Evaluation Curves for C-5A Aircraft Emergency Operational Category and Capacity Operational Category for Overruns (Contact Area 285 sq in.)
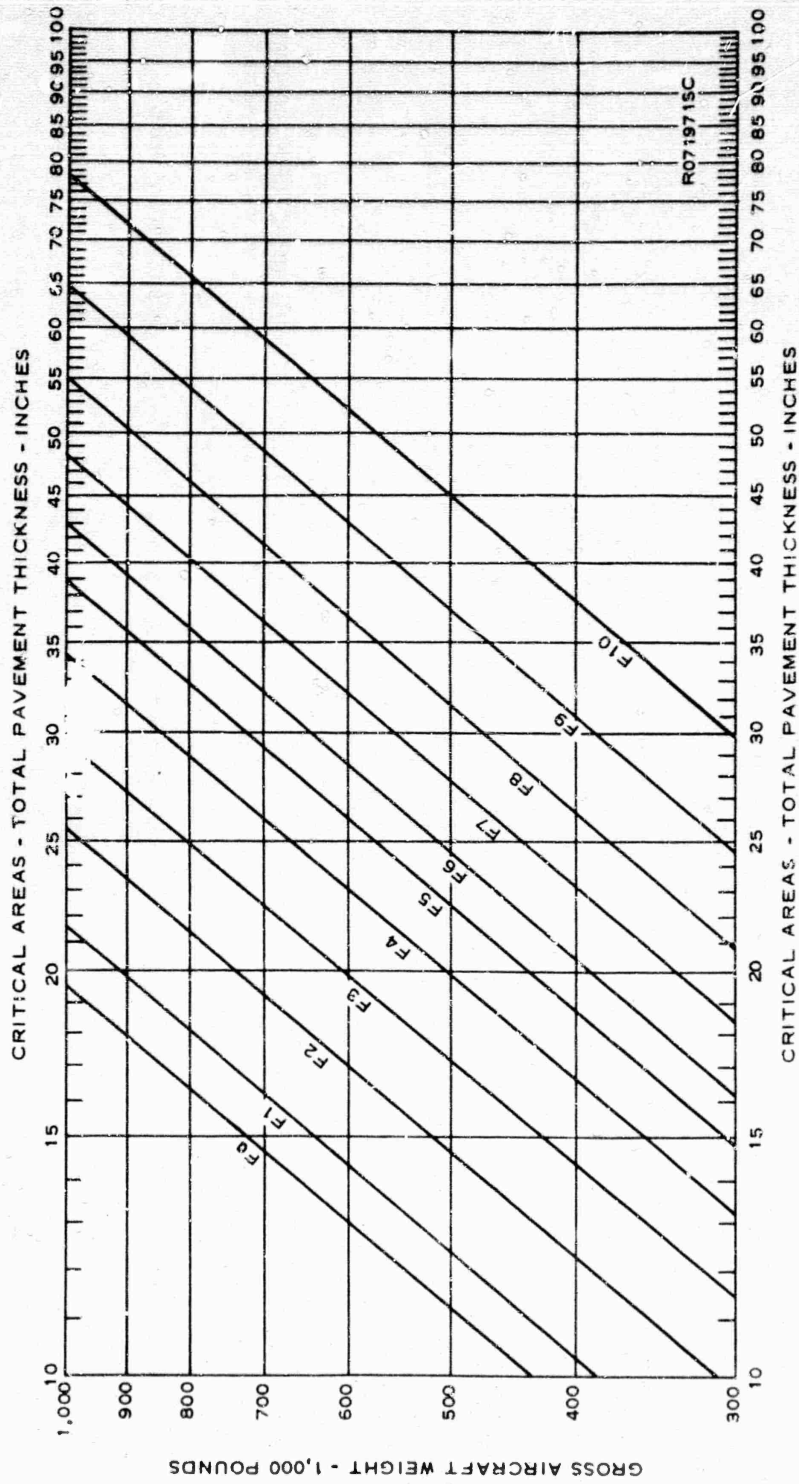
Figure 89. Flexible Pavement Design Curves in FAA Format for Boeing 747 Aircraft (Contact Area 208 sq in.)

165
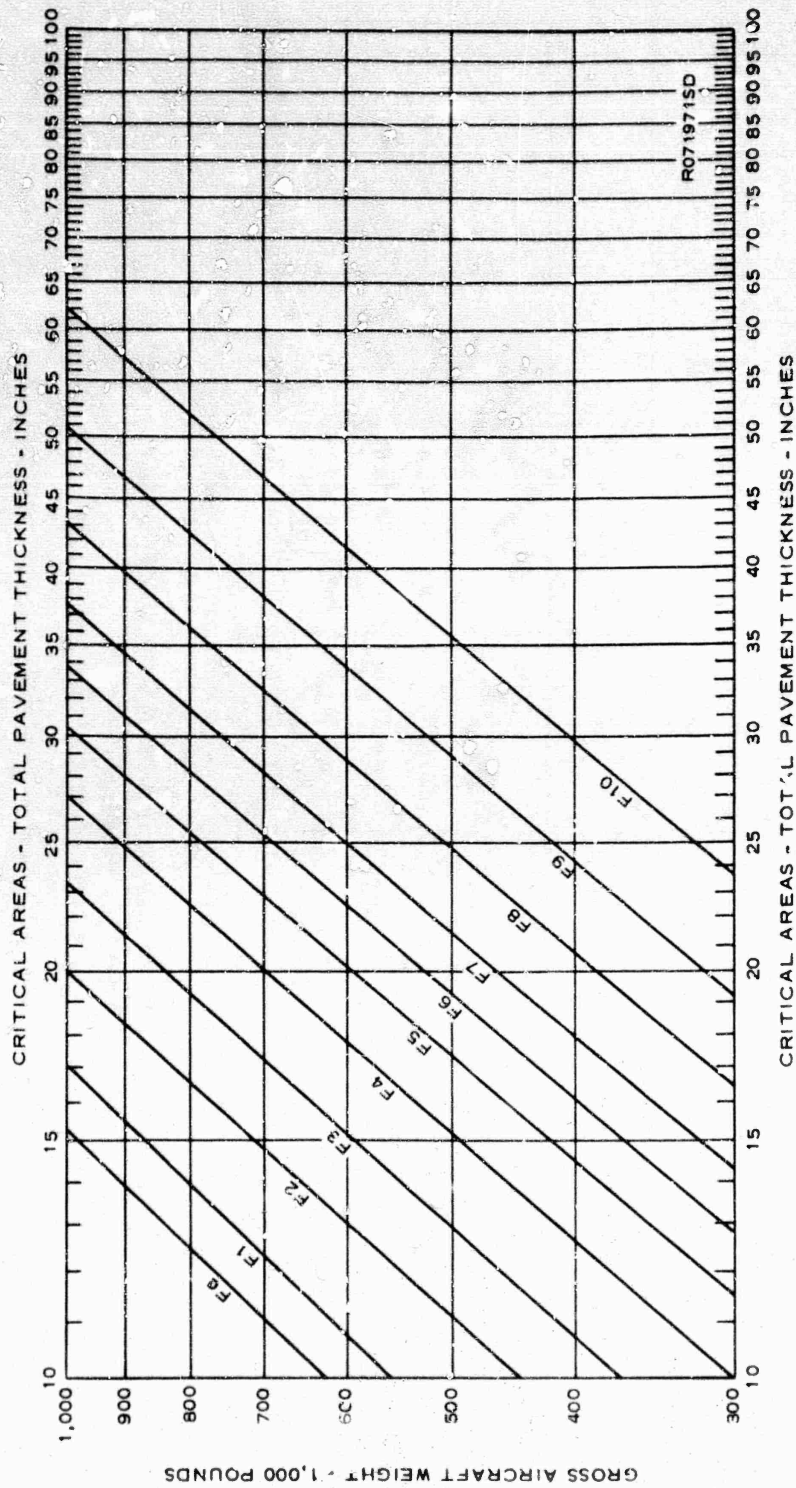
Figure 90. Flexible Pavement Design Curves in FAA Format for C-5A Aircraft (Contact Area 285 sq in.)

166
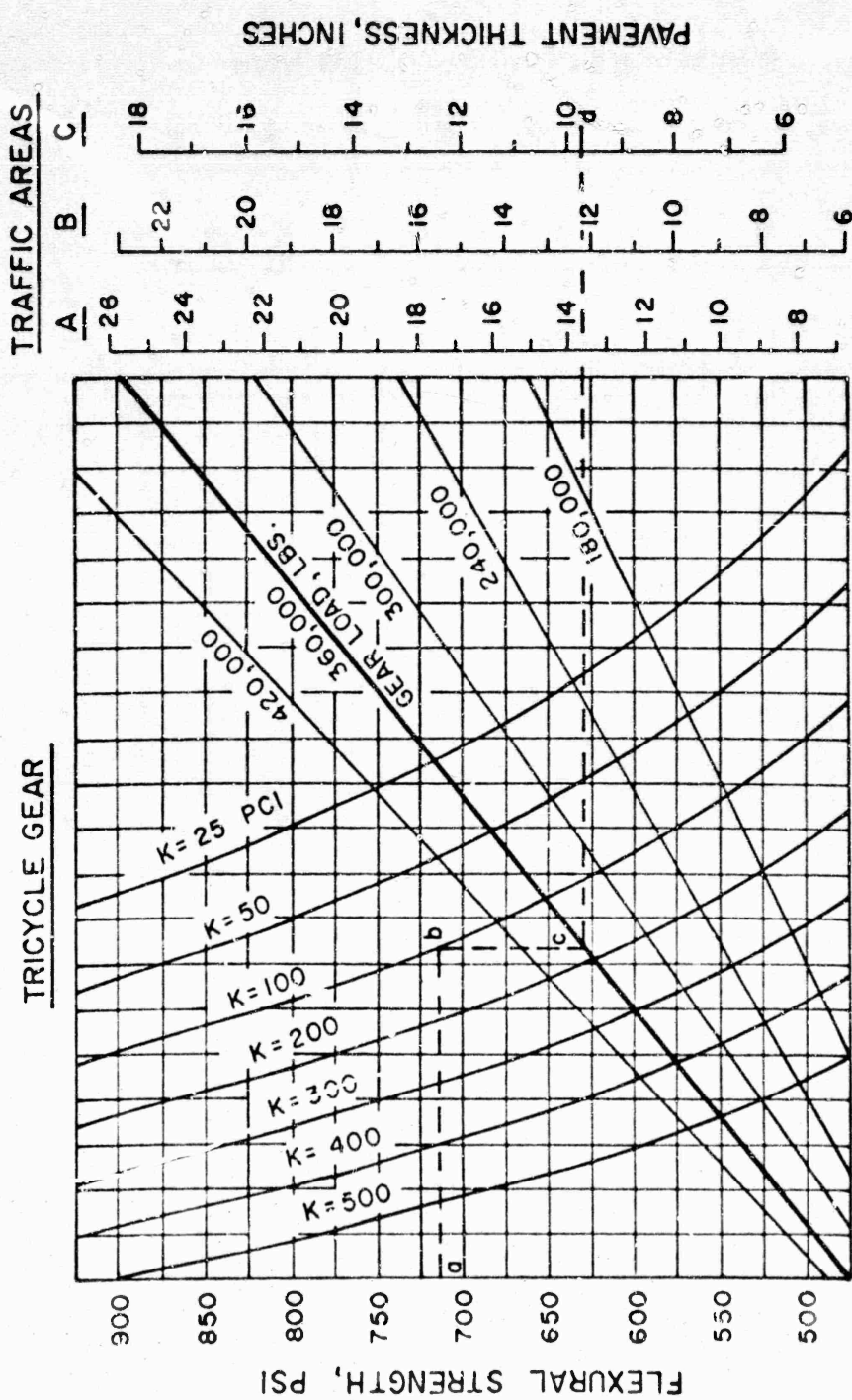
Figure 91. Rigid Pavement Design Curves for C-5A Aircraft (285-sq-in. Contact Area Each Wheel)

167
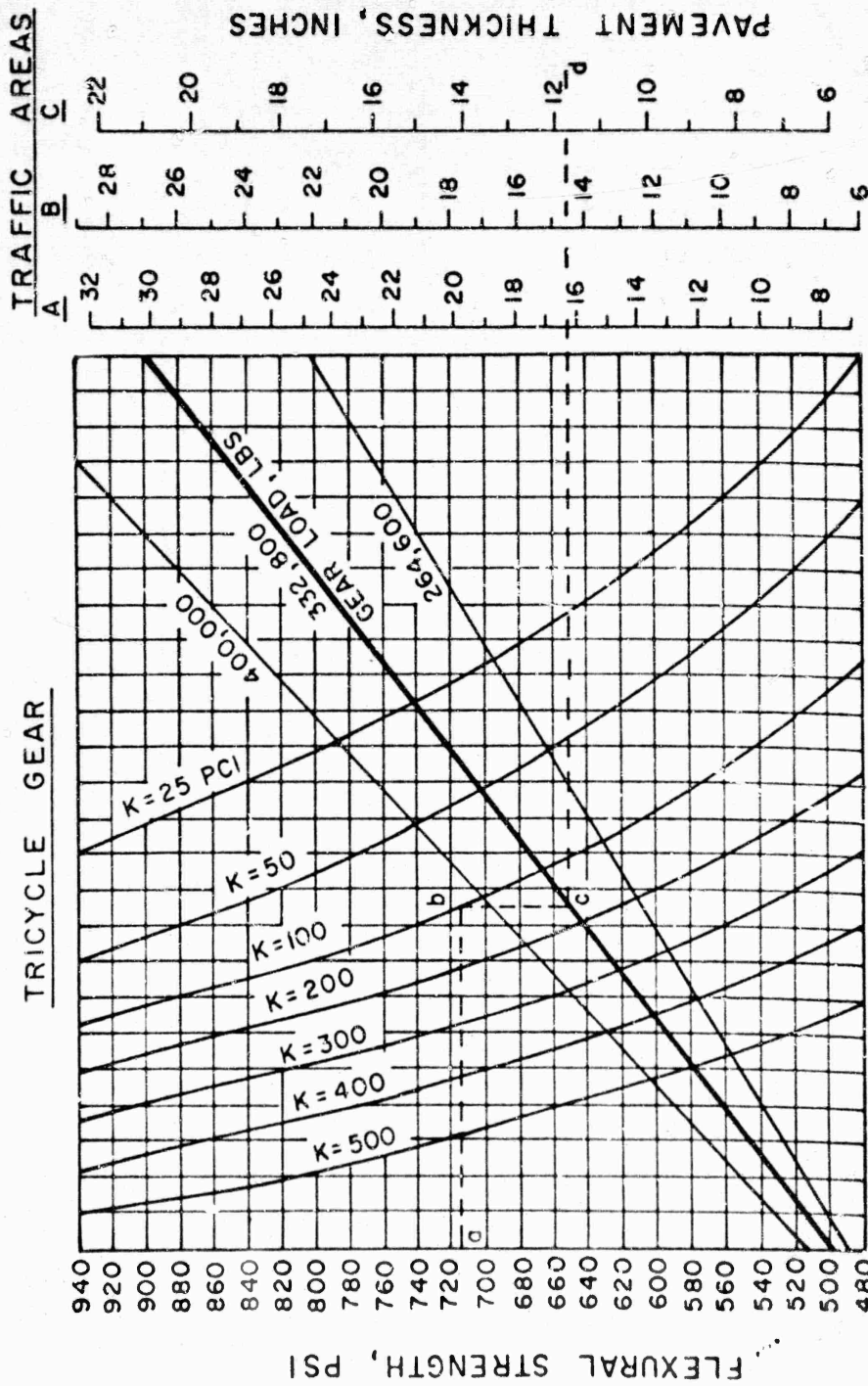
Figure 92. Rigid Pavement Design Curves for Boeing 747 Aircraft (208-sq-in. Contact Area Each Wheel)

168

Table 1

As-Constructed Thickness, CBR, Water Content, and Density Data

for Flexible Pavement Test Section

Test Item	Material	Station	Elev ft	Layer Thickness*		Total Thickness in.**		CBR	Water Content %	Dry Density, pcf		Percent CE 55 Density
				ft	in.	Design	Actual			In Place (A)	CE 55† (B)	(A/B)
West maneuver area	Cr stone base	3+90	194.05	0.90	10.8	12	13	34	1.4	135.2	140	97
	Subgrade		193.15					11	19.0	105.8	106	100
1	Cr stone	3+30	193.67	0.30	3.6	15	15	51	1.9	136.6	140	98
	Subbase		193.37	0.89	10.7			13	5.0	124.1	126	98
	Subgrade (CH)		192.48					3.0	33.2	86.0	85	101
	(CH)		191.64					3.7	31.8	88.0	86	98
	(CH)		190.79					3.4	32.5	83.3	87	96
	(CL)		189.82					2.2	23.8	97.0	97	100
	(CL)		188.88					4.0	23.5	98.9	97	102
2	Cr stone	2+70	193.42	0.60	7.2	24	24	81	1.8	141.3	140	101
	Subbase		192.82	1.26	15.1			12	5.0	129.4	126	103
	Subgrade (CH)		191.56					4.5	30.9	88.6	89	100
	(CH)		190.44					3.6	33.4	82.9	85	98
	(CH)		189.70					3.4	33.9	87.6	84	103
	(CL)		188.45					3.6	24.8	97.3	95	102
	(CL)		187.56					3.8	21.4	92.0	101	92
3	Cr stone	2+10	193.15	0.69	8.1	33	33	61	2.0	142.2	140	102
	Subbase		192.46	2.0	24.0			13	3.4	121.6	126	96
	Subgrade (CH)		190.46					3.4	30.9	87.6	89	99
	(CH)		189.55					2.4	32.5	85.4	86	99
	(CH)		188.54					3.3	34.8	84.0	83	102
	(CL)		187.74					4.5	20.9	102.8	102	101
	(CL)		186.59					3.7	20.6	101.9	102	100
	(CL)		185.61					3.9	23.0	99.7	98	101
	(CL)		184.81					1.8	22.1	99.0	100	99
	(CL)		184.00					1.1	23.2	98.6	98	101
	(CL)		182.65					1.9	21.7	98.1	99	99
	(CL)		181.78					2.2	22.2	96.7	99	98
4	Cr stone	1+50	192.84	0.65	7.8	33	33	72	1.4	142.0	140	101
	Subbase		192.19	1.93	23.2			15	3.0	130.4	126	103
	Subgrade (CH) 4-CBR design		190.26					3.5	30.2	89.3	84	100
			189.43					3.1	33.4	84.4	85	99
			188.65					3.3	33.0	84.2	85	99
	2-CBR design		187.69			54	53	2.7	36.7	79.9	80	100
			186.75					2.0	33.2	83.2	85	98
	(CL)		185.68					2.9	24.0	97.3	96	101
	(CL)		184.71					1.4	22.4	98.4	99	99
5	Cr stone	0+90	192.50	0.64	7.7	42	41	37	1.0	140.5	140	100
	Subbase		191.86	2.64	31.7			11	2.7	131.1	126	104
	Subgrade (CH)		189.22					4.0	31.8	87.5	85	100
	(CH)		188.13					2.7	34.1	83.5	84	100
	(CH)		187.29					3.1	31.5	84.1	83	102
	(CL)		186.19					2.7	23.5	98.1	97	101
	(CL)		185.23					2.0	22.6	98.6	99	100
East maneuver area	Cr stone	0+30	192.20	0.63	7.5	33	32	41	1.6	135.0	140	96
	Subbase		191.57	1.91	23.0			16	2.9	126.5	126	100
	Subgrade (CL)		189.66					8	20.5	103.4	103	100

* Layer thicknesses measured at test pit locations.
** Total actual thicknesses derived from cross sections taken during construction at the top of each pavement element.
† Laboratory densities shown in this column are the CE 55 maximum densities at optimum water content for the crushed-stone base and the gravelly sand subbase material and the CE 55 density corresponding to the field in-place water contents for the subgrade material.

Table 2

Stability, Flow, Voids, and Density Data for Asphaltic Concrete

Test Item	Cov- erages	Asphalt Content % Total Wt	Sta- bility lb	Flow 1/100 in.	Percent Voids		Unit Wt Total Mix pcf	% Plant Laboratory Density
					Total Mix	Filled/AC		
Laboratory Mix Design*								
--	--	5.0	2420	14	4.1	74.0	150.9	--
Plant-Mixed, Laboratory-Compacted Samples*								
--	--	5.0	2200	10	4.5	73.0	150.3	100.0
Field Cores**								
1-5	0	5.0	650	9	7.5	60.5	145.4	96.8
1	12	5.0	1310	18	6.6	63.6	147.0	97.5
2	200	5.0	1362	18	6.0	65.9	147.8	98.0
3	3334	5.0	1593	15	4.3	73.3	150.6	100.2
4	3343	5.0	1455	16	4.5	70.6	149.7	99.3
5	3848	5.0	1700	16	3.7	76.8	151.5	100.8

* Specimens compacted by gyratory compaction, 200-psi pressure, 1-deg pitch, and 30 revolutions.
** Field cores obtained from traffic lane 1 360,000-lb, 12-wheel-gear assembly.

Table 3

As-Constructed Pavement and Foundation Properties of Rigid Pavement Test Section

Item No.	Material	Elevation ft	Thickness in.*		Flexural Strength, psi**		Modulus of Soil Reaction k lb/cu in.	CBR	Water Content %	Dry Density pcf
			North Lane	South Lane	North Lane	South Lane				
West maneuver area	Asphaltic concrete	--	3.0	3.0	--	--	--	--	--	--
	Crushed stone	--	6.0	6.0	--	--	--	--	--	--
	Subbase	--	24.0	24.0	--	--	--	--	--	--
	Subgrade (CL)	191.02	--	--	--	--	--	6.3	19.5	101.8
1	Asphaltic concrete	--	4.0	4.5	--	--	--	--	--	--
	PCC	--	9.7	10.2	585	640	--	--	--	--
	Subgrade (CH)	192.47	--	--	--	--	62	2.8	32.2	85.5
	Subgrade (CL)	189.47	--	--	--	--	--	2.1	23.4	98.1
	Subgrade (CL)	180.83	--	--	--	--	--	6.0	91.5	24.8
2	PCC	--	11.4	12.1	600	730	--	--	--	--
	Subgrade (CH)	191.93	--	--	--	--	70	2.5	32.9	83.9
	Subgrade (CL)	189.32	--	--	--	--	--	2.1	23.1	98.6
	Subgrade (CL)	180.16	--	--	--	--	--	4.5	20.8	99.2
3	PCC	--	13.6	14.0	630	760	--	--	--	--
	Subgrade (CH)	191.38	--	--	--	--	74	3.2	32.0	86.0
	Subgrade (CL)	188.87	--	--	--	--	--	3.2	23.5	98.4
	Subgrade (CL)	181.27	--	--	--	--	--	--	--	--
4	Asphaltic concrete	--	5.6	5.3	--	--	--	--	--	--
	PCC	--	7.5	8.0	560	720	--	--	--	--
	Subgrade	191.65	--	--	--	--	74	2.9	31.5	86.1
	Subgrade	188.57	--	--	--	--	--	2.2	23.3	98.0
	Subgrade	181.13	--	--	--	--	--	7.7	18.7	104.5
East maneuver area	Asphaltic concrete	--	3.0	3.0	--	--	--	--	--	--
	Crushed stone	--	6.0	6.0	--	--	--	--	--	--
	Subbase	--	24.0	24.0	--	--	--	--	--	--
	Subgrade (CL)	189.15	--	--	--	--	--	7.2	19.6	100.5

* Thicknesses were obtained from level readings made on the subgrade prior to concrete placement and on the concrete after placement.

** Average 28-day value.

Table 4

28-Day Flexural Strength Data for Concrete Used in

Rigid Pavement Test Section

Curing Condition	Item No.	Specimen No.*	Beam Dimensions in.		Cement Factor bag/cu yd	Slump in.	Entrained Air %	Flexural Strength psi**
			Depth	Width				
North Paving Lane								
Field	1	1	6.00	6.05	5.0	3.50	3.9	390
	2	4	6.05	6.10	5.5	3.50	4.2	575
	3	7	6.05	6.10	5.5	3.75	3.8	485
							Avg	485
Standard	1	2	5.85	6.20	5.0	3.50	3.9	585
	2	5	6.00	6.00	5.5	3.50	4.2	620
	2	6	6.05	6.15	5.5	3.50	4.2	575
	3	8	6.10	6.10	5.5	3.75	3.8	630
	4	10	6.00	6.00	5.5	3.75	4.9	580
	4	11	6.05	6.15	5.5	3.75	4.9	535
							Avg	590
South Paving Lane								
Field	1	3	6.05	6.20	6.5	3.25	4.5	620
	3	9	6.00	6.00	6.5	3.50	4.9	615
	4	12	6.05	6.05	6.5	3.75	4.7	590
							Avg	620
Standard	1	2	6.10	6.15	6.5	3.25	4.5	640
	2	5	6.00	6.10	6.5	3.50	3.8	705
	2	6	6.00	6.00	6.5	3.50	3.8	750
	3	7	6.00	6.00	6.5	3.50	4.9	745
	3	8	6.10	6.15	6.5	3.50	4.9	775
	4	11	5.85	6.20	6.5	3.75	4.7	720
							Avg	720

* Specimens taken during concrete placement.
** Average of two breaks.

Table 5

28-Day Compressive Strength Data for Concrete Used in

Rigid Pavement Test Section

Curing Condition	Item No.	Specimen No.*	Cylinder Dimensions, in.		Cement Factor bag/cu yd	Slump in.	Entrained Air, %	Compressive Strength psi**	
			Height	Diameter					
North Paving Lane									
Field	1	3	12	6	5.0	3.50	3.9	3750	
	2	5	12	6	5.5	3.50	4.2	3910	
	4	9	12	6	5.5	3.75	4.9	3960	
								Avg	3870
Standard	1	1	12	6	5.0	3.50	3.9	4110	
	2	4	12	6	5.5	3.50	4.2	3980	
	3	6	12	6	- 5.5	3.75	3.8	4030	
								Avg	4040
South Paving Lane									
Field	1	3	12	6	6.5	3.25	4.5	3750	
	3	9	12	6	6.5	3.50	4.9	4290	
	4	12	12	6	6.5	3.75	4.7	4320	
								Avg	4120
Standard	1	2	12	6	6.5	3.25	4.5	4520	
	2	5	12	6	6.5	3.50	3.8	5780	
	2	6	12	6	6.5	3.50	3.8	5680	
	3	7	12	6	6.5	3.50	4.9	4610	
	3	8	12	6	6.5	3.50	4.9	4640	
	4	11	12	6	6.5	3.75	4.7	5210	
								Avg	5070

* Specimens taken during concrete placement.
** Average of two breaks.

Table 6

Field Compaction Data for Nonrigid Overlay Placed on

Rigid Pavement Test Section

Test Item No.	Layer Thickness in.	Asphalt Content % Total Wt	Stability lb	Flow 1/100 in.	Percent Voids		Unit Wt Total Mix pcf	% Plant Laboratory Density
					Total Mix	Filled/AC		
Plant-Mixed, Laboratory-Compacted Samples*								
--	--	2.6	2320	9	10.3	36.4	146.5	100
--	--	2.8	2242	9	9.7	39.8	147.0	100
Field Cores**								
1	4	2.6	--	--	10.9	35.1	145.5	99.3
1	4	2.8	500	20	10.2	38.6	146.2	99.7
4	3	2.6	700	15	10.2	36.6	146.6	100
4	6	2.6	800	15	10.6	35.8	146.0	99.7

* 75-blow Marshall compaction.
** Cores cut immediately after compaction.

Table 7

Summary of After-Traffic Water Content, Density, and CBR Data

for Flexible Pavement Test Section

Lane	Assembly	Test Item	Fill No.	Sta	Location	Material	Elev ft	Layer Thickness %	Layer Thickness ft	Total Thickness Design in.	Total Thickness Actual in.	Traffic Cov	CBR	Water Content %	Dry Density In Place (A)	Dry Density CE 55 (B)	Percent CE 55 Density (A/B)
1	360 kip 12 wheel	1	1	3+5	Inside traffic lane	Asphaltic conc	193.83	0.28	3.36	15	15.36	8	-	-	137.1	-	-
						Cr stone base	193.55	0.42	5.04				8	1.9	135.4	140	96*
						Subbase	193.13	0.58	6.96				4.3	3.8	88.5	126	107*
						(CH)	192.55						2.7	32.7	86.2	87	102***
						(CH)	191.50						4.2	31.2	81.3	89	97
						(CH)	190.50						3.8	32.7	81.3	87	97
						(CL)	189.50						3.6	20.5	102.2	103	99
					Outside traffic lane	Asphaltic conc	193.76	0.28	3.36	15	15.48		-	-	136.9	-	-
						Cr stone base	193.48	0.56	6.72				36	2.0	133.8	140	98*
						Subbase	192.92	0.45	5.40				21	6.5	88.5	126	106*
						(CH)	192.47						3.4	30.3	86.5	89	98***
						(CH)	191.50						6.2	31.1	86.4	87	97
						(CH)	190.50						4.8	30.8	86.4	90	97
		1	2	3+05	Inside traffic lane	Asphaltic conc	193.68	0.39	4.68	15	14.10	12	-	-	132.5	-	95*
						Cr stone base	193.29	0.44	4.26				11	1.4	128.0	140	95*
						Subbase	192.94	0.43	5.16				4.2	3.6	87.4	126	102*
						(CH)	192.51						2.8	30.9		90	97*
					Outside traffic lane	Asphaltic conc	193.62	0.25	3.00	15	14.40		-	-	141.1	-	-
						Cr stone base	193.37	0.52	6.24				58	0.9	126.5	140	101*
						Subbase	192.85	0.43	5.16				7	3.2	85.6	126	100*
						Subgrade (CH)	192.42						3.1	32.2		87	98**
	2		3	2+70	Inside traffic lane	Asphaltic conc	193.39	0.35	4.20	24	23.64	200	-	-	140.3	-	-
						Cr stone base	193.04	0.49	5.88				79	1.0	130.7	140	100*
						Subbase	192.55	1.13	13.56				15	3.8	87.5	126	104*
						(CH)	191.42						4	31.3	87.7	89	98**
						(CH)	190.48						6	30.8	85.7	90	97
						(CH)	189.48						6	31.7	101.6	89	96
						(CL)	188.28						4.5	20.8		102	100
					Outside traffic lane	Asphaltic conc	193.43	0.30	3.60	24	24.72		-	-	141.0	-	-
						Cr stone base	193.13	0.50	6.00				67	1.1	128.1	140	101*
						Subbase	192.63	1.26	15.12				20	3.0	88.5	126	102***
						Subgrade (CH)	191.37						5	30.6	86.9	90	98**
						(CH)	190.35						7	30.8	82.4	90	97
						(CH)	189.35						4.0	34.1		84	98

Table 7 (cont'd)

3	2+30	Inside traffic lane	Asphaltic conc	193.16	0.33	3.96	33	31.32	2342	103	-	-	-
			Cr stone base	192.63	0.42	5.04				23	0.6	139.8	140	100
			Subbase	192.4	1.86	20.34				4.3	2.9	129.2	126	103
			(CL)	190.55						5	32.4	86.7	97	100
			(CH)	189.56						3.6	32.6	84.8	87	98
			(CH)	188.56						3.5	32.4	83.0	87	95
			(CL)	187.85							20.1	98.1	100	98
		Outside traffic lane	Asphaltic conc	191.32	0.32	3.84	33	34.44		92	-	-	-	-
			Cr stone base	193.00	0.56	6.72				32	1.1	161.7	140	102
			Subbase	192.44	1.90	23.68					1.9	129.4	126	103
			Subgrade (CH)	190.45						3.9	32.1	85.8	88	97
			(CH)	189.35						6	31.7	85.7	89	96
			(CH)	188.85						3.8	33.4	83.0	85	98
			(CL)	187.44						3.7	22.1	101.4	100	101
4	1+90	Inside traffic lane	Asphaltic conc	192.98	0.37	4.44	33	33.36	2342	86	-	-	-	-
			Cr stone base	192.61	0.37	4.44				27	1.1	143.9	140	102
			Subbase	192.24	2.04	24.18				4.9	0.3	137.6	126	109
			Subgrade (CH)	190.20						5	31.5	86.0	89	97
			(CH)	189.20						2.5	31.9	85.0	88	97
			(CL)	188.20						6	36.4	79.7	80	100
			(CL)	187.35						6	21.7	100.2	101	99
			(CL)	186.38						5	19.6	101.6	105	97
5	1+90	Inside traffic lane	Asphaltic conc	192.72	0.37	4.44	33	32.40	2351	6.0	-	-	-	-
			Cr stone base	192.35	0.32	3.84				38	0.9	143.0	140	102
			Subbase	192.03	2.01	24.12					3.4	130.1	126	103
			Subgrade (CH)	190.02						4.5	31.4	87.0	89	96
			(CH)	189.04						2.7	33.9	84.6	65	100
			(CH)	187.54						2.2	34.7	83.1	84	99
			(CH)	186.54						4.2	33.9	82.5	85	97
			(CL)	185.54						2.5	33.7	82.3	85	97
			(CL)	185.45						3.0	22.3	99.0	100	99
			(CL)	184.52						3.3	22.3	100.3	100	100
			(CL)	183.52							21.8			
			(CL)	182.52							21.0			
			(CL)	181.52							20.1			
			(CL)	180.72							20.9			
6	1+90	Outside traffic lane	Asphaltic conc	191.76	0.35	4.20	33	33.24		65	-	-	-	-
			Cr stone base	192.41	0.49	4.88				31	1.7	146.0	140	104
			Subbase	191.92	1.04	22.28				4.1	2.0	130.2	126	104
			Subgrade (CH)	189.08						3.7	32.3	86.2	89	97
			(CH)	189.07						2.5	32.3	85.5	87	98
			(CH)	187.47						2.0	55.9	81.2	83	100
			(CH)	186.47							33.3	83.9	86	98
7	0+90	Inside traffic lane	Asphaltic conc	192.37	0.22	3.48	40	41.04	3850	104	-	-	-	-
			Cr stone base	192.08	0.47	4.44				33	1.0	151.0	140	108
			Subbase	191.71	2.76	33.12					2.8	138.6	126	110
			Subgrade (CH)	188.95						2.0	34.3	85.4	84	102
			(CH)	188.45						3.6	33.5	84.9	85	100
			(CH)	187.05						3.0	37.6	79.3	79	100

Table 7 (cont'd)

				Material	Elev.										
3A	30 kip Single wheel	1	3+45	Outside traffic lane	Asphaltic conc	192.45	0.29	3.48	42	41.76	120	107	—	145.6	140	204*
					Cr stone base	092.16	0.50	6.00				19	1.6	139.7	126	111*
					Subbase	191.66	2.69	32.34				1.5	3.7	96.2	88	98
					(CH)	188.47						3.8	32.0	87.5	86	99
					(CH)	187.97						3.1	32.5	85.1	87	98
		8		Inside traffic lane	Asphaltic conc	194.06	0.35	4.20	25	19.20		59	—	144.4	140	103*
					Cr stone base	193.71	0.55	6.60					1.0	—	—	—
					Subbase	193.16	0.70	8.40				3.8	33.4	85.4	86	99*
					(CH)	192.46						3.5	31.6	95.8	89	96
					(CH)	190.46						2.7	34.7	61.7	84	97
2	50 kip Single wheel	9	2+90	Inside traffic lane	Asphaltic conc	193.63	0.36	4.32	24	23.52	200	69	—	133.0	140	95*
					Cr stone base	193.27	0.45	5.40					2.9	—	—	—
					Subbase	193.82	1.15	13.80				4.1	33.2	86.0	86	100*
					(CH)	191.67						4.9	31.4	85.8	89	96
					(CH)	190.67										
		2	2+48	Inside traffic lane	Asphaltic conc	193.20	0.34	4.08	24	24.60	200	60	—	140.5	140	100*
					Cr stone base	192.86	0.32	3.84					1.8	—	—	—
					Subbase	192.54	1.39	16.68				3.5	31.5	87.3	89	98*
					(CH)	191.15						4.3	32.2	85.0	87	98
					(CH)	190.15										
2A	50 kip Single wheel	11	2+50	Inside traffic lane	Asphaltic conc	193.15	0.34	4.08	24	22.20	200	67	—	238.1	140	99*
					Cr stone base	192.81	0.37	4.44				17	1.9	—	—	—
					Subbase	192.44	1.14	13.68				2.5	30.8	91.8	90	102*
					(CH)	191.30							31.6	86.5	89	97
					(CH)	190.30										
2B	200 kip Twin tandem	12	4+10	Inside traffic lane	Asphaltic conc	193.12	0.33	3.96	33	33.00	40	55	—	143.2	140	102*
					Cr stone base	192.79	0.39	4.68					1.2	—	—	—
					Subbase	192.40	2.03	24.36				5.4	30.8	58.0	90	98*
					(CH)	190.37						2.6	34.5	82.8	84	99
					(CH)	189.37										
				Outside traffic lane	Asphaltic conc	193.33	0.30	3.60	33	34.00			—	—	140	—
					Cr stone base	193.03	0.44	5.28					—	—	—	—
					Subbase	192.59	2.11	25.32				4.2	30.1	88.6	91	97*
					(CH)	190.48						3.4	33.2	84.2	86	98
					(CH)	189.48										
		13	1+50	Inside traffic lane	Asphaltic conc	192.86	0.31	3.72	33	32.16	40	76	—	137.7	140	98*
					Cr stone base	192.55	0.54	6.48					1.4	—	—	—
					Subbase	192.01	1.83	21.96				4.5	31.3	88.2	89	99*
					(CH)	190.18						5.7	33.2	84.8	86	99
					(CH)	189.18										

Table 7 (concl'd)

Location	Item		Layer											
Outside traffic lane			Asphaltic conc	193.08	0.39	4.68	33	32.88		-	-	-	-	-
			Cr stone base	192.69	0.44	5.28				-	-	-	-	-
			Subbase	190.34	1.91	22.92				6	31.7	86.3	88	98**
			Subgrade (CH)	189.34						3.2	35.6	83.0	85	100
Inside traffic lane	14	1.05	Asphaltic conc	192.51	0.26	3.12	42	40.21	280	-	-	-	-	-
			Cr stone base	192.25	0.51	6.13				-	-	-	-	-
			Subbase	191.74	2.58	30.96				55	1.5	139.5	140	100**
			Subgrade (CH)	189.16						4.4	33.4	86.5	86	101**
			Subgrade (CH)	188.16						5.3	30.6	86.4	90	96
Outside traffic lane			Asphaltic conc	192.85	0.35	4.20	42	42.60		-	-	-	-	-
			Cr stone base	192.50	0.41	4.92				-	-	-	-	-
			Subbase	192.05	2.79	33.48				-	-	-	-	-
			Subgrade (CH)	189.30						4.8	33.5	85.3	86	99**
			Subgrade (CH)	188.30						4.5	30.7	89.0	90	99
Inside traffic lane	15	0.75	Asphaltic conc	192.43	0.33	3.95	42	40.88	280	-	-	-	-	-
			Cr stone base	192.10	0.46	5.80				-	-	-	-	-
			Subbase	191.62	2.59	31.13				-	-	-	-	-
			Subgrade (CH)	189.03						4.9	32.0	89.6	88	99**
			Subgrade (CH)	188.03						3.9	32.7	85.9	87	99
East maneuver area Inside traffic lane	16	0.40	Asphaltic conc	192.34	0.31	3.70	33	33.63	120	-	-	-	-	-
			Cr stone base	192.03	0.48	5.73				41	1.3	140.1	140	100*
			Subbase	191.55	2.02	24.20				-	-	-	-	-
			Subgrade (CL)	189.53						8	21.1	103.8	102	102**
			Subgrade (CL)	188.53						6	22.0	100.7	100	101

* Based on CE 55 maximum density at optimum water content.
** Based on CE 55 maximum density at field in-place water content.

Table 8

Traffic Test Data for Flexible Pavement Test Section

Traffic Lane	Assembly	Load per Tire lb	Tire Inflation Pressure psi	Tire Contact Area sq in.*	Pavement Temperature Range F	Item	Rated Subgrade CBR	Coverages	Total Deflection in.	Maximum Permanent Deformation in.	Upheaval in.	Pavement Cracking	Rating of Test Item
1	360 kip 12 wheel	30,000	100	285	90-135	1	3.7	0	0.63	--	--	--	--
							--	8	--	1.8	1.8	Severe	Failed
							--	12	--	3.6	--	Severe	Failed
						2	4.4	0	--	--	--	--	--
							--	104	0.43	0.5	0.4	Severe	Failed
							--	200	0.53	1.1	0.5	Severe	Failed
						3	3.8	0	--	--	--	--	--
							--	1500	0.30	1.8	0.7	Severe	Failed
							--	3334	0.31	2.6	1.1	Severe	Failed
						4	4.0	0	--	--	--	--	--
							--	1500	0.30	1.3	0.5	Severe	Failed
							--	3343	0.33	2.8	0.7	Severe	Failed
						5	4.0	0	0.27	--	--	--	--
							--	456	--	0.5	0.1	None	Satisfactory
							--	1500	0.25	1.1	0.3	Slight	Satisfactory
							--	2360	--	1.4	0.3	Slight	Satisfactory
							--	3850**	--	1.7	0.3	Slight	Satisfactory
2	30 kip Single wheel	30,000	100	285	90-120	1	3.7	0	0.22	--	--	--	--
							--	120	0.28	1.4	0.2	Severe	Failed
						2	4.4	0	0.11	--	--	--	--
							--	450**	0.08	0.8	0.1	None	Excellent
2A	50 kip Single wheel	50,000	165	285	90-115	1	3.7	0	0.48	--	--	--	--
							--	5	--	1.2	0.6	Severe	Failed
						2	4.4	0	0.19	--	--	--	--
							--	200	0.47	2.4	0.6	Severe	Failed
3A	60 kip Single wheel	60,000	165	285	60-70	1	3.7	0	0.42	--	--	--	--
							--	6	--	1.5	1.2	Severe	Failed
						2	4.4	0	0.23	--	--	--	--
							--	200	0.57	1.5	0.4	Severe	Failed
						3	3.8	0	0.56	--	--	--	--
							--	40	0.72	2.4	0.9	Severe	Failed
3B	240 kip Twin tandem	60,000	225	290	45-85	4	4.0	0	0.56	--	--	--	--
							--	40	0.72	2.4	1.0	Severe	Failed
						5	4.0	0	0.50	--	--	--	--
							--	40	--	1.3	0.2	Slight	Satisfactory
							--	280	0.74	3.5	0.7	Severe	Failed

* Average measured area.
** No failure developed.

178

Note: Table 9 has been placed in the
text proper for the reader's
convienence.

Table 10

MWHGL Static and Dynamic Instrumentation Loadings of

Flexible Pavement Test Section

Test Loading No.	Loading	Date Collection of Readings Completed	Static Loading Grid Pattern	Number of Static Readings
1	Preliminary tests	25 Apr 69	*	2,660
2	15 kips, 12 wheels, 45 psi	30 Apr 69	Partial	5,320
3	15 kips, SWL, 45 psi	6 Jun 69	Partial	2,660
4	30 kips, 1" wheels, 100 psi	19 Jun 69	Complete	5,360
5	30 kips, SWL, 100 psi	26 Jun 69	Complete	4,280
6	30 kips, 6 wheels, 100 psi	2 Jul 69	Partial	5,320
7	Prime mover (12 wheels)	9 Jul 69	*	1,660
8	30 kips, twin tandem, 100 psi	15 Jul 69	Complete	8,640
9	30 kips, twin tandem, 150 psi	18 Jul 69	Partial	2,760
10	Prime mover (twin tandem)	23 Jul 69	*	1,660
10a	30 kips, SWL, 100 psi (speed test)		--	
11**	6 kips, SWL, 10 psi	25 Jul 69	Partial	2,660
11a	30 kips, 12 wheel, 100 psi		*	
12	50 kips, SWL, 165 psi	30 Oct 69	Partial	2,660
13	60 kips, twin tandem, 225 psi	6 Nov 69	Partial	2,760
			Total	48,400

Note: Each test loading number and loading represents both static and dynamic load tests, except for test Nos. 10a and 11a. Test No. 10a represents only dynamic loading, and test Nos. 11-13 represent only static loadings.

* Selected locations.

** Performed in conjunction with another project.

Table 11

Summary of Tests with Load Cart

Assembly	Load kips	Tire Infla- tion Pressure psi*	Prelim- inary Tests	Pretraffic Tests			During Traffic Static	Additional Static Tests
				Static	Dynamic	Speed		
12 wheel	180	45	--	2	2	--	--	--
	360	100	--	4	4	--	11a	--
6 wheel	180	100	--	6	6	--	--	--
Twin tandem	120	100	--	8	8	--	--	--
		150	--	9	9	--	--	--
	240	225	--	--	--	--	--	13
Single wheel	5	10	--	11	--	--	--	--
	15	45	--	3	3	--	--	--
	30	100	1	5	5	10a	--	--
	50	165	--	--	--	--	--	12

* Tire contact area for 120-kip twin-tandem load (tire pressure 150 psi) was 212 sq in. Tire contact area for all other test carts was 285 sq in.
** Test load numbers correspond to the numbers shown in table 10.

Table 12

Summary of Tests with Empty Prime Movers

Test Loading No.*	Prime Mover	Dead Weight, lb	Tire Inflation Pressure, psi
7	6 and 12 wheel	2 front tires - 58,000 2 rear tires - 44,000	25 24
10	Twin tandem pulled by a tractor	1 tire - 6,500 1 tire - 5,900	15 15

* Test load numbers correspond to the numbers shown in table 10.

Note: Table 13 has been placed in the
text proper for the reader's
convienence.

Table 14

Comparison of Existing Criteria with Performance
of Multiple-Wheel Heavy Gear Load Test Section

Identification	CBR	ESWL* lb	Thickness t, in. Actual	Thickness t, in. Indicated**	Failure Coverages Actual	Failure Coverages Predicted
Lane 1, item 1	3.7	52,200	15	14.5	8	9
item 2	4.4	63,000	24	25.1	104	79
item 3	3.8	74,900	33	42.6	1500	206
item 4	4.0	74,900	33	41.5	1500	248
item 5	4.0	84,250	41	48.3	3850†	810
Lane 2, item 1	3.7	50,000	15	13.1	6	10
item 2	4.4	50,000	24	24.6	200	170
Lane 3A, item 1	3.7	30,000	15	19.0	120	33
item 2	4.4	30,000	24	20.8	450†	1438
Lane 3B, item 3	3.8	124,800	33	32.6	40	43
item 4	4.0	124,800	33	31.8	40	49
item 5	4.0	144,000	41	47.0	280	113

* Lane 1 ESWL computations were made using elastic theory with 20-radii cutoff modification. In all other lanes, ESWL was computed using elastic theory with no modification.
** Thickness indicated by number of coverages at failure.
† Nonfailure.

Note: Table 15 has been placed in the
        text proper for the reader's
        convienence.

Table 16

Comparison of α and f with Coverages

Identification	Failure Coverages	Actual Thickness t in.	ESWL* lb	CBR	A sq in.	α	f
Lane 1, item 1	8	15	62,280	3.7	285	0.336	0.357
item 2	104	24	77,760	4.4	285	0.525	0.614
item 3	1500	33	94,320	3.8	285	0.605	0.880
item 4	1500	33	94,320	4.0	285	0.621	0.975
item 5**	3850**	41	108,360	4.0	285	0.719	0.825
Lane 2, item 1	6	15	50,000	3.7	285	0.378	0.329
item 2	200	24	50,000	4.4	285	0.662	0.679
Lane 3A, item 1	120	15	30,000	3.7	285	0.497	0.628
item 2**	450*	24	30,000	4.4	285	0.875	0.760
Lane 3B, item 3	40	33	124,800	3.8	290	0.524	0.518
item 4	40	33	124,800	4.0	290	0.538	0.518
item 5	280	41	144,000	4.0	290	0.621	0.713

 * Obtained from figure 64 or 69, as appropriate. All computed using elastic theory without modification.
** Nonfailure.

Table 17

Comparison of Predicted Thicknesses
with Test Section Thicknesses

Identification	α	$\sqrt{\dfrac{ESWL}{8.1\ CBR}} - \dfrac{A^*}{n}$	Thickness t, in. Predicted	Actual
Lane 1, item 1	0.340	44.5	15.1	15
item 2	0.550	45.7	25.1	24
item 3	0.661	54.5	36.0	33
item 4	0.661	53.1	35.1	33
item 5**	0.692	57.0	39.4	41
Lane 2, item 1	0.360	39.7	14.3	15
item 2	0.670	36.2	24.2	24
Lane 3A, item 1	0.625	30.2	18.9	15
item 2**	0.740	27.4	20.3	24
Lane 3B, item 3	0.510	62.9	32.1	33
item 4	0.510	61.3	31.3	33
item 5	0.640	66.0	42.2	41

* ESWL was determined using elastic theory without modifications.
** No failure occurred in this item.

Table 18

Conversion of MWHGL Test Section Coverages
to Actual Airfield Facility Passes

Identification	Assembly	A sq in.	Failure Coverages	α_i Factor	P/c Factor	Failure Passes
Lane 1, item 1	12 wheel	285	8	0.340	0.66	5
item 2	12 wheel	285	104	0.550	0.66	69
item 3	12 wheel	285	1500	0.661	0.66	990
item 4	12 wheel	285	1500	0.661	0.66	990
item 5	12 wheel	285	3850*	0.692	0.66	2541
Lane 2, item 1	Single wheel	285	6	0.360	2.9	17
item 2	Single wheel	285	200	0.670	2.9	580
Lane 3A, item 1	Single wheel	285	120	0.625	2.9	348
item 2	Single wheel	285	450*	0.740	2.9	1305
Lane 3B, item 3	Twin tandem	290	40	0.510	1.62	65
item 4	Twin tandem	290	40	0.510	1.62	65
item 5	Twin tandem	290	280	0.640	1.62	454

* Nonfailure.

187

Table 19

Previous Related Studies

Reference No.	Assembly	Wheel Load kips	Tire Contact Area sq in.	CBR	Failure Passes	α, Load Repetitions Factor
46 & 51	Single wheel	200	1501	6.0	190	0.646
		200	1501	9.0	2,140	0.924
		200	1501	16.0	13	0.550
		200	1501	18.0	76	0.686
		200	1501	15.5	455	0.704
		200	1501	17.5	1,890	0.980
		200	1501	8.0	1,640	0.959
		15	250	8.0	11,650	0.813
		15	250	9.0	11,650	0.893
53	Twin wheels	35	330	20.0	5,250	0.787
57	Twin tandem	30	150	12.0	410	0.758
		30	150	5.0	135	0.475
		30	150	15.0	2,250	0.870
58	Twin tandem	37.5	262	16.0	1,310	0.693

Note: Table 20 has been placed in the
text proper for the reader's
convience.

Note: Table 21 is a folded sheet and
is enclosed at the back of this
volume.

Note: Tables 22 through 24 have been placed
       in the text proper for the reader's
       convienence.

REFERENCES

1. Ladd, D. M.; Ground-Flotation Requirements for Aircraft Landing Gear, Miscellaneous Paper No. 4-459, U. S. Army Engineer Waterways Experiment Station, CE, Vicksburg, Miss., December 1961, revised July 1965.

2. Ladd, D. M., and Ulery, H. H., Jr.; Aircraft Ground-Flotation Investigation, Technical Documentary Report AFFD. TDR-66-43 (consists of a basic report and separate data reports, Parts I-XIX), Wright-Patterson AFB, Ohio. Prepared by U. S. Army Engineer Waterways Experiment Station, CE, Vicksburg, Miss., August 1967.

3. Ahlvin, R. G., and Brown, D. N.; "Flotation Requirements for Aircraft," Aerospace Systems Conference, Conference Proceedings, Society of Automotive Engineers, Inc., Paper 670559, June 1967.

4. Burns, C. D., Brabston, W. N., and Grau, R. W.; Feasibility of Membrane-Encased Soil Layers as Pavement Elements for Multiple-Wheel Heavy Gear Load Pavement, Miscellaneous Paper in preparation, U. S. Army Engineer Waterways Experiment Station, CE, Vicksburg, Miss.

5. Departments of the Army and the Air Force; Airfield Flexible Pavements - Air Force, TM 5-824-2/AFM 88-6, Chapter 2, Washington, D. C., February 1969.

6. Behrmann, R. M.; Small-Scale Static Load Model Study of Pavement Stresses Resulting from C-141 and C-5A Aircraft Loadings, AFWL-TR-69-2; prepared by Construction Engineering Research Laboratory, U. S. Army Engineer Division, Ohio River, for Air Force Weapons Laboratory, Albuquerque, N. Mex., August 1969.

7. Departments of the Army and the Air Force; Rigid Airfield Pavements, TM 5-824-3/AFM 88-6, Chapter 3, Washington, D. C., February 1958.

8. Department of Defense; Military Standard for Unified Soil Classification System for Roads, Airfields, Embankments, and Foundations, MIL-STD-619F, Washington, D. C., June 1968.

9. Department of the Army, CE, Office, Chief of Engineers; Guide Specification for Military Construction, Subbase Course, CE-807.02, Washington, D. C., January 1968.

10. Department of the Army, CE, Office, Chief of Engineers; Guide Specification for Military Construction, Graded-Crushed Aggregate Base Course, CE-807.07, Washington, D. C., January 1968.

11. Department of the Army, CE, Office, Chief of Engineers; Guide Specification for Military Construction, Bituminous Binder and Surface Courses for Airfields, Heliports, and Tank Roads (Central-Plant Hot-Mix), CE-807.22, Washington, D. C., October 1959.

12. Department of Defense; Military Standard for Test Methods for Pavement, Subgrade, Subbase, and Base-Course Materials, MIL-STD-621A, Washington, D. C., December 1964.

13. U. S. Army Engineer Waterways Experiment Station, CE; Investigations of Pressures and Deflections for Flexible Pavements: Homogeneous Clayey-Silt Test Section, Report No. 1, Technical Memorandum No. 3-323, Vicksburg, Miss., March 1951.

14. Ahlvin, R. G., and Ulery, H. H., Jr.; "Tabulated Values for Determining the Complete Pattern of Stresses, Strains, and Deflections Beneath a Uniform Circular Load on a Homogeneous Half Space," Stress Distribution in Earth Masses, Highway Research Board Publication No. 1025, Bulletin 342, pp. 1-13, 1962.

15. Hall, J. W., Jr.; Nondestructive Testing of Pavements: Tests on Multiple-Wheel Heavy Gear Load Test Sections, and Eglin and Hurlburt Airfields, Technical Report AFWL-TR-71-64, being prepared by U. S. Army Engineer Waterways Experiment Station, CE, for Air Force Weapons Laboratory, Kirtland AFB, N. Mex.

16. Peutz, M. G. F., Jones, A., and van Kempten, H. P.; Layered Systems Under Normal Surface Loads, Computer Program, Koninklijke/Shell Laboratorium, Amsterdam, Holland.

17. Michelow, J.; Analysis of Stresses and Displacements in an N-Layered Elastic System Under a Load Uniformly Distributed on a Circular Area, Computer Program, California Research Corporation, Richmond, Calif., September 1963.

18. Peattie, K. R.; "A Fundamental Approach to the Design of Flexible Pavements," Proceedings, International Conference on Structural Design of Asphalt Pavements, pp. 403-411, 1962.

19. Pletta, F.; Engineering Mechanics, Ronald Press, N. Y., pp. 265-271, 1964.

20. Timoshenko, S., and Young, D. H.; Advanced Dynamics, McGraw-Hill, N. Y., pp. 153-181, 1948.

21. Boresi, A. P.; Elasticity in Engineering Mechanics, Prentiss Hall, pp. 103-112, 1965.

22. Smith, G. L., and Smith, G. M.; Advanced Dynamics, International Textbook Co., Scranton, Pa., pp. 117-153, 1960.

23. Kristnamurthy, N.; Short Course Matrix Operations - Finite Elements as Applied to Structural Analysis, Auburn University, Auburn, Ala., February 1970.

24. Wang, C. K.; Matrix Methods of Structural Analysis, International Textbook Co., Scranton, Pa., 1966.

25. Kristnamurthy, N.; Short Course in Finite Elements, Auburn University, Auburn, Ala., March 1970.

26. Scheid, Francis; Theory and Problems of Numerical Analysis, McGraw-Hill, N. Y., pp. 15-21, 1968.

27. Banks, D. C., and Palmerton, J. B.; *Application of Finite Element Method in Determining Stability of Crater Slopes, Preliminary Report*, Miscellaneous Paper S-68-3, U. S. Army Engineer Waterways Experiment Station, CE, Vicksburg, Miss., May 1968.

28. Timoshenko, S. P., and Goodier, J. N.; *Theory of Elasticity*, McGraw-Hill, N. Y., pp. 235-244, 1970.

29. Duncan, J. M., Monismith, C. L., and Wilson, E. L.; "Finite Element Analysis of Pavements," *47th Annual Meeting of Highway Research Board*, January 1968.

30. U. S. Naval Civil Engineering Laboratory; *Rational Pavement Evaluation-Review of Present Technology*, AFWL-TR-69-9; prepared under MIPR's 68-15, 68-28, and 69-17 for Air Force Weapons Laboratory, Kirtland AFB, N. Mex., October 1969.

31. Wilson, E. L.; *A Digital Computer Program for the Finite Element Analysis of Solids with Nonlinear Material Properties*, Department of Civil Engineering, University of California, Berkeley, Calif., July 1965.

32. Harr, M. E., and Rosner, J. C.; *Theoretical Study of Landing Mat Behavior*, Contract Report S-69-7; prepared by Purdue Research Foundation, Purdue University, under Contract No. DACA 39-67-C-004 for the U. S. Army Engineer Waterways Experiment Station, CE, Vicksburg, Miss., June 1970.

33. Vlasov, V. Z., and Leont'ev, N. N.; *Beams, Plates, and Shells on an Elastic Foundation*, Israel Program for Scientific Translations, Jerusalem, 1966.

34. Freudenthal, A. M., and Lorsch, H. G.; "The Infinite Elastic Beam on a Linear Viscoelastic Foundation," *Proceedings of the ASCE*, Journal of Engineering Mechanics Division, Vol. 83, No. EM 1, pp. 1158, 1-1158, 22, January 1957.

35. Barksdale, R. D.; *Elastic and Viscoelastic Analysis of Layered Pavement Systems*, PhD Thesis, Purdue University, Lafayette, Ind., 1966.

36. Chou, Y. T.; "A General Theory of Stresses and Displacements in Elastic and Viscoelastic Layered Systems," *Transactions of the Fifteenth Conference of Army Mathematicians*, ARD-D Report 70-1, pp. 141-168, June 1969.

37. Hudson, R. N.; *Discontinuous Orthotropic Plates and Pavement Slabs*. Computer Program, No. 56-9, Center for Highway Research, University of Texas, Austin, Tex., October 1967.

38. Westergaard, H. M.; "A Problem of Elasticity Suggested by a Problem in Soil Mechanics" and "Soft Material Reinforced by Numerous Strong Horizontal Sheets," *Contributions to the Mechanics of Solids*, Timoshenko Sixtieth Anniversary Volume, Macmillan, N. Y., 1938.

39. Odemark, N.; *Investigations as to Elastic Properties of Soils and Design of Pavements According to Theory of Elasticity*, Statens Vaginstitute, Meddelande No. 77, Stockholm, Sweden, 1949.

194

40. Hogg, A. H. A.; "Equilibrium of a Thin Plate, Symmetrically Loaded, Resting on an Elastic Subgrade of Infinite Depth," _Philosophical Magazine_, Series 7, Vol. 25, March 1938.

41. Holl, D. L.; "Thin Plates on Elastic Foundations," _Proceedings_, Fifth International Congress of Applied Mechanics, Cambridge, Mass., 1938.

42. Barenberg, E. J.; _A Structural Design Classification of Pavements Based on an Analysis of Pavement Behavior, Material Properties, and Modes of Failure_, PhD Thesis, University of Illinois, Urbana, Ill., 1965.

43. Vesic, A. S., and Domaschuk, L.; _Theoretical Analysis of Structural Behavior of Road Test Flexible Pavements_, Georgia Institute of Technology, Atlanta, Ga., p. 29, 1964.

44. Brandt, E. W.; _Concentration Factors for Stress Distribution in Soils_, Sols Soils No. 21, pp. 11-20, 1968.

45. Foster, C. R., and Ahlvin, R. G.; "Development of Multiple-Wheel CBR Design Curves," in _Proceedings of the American Society of Civil Engineers_, Journal of Soil Mechanics, Foundations Division, Paper 1647, May 1958.

46. U. S. Army Engineer Waterways Experiment Station, CE; _Collection of Letter Reports on Flexible Pavement Design Curves_, Miscellaneous Paper No. 4-61, Vicksburg, Miss., June 1951.

47. Cooksey, D. L., and Ladd, D. M.; _Pavement Design for Various Levels of Traffic Volume_, AFWL-TR-70-133; prepared by U. S. Army Engineer Waterways Experiment Station, CE, for Air Force Weapons Laboratory, Kirtland AFB, N. Mex., July 1970.

48. Bryant, E. C.; _Statistical Analysis_, McGraw-Hill, N. Y., pp. 113-135, 198-224, 1960.

49. Snedeior, G. W., and Cochran, W. G.; _Statistical Methods_, Iowa State University Press, 1967.

50. Brown, D. N., and Thompson, O. O.; _Lateral Distribution of Aircraft Traffic_, Miscellaneous Paper in preparation, U. S. Army Engineer Waterways Experiment Station, CE, Vicksburg, Miss.

51. O. J. Porter and Co.; _Accelerated Traffic Tests at Stockton Airfield_, Stockton, Calif., Stockton Test No. 2, 7 vols., for U. S. Engineer Office, Sacramento, Calif., May 1948.

52. U. S. Army Engineer Waterways Experiment Station, CE; _Rigid Pavement Tests, Marietta, Georgia, Construction, Testing and Data Report_, Vicksburg, Miss., August 1945.

53. U. S. Army Engineer Waterways Experiment Station, CE; _Effects of Traffic with Small High-Pressure Tires on Asphalt Pavements_, Technical Memorandum No. 3-314, Vicksburg, Miss., June 1950.

54. U. S. Army Engineer Waterways Experiment Station, CE; Design of Flexible Airfield Pavements for Multiple-Wheel Landing Gear Assemblies, Report No. 1, Technical Memorandum No. 3-349, Vicksburg, Miss., September 1952.

55. U. S. Army Engineer Waterways Experiment Station, CE; Design of Upper Base Courses for High-Pressure Tires, Report No. 1, Technical Memorandum No. 3-373, Vicksburg, Miss., December 1953.

56. U. S. Army Engineer Waterways Experiment Station, CE; Proof-Test Section. Columbus Air Force Base, Technical Report No. 3-490, Vicksburg, Miss., December 1958.

57. U. S. Army Engineer Waterways Experiment Station, CE; Investigation of the Design and Control of Asphalt Paving Mixtures, Technical Memorandum No. 3-254, Vol. 3, App. D, Vicksburg, Miss., May 1948.

58. U. S. Army Engineer Waterways Experiment Station, CE; Investigation of Effects of Traffic with High-Pressure Tires on Asphalt Pavements, Technical Memorandum No. 3-312, Vicksburg, Miss., May 1950.

59. Ahlvin, R. G.; "Consolidated CBR Criteria," Journal of Soil Mechanics and Foundations Division, ASCE, Vol. 84, No. SM4, Paper 1825, pp. 1825, 1-1825, 16, October 1958.

60. U. S. Army Engineer Waterways Experiment Station, CE; Developing a Set of CBR Design Curves, Instruction Report No. 4, Vicksburg, Miss., November 1959.

61. Department of Transportation; Airport Paving, AC 150/5320-6A, Federal Aviation Administration, May 1967, reprinted September 1968.

BIBLIOGRAPHY

Ahlvin, R. G.; Pavement Test to Provide for the Jumbo Jets, Presentation at the 13th Annual Alabama Highway Engineering Conference, Auburn University, Auburn, Ala., March 1970

Brown, D. N., and Rice, J. L.; Airfield Pavement Requirements for Multiple-Wheel Heavy Gear Loads, FAA-RD-70-77 (Final Report) (also Waterways Experiment Station Miscellaneous Paper S-71-5), prepared by U. S. Army Engineer Waterways Experiment Station, CE, for Federal Aviation Administration, Washington, January 1971.

Burmister, D. M., "The Theory of Stresses and Displacements in Layered Systems and Applications to Design of Airport Runways," Proceedings Highway Research Board, Vol. 23, pp. 126-144, 1943.

Compaction Requirements for Soil Components of Flexible Airfield Pavements, Technical Report No. 3-529, U. S. Army Engineer Waterways Experiment Station, CE, Vicksburg, Miss., November 1959.

Handbook of Instructions for Aircraft Design, AFSC Manual No. 80-1, U. S. Air Force Systems Command, Headquarters, Revised October 1964.

Investigations of Pressures and Deflections for Flexible Pavements, Homogeneous Sand Test Section, Technical Memorandum No. 3-323, Report No. 4, U. S. Army Engineer Waterways Experiment Station, CE, Vicksburg, Miss., December 1954.

Jester, G. E., *An Experimental Investigation of Soil-Structure Interaction in a Cohesive Soil*, Technical Report No. N-70-7, Vols. 1 and II, U. S. Army Engineer Waterways Experiment Station, CE, Vicksburg, Miss., March 1970.

Jurgenson, Leo, "Application of Elastic Theory and Plasticity of Foundation Problems," *Journal*, Boston Society of Civil Engineers, p. 242, July 1934.

McFadden, G., et al., "Development of CBR Flexible Pavement Design Method for Airfields," *Transactions of an ASCE Symposium*, Vol. 115, pp. 453-589, 1950.

Middlebrooks, T. A., and Bertram, G. E., "Adaptation to the Design of Airfield Pavements," *ASCE Transactions*, Vol. 115, p. 468, 1950.

Pickett, G., and Ray, G. K., "Influence Charts for Concrete Pavements," *ASCE Transactions*, Paper No. 2425, April 1950.

Porter, O. J., "Development of Original Method of Highway Design," *ASCE Transactions*, Vol. 115, p. 461, 1950.

Pressure Cells for Field Use, Bulletin No. 40, U. S. Army Engineer Waterways Experiment Station, CE, Vicksburg, Miss., January 1955.

Standard Practices for Bituminous Pavements, Technical Manual No. 5-822-8, in process of publication, Headquarters, Department of the Army, Washington, D. C.

Taylor, D. W., *Soil Mechanics*, John Wiley & Sons, Inc., N. Y., 1948.

Tentative Method of Test for Pulse Velocity Through Concrete, CRD-C 51-68, U. S. Army Engineer Waterways Experiment Station, CE, Vicksburg, Miss., June 1968; *Handbook for Concrete and Cement* (with quarterly supplements), Vicksburg, Miss., August 1949.

Ulery, H. H., Jr., and Trawle, M. J.; "Pavement Tests for the Jumbo Jets," in *The Military Engineer*, Vol. 63, No. 413, May-June 1971.

Test Item	Slab	Water Content, % Top 6" Subgrade As Constr.	After Traffic	Dry Density, pcf Top 6" Subgrade As Constr.	After Traffic	Modulus of Soil Reaction, pci As Constr.	After Traffic	Thickness, inches As-Constructed AC(2)	PCC(1)	After Traffic AC(2)	PCC(2)	As Co
1	SW	32.2	34.2	85.5	84.1	62	140	--	10.2	--	10.6	
	SE	"	"	"	"	"	"	--	"	--	9.8	
	NW	"	33.3	"	83.7	"	169	--	9.7	--	9.6	
	NE	"	"	"	"	"	"	--	"	--	9.5	
1 (Overlay)	SW	"	34.2	"	84.1	"	140	4.3	10.2	3.9	10.6	1
	SE	"	"	"	"	"	"	4.7	"	4.5	9.8	
	NW	"	33.3	"	83.7	"	169	4.0	9.7	3.9	9.6	1
	NE	"	"	"	"	"	"	4.0	"	3.8	9.5	
2	SW	32.9	35.0	83.9	81.5	70	78	--	12.1	--	12.0	
	SE	"	"	"	"	"	"	--	"	--	12.1	
	NW	"	33.2	"	84.6	"	111	--	11.4	--	11.5	
	NE	"	"	"	"	"	"	--	"	--	11.3	
3	SW	32.0	36.9	86.0	81.8	74	59	--	14.0	--	14.1	
	SE	"	"	"	"	"	"	--	"	--	13.8	
	NW	"	33.1	"	83.4	"	115	--	13.6	--	13.6	
	NE	"	"	"	"	"	"	--	"	--	14.1	
4	SW	31.5	32.6	86.1	87.3	74	125	--	8.0	--	8.2	
	SE	"	"	"	"	"	"	--	"	--	8.2	
	NW	"	32.4	"	87.6	"	128	--	7.6	--	7.4	
	NE	"	"	"	"	"	"	--	"	--	7.2	
4 (Overlay)	SW	"	32.6	"	87.3	"	125	5.3	8.0	5.3	8.2	1
	SE	"	"	"	"	"	"	5.6	"	5.6	8.2	
	NW	"	32.4	"	87.6	"	128	5.6	7.6	5.4	7.4	1
	NE	"	"	"	"	"	"	5.6	"	5.6	7.2	

NOTES: (1) Determined from level readings.
(2) Measured from cores.
(3) 28-day construction control tests.
(4) Representative values based on modulus of rupture tests on sawed beams, compression tests on cores, and pulse velocity measurements.

(5) Item or slab not instrumented o
(6) Measured along longitudinal joi
(7) Measured along transverse joint
(8) Traffic discontinued before ite

1

Table 21

Traffic Test Data for Rigid Pavement Test Section

Traffic PCC[2]	Unit Weight of Asph. Conc., pcf		Concrete Flexural Strength, psi		Assembly Used for Traffic	Load Per Tire lb	Tire Contact Area psi	Minimum Transient Deformation in.	Maximum Permanent Defl., in.	Coverages for Failure Condition	
	As Constr.	After Traffic	As[3] Constr.	After[4] Traffic						1st Crack	Shatter Slab
10.6	--	--	640	725	12-Wheel	30,000	285	(5)	0.36	251	(8)
9.8	--	--	"	"	" "	"	"	0.147(6)	0.36	192	592
9.6	--	--	585	695	--	--	--	(5)	--	--	--
9.5	--	--	"	"	--	--	--	(5)	--	--	--
10.6	145.5	148.4	640	725	12-Wheel	30,000	285	(5)	0.72	N/A	N/A
9.8	"	"	"	"	" "	"	"	0.270(6)	1.08	N/A	N/A
9.6	146.2	149.1	585	695	Twin-Tandem	41,500	207	(5)	0.84	N/A	N/A
9.5	"	"	"	"	" "	"	"	(5)	0.72	N/A	N/A
12.0	--	--	730	800	12-Wheel	30,000	285	0.173(6)	0.96	4496	(8)
12.1	--	--	"	"	" "	"	"	0.174(6)	0.96	3963	(8)
11.5	--	--	600	700	Twin-Tandem	41,500	207	(5)	0.48	40	680
11.3	--	--	"	"	" "	"	"	(5)	0.48	150	680
14.1	--	--	760	760	12-Wheel	30,000	285	0.197(7)	1.20	2208	(8)
13.8	--	--	"	"	" "	"	"	0.212(7)	1.44	592	(8)
13.6	--	--	630	660	Twin-Tandem	41,500	207	(5)	0.36	260	(8)
14.1	--	--	"	"	" "	"	"	(5)	0.48	150	(8)
8.2	--	--	720	775	12-Wheel	30,000	285	(5)	0.48	180	240
8.2	--	--	"	"	" "	"	"	(5)	0.40	181	240
7.4	--	--	560	605	-- --	--	--	(5)	--	--	--
7.2	--	--	"	"	-- --	--	--	(5)	--	--	--
8.2	146.6	147.5	720	775	12-Wheel	30,000	285	(5)	1.56	N/A	N/A
8.2	"	"	"	"	" "	"	"	(5)	1.20	N/A	N/A
7.4	146.0	149.2	560	605	Twin-Tandem	41,500	207	(5)	1.56	N/A	N/A
7.2	"	"	"	"	" "	"	"	(5)	1.68	N/A	N/A

instrumented or gage failed prior to traffic.
Longitudinal joint.
Transverse joint.
ued before item reached failure condition shown.

2

mbly d for ffic	Load Per Tire lb	Tire Contact Area psi	Maximum Transient Deformation in.	Maximum Permanent Defl., in.	Coverages for Failure Condition			Remarks
					1st Crack	Shatter Slab	Compl. Failure	
heel	30,000	285	(5)	0.36	251	(8)	(8)	
"	"	"	0.147(6)	0.36	192	592	(8)	
--	--	--	(5)	--	--	--	--	Not trafficked prior to overlay
--	--	--	(5)	--	--	--	--	" " " "
heel	30,000	285	(5)	0.72	N/A	N/A	--	Not failed - 4416 coverages
"	"	"	0.270(5)	1.08	N/A	N/A	--	" " " "
-Tandem	41,500	207	(5)	0.84	N/A	N/A	--	" " 680 coverages
"	"	"	(5)	0.72	N/A	N/A	--	" " " "
heel	30,000	285	0.173(6)	0.96	4496	(8)	(8)	
"	"	"	0.174(6)	0.96	3963	(8)	(8)	
-Tandem	41,500	207	(5)	0.48	40	680	(8)	
"	"	"	(5)	0.48	150	680	(8)	
heel	30,000	285	0.197(7)	1.20	2208	(8)	(8)	Performance affected by pumping
"	"	"	0.212(7)	1.44	592	(8)	(8)	" " " "
-Tandem	41,500	207	(5)	0.36	260	(8)	(8)	
"	"	"	(5)	0.48	150	(8)	(8)	
heel	30,000	285	(5)	0.48	180	240	(8)	
"	"	"	(5)	0.48	181	240	(8)	
--	--	--	(5)	--	--	--	--	Not trafficked prior to overlay
--	--	--	(5)	--	--	--	--	" " " " "
heel	30,000	285	(5)	1.56	N/A	N/A	--	Not failed - 4416 coverages
"	"	"	(5)	1.20	N/A	N/A	--	" " " "
-Tandem	41,500	207	(5)	1.56	N/A	N A	680	
"	"	"	(5)	1.68	N/A	N/A	680	

3

DOCUMENT CONTROL DATA - R & D

(Security classification of title, body of abstract and indexing annotation must be entered when the overall report is classified)

1. ORIGINATING ACTIVITY (Corporate author)	2a. REPORT SECURITY CLASSIFICATION
U. S. Army Engineer Waterways Experiment Station Vicksburg, Mississippi 39181	UNCLASSIFIED
	2b. GROUP

3. REPORT TITLE

MULTIPLE-WHEEL HEAVY GEAR LOAD PAVEMENT TESTS: Volume I, Basic Report

4. DESCRIPTIVE NOTES (Type of report and inclusive dates)

1 January 1968 through 1 August 1971

5. AUTHOR(S) (First name, middle initial, last name)

R. G. Ahlvin, et al.

6. REPORT DATE	7a. TOTAL NO. OF PAGES	7b. NO. OF REFS
November 1971	212	61

8a. CONTRACT OR GRANT NO. MIPR 68-7	9a. ORIGINATOR'S REPORT NUMBER(S)
b. PROJECT NO. 5224	AFWL-TR-70-113, Vol I
c.	9b. OTHER REPORT NO(S) (Any other numbers that may be assigned this report)
d.	

10. DISTRIBUTION STATEMENT

Distribution limited to U S Government agencies only because of test and evaluation (1 Nov 1971). Other requests for this document must be referred to AFWL (DEZ), Kirtland AFB, New Mexico 87117.

11. SUPPLEMENTARY NOTES	12. SPONSORING MILITARY ACTIVITY
	AFWL (DEZ) Kirtland AFB, NM 87117

13. ABSTRACT (Distribution Limitation Statement B)

Flexible and rigid pavements were constructed and tested to obtain data on pavement and soil behavior under large aircraft loadings for use in developing criteria for evaluating and designing airfield pavements subjected to multiple-wheel heavy gear loads (WMHGL).

The test sections incorporated instrumentation systems designed to determine the response of the pavement structures to static, dynamic (slowly moving), and vibratory loads and to traffic by full prototype loadings of a 12-wheel assembly (one main gear of a C-5A aircraft), a twin-tandem assembly (one twin-tandem component of the Boeing 747 assembly), and a single wheel.

Analysis of static load response data from the flexible pavement instrumentation program resulted in the establishment of maximum elastic deflection and vertical elastic stress versus depth curves. Comparisons showed that the same relationships were true for static and dynamic load tests, as well as for speed tests. The findings for the rigid pavement test section indicated that the Westergaard algorithm can be used for reasonable prediction of pavement response to test loadings.

The data from the instrumentation program and the traffic tests were used in the analysis of the flexible and rigid pavement test sections. The analysis resulted in a modification of the basic flexible pavement CBR design method. The recommended method reflects a reduction of existing Corps of Engineers (CE) thickness requirements that is especially significant for multiple-wheel assemblies in the higher operational level.

DD FORM 1473 NOV 68

14. KEY WORDS	LINK A		LINK B		LINK C	
	ROLE	WT	ROLE	WT	ROLE	WT
Heavy duty airfield pavements						
Airfield pavements						
Strength criteria for airfield pavements						
Pavement deflections						
Pavement requirements for heavy gear load aircraft						
Accelerated traffic tests of airfield pavements						
Multi-wheel airfield pavement tests						

Item 13 Continued:

Current CE evaluation and design methods for rigid pavements are based on stress in the concrete pavement as calculated from the Westergaard analysis; extrapolations to the existing criteria were found to be valid for MWHGL assemblies insofar as pavement thicknesses were concerned. Rigid pavement testing indicated that current jointing recommendations allowing keyed construction joints may be unconservative for MWHGL assemblies trafficking a pavement overlying a low-strength subgrade.